Development of A Highly Efficient Nb/V/S Co-doped Ta_3N_5 Solar Catalyst Immobilized/Protected With Biomass Soot Carbon and PANI Utilizing Solar Energy for Efficient Water Splitting

Thesis Submitted for the Award of the Degree of

DOCTOR OF PHILOSOPHY

In

Chemistry

By

Monika

Registration Number: 11919263

Supervised By

Dr. Ajit kumar Sharma

Chemistry (Associate professor)

Lovely professional University

Co-Supervised by

Dr Dai-Viet N. Vo

Environment Science(Deputy Director)

Nguyen Tat Thanh University-Vietnam

LOVELY PROFESSIONAL UNIVERSITY, PUNJAB
2023

DECLARATION

I, hereby declared that the presented work in the thesis entitled "Development of a highly efficient Nb/V/S co-doped Ta_3N_5 solar catalyst immobilized/protected with biomass soot carbon and PANI utilizing solar energy for efficient water splitting" in fulfilment of degree of **Doctor of Philosophy (Ph. D.)** is outcome of research work carried out by me under the supervision Dr Ajit Kumar Sharma, working as Associate Professor, in the Department of Chemistry, School of Chemical Engineering and Physical Sciences of Lovely Professional University, Punjab, India. In keeping with general practice of reporting scientific observations, due acknowledgements have been made whenever work described here has been based on findings of another investigator. This work has not been submitted in part or full to any other University or Institute for the award of any degree.

Name of the scholar: Monika

Registration No.:11919263

Department of Chemistry, School of Chemical Engineering and Physical Sciences of Lovely Professional University

Lovely Professional University,

Punjab, India

CERTIFICATE

This is to certify that the work reported in the Ph. D. thesis entitled "Development of a highly efficient Nb/V/S co-doped Ta_3N_5 solar catalyst immobilized/protected with biomass soot carbon and PANI utilizing solar energy for efficient water splitting" submitted in fulfillment of the requirement for the reward of degree of **Doctor of Philosophy (Ph.D.)** in the Department of Chemistry, School of Chemical Engineering and Physical Sciences of Lovely Professional University, is a research work carried out by Monika, 11919263, is bonafide record of his original work carried out under my supervision and that no part of thesis has been submitted for any other degree, diploma or equivalent course.

(Signature of Supervisor)

Dr Ajit KumarSharma

Designation: Associate Professor

Department;
School of Chemical Engineering
And Physical Science University

(Signature of Co-Supervisor)

Dr Dai-Viet N. Vo

Designation: Deputy Director

Department;
Environment Science
Nguyen Tat Thanh University

Abstract

Extensive industrialization and rapid population growth with the global energy demands are rising due to high growth rate of urbanization and industrial expansion, which are some of the greatest challenges of this century. The rapid depletion of the world's primary energy resources, carbon-derived fossil fuels, and the deleterious environmental impacts associated with their use and processing, such as global warming and disruption of ecological balance, have induced growing concerns in global communities. As fossil fuels are the primary contributor to global warming, provide the majority of the world's energy demands, energy generation from alternative renewable resources become indispensable. The quantity of solar energy that enters the atmosphere of earth every hour greatly exceeds the yearly global energy needs. Conversion of solar energy to generate hydrogen (H_2), which is an ideal fuel, abundant, free of cost and clean source of energy has emerged as a potential long- term alternative. After Fujishima-Honda's discovery of water-photolysis on a semiconductor electrode made of TiO_2 in 1972, vast majority of research has been devoted on semiconductor photocatalysis that continues to grow even today, despite the fact that the UV activity of TiO_2 and many other oxide semiconductors limits their utility in solar radiation. Considering the abundance of 'visible light' amounting to $\sim 43\%$ of incoming solar energy, a lot of research efforts in the global arena have been dedicated toward the synthesis of photocatalysts that are visible light active for the effective use of solar energy. Semiconductor photocatalysis for CO_2 reduction and hydrogen production from water renders a sustainable solution toward use and generation of renewable energy. An effective photocatalyst powered by sunlight would ideally find niche uses in some of the growing fields of environment and energy. Generally, the efficiency or usage of photocatalysts are limited due to issues related to photocorrosion, photostability, reusability, inefficient charge-carrier separation and fast recombination resulting in low photocatalytic efficiencies for visible-light/sunlight utilization. Several

methodological techniques are used for the production of visible light driven photocatalysts through band gap engineering. To develop visible-light active semiconductors, doping of metal ions with partially filled d orbitals in oxides is being widely investigated. Moreover, for improving upon the efficiencies of photocatalysts, use of co-catalysts or metal nanoparticles in the form of heterojunction or composites has been explored. The loading of cocatalysts or metal nanoparticles enhances charge separation due to suitable band level positioning or high conductivity of metals, respectively.

In view of this, one of the cleanest and most sustainable routes for H_2 evolution is solar-assisted photocatalytic (PC) water splitting. Nevertheless, the efficiency of PC water splitting systems is rather low till date, owing to the low solar conversion productivity of singular semiconductor photocatalyst. Thus, this thesis work aims to rationally design and develops an efficient novel cost-effective, stable and eco-friendly Ta_3N_5-based photocatalyst and suitably modified novel co-doped Ta_3N_5/BSC@PANI photocatalyst, and integrates them into a PC system for effective solar driven overall water splitting. Despite its excellent PC performance as a base Ta_3N_5 photocatalyst, its efficiency is limited by its sluggish charge transfer kinetics and rapid electron-hole recombination rate. To alleviate these intrinsic material issues, novel surface modification is done by introducing BSC on the surface of Ta_3N_5 photocatalyst. Hole-transporting conductive polyaniline (PANI) are synthesized on the surface of BSC/Ta_3N_5 through chemisorption process means to construct the novel hierarchical BSC/Ta_3N_5@PANI photocatalyst. The PANI allows the effective transport of photogenerated holes to PANI surface from the Ta_3N_5 surface to deter electron-hole recombination. The synergistic interactions between Ta_3N_5, PANI, and BSC collectively contribute to enhanced solar absorption, improved charge transfer and hindered charge recombination.

One of the important solutions for resolving the energy crisis is photocatalytic hydrogen generation. Therefore, this thesis has discussed inexpensive, stable and environmental

friendly Ta_3N_5 based photocatalysts with heterojunction, namely Ta_3N_5/BSC@PANI, V@S-Ta_3N_5/PANI and Nb-Ta_3N_5/PANI photocatalysts for improved water splitting to produce hydrogen. We have designed simple, cost-effective photoreactor to boost photocatalytic activity for efficient water-splitting processes for H_2 evolution.

In the first work, one-pot hydrothermal method was used to synthesize Ta_3N_5/BSC@PANI photocatalyst. It was noted that Ta_3N_5/BSC@PANI (76.9 $\mu mol g^{-1} h^{-1}$) photocatalysts showed ~3.42 folds enhanced photocatalytic hydrogen production activity as compared to bare Ta_3N_5 (22.5 $\mu mol g^{-1} h^{-1}$). The improved hydrogen production was attributed to better light absorption and rapid charge carrier separation characteristics of Ta_3N_5/BSC@PANI photocatalyst as analyzed by photoluminescence (PL), electrochemical impedance sepectroscopy (EIS) and ultraviolet–visible diffuse reflectance spectroscopy (UV–vis DRS) studies. In the second work, simple hydrothermal and chemisorption methods were used to synthesize V@S-Ta_3N_5/PANI photocatalyst. V@S-Ta_3N_5/PANI photocatalyst was responsible for visible light absorbance as evidenced by UV-DRS spectra. Moreover, V@S-Ta_3N_5/PANI (98.4 $\mu mol g^{-1} h^{-1}$) photocatalyst exhibited ~ 4 folds enhanced hydrogen production activity compared to Ta_3N_5.

In the third work, composite photocatalyst was synthesized by using chemisorption process. The H_2 yield of Nb-Ta_3N_5@PANI composites photocatalyst is 71.3 $\mu mol g^{-1} h^{-1}$, 3.17 folds greater than Ta_3N_5.

As a result, all the synthesized composite photocatalyst is cost-effective, stable and eco-friendlyand shows superior photocatalytic activity for H_2 evolution. Although, co-doped V@S-Ta_3N_5/PANI hybrid photocatalyst with enhanced photocatalytic performance could be promising candidate for water splitting with significant application potential toward environmental sustainability.While Ta_3N_5/BSC@PANI shows excellent photostability upto 6 cycles among all the synthesized photocatalysts. The invention of pn-heterojunctions has

resulted in improved charge carrier separation and transfer, which was supported by UV-vis DRS analysis, was the cause of the increased photocatalytic activity. It is anticipated that the outcomes of this thesis are pivotal for the building of a solid foundation for future work in the research field and to drive continuous efforts for the eventual global transition to a decarbonised H_2 economy.

Acknowledgement

At first, I owe my thanks to GOD **(MAHADEV)** Almighty for sustaining me with his grace and strength while doing my research work.

First and Foremost, I would like to express my sincere gratitude to my research supervisors **Dr. Ajit Kumar Sharma,** Associate Professor of Chemistry, Department of Chemistry, School of Chemical Engineering and Physical Science, Lovely Professional University, Phagwara-Punjab, for their patient guidance, extraordinary motivation, kindness, moral instruction, endless support, encouragement, advices, and countless discussions over the last three years. This achievement been accomplished, in no small measures, due to their sheer professionalism and dedication. It is to them that I owe my heartfelt thanks and the overwhelming sense of satisfaction that I feel at this stage.

I feel privileged to my sincere regards and gratitude to my Co-supervisors, **Dr. Dai-Viet N. Vo,** Deputy Director, Department of Environmental Science, Nguyen Tat Thanh University, Vietnam, for their valuable guidance, constant encourgment, motivation, endless support, and countless discussions over the last three years. This achievement been accomplished, in no small measures, due to their sheer professionalism and dedication. It is to them that I owe my heartfelt thanks and the overwhelming sense of satisfaction that I feel at this stage.

I express thanks to the **Principle of Scientific advisor to the Govt. of India** [SSF- Award no.: Dated 1/10/22] for providing financial support to carry out my research works ("Waste to Wealth" Mission under SSF fellowship).

For the past three years I have been working on this dissertation, I have been most fortunate to be offered the intelligence, inspiration and support of so many people. Thus, special thanks are due to all my colleagues from our research group, who were engaged in establishing a nice and friendly atmosphere. Thus, I would like to thank my lab colleagues Ms. Sahima Tabasum, Karan Singh Mann, Suman Rani, Qurat Ul-Ain, Nancy George and Mankomal

List of Contents

Table of contents

List of Abbreviation

Abbreviations	Expansion
H_2	Hydrogen
CO_2	Carbon dioxide
PC	Photocatalytic
PEC	Photoelectrochemical
WS	Water splitting
POWS	Photocatalytic overall water splitting
PIWS	Photocatalytic intermediate water splitting
PPWS	Photocatalytic partial water splitting
VB	Valance Band
CB	Conduction Band
Eg	Band Gap
PANI	Polyaniline
BSC	Biomass soot carbon
Ta_3N_5	Tantalum Nitride
QDs	Quantum dot
UV-Vis	Ultraviolet-visible Spectroscopy
Fe-SEM	Field Emission Spectroscopy
XRD	X-ray Diffraction
PL	Photoluminescence
EIS	Electrochemical impedance Spectroscopy
GHS	Green house gas
WSR	Water splitting reaction
OER	Oxygen evolution reaction
HER	Hydrogen evolution reaction
FCIL	Fertiliser Corporation of India
AE	Alkaline Electrolyser
NG	Natural Gas

List of Tables

List of Figures

	stability up to 3 cycles and (c) XRD image of synthesized photocatalyst before and after the reaction.
Fig. 4.4	Schematic representation of the photocatalytic mechanism for all photocatalysts.

Chapter 1

1. Introduction

1.1. Background and Research Motivation

1.2. Energy and Environmental Scenario (Crisis and Solutions)

Since natural scientists describe energy as the "ability to do work" (without energy, there is no life), they rarely make observations about the nature of the work that is made possible or how this impacts the definition of energy [1]. While there are numerous types of energy, they can be roughly classified as follows: First, there is kinetic energy, also known as "energy in motion," that includes the subfields of electricity, motion, radio waves, sound, and thermal. Second, there is potential energy, which is stored energy in an object, while there are several different kinds of potential energy, including gravitational, chemical, mechanical, nuclear (both strong and weak), and solar energy [2-3]. Energy is the capacity to perform work, but energy is also required to perform that task. Indeed, potential energy can be converted into kinetic energy, and the reverse is also true [4]. We now understand that there are two primary categories of energy: kinetic energy and potential energy. But exactly what is the much energy that exists? There are many diverse manifestations of energy, after all. Some examples of energy sources are: chemical, electrical, electromagnetic, gravitational, heat, hydro, magnetic, mechanical, nuclear, radiated, mechanical, wind, sound, thermal, and solar [5]. Energy cannot be created or destroyed, according to the fundamental law of science known as the law of conservation of energy. Only an object can be moved, or a form can be converted into another [6-7]. Where can energy be found if it cannot be created? There are basically three different kinds of energy sources. They have been classified into three distinct groups: non-renewable energy (fossil fuels), energy from renewable sources, and alternative energy [8]. Fossil fuels, because of the significant quantity of carbon dioxide they emit are non-renewable sources of energy and, are commonly referred to as filthy energy sources. The

1

major energy comes from the non-renewable sources are about 35% is comes from oil, 27% from coal, 23% from natural gas, 6% from nuclear (nuclear energy is a non-renewable resource because the uranium is most commonly used material that is finite. Nuclear energy is considered as a clean energy, but there is a subject of major debate over whether it belongs on the list of renewable energy sources. For the better understanding of this debate firstly we need to understand the definition of renewable energy and nuclear energy. Renewable energy is defined as an energy source that has an infinite capacity to regenerate and replenish itself. On the other hand nuclear energy is a result of heat generated through the fission process of atoms. The fission releases energy in the form of heat and neutrons. The released neutrons then go on to hit other neutrons and repeat the process, hence generating more heat. Mostly uranium is used as a fuel for nuclear fission [9]. Advanced nuclear energy is truly renewable, while proven uranium reserves only provide an additional 90 years of useful life for legacy technology, advanced technology can last for thousands of years [10]), and the rest from sunlight, wind, biomass, and geothermal. However, over 80% of the energy we consume globally now comes from fossil fuels [11]. There are four different kinds of fossil fuels: petroleum, coal, natural gas and orimulsion [12].

As the human population is increasing day by day leading to the expansion of industrialization. There are currently more than 7 billion people on the planet, with a projected growth to 9 billion by 2050 [13, 14]. The expected increase in energy demand would more than double due to the growing population, rapid expansion, and global economic growth. By the end of the 21st century, the demand for energy is expected to more than quadruple, from its projected peak of 30 TW in 2050 [15-17]. With the steadily increasing need for energy, particularly in developing nations, it is a major difficulty to supply such a vast amount of energy to society. At the moment, fossil fuels like natural gas, oil, and coal provide the majority of the energy [18]. However, long-term use will deplete the

amount of fossil fuels. Furthermore, even though fossil fuels are infinite, their on-going usage has undesirable side effects like pollution ('Pollutants' are defined as anthropogenically-introduced substances that have harmful effects on the environment and human health while 'Contaminants' are well-defined as inputs of unfamiliar and potentially toxic substances into the environment; not all contaminants cause pollution, due to their low concentrations.) that endangers to human health and production of GHG which causes to the environmental damage [19]. Carbon dioxide (CO_2) is the major GHS which is produced due to combustion of fossil fuels. CO_2 concentrations in the atmosphere have risen rapidly during the preceding century, with an average annual increase of 2 ppmv in the last ten years [20]. Methane (CH_4) and nitrous oxide (N_2O) levels have also increased significantly. CO_2 emissions from energy use account for over 70% of global emissions. Smaller shares are accounted for by agriculture, which mostly relies on domestic livestock and rice farming to produce CH_4 and N_2O, and by industrial operations distinct to energy, which primarily produce fluorinated gases and N_2O [21, 22].

1.1.1. Non-renewable sources of Energy (Fuels from fossil sources and GHGs)

Coal, gas, oil and other fossil fuels are called non-renewable sources of energy since they need decades to refill. Although fossil fuels are utilised extensively, their efficiency and affordability are dwarfed by their consumption, resulting in their elimination from the earth's crust. Fossil fuels are the primary energy sources and electricity productions are the main cause of CO_2 emissions, according to fig. 1.1 oil accounted for 33% of global fossil fuel consumption in 2019. Coal (27%) and natural gas (21%) came in second and third, respectively. Renewable energy use is rather modest, with hydropower leading the way with a 2% consumption rate [23].
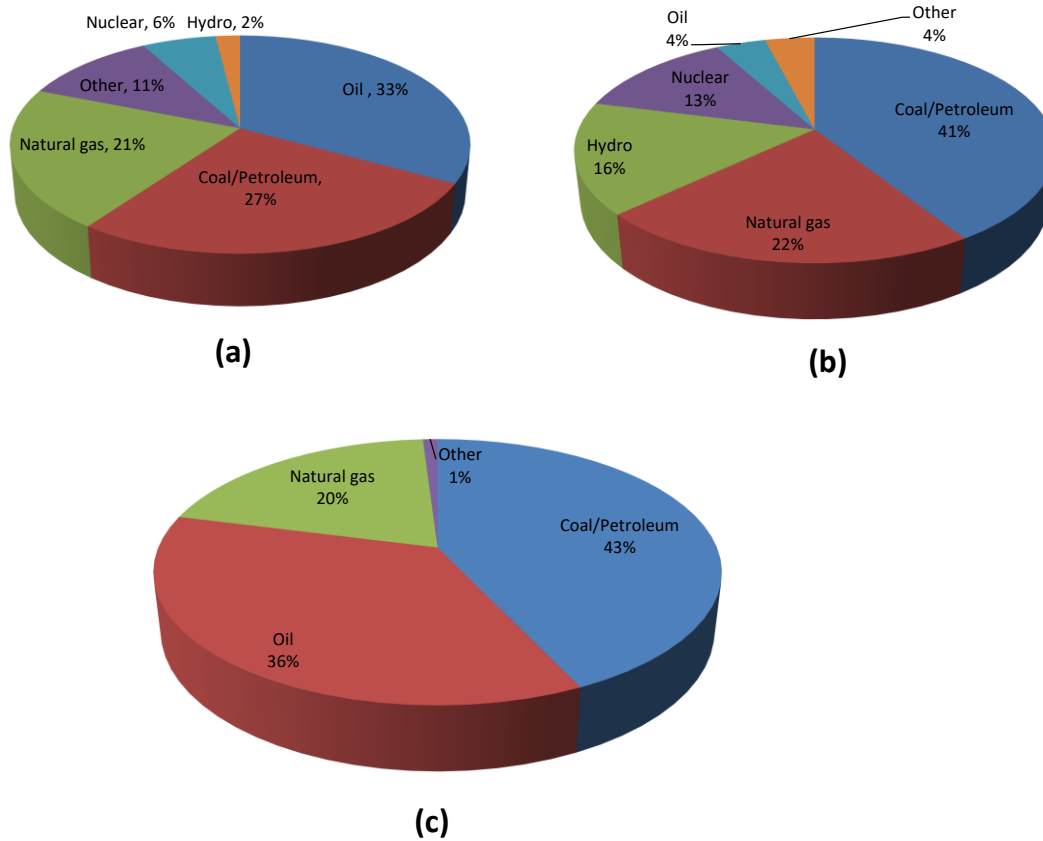
Fig.1.1 (a) Total primary energy supply (TPES), (b) total electricity production (TEP), and (c) total carbon dioxide emissions (CO_2) by energy source (other includes biofuels, geothermal, solar, waste, heat, and wind, and others) [24]

The fundamental concern with fossil fuel usage is that it directly adds to GHG emissions, resulting in a damaged environment and an ongoing temperature increase in the Earth's atmosphere. In light of the aforementioned information, the rise in average world temperature to 1.5-2°C recommended by conference of Intergovernmental Panel on Climate Change (IPCC), which would need around 275 billion tons of carbon dioxide being released into the atmosphere. Additionally, the global temperature will rise by 2 to 6 degree Celsius by the end of the twenty-first century the predicted by the International Energy Agency [25, 26]. In order to deal with it, there are two basic options: We can either cease using fossil fuels (which is very impossible), or we attempt to recycle these GHGs by transforming into fuels. Table 1.1 provides the percentage of energy consumption sources in India [27]. In addition,

environmental pollution caused by fossil fuels increasing energy costs has made us work on alternative energy fuels [28].

Table 1.1 Source-wise energy consumption in 2018-19 (India) [27]

Sources of Energy	Consumption in Percentage
Coal	43
Crude Oil	35
Electricity from Hydro, Nuclear and ORS	13
Natural Gas	7
Lignite	2

1.1.2. Natural Energy Sources

Alternative energy could be utilised in place of fossil fuels which usually has little impact on the environment. Renewable energy is derived from natural processes that are replenished constantly. Here are a number of alternative energy sources, including sun, wind, rain, tides of ocean, biomass and geothermal resources from heat generated deep within the earth [29, 30].

1.1.3. Greenhouse Effect remedy: renewable energy

For alleviating energy issues, renewable energy sources are vital. Renewable energy is defined as energy produced from regularly occurring, consistent energy fluxes in a given environment. Along with a few constraints on efficiency, utility, or applicability, this energy must be used to reduce the greenhouse gases emission and negative influence on the environment. With 7% of all energy 60% and of all renewable energy coming from hydropower, it is one of the most widespread, well-known, and long-lasting sources of energy [31, 32]. The largest hydropower producer in 2019 was China, which produced 1302 TWh of

hydropower annually, followed by India, which generated about 164 TWh. On the contrary, wind energy is pure and among the most environmentally beneficial forms of energy generation. It is obtained through the rotation of turbines and transformed into usable power for water pumping, grain milling, and marine shipping [33]. Wind energy accounts for only 2% of all energy output in India [34]. Geothermal energy, the heat in the interior of the earth, is not related to solar energy but is ultimately generated by gravitational energy and the radioactive decay of unstable atoms. It is renewable in the sense that there is a huge amount of heat stored in the body of the planet and human consumption cannot deplete the energy reservoir [35]. Despite the fact that geothermal energy produces less greenhouse gas than burning fossil fuels, hot water supply and power can still be provided [36, 37]. Additionally, biomass produces 10% of the world's fuel, which burns at temperatures above 400°C and can be utilised to generate energy [38]. However, biomass energy production suffers from high installation costs and environmentally unfavourable temperatures. Furthermore, the majority of biomass, especially agricultural biomass, originates in rural areas and can only be adequately managed with significant local community involvement [39].

Solar energy offers the best chance of supplying the world's rising energy needs among renewable energy sources. Comparing the cost of installing the equipment to other high efficiency energy sources, it is noticeably less expensive [40]. The only problem with solar power generation is that its production efficiency is dependent on the weather, but that can be fixed with suitable storage devices [41].

In the modern era, worldwide researchers are working to find sustainable, clean energy sources to replace conventional fossil fuels. Renewable energy offers a practical solution to this enormous dilemma. Renewable energy growth is required to maintain a balance between energy supply and demand, even if it is currently far from viable in terms of capacity and cost as compared to fossil fuels. The sun is among the most plentiful source of energy on planet

[42]. Even in the most extreme scenarios of energy demand, it provides 120,000 TW of radiation on the surface of earth, considerably in excess of what humans will ever need [43, 44]. Solar energy has the capability to replace the widely used fossil fuel resource in the near future. While the contribution of solar energy to global electricity production remains generally low due to the solar energy accessibility varies it depends on the location, a cycle of night/day, the existence of clouds, etc. It is due to the sun erratic behavior, there are significant technological challenges associated with the practical use of solar energy, including efficiently converting sunlight into valuable energy and storing and distributing that energy to consumers in a form that is both affordable and practical [45]. Globally, solar photovoltaic (PV), the simple method for the direct transformation into electrical energy of solar energy, is experiencing significant expansion. Though, scalability and large initial expense are disadvantages of this method. Transportable fuels or chemicals are preferred for the conversion of solar energy. By using solar power to electrolyze water into H_2 and O_2, it has been possible to develop an established and mature technique to produe chemical fuels from solar energy. The challenge associated with this particular technique is linked to scalability limitations, which makes it arduous to achieve energy production at a terawatt (TW) level [46, 47]. Therefore, direct conversion into chemical fuels of solar energy is preferable because it offers a built-in way to extract solar energy, distribute it economically through the current infrastructure, and utilize it in the industrial, residential, and transport sectors [48]. The main merits and demerits of sources of renewable energy, such as hydro, wind, biomass, geothermal and solar, are given in Table 1.2 [49-56]

Table 1.2 Merits and demerits of renewable energy technologies

Type of Renewable Energy	Energy source	Merits	Demerits	Ref.

Hydropower	The energy produced from the falling or fastflowing water to electricity or power machines	Reliable, low operating and maintenance cost, and adjustable to change in the load	High capital cost, depending on precipitation, and displacement of the people from reservoir area requires	[52]
Wind	Wind energy is converted into electricity using turbines	Unlimited wind availability	Expensive maintenance cost, irregularity in wind, noisy, interfering radio signals and kills the migratory bird	[53]
Geothermal	The underground heat is converted into electricity	Low operating cost	Limited amount of geothermal energy locations, limited energy, and transportation of the stored energy is difficult	[54]
Biomass	The energy is produced from plant or animal materials	Most of the raw materials from agricultural and forest waste	Limited resources	[55]
Solar	Utilizes energy from solar light and is converted into electricity or thermal energy	Low operating costs, unlimited source of energy, and very little maintenance costs	Currently expensive due to raw material processing and depends on the sunshine	[56]

India produced 4% of its electricity from solar energy in 2020 [57]. Furthermore, it can be used to generate hydrogen (H_2) from organic waste and polymers, which is affordable as a fuel, doesn't require a lot of industrial machinery, and can function at lower temperatures and pressures [58]. A brief description of hydrogen (H_2) as a fuel for various technologies is provided in the section that follows.

1.1.3.1. Hydrogen (H_2) as fuel

Regardless of the above-listed renewable energy sources (in Table 1.2) researchers are still investigating other clean and carbon-neutral energy sources to replace fossil fuels. In this aspect, hydrogen is considered a suitable candidate and can be obtained from various abundant sources [59]. Hydrogen is carbon neutral and portable fuel carrier with high energy density (120 to 140 MJ/kg), a potential substitute for current fossil fuels with clean emissions. The supreme attractive quality of hydrogen as fuel is its non-toxic combustion by-product (H_2O) in addition to having a high calorific value than other fuels. Moreover, through the Fischer-Tropsch method, it has been employed in the manufacturing of ammonia, processing of fossil fuels, methanol production, and hydrogenation processes industries to produce liquid hydrocarbon fuel [60]. In recognition of its low capacity to emit harmful emissions, hydrogen has emerged to be a viable energy source. When we switch to hydrogen fuel cells from our existing fossil fuels, it is predicted that human-caused hydrogen emissions will increase by 60–120 Tg/year. This would directly cool the lower stratosphere and have an influence on ozone chemistry by delaying the expected retrieval from chlorofluorocarbons [61]. Depending on its production process and the energy conversion system applied, lower emissions of carbon dioxide (CO_2), particles, and nitrogen oxides (NO_x) are possible with pure hydrogen, the most basic and powerful chemical fuel. More than 200 years ago, one of the earliest internal combustion engines (ICE) automobiles used hydrogen as fuel [62]. Like

conventional fuels, hydrogen fuel-powered vehicles can be filled up relatively rapidly. Fuel cells (FCs) are effective and scalable apparatus that can convert and store the chemical energy held by H_2 molecules in the form of electricity [63, 64]. To boost electrical efficiency, power generators and turbines operate at higher temperatures (600–1000°C) using molten carbonate fuel cells (MCFCs) and solid oxide fuel cells (SOFCs) [65]. Alkaline fuel cells (AFCs), often referred to as low temperature fuel cells (LTFCs), are described as reasonably priced fuel cells with changeable parts and are employed at low operating temperatures (60-100°C). With low working temperatures (50–80°C) and a small footprint, the proton exchange membrane fuel cell (PEMFC) is widely investigated and utilised FC and a viable choice for portable electronics and electric vehicles [66, 67]. Astronauts can also use the water created as a byproduct of using hydrogen fuel cells as their source of drinking water [68]. In addition to these fuel cells, portable electronic vehicles and forklifts run on hydrogen and require less maintenance because they don't need to be charged, balanced, watered, or cleaned [69]. In addition, hydrogen is utilised to fuel aircraft, heat homes, and power mining equipment [70]. The ability to transport hydrogen by sea is one of its main benefits. In contrast to ordinary oil spills that harm marine habitats, cause pollution, and increase the cost of moving heavy equipment and clean up, hydrogen spills are impossible [71]. Additionally, if we use hydrogen, we do not need to drill far below the surface to get oil, damaging the land's ecosystems in the process.

1.1.4. Hydrogen generation

H_2 is not available on earth in its pure form. However, it naturally occurs in the form of hydrocarbons, biomass, or water [72]. In order to reduce greenhouse gas emissions and decarbonize the energy, transportation, and chemical industries, hydrogen is a promising energy source and feedstock. Therefore, various processes are being developed to produce hydrogen from different raw materials and sources, categorized under conventional

techniques (fossil fuel-based) or renewable techniques, as shown in Fig 1.2. Conventional techniques, such as hydrocarbon reformation and hydrocarbon pyrolysis, require high energy and emit greenhouse gases [73]. On the other hand, hydrogen production from renewable sources, such as water and biomass, can be economical. The selected technologies rely on feedstocks with an existing large-scale distribution network, i.e. natural gas and water, and are preferentially characterized by a high technology readiness level (TRL). Moreover, the hydrogen generation technologies are designated to comprise one example for each of the hydrogen colors: (i) grey hydrogen obtained by steam methane reforming, (ii) blue hydrogen obtained via steam methane reforming with carbon capture and storage, (iii) turquoise hydrogen obtained through methane pyrolysis, and (iv) green hydrogen obtained by polymer electrolyte membrane water electrolysis [74].

On the contrary, electrolysis of H_2O molecules emerged as a potentially useful method for producing hydrogen gas with high efficiency (70-80%) and negligible transit cost [75]. Thermochemical water splitting refers to a technique in which heat is used to drive chemical processes in the presence of a catalyst, yielding hydrogen gas [76]. Additionally, H_2 gas can be produced from the dissociation of H_2O molecules by radiolysis (the application of radioactive radiation) in a nuclear power plant [77].
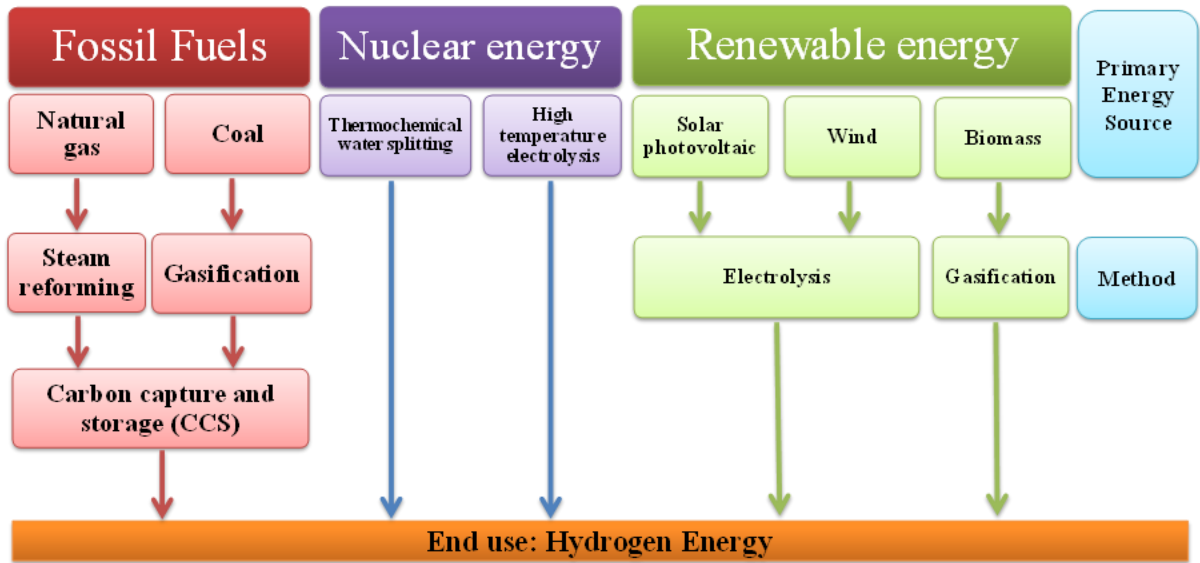
Fig. 1.2 Hydrogen production methods (a) Fossil fuel source (b) Nuclear energy and (c) Renewable source [78]

The complexity of the equipment needed for each of the aforementioned approaches, as well as their high working temperatures, are seen as substantial barriers to effective and mountable technological advancement in the field of hydrogen generation. Hydrogen production from water has advantages, which include abundant and clean sources for hydrogen than biomass [79]. Therefore, hydrogen production from water has gained significant attention. Honda and Fujishima in 1970s suggested the water splitting process is catalysed by TiO_2 at room temperature [80]. After that, a number of scientists have investigated novel approaches to the manufacture of catalysts for water splitting at room-temperature to create hydrogen gas. Water splitting in this context refers to the separation of the water molecule into its hydrogen and oxygen components. Hydrogen synthesis through water splitting has been regarded as a safe and effective method. There are several ways for producing hydrogen, both renewable and non-renewable, including natural gas steam reforming, coal gasification, wind and sun electrolysis, thermochemical water splitting and high temperature electrolysis.

Most of the hydrogen manufactured from non-renewable sources (96%) while 4% is responsible for the electrolysis of water/water splitting (renewable source) as shown in figure

1.3.
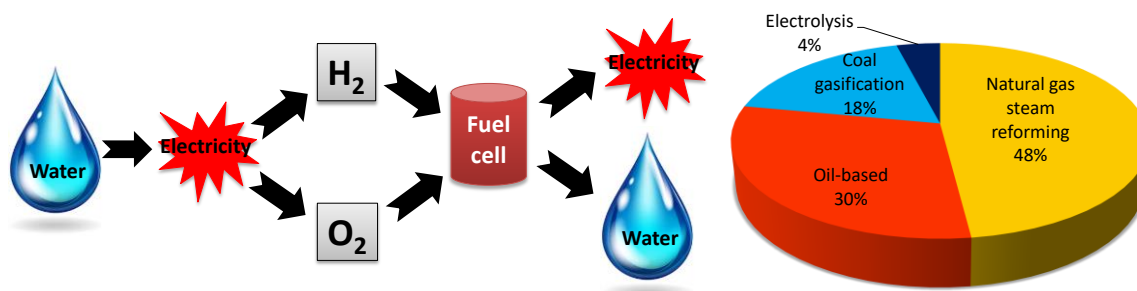
Fig. 1.3 schematic representation of the H$_2$ production from H$_2$O and overall percentage of H$_2$ production from others sources [81]

1.1.4.1 Production of H$_2$ using fossil fuels (non-renewable)

1.1.4.1.1. Steam reforming

At the moment, it is the most popular and affordable technique of producing hydrogen. Before being fed through a reactor heated from the outside and steam reforming to produce carbon monoxide (CO) and hydrogen (H$_2$), natural gas must first be purified of any contaminants. Following that, the CO and H$_2$O are transformed into H$_2$ and CO$_2$ through a catalytic water-gas shift process. After that, the hydrogen gas is purified. Large reformers (e.g., 100,000 tonnes annually) may achieve yields of more than 80% with this technique [82]. Smaller reformers have been demonstrated to be less efficient, especially when used with tiny fuel cells.

1.1.4.1.2. Gasification

Gasification is defined as the process of converting any carbon-based raw material into synthetic gas using air, water vapour, or oxygen. Many raw materials and wastes, including coal, car tyres, sewage sludge, wood, sawdust, and plastic waste, can be easily and effectively converted into useful products by using gasification techniques. Because of the number of coal reserves globally and economically accessible technology, coal is feasible choice for producing hydrogen in big plants. Gasification is a more suited process than the currently

13

used ones (such as electrolysis) for turning coal to H_2. Coal is partially oxidised in a high-pressure, high-temperature reactor during the coal gasification process using steam and oxygen. The main end products are syngas, which are primarily CO and H_2. The syngas passes through a shift process to produce more hydrogen. The gas can be typically purified to extract elemental sulphur or create sulfuric acid. A gas turbine may be used to generate electricity by burning part of the syngas. Coal gasification appears to be a significant process for cleaner and more cost-effective generation of energy and other chemical products due to coal high carbon content as compared to alternative feedstock options [83]. To address this problem, Carbon Capture and Storage (CCS) systems are being developed. Today, a major coal gasification plants, it costs slightly more to produce hydrogen than it would if it were made from natural gas. However, compared to those employed in the steam reforming of coal gasification and natural gas procedures are less clearly defined. Examining the economics of creating hydrogen from coal vs other fossil fuels, coal gasification plants have higher unit capital costs while their unit raw material costs are lesser [84].

1.1.4.2. Hydrogen production from nuclear energy

1.1.4.2.1.   Thermochemical water splitting

Hydrogen may be produced in nuclear reactors through thermochemical water splitting cycles when the temperature is 500 °C or greater [85, 86]. At higher temperatures, better efficiencies and reaction speeds can be attained. There have been over 100 putative high temperature water-splitting thermochemical methods put out so far [87]. This study investigates the Cu-Cl and S-I thermochemical cycles. The thermochemical Cu-Cl cycle was first proposed in the 1970s. Currently, certain commercially available Cu-Cl cycles are being evaluated. At operating temperatures of around 550 °C, Cu-Cl cycles are projected to achieve efficiencies of about 40% (cogeneration of electricity is excluded). The reduction of the temperatures required for good efficiency in thermochemical Cu-Cl cycles is one of the primary issues.

Thermochemical S-I cycles can achieve higher efficiency (around 60% with cogeneration of electricity). However, for these cycles, temperatures between 825 and 900 °C are required [88, 89]. Special reactors must be built for these thermochemical cycles employing unique chemically inert materials proficient of withstanding high temperatures. Another key obstacle for thermochemical cycles is the development of these unique materials in a way that is commercially viable. Thermochemical cycles, however, exhibit encouraging outcomes to be taken into consideration as prospective strategies to create hydrogen [90].

1.1.4.2.2. High temperature electrolysis

The nuclear power plant's efficiency (about 33% with modern reactors) limits the electricity-to-hydrogen conversion efficiency of this technology, even though it can touch as high as 80% under pressure [91]. Reactors with higher outlet temperatures could be created as a solution to the poor efficiency issue. For instance, at 950 °C, the 20% efficiency from 350 °C rises to nearly 50% [92].

1.1.4.3. Hydrogen production from renewable energies

1.1.4.3.1. Electrolysis

Many years ago, coal gasification and water electrolysis processes were used in India to produce hydrogen for ammonia synthesis. FCIL owned and operated five fertiliser plants in Gorakhpur, Korba, Ramagundam, Sindri, and Talcher. Three of these fertiliser plants, located in Ramagundam, Sindri, and Talcher, used coal gasification technology to synthesise ammonia, but they were closed in the late 1990s to early 2000s due to economic unviability [93]. However, because India has large reserves of coal and import dependence on NG is increasing, the Talcher plant is likely to be operational again by 2023 using coal gasification technology. During the 1960s, the urea production plant in Nangal, Punjab, was equipped with AE for hydrogen production because it was relatively inexpensive, and surplus hydroelectricity was used from the nearby Bhakra multipurpose project. When the demand

for electricity increased, it was later replaced by a fuel oil-based system [94]. Electrolysis generates clean hydrogen, devoid of impurities like carbon and sulphur. However, the prices and energy needs of electrolysis are greater than those of fossil fuel-based alternatives [95]. Nevertheless, owing to its portability and suitability for niche applications, electrolysis is still considered a viable option for producing hydrogen on a smaller scale at an affordable cost. They are also compatible with all standard gas stations.

1.1.4.3.2   Solar photovoltaic

This is one of the most expensive ways to produce H_2. With current technology, photovoltaic electrolysis costs around 25 times more to produce hydrogen than fossil fuel alternatives. However, this factor is predicted to decline as the price of solar cells [96].

1.1.4.3.3.   Wind

This approach, especially for distributed systems, has perhaps the most potential amid renewable sources to generate pollution-free hydrogen by electrolysis using wind turbine electricity. The expense of wind turbines and electrolyzer is one of the difficulties of this technique. Another obstacle to harnessing wind energy to generate H_2 is the optimisation of the turbine electrolyzer storage system. Utilizing wind turbines to produce hydrogen is almost 6–10 times more costly than doing it using fossil fuels. In the future, this gap is anticipated to be cut in half [97].

1.1.4.3.4.   Biomass gasification

Biomass resources may be used to produce hydrogen, such as waste from the processing of wood, forestry, and agriculture, as well as from municipal and animal waste and/or crops. Currently, a large-scale, cost-effective hydrogen production technique using biomass gasification is not possible. On the other hand, this strategy enables the clean recovery of energy from municipal and agricultural waste. Since the carbon dioxide emitted when the

biomass is oxidised may be taken from the environment and repaired by photosynthesis in the biomass growth process, this technique has the potential to reduce the net CO_2 emissions more than fossil fuels. A major concern with this approach is the potential for problems with natural resources and land needs as a result of growing huge volumes of biomass as energy outputs. One of the many ecological and sustainable methods for producing H_2 that were mentioned above is solar water splitting [98].

1.2. Water Electrolysis/splitting

The earth surface is enclosed with more than 70% water which makes it an attractive and alternative feedstock of energy as it is regenerated back into nature. It is a possible substitute of liquid and fossil fuels to generate energy via hydrogen production [99]. Hydrogen is the first and simplest element of the periodic table and presents plenty in nature. It has a very high heat of combustion 34.19 kcal/g and very high energy storage capacity 120 kJ/g. Because of significant energy storage capacity, it could be used as fuel to release energy for the targeted mechanical processes. H_2 is produced industrially from coal gasification, steam methane reforming and water electrolysis, except for water electrolysis, these methods generate CO_2 or other by-products creating 'greenhouse effect'. When hydrogen burns as fuel or oxidizes, it gives water vapour with heat. Therefore, it could be used as no pollution fuel [100]. "When sufficient amount of electrical energy passed into the aqueous electrolyte solution by applying potential on the electrodes, the protons which are present in the electrolyte absorbed on the surface of the electro catalyst and these protons gets reduce on the surface to evolve hydrogen gas." Decomposition of H_2O into H_2 and O_2 through the supply of energy like (electricity, photon and heat) is known as water splitting reaction. This is a thermodynamically uphill reaction; therefore, it requires some energy to conduct the reaction. This is a multi-electron transfer process involving slow reaction kinetics. When enough energy exists, water splits, converting into gaseous oxygen and hydrogen. It can be carried

17

out using a variety of mechanisms that can be divided in 5 main types (types as demonstrated in Fig. 1.4) depending on the energy source used to start the chemical reaction: electrolytic, photobiological, thermochemical, photoelectrochemical, and photocatalytic water splitting. Any of these approaches or a combination of two methods may be used to carry it out [101]. The photobiological water splitting method has several disadvantages, including a high system cost, a large size system (to contain an eco-system), poor production efficiency and a significant volume of recycled or reused water as a byproduct [102]. We can assume that H_2O splitting consists of two separate processes, the first of which involves oxidising water to produce oxygen and the second of which involves reducing protons (H^+) to hydrogen [103]. The hardest portion of this reaction is the water oxidation phase because, as seen during natural and artificial photosynthesis, oxygen evolves more than four times more slowly than hydrogen.
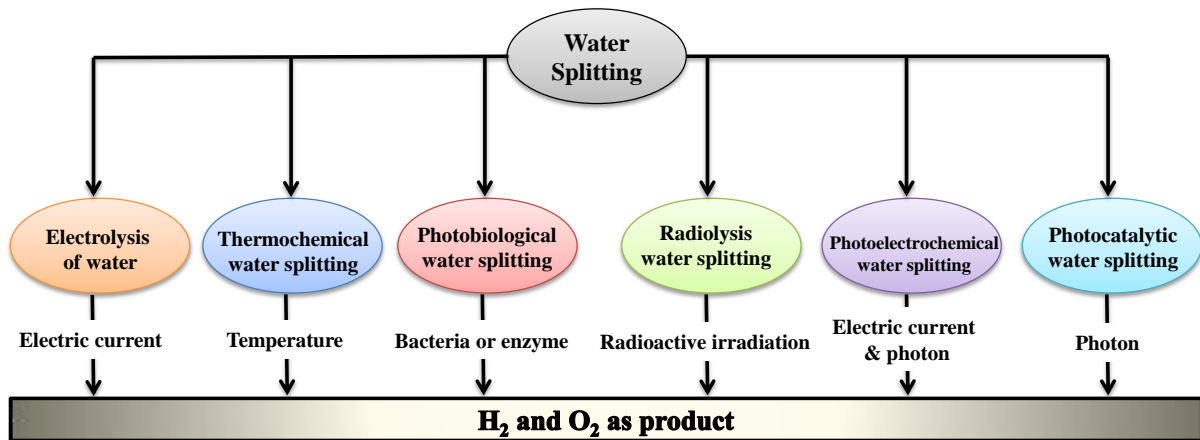
Fig. 1.4 Different types of water splitting process to produce H_2 and O_2 [104]

1.2.1. Types of water splitting reaction

Based on energy source methods, it could be explored into the following categories such as electrocatalytic/electrolysis of water, thermolysis/thermochemical water splitting photobiological, Radiolysis, Photoelectrocatalytic/photo-electrochemical and photocatalytic water splitting as shown in Fig. 1.4.

1.2.2. Electrocatalytic water splitting reactions

1.2.2.1. Electro-catalytic HERs/OERs in different electrolyte medium

Splitting of water is a redox process which is composed of two half-cell reactions, one is acknowledged as water oxidation for oxygen evolution reaction (OER) and another is called reduction of water for hydrogen evolution reaction (HER) [105]. Water splitting reactions (WSR) are thermodynamically unfavorable, so catalyst plays a crucial role in making reactions feasible under various electrolytic mediums. The mechanism of WSR is different in different mediums. Firstly, the decomposition of water molecule takes place before other following consecutive reactions.

The WSR are majorly depended upon the reactions taking place in the vicinity of the electrode and by the concentration of charged species (H^+, OH^-) generated from water. Moreover, the formation of these ionic species is proportional to the applied potential on the electrodes. The WSR reactions involve two different kinds of redox reactions, different voltammetry curves obtained for these reactions. The first one which occurred at anode is called OER and the one at cathode is known as HER. Oxygen evolution reaction (OER): In recent times, a lot of research attempts have been attributed to prove the mechanism of OER, but still the knowledge at the atomic level is scarce because of complications in isolating the reaction intermediates formed during the electrochemical processes [106, 107]. Bockris et al. for the very first time elaborated the different pathways of OER. In general, OER involved of numerous electron transfer reactions which are consequently followed by each other [108]. HER reactions take place at the cathode and are more favorable under acidic conditions due to easy availability of protons. The energy associated with adsorption of hydrogen on a catalyst surface is directly responsible for its reactivity. A moderate value of hydrogen adsorption energy is accountable for excellent HER activity which accelerates the Volmer process and consequently the Heyrovsky and Tafel processes. The Volmer process is the proton adsorption, Tafel step is the physical desorption, and Heyrovsky process is the

chemical desorption. The role of the adsorbed intermediate in the Volmer-Heyrovsky-Tafel mechanism for the hydrogen evolution reaction (HER) on metallic electrodes has been extensively analyzed [109, 110]. Numerous nanoparticles based on transition metals can produce high potential energy from water at lower prices and with zero carbon emissions such as metal oxides, spinels, perovskites, metal sulphides, selenides, metal phosphides and metal nitride.

1.2.3. Photoelectrochemical (PEC) water splitting

A novel method to address energy problems is to use solar energy to produce chemical fuels from carbon dioxide and water, such as hydrogen (H_2) and methanol (CH_3OH), respectively. TiO_2 was initially used as a photo anode in photo electrochemical water oxidation due to its characteristics as an n-type semiconductor [111]. Researchers have tried multiple times over many decades to assess Earth's enormous collection of reliable photo electrode samples. In a perfect PEC water splitting cell, the p-type semiconductor photocathode splits the water while the n-type semiconductor photo anode oxidises it. The ecologically friendly synthesis of H_2 and O_2 by water splitting by photo- and electrochemistry is anxiously anticipated by many people. The OER is one out of the two half-reactions needed to split water, which calls for challenging electron and ion mobility [112]. Photoelectrochemical mechanisms are depicted Fig. 1.5.
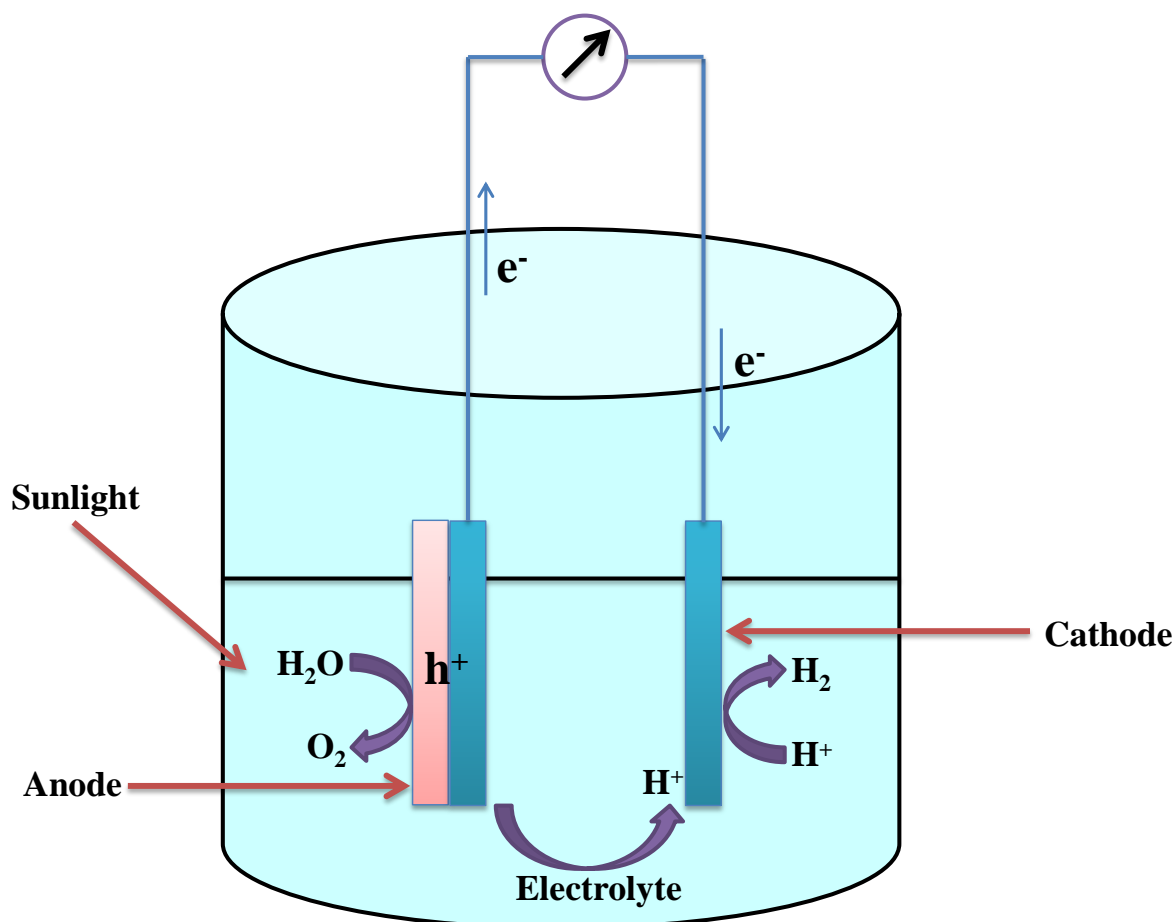
Fig. 1.5 Mechanism of Photo Electrochemical water splitting process

1.2.4. Photocatalytic water splitting

Given the importance of renewable, clean, and environmentally friendly energy, photocatalytic water splitting, which employs solar energy, is a common technique. Figure 1.6 is a schematic representation of a possible hydrogen production and utilisation facility, where photocatalysis drives the decomposition of water to produce H_2 as a platform for clean fuel generation. A solar water splitting module is used to split water into hydrogen and oxygen, which are then utilized in systems for producing high-efficiency electricity such fuel cells and internal combustion engines to produce electricity. Power is generated using both water and sunlight. Methanol and precursors for the plastics and fertilizer industries can be produced by combining H_2 with CO_2 (emitted from combustion of fossil fuels or collected from the air). Generally, semiconductor photocatalysts are solid powder samples, which are

(i) visible and/or UV light absorbers, (ii) chemically inert and photostable, (iii) inexpensive and (iv) non-toxic [113]. A catalyst responds to EM illumination by harvesting solar energy in the form of chemical energy, which is what photocatalysis is characterized as. Nearly 9600 times more solar energy than the entire world uses is provided to the surface of the globe.
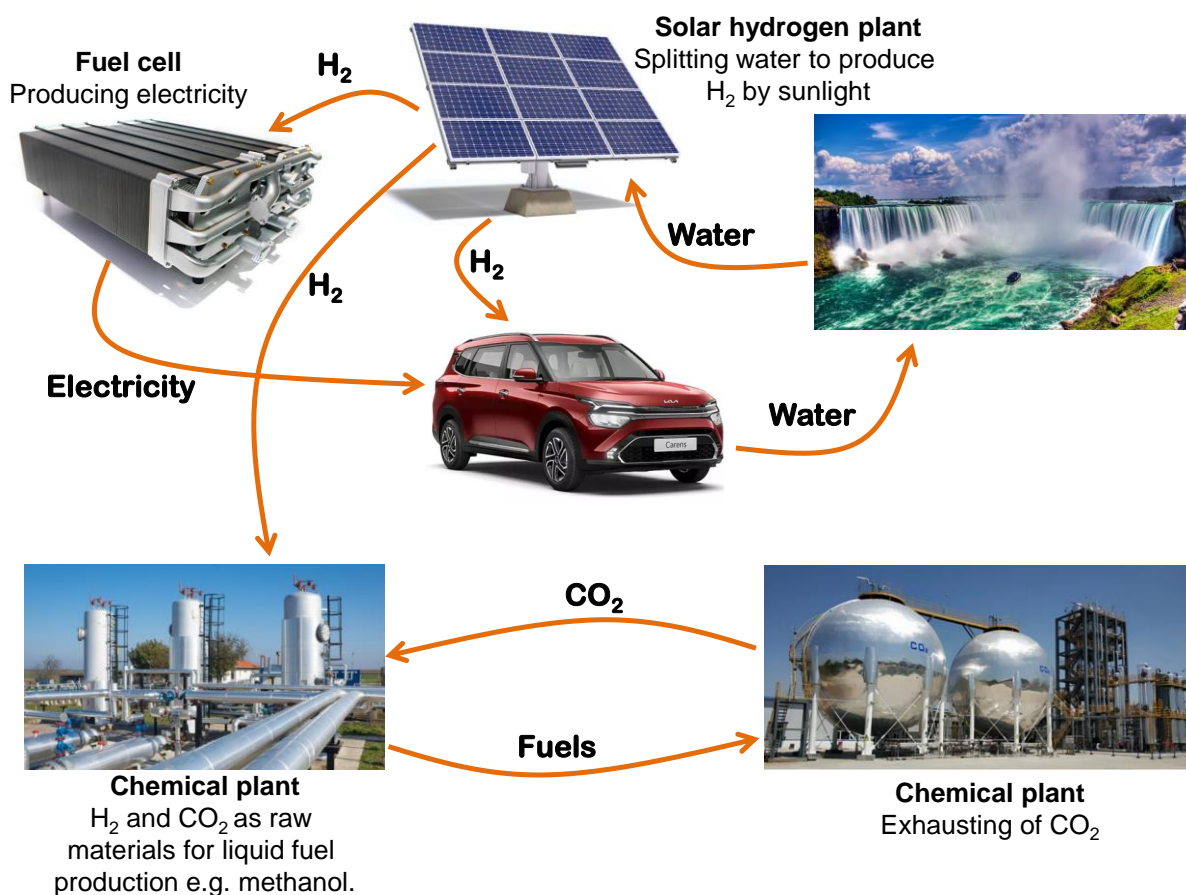
Fig. 1.6 Schematic representation of potential sustainable hydrogen fuel plant based on photocatalytic water splitting [114]

Here, the multidisciplinary field of photocatalytic water-splitting research necessitates expert understanding of chemical engineering, physics, nanotechnology, chemistry, nanoscience and materials science. It should be noted that a crucial element in photocatalysis is an electronic structure with a lower occupied energy level (valence band; VB) and a higher unoccupied energy level (conduction band; CB), which is used when semiconductors are used as

catalysts. As a result of the difference between these two levels, a particular amount of optical band gap (Eg) is introduced. 1.23 eV is thought to be the semiconductor's optimal band gap value. However, a wider approximation is taken into account between 1.5 and 2.5 eV for the same purpose due to some specific energy losses [115]. H^+ reduction and $4e^-$ H_2O oxidation are the two fundamental processes involved in the direct splitting of $H_2O_{(l)}$ into $H_{2(g)}$ and $O_{2(g)}$. Photocatalytic water splitting is classified into 3 different categories (Schematically shown in Fig. 1.7), (i) POWS, (ii) PIWS, and (iii) PPWS [116].

(i) Photocatalytic overall water splitting (POWS): In this technique, two molecules of H_2O split into two molecules of hydrogen and one molecule of oxygen according to (shown in Fig. 1.7) stoichiometry, which requires four electrons. An efficiency of ~5-10% can be achieved in this process to commercialize hydrogen as an economically viable fuel.

(ii) Photocatalytic intermediate water splitting (PIWS): In this process, two molecules of H_2O are converted into one molecule of hydrogen peroxide (H_2O_2) and hydrogen (shown in Fig. 1.7), which is the two-electron process. The advantage of this is that no purification and separation of hydrogen is required. However, controlling reaction kinetics at the surface of the photocatalyst is tricky (especially preventing H_2O_2 from decomposing into water and oxygen).

(iii) Photocatalytic partial water splitting (PPWS): In this method, a molecule of water, with the help of a sacrificial electron donor, produces hydrogen along with other by-products formed through oxidation (shown in Fig. 1.7). This method is also a two electron process, and the holes in the VB are rapidly captured by the sacrificial electron donor, which helps produce hydrogen. In addition, this process can separate charge carriers with a high efficiency of ~100%. In this technique,

waste organic pollutants such as glycerol (biodiesel by-product) can be used as a

sacrificial electron donor, which also helps in environmental remediation.

(1) POWS

4e⁻ → 2H₂

4h⁺ → O₂

(2) PIWS

2e⁻ → H₂

2h⁺ → H₂O₂

(3) PPWS

2e⁻ → H₂

Electron donor

2h⁺ → **Oxidation products**
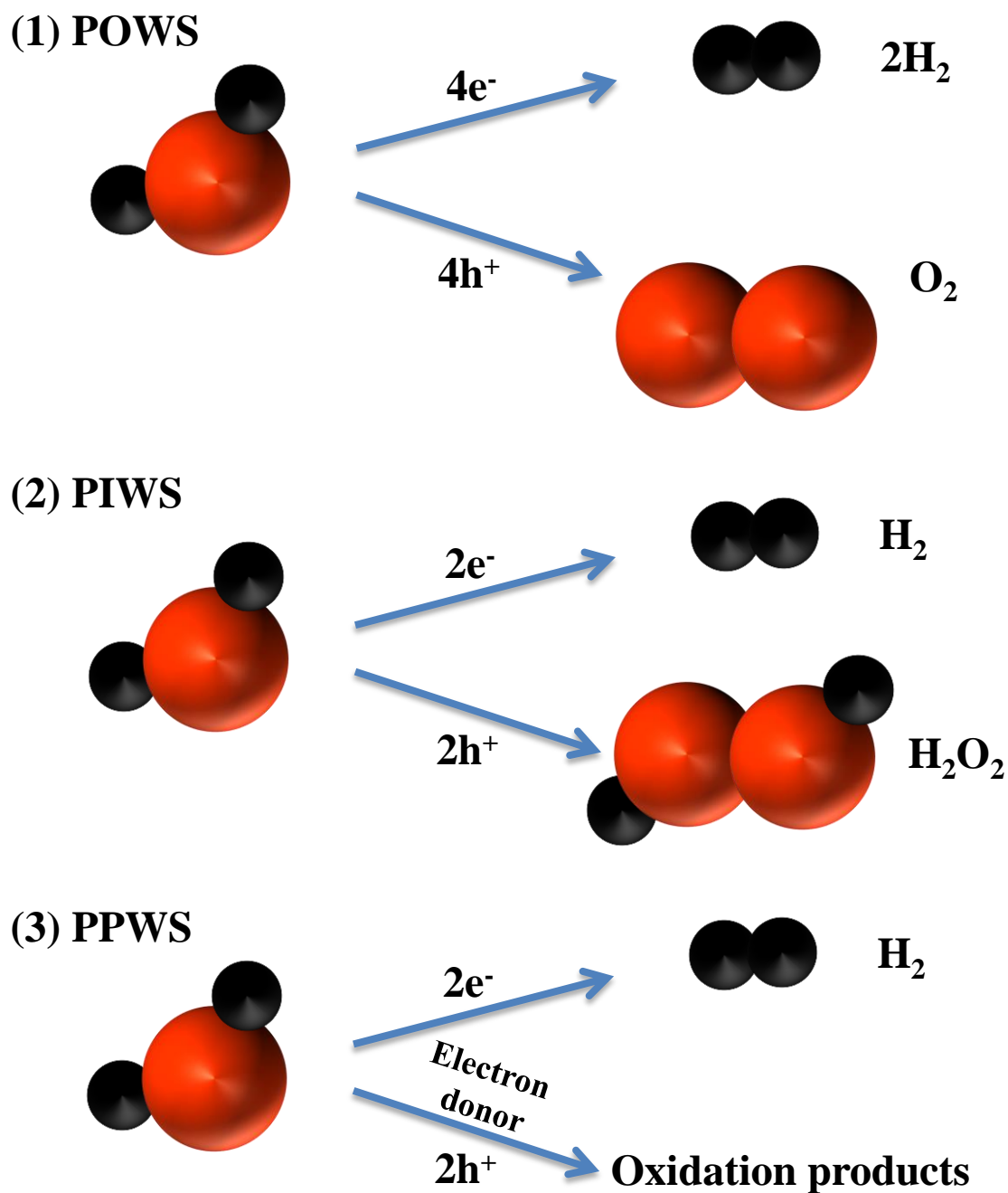
Fig. 1.7 Different types of photocatalytic water splitting methods for H₂ evolution

Further, a detailed discussion of a photochemical reaction (PCR) mechanism is depicted

above. A photocatalytic surface absorbs photons when exposed to energy above or equivalent

to its band gap, which eventually outcomes in the creation of an electron-hole (e⁻/h⁺) pair. A

vacancy, or hole (h^+), or photogenerated electron (e^-), is created in the VB when the photogenerated electron (e^-) is accommodated in CB. The produced e^-- h^+ pairs, also known as charge carriers, migrate to the photocatalyst's surface and are compelled to interact with the H_2O molecules there. By transferring electrons and holes at different reaction sites, the charge carriers engage in reduction and oxidation reactions, causing the generation of gaseous H_2 and O_2. The oxidation potential required to convert H_2O to O_2 must be positive than the bottom of the VB, and the reduction potential required to convert H^+ to H_2 must be negative than the bottom of the CB [117]. In addition to these photochemical processes, the photogenerated charge carriers also take part in recombination, radiation-nonradiative transitions [118], and trapping at defect locations. For a photochemical system to be optimised for effective H_2 evolution, all of these physical processes must be taken into account. In Fig. 1.8, the entire photochemical process is depicted. Photocatalytic water splitting may make use of either a one-step or two-step excitation method, and both are described here.
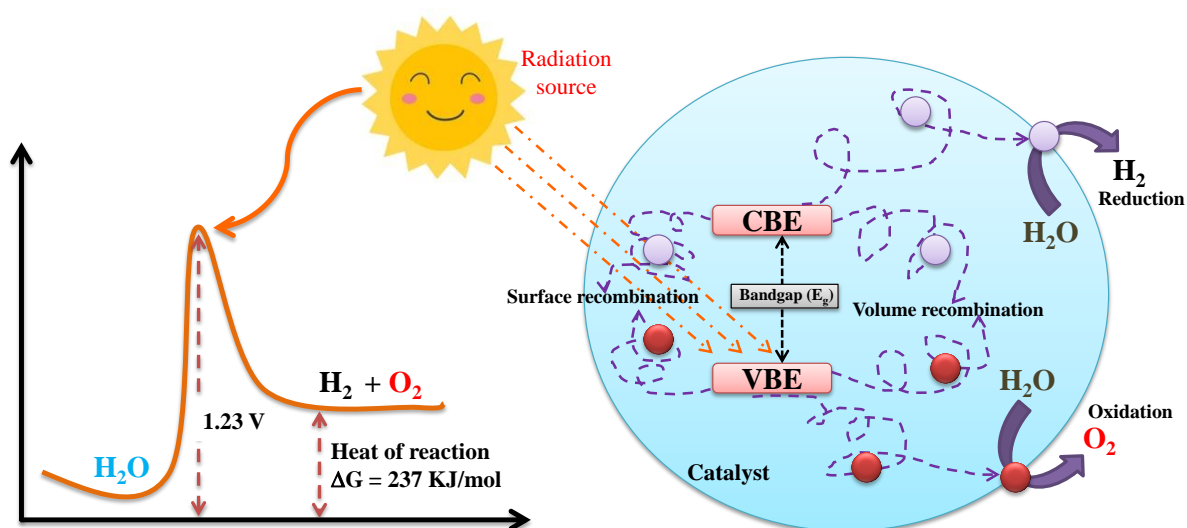
Fig. 1.8 Illustration of the water splitting reaction that leads to the evolution of H_2/O_2 gas and photoexcitation of the catalyst.

$$\text{Photon} + \text{catalyst} \rightarrow \text{catalyst} + h^+ + e^- + H_2O \rightarrow \text{catalyst} + H_2 + O_2 \qquad (1.1)$$

One-step mechanism:

$$\text{At VBE, } 2O^{2-} \rightarrow O_2 + 4e^- \qquad (1.2)$$

$$\text{At CBE, } 2H^+ + 2e^- \rightarrow H_2 \qquad (1.3)$$

Two-step mechanism:

$$\text{At VBE, Donor} + h^+ \rightarrow \text{Accepter} \qquad 2H_2O + 4h^+ \rightarrow O_2 + 4H^+ \qquad (1.4)$$

$$\text{At CBE, } 2H^+ + 2e^- \rightarrow H_2 \qquad \text{Accepter} + e^- \rightarrow \text{Donor} \qquad (1.5)$$
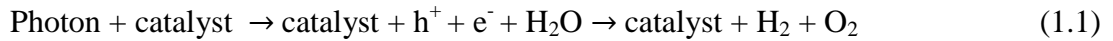
1.2.4.1.Photocatalytic water splitting reactions

Sustainable energy production from water is a critical issue and has become a great challenge for clean-energy technologies. Therefore, the generation of H_2 fuel from the H_2O with help of various energy sources is getting enormous attention. Photocatalytic water splitting is an effective alternative for the promising H_2 production, also known as artificial photosynthesis. Lewis and Nocera, in their research article 'Powering the planet', revealed that solar light falling on earth surface has an illumination power of 103 W/m^2 which can be used as an optional energy source as compared to the fossil fuels [119, 120]. But the concept of water splitting by use of the energy of photons was become real by the efforts of Fujishima and Honda. They split water into hydrogen and oxygen using semiconductor photocatalyst to absorb solar energy. After that, a number of semiconductor nanoparticles have been discovered as an excellent photocatalyst. Their activity can be improved by tailoring their size and shape. Among the various semiconductor nanoparticles oxides, sulphides and nitrides are quite popular. Further the optical activity of semiconductor nanoparticles can be improved by doping of Au, Pt, Pd etc., as these metals work as a co-catalyst during the photocatalysis process. These features are responsible for substantial increment in hydrogen generation from water and work as ideal photocatalyst under visible light region [121]. Various semiconductor photocatalysts for photocatalytic water splitting reaction. In general, a

photocatalyst absorbs photons of appropriate energy and transfer this energy to the H free radical of water in the form of photoelectrons, these radicals are reduced on the surface of the photocatalyst and hydrogen evolution takes place.

Because water is transparent to the visible spectrum, a photosensitizer capable of absorbing solar radiation must be dissolved in solution before using solar irradiation directly for photocatalytic water splitting [122]. To work as an efficient photocatalyst, the semiconductor nanoparticles must have their band position in the range of energy required for water splitting reaction. In photocatalysis process, when a catalyst absorbs photons, electrons jump from the VB to the CB of the catalyst producing holes in VB. Both the electrons and holes travel to the surface reaction sites where holes are scavenged by sacrificial agents and using the electrons for water to generate H_2. The efficiency of catalyst is directly proportional to its light harvesting property and efficient electron-hole separation [123].

As shown in Fig. 1.9, there are multiple processes involved in the whole photochemical H_2 production through the water splitting reaction, commencing with photon absorption and ending with the formation of an H_2 molecule. It depicts a stepwise reaction pathway where different factors influence each stage and the efficiency of each phase affects the overall process as a whole.
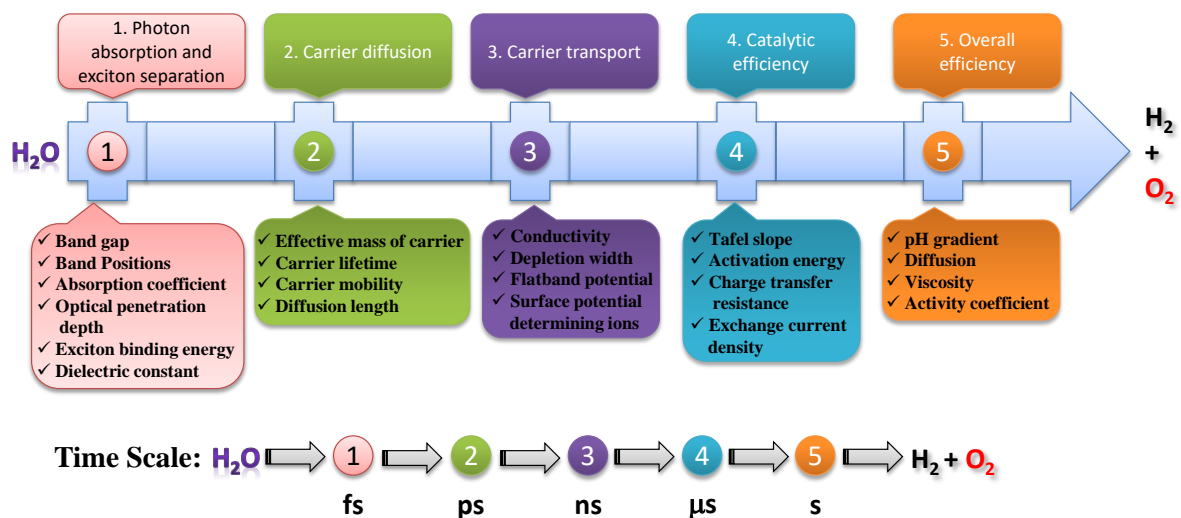
Fig. 1.9 A step-by-step breakdown of the photocatalytic water splitting process's

27

contributing elements with a time-scaled profile of several chemical reaction steps.

1.2.4.1.1. Photocatalyst requirement for photocatalytic water splitting

The sun's potential to deliver a clean, renewable, and limitless supply of energy has piqued the imagination of many [124]. Because just sunlight and a catalyst are needed to solve these problems, photocatalytic technology has attracted attention around the world [125]. Environmental remediation (pollutants degradation) encompasses air purification and waste water treatments [126], whereas energy conversion (nitrogen fixation, carbon dioxide reduction and hydrogen evolution) is characteristic of photocatalysts. As a result, the creation of a workable photocatalyst has become a popular topic of international study in an effort to alleviate the world's pressing energy and ecological problems.

1.3. Photocatalysis

In photocatalysis process, the photocatalysts must absorb light and then transmit the light energy to the reacting molecules for participating in the redox reactions [127]. To provide a strong enough platforms from photon absorption to desorption of the H_2 gas produced as a result of the photochemical reaction, a solid substrate (i.e., photocatalyst) is needed, as was discussed above. Photocatalysis is the term used for the process in which rate of reaction is enhanced by the addition of a substance (photocatalyst) in the presence of light (UV or visible) without any chemical change in the photocatalyst after the reaction and the reactants get transformed to the desired products in the procedure. Light plays the crucial role in the photocatalysis process contrary to typical catalysis processes; the chemical reactions which are thermodynamically unfavorable can be carried out by utilizing the energy available from photons of light [128]. In homogeneous photocatalysis, the reactants and photocatalyst are in the same phase, but in heterogeneous photocatalysis, the reactants and photocatalyst are in the different phase [129]. In heterogeneous photocatalysis, the photocatalyst is in particulate form while the reactants can be in gaseous or liquid form, and all the reactions take place at

the photocatalyst interface. Mostly, semiconductors compounds are used as photocatalysts in heterogeneous photocatalysis due to their unique bandgap energies. The term "photocatalyst" refers to a solid substrate employed in a heterogeneous photocatalytic process, which often kick starts the photochemical reaction by delivering charge carriers [130]. While there has been significant progress in photocatalytic technology, no photocatalytic system that meets all the requirements for widespread use has yet been designed. New photocatalytic materials are being designed and produced with a lot of effort in order to improve photocatalytic performance, particularly in the spectrum of visible light. For a photocatalytic system to be useful, it must satisfy the following conditions: (a) Surface redox reactions should occur uniformly as a result of the contribution of charges; (b) the catalyst must have a narrow enough photonic band gap to absorb the entire solar spectrum; (c) excessive separation followed by a quick transfer of photoinduced charge carriers (e^- and h^+) to the surface of the photocatalyst is necessary to reduce the rate at which redox reactions occur and prevent back reactions. That's why it's so important for scientists to zero down on a photocatalyst that can effectively separate and transfer charges. Attempts to increase photocatalytic efficiency by altering the morphologies and structural properties of photocatalysts have led to the development of an unbalanced outlet having poor photocatalytic performance, as shown in a number of studies. Strategically designing many active sites and alterations to electronic properties are necessary to accelerate the pace of kinetically viable surface redox reactions and enhance the catalyst's performance and stability [131]. As a rapidly developing area of interest in disciplines as diverse as chemistry, materials science, physics, nanoscience, and engineering, photocatalysis has recently been the subject of extensive research. Finding a candidate whose performance may get improved to meet industry requirements, scientists from a wide range of fields have been working hard to improve photocatalyst efficiency. According to a search of Web of Science for the term "photocatalyst," around 8850 scholarly

articles focused on photocatalysis and its many applications were published in 2021. Some very good evaluations of methods used to create novel photocatalysts for a variety of photocatalytic purposes have been published, but no contemporary, all-encompassing review has been found.

1.3.1. Applications of Photocatalyst

Photocatalytic hydrogen evolution, carbon dioxide reduction, Nitrogen fixation, and pollutant degradation [132] are a few of the various applications for photocatalysts shown in fig. 1.10.
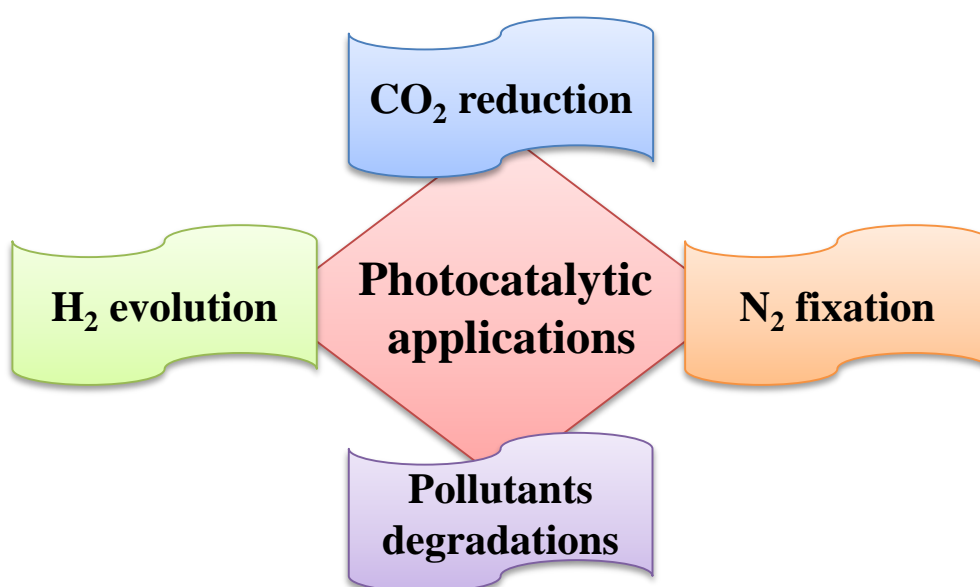
Fig. 1.10 shows the different applications of photocatalyst.

1.3.1.1. Photocatalytic N_2 fixation

In order to convert N_2 into an eco-friendly product, such as NH_3, photocatalytic fixation of nitrogen is an effective method. The substance is generated out of N_2 and H_2O under mild environmental circumstances with the help of pollution-free and long-lasting sunlight [133]. Except for the final phase, wherein electrons and holes take part in the redox reactions of fixation of N_2 controlled by electrons and H^+, the steps involved in photocatalytic N_2 fixation are the same as those involved in CO_2 reduction. The Haber-Bosch process is a common method for obtaining nitrogen fixation; it can efficiently transform nitrogen into ammonia,

energy-intensive reaction conditions are required, including high pressure (15-25 MPa) and temperature (673-873 K) over long duration of time, which necessitates a lot of effort [134]. The conventional approach has the additional issue of contributing to global warming through the discharge of carbon dioxide (less than 1%) throughout the nitrogen fixation process. Accordingly, it is essential to replace the current, time-consuming, and polluting method of converting N_2 with a sustainable, low-energy one that produces no secondary pollutants. Since just sunlight is needed to derive the reaction, photocatalysis is now recognised as exciting technology that could serve as a suitable replacement. To be an effective photocatalyst for N_2 fixation, a material needs to meet certain criteria [135]. Large surface area, high N_2 adsorption ability, and insufficient photoinduced charge carrier recombination rate are a few of these. Hu et al. developed a method to create a heterojunction system where charges are effectively separated in space through the integration of rGO and protonated g-C_3N_4 via an electrostatic self-assembly process [136]. In the presence of visible light, the photocatalytic activity presented by the composite as-prepared for N_2 fixation was assessed. The relevance of the interaction among the two components that comprise the enhanced surface contact area was supported by FTIR and PL experiments that clarified paths for quick charge transit and prevented charge carrier recombination. It was discovered that the ideal PCN/rGO composite fixed N_2 to NH_4^+ 8.3 times more efficiently than the pure g-C_3N_4 composite.

1.3.1.2. Photocatalytic pollutants degradation

Constant discharges of harmful effluents from a wide range of expanding industries into water bodies are damaging aquatic life and posing a threat to human health. Thus, it is of critical importance to create a technology to lessen pollution and protect people's health [137]. Photocatalytic elimination of pollutants without producing secondary pollutants is one technology that has garnered a lot of interest. Regarding the photocatalytic elimination of

environmental contaminants, the main goal of research and development has been to create an effective photocatalyst with broad optical absorption, a greatly reduced rate of recombine for photoinduced charge carriers, and robust redox potentials. Numerous cutting-edge methods have recently been implemented for photocatalytic elimination of various pollutants. To test the photocatalytic efficiency of a system for degrading NO pollutants, Hu's team, for instance, built a Z-scheme heterojunction of 2D/2D BP/monolayer Bi_2WO_6 hybrid system [138]. To make the BP/monolayer Bi_2WO_6 composite, they ultrasonically mixed Bi_2WO_6 generated hydrothermally with BP nanosheets obtained by exfoliating bulk BP. SEM and TEM examinations verified the incorporation of BP and Bi_2WO_6 nanosheets into a functioning 2D/2D heterojunction. The results of photocatalytic NO degradation showed that BP/MBWO composites performed better than individual component photocatalysts. Under the same testing settings, the optimum candidate showed an optimal NO degrading rate of 67% after 30 min, while pure MBWO only managed a rate of 26%. Photocatalysts' crystal lattices may accommodate surface oxygen vacancies and bulk defects; nevertheless, these two types of defects have opposite effects on photocatalytic activity. Perovskite materials like $CaCu_3Ti_4O_{12}$ are good in photo catalytically degrading TC [139].

1.3.1.3. Photocatalytic CO_2 reduction

The main cause of global warming is the emissions of carbon dioxide (CO_2) in the atmosphere, which is steadily rising because of the excessive burning of fossil fuels. Until 40% of total CO_2 emissions come from the cement, chemical, transportation, and steel industries; therefore, low-carbon cost chemicals and fuels that result in CO_2 reduction and the utilization of clean energy would play an essential part in decarbonizing practical applications in these sectors [140]. Humanity's greatest concern is ensuring the safety of future generations in the face of an eventual lack of renewable energy brought on by our increasing reliance on fossil fuels and our efforts to reduce atmospheric concentrations of CO_2. The use

of photocatalysis to transform CO_2 into a fuel product is a sustainable way to meet the energy need of world. Subsequently the beginning of the industrial age, the world's attention has been focused on energy shortages and the burning of primary sources of energy contributes to global warming, which releases substantial CO_2. The use of CO_2 has drawn a lot of interest as a potential remedy for the problems of global warming and energy constraint [141]. One possible approach to addressing this predicament is to turn CO_2 into high-value end products. However, a linear CO_2 molecule has a C=O bond enthalpy is 750 kJ/mol, therefore a lot of energy is needed to break it. For instance, conventional gas-solid thermal catalysis typically necessitates severe conditions, large energy costs, and uncontrolled product selectivity [142] in order to accomplish effective CO_2 conversion. Mild electrocatalysis techniques, on the other hand, require expensive membrane modules to partition the reactor into two halves, making industrialization difficult. In addition, the primary means by which both of these energies are obtained is still the ignition of fossil fuels, which results release of CO_2 as a by-product [143]. Alternatively, photocatalytic technology can use the abundant and cost-free solar energy to achieve CO_2 reduction. Its rapid regenerativeness and ecological friendliness make it a popular topic of conversation [144]. However, current response efficiency remains significantly lower than what is needed for industrial manufacturing. This is mainly because the catalysts often utilized in traditional photocatalysis have a relatively wide prohibited bandwidth, limiting the improper use of the solar radiation. Indeed, there is a great need for extensive research into various forms of efficient photocatalysts in this area. The following five sequential processes [145] make up the majority of the CO_2 photocatalytic reduction: because (1) uses the sun's rays to create a pair of electrons and holes. In order to distinguish photogenerated electrons from photogenerated holes, energy levels must exceed or be equivalent to bandgap levels. As a result, an equal number of holes in the valence band (VB) are also left behind as the excited electron moves from the VB to the CB. As a result,

photogenerated electrons and holes may be separated. (2) Photocarriers are produced, scatter, and go to the surface where they participate in oxidation and reduction processes. In order to boost photocatalytic performance, it may be required to improve the efficiency with which photocarriers are separated and their recombination is suppressed [146]. (3) Adsorption of carbon dioxide (CO_2). This is necessary for the photocatalyst to transmit an electron to the carbon dioxide molecule. The CO_2 adsorption and activation process might be accelerated by changing the surface alkali and increasing the specific surface area; (4) to occur the CO_2 reduction reaction, an oxidation-reduction reaction requires a photocatalyst with a wide enough bandgap [147]. Conduction band potential is lower than valence band potential, and vice versa. The surface electron acceptor potential is smaller than the valence band potential. The effectiveness of the catalyst was crucial throughout the procedure. Improvements in light conversion efficiency and the ability to absorb a wider spectrum of light have been made in recent decades. However, the efficiency of photocatalytic CO_2 reduction is still quite low. The reserves and price of the catalyst will also restrict how widely it may be used. Therefore, the key to fixing the aforementioned issues is discovering a catalyst having abundant reserves, low price, and great catalytic performance. In response to these two issues, numerous photo-catalytic technologies have evolved; among these, photo-catalytic CO_2 reduction technique has garnered great attention due to its potential applicability in addressing those problems [148]. The photo-catalyst, when exposed to constant sun radiation, may transform CO_2 into valued organics such CO, CH_4, CH_3OH, HCOOH, and HCHO. These products, if purified, can be utilised as basic components and fuels to address the world's pressing energy needs. The steps that follow are the foundation of the photo-catalytic reaction. Surface reactions include hole-catalysed oxidation of H_2O and electron-catalyzed reduction of CO_2 [149]. The production of electricity and the use of fossil fuels in manufacturing are the two most significant human activities. CO_2 emissions are another

major problem caused by deforestation [150]. Therefore, one of the most appealing solutions to combat climate change and the energy issue is the transformation of CO_2 into fuels like formic acid, methanol, and methane. CuO-ZnO, TiO_2-ZrO_2, ZrO_2, TiO_2, and a carbon-based photocatalytic NC system are a few examples of photocatalytic materials and nanocomposites (NCs) that have been investigated for their effectiveness in the photocatalytic transformation of CO_2 into fuels [151]. To be able to assess the photocatalytic effectiveness of $SrTiO_3$ for CO_2 conversion, for instance, Humayun et al. [152] constructed co-catalyst-free iron and boron co-doped $SrTiO_3$ photocatalyst. It was determined by XRD and DRS those B ions were substituted for Ti^{+4} ions. When Fe ions replaced O^{2-} ions in the $SrTiO_3$ crystal lattice, new energy states were created at the VB but below the CB, prompting a significant red shift in the optical absorption. The best composite outperformed the best individual photocatalyst by a factor of five, with CO and methane yields of 21 $\mu mol g^{-1} h^{-1}$ and 17 $\mu mol g^{-1} h^{-1}$, respectively.

1.3.1.4. Photocatalytic H_2 evolution

Because of the zero pollution and excellent energy aptitude qualities, a focus of photocatalytic technology has been the water splitting method for photocatalytic hydrogen generation. Meanwhile, sunshine is acknowledged as a abundant, unlimited, sustainable, and renewable energy source that might meet the energy need of world in its whole. The efficacy of water splitting remains too low despite significant progress in H_2 through water splitting. Researchers have tried using sacrificial agents to boost the rate of hydrogen evolution, but the high cost of the sacrificial agents means that this route is not yet widely accepted. There must be more effort put towards creating cutting-edge photocatalytic candidates. In this section, we will review the most up-to-date efforts to enhance the efficiency of photocatalytic H_2 evolution [153].

1.4. Photocatalyst selection criteria

Light is captured to create electrons and holes, charge carriers are dissociated and migrate from the bulk to the catalyst's surface, and interfacial charges contribute to reduction and oxidation reactions at the surface's reactive sites, making up the three main steps of the photocatalytic process [154].

By examining the light-harvesting extent (The extent of light harvested depends on the surface area of photocatalyst/materials. Capturing the amount of sunlight depends on the photocatalyst surface area if the solar harvesting surface area is enlarge it allows for capturing a greater amount of sunlight which increasing the overall energy generation.), it is feasible to calculate how much solar light is being utilised. To take part in the interface oxidation/reduction reactions, charge carriers must first travel to the surface of the catalyst from the bulk, where some are dissipates as a result of recombination and heat generation [155]. Thus, their recombination rate significantly affects the ability of excited charges to dissociate and diffuse. The exceptionally high effectiveness of fuel generation requires a photocatalyst that satisfies the following conditions. (i) A lower potential is required for the CB edge of the photocatalyst than the potential for the evolution of hydrogen (H_2), which is 0 eV; (ii) The potential of the VB edge of the photocatalyst must remain positive in comparison to the 1.23 eV potential for the formation of oxygen (O_2). Therefore, the minimum band gap value required of a photocatalyst to show its photocatalytic effect is 1.23 eV. In order for a photocatalytic process to be successful, to produce a large enough flux of charges, the photocatalyst must be able to absorb light over a variety of wavelengths [156]. The maximum amount of light that may be absorbed is significantly determined by the photocatalyst in band gap ($Eg = hc/\lambda$). As a result, while possessing adequate band edge potentials, photocatalytic materials with large band gap energies are not suitable for effective light absorption and cannot provide useful photocatalytic results. Furthermore, the photocatalytic efficacy of a

material is tightly regulated by the effective segregation and transport of photogenerated e$^-$ and h$^+$ within the photocatalyst. Fast charge carrier transfers help the photocatalytic process, which decreases recombination of charges. It is important that the photocatalytic material chosen for the procedure is both economically viable and photochemically viable during the reaction [157].

1.4.1. Photocatalytic water-splitting material

A semiconductor must fulfil a number of requirements in order to be considered an excellent substance for photocatalytic water splitting. First, it requires having narrow bandgap energy [159] so that visible light may be used. All that is required for this is a photocatalyst with bandgap energy of around 2.1 eV, or a wavelength of about 600 nm. Second, the photocatalyst's band locations must cross the redox potential of H_2O [159]. The water reduction potential and oxidation potential must be less than or equal to the photocatalyst's lowest and highest conduction and valence bands, respectively, enabling a single photocatalyst system to function. The electrical and crystal structures of a material are the primary factors in determining the energy and location of the bandgap. In order to select an efficient photocatalyst, it is necessary to have a firm grasp on the fundamentals and a thorough characterization of specific photocatalysts. The next need for a successful photocatalytic reaction is that the photocatalyst be highly stable both in the presence and absence of light [160]. Due to their instability, many promising photo-active materials can't be used in photocatalytic water splitting, making this criterion extremely important. Hydrogen evolution activity is high in some candidates for narrow bandgap energy photocatalysts, including CdS and CdSe. The bottom of CB position of CdX based-photocatalysts is more negative than the water reduction potential, while the top of VB should be lower (more positive) than the water oxidation potential [161]. Oxygen evolution is greatly aided by WO_3, but its Conduction band location is additional favourable as the

reduction potential of water [162]. As a result, there is a smaller pool of viable photocatalyst options for a single photocatalyst system compared to a PEC setup. The fourth criterion is that the semiconductor catalyses the reduction or oxidation of water strongly. In the end, the semiconductor has to be cost-effective. In order for the powdered photocatalyst system to be scalable, the photocatalyst itself needs to be made from low-cost, plentiful ingredients and to be synthesised in huge quantities.

High-efficiency photocatalytic water splitting has reportedly been achieved with a wide range of materials. La doped-$NaTaO_3$ photocatalyst has a potential quantum efficiency of 56 % at 270 nm [163]. Electronic structures with a single d orbital filled (d10, s2d10) or a single d orbital empty (d0, d0f0) are typical of efficient photocatalysts. The highest oxidation states of the metals Ti, Sb, V, Zn, Nb, Zr, W, Ga, In, Bi, Ge, and Ta, all have such electron configurations [164]. The metal oxides formed by these photocatalysts often have conduction bands that appear more negative than 0 eV and valence bands that are around 3.0 eV vs. NHE because of the presence of O 2p orbitals. This means that these materials can only be activated by exposure to UV light. These materials' photocatalytic activity is greatly influenced by their electrical and crystal structures. Although $Sr_2Nb_2O_7$ and $Sr_2Ta_2O_7$ photocatalysts share a similar crystal structure, the former is thought to exhibit more photocatalytic activity due to the higher location of its conduction band [165]. Both photocatalysts have a distorted framework within a layered perovskite structure. $NaTaO_3$ is the most active of the $ATaO_3$ (a: Li, Na, and K) photocatalysts, but the activity of the others has been demonstrated to be affected by framework distortion [166]. $NiO/NaTaO_3$ strong activity can be attributed to the combination of a sufficiently distorted TaO_6 connection network and the Ta 5d in the conduction band [167].

Maintaining the locations of CB and VB with respect to the oxidation and reduction potentials of water can be difficult with a photocatalyst that has low bandgap energy. Several

solutions have been proposed to meet this difficulty. There are essentially four classes into which the various attempts might be placed [168, 169].

1. Oxides sensitive to ultraviolet light that have been doped with metals in the d1-d9 d orbital to achieve significant doping.

2. S, Se, N, P, and C are examples of non-metallic hetero-elements that can be doped.

3. Synthesis of d0 or d10 and d10 2s electrical configuration double metal oxides.

4. Metal d0 or d10 oxynitride and oxysulfide synthesis.

As previously stated, the valence band of UV-responsive photocatalysts is made up of O 2p orbitals, whereas the conduction band is made up of empty orbital (LUMO) states of metal cations (M^{+n}) in the d^0 and d^{10} configurations. Because the conduction band cannot be reduced, the bandgap energy must be decreased by adding a second valence band or by using an electron donor with an orbital other than O 2p. However, during this bandgap energy reduction, it is important to take into account the thermodynamic and kinetic properties of the newly forming level that experiences water oxidation.

The development of (oxy) nitrides and (oxy) sulphides demonstrates the effective synthesis of a visible-responsive photocatalyst. These photocatalysts are made by either partially or completely exchanging oxygen for nitrogen or sulphur. The bandgap is shrunk as N 2p and S 3p orbitals are substituted for O 2p ones, due to their higher energy levels [170]. In contrast to doped-oxide photocatalysts, the valence bands of these materials are not dependent on the concentration of dopants but rather on their concrete electronic structure. Photogenerated holes are more easily transferred to the photocatalyst's valence band thanks to this feature. Absorption behaviour of several (oxy) nitrides with d0 electronic configuration transition-metal cations of theses Ta^{5+}, Nb^{5+}, and Ti^{4+} [171]. Simultaneous nitridation of the

appropriate metal oxides in the presence of NH_3 at high temperature is a common method for synthesising these photocatalysts. These photocatalysts have a bandgap energy of about 1.7-2.5 eV, having an absorption edge at 500-700 nm. The DFT prediction that these photocatalysts have ideal band positions for water splitting is supported by activity in a photocatalytic process when sufficient sacrificial reagents are present. As a result, when exposed to visible light, they appear to be a potential candidate for worldwide water splitting.

1.4.2. Few dynamic photocatalysts which are explored for hydrogen generation are:

1.4.2.1.Oxides

Transition metal oxides with unfilled or fully filled d orbital like oxides of Ti^{4+}, Zr^{4+}, Nb^{5+}, W^{6+}, Ga^{3+}, In^{3+} are highly efficient photocatalysts. However, these are active in near ultraviolet region; therefore their solar to hydrogen efficiency is low. Furthermore, Fe_2O_3, WO_3, $BiVO_4$, NiO, CoO, ZnO have also been reported as promising photocatalysts under visible region [172].

1.4.2.2.Metal sulphides

Transition metal sulphides are also well studied as semiconductor photocatalyst for water splitting reactions. For significant photocatalysis semiconductor materials should have 20-30% ionic character and only metal sulfides lies in this range. Moreover, metal sulfide has fewer tendencies to form metal hydride bonds during WSR reactions therefore rate of HER is high for the sulfide. These can be single metal sulphides like CdS, Bisulphide, and MoS2, bimetallic sulphides as CdGaS, ZnGaS, $CuInS_2$ and ZnInS. Further multi-metal sulphides also result remarkable photocatalytic activity e.g. Cu_2ZnSnS_2, $ZnCoS_4$, CuGa1-xZn_2xS4 etc. [173].

1.4.2.3. Nitrides

Among these conjugated metal free carbon-based nitrides (C_3N_4) are very well recognised as

promising photocatalyst for water splitting reactions. It exists in different allotropes (alpha, beta, graphitic and quasi cubic) from which graphitic C_3N_4 is more active as it has graphite like sheet nature and high surface area. The discovery of H_2 evolution from H_2O under visible light using graphitic C_3N_4 was made by Wang and colleagues. Further to remove limitations like lower charge ion movement and less light harvesting nature, it can be modified with iron or gold [174].

1.4.2.4. Metal Nitride

Metal nitrides (MNs) are relatively new in the chemical world, but their unusual features have attracted a lot of interest. Importantly, "N_3" forms unusual bonds with metals, enabling the formation of metal nitrides with surprising novel characteristics that resemble even platinum and gold, favouring the delivery of remarkable new compounds [175]. Despite their obvious appeal, however, the entire potential of these materials has not been investigated in many published papers. TiN, TaN, and ZrN are examples of MNs that are optically transparent because they are naturally metallic; some MNs are superconductors because they have small band gaps; and the others act as semiconductors because they have a wide bandgap, like GaN. Therefore, they are trustworthy substitutes for Au and Ag [176]. Melting points of MNs are high, their metallic strength is unparalleled, they are extremely stable, and their bandgap is similar to that of platinum-class elements. Because of their prospective uses as electrochemical and optical sensors and as effective adsorbents from effluents [177], the development of innovative MN materials has garnered fresh interest. Metal oxides and hydroxides are mitigated by their essential features. MNs have the potential to be useful photocatalysts because they are electrically conductive and feature band structures that are analogous to those of noble metals. When it comes to redox processes, the bandgap of MN nanoparticles is ideal. In addition, in the case of hybrid MNs desorption of adsorbed material and interface engineering can be accelerated by optimising their doping strategies and

modifying their d-bands, respectively [178].

1.4.2.4.1. Recent research on metal nitrides and their potential uses

Because of their unique physical properties, outstanding electronic composition, numerous oxidation states, and cost efficiency [179], MNs have become popular with growing attention in photocatalysis, electrochemistry and storage of energy related fields like supercapacitors, batteries (SC), detectors, active electrodes, electrocatalysts, photocatalysts [180]. Important reactions for creating hydrogen as cleaner fuel are the hydrogen evolution reaction (HER) and the oxygen evolution reaction (OER) that occur during electrochemical water splitting reactions [181]. MNs are useful in many chemical reactions, like oxygen evolution reactions, hydrogen evolution reactions, urea oxidation reactions, ammonia oxidation reactions, oxygen reduction reactions, including ammonia borane the dehydrogenation.

In recent years, researchers have focused on tantalum oxynitride (TaON) and tantalum nitride (Ta_3N_5) as potential photocatalysts for water splitting because of their narrow bandgap energy and favorable band locations. Ta_3N_5 absorption spectra, which may reach up to 600 nm, have drawn a lot of interest as a promising material for efficient photocatalytic water splitting. In experiments, TaON and Ta_3N_5 powders are produced by the high-temperature nitridation of crystalline or amorphous Ta_2O_5 under various temperature and time-of-heating regimes [182]. The resultant samples were characterised by neutron and synchrotron diffraction of powder analyses, which showed that TaON and Ta_3N_5 had monoclinic (phase) and orthorhombic crystal structures, respectively [183]. Nitridation of oxides materials yields the N 2p electrical configuration, which can be used for band engineering. Nitrogen replaces oxygen, making the valence band more negative, whereas the conduction band, which consists of empty orbitals derived from the Ta d^0 orbital, remains mostly unchanged during nitridation. The time of the nitridation process, flow rate, and temperature were also observed to affect both the photocatalytic efficiency and band gap of these materials [184].

Both materials have been demonstrated to produce hydrogen or oxygen from water when exposed to visible light and sacrificial reagents [185]. These photocatalysts have not been able to split water efficiently thus far. When exposed to visible light, these photocatalysts show relatively high activity in oxygen evolution. However, their contribution to hydrogen evolution is still negligible, falling roughly an order of magnitude behind their contribution to oxygen evolution. Hydrogen production also calls for some sort of tweaking. Efforts have been made to boost performance in hydrogen evolution. Hydrogen evolution can be significantly boosted by photo depositing Ru nanoparticles on top of a TaON photocatalyst [186]. Although Pt has been utilised as a co-catalyst in the instance of Ta_3N_5, the generation of hydrogen rate is significantly lesser even now [187]. One of the most efficient ways to speed up the Ta_3N_5 hydrogen evolution process is to subject the material to high pressure treatment using NH_3 gas. This strategy makes sense since nitrogen vacancies are created in the crystal lattice through the synthesis of the (oxy) nitrides. After forming, these vacancies induce substantial band-bending at the photocatalyst-electrolyte interface, leading to the formation of a Schottky barrier that impedes electron passage to the reaction sites of surface from the bulk. Efforts have been made to boost performance in hydrogen evolution. Thus, it is considered that modifying the production technique to lower the defect density in d^0 (oxy) nitrides materials is a powerful technique to boost photocatalytic activity [188].

1.4.2.4.2. Ta_3N_5 Metal nitride semiconductor photocatalyst

Ta_3N_5 is regarded as the most effective catalyst for water splitting, pollutant degradation and CO_2 reduction because of its suitable bandgap (2.1 eV). It has a strong visible light absorption wavelength of 600 nm [189]. Since 1972, ingenious research has emphasised TiO_2 capability to break down water under solar irradiation. Additionally, several photocatalyst materials have been investigated such as $SrTiO_3$, CdS, GaN, and Ge_3N_4 for water splitting. Despite this, many of these materials have band gaps that can only absorb ultraviolet light,

which accounts for just about 10% of the light that hits the earth's surface compared to about 40% and 50% for visible and infrared light, respectively [190, 191]. Therefore, a band gap that's able to absorbing visible light is required of a good photo-electrode material. Two, it must have valence and conduction band edges that exist across the oxidation as well as reduction potentials of water; three, it must be stable under water splitting circumstances; four, it must include no harmful substances; and five, it must be cost-effective. Research into tantalum nitride (Ta_3N_5) has been intense since it was first described in 2002 as a material with solar water splitting potential. Ta_3N_5 has an absorption edge at 610 nm and a band gap of 2.1 eV, it can absorb light from the visible spectrum (380-750 nm) [192]. Researchers are intrigued by Ta_3N_5 due to their excellent conduction and valence band edges, which allow it to perform both half processes (oxidation and reduction of water) concurrently. However, despite these benefits, the material's weak durability under water splitting circumstances and poor photovoltaic performance are major drawbacks. An oxide layer one nanometer thick forms over the exterior of the material under water splitting conditions, which has been connected to these problems [193]. The entire photocurrent of Ta_3N_5 water splitting devices is lowered as a result of this photo-oxidation byproduct. Isolating the Ta_3N_5 electrode from H_2O or stabilising it with hole storage layers are two approaches that have met with mediocre results. Numerous strategies for enhancing Ta_3N_5 photocatalytic activity have been investigated by scientists. These include nanostructuring, dopant inclusion, multilayer films, co-catalysts, and sensitization. Doping and sensitization are looked at as the best way to regulate and enhance the photocatalytic activities of Ta_3N_5 [194].

1.5. Techniques to increase the photocatalytic efficiency of the Photocatalyst

The electron in the photocatalyst VB becomes excited when it is exposed to the light photon flux, absorbs the energy of the flux to the photocatalyst's band gap, and then goes towards the CB, but the h^+ remain in the VB. Figure 1.10 depicts the four main steps that typically make

up a photocatalytic reaction. The following stages are involved: (i) light absorption and coordinated activation of the photocatalyst; (ii) the creation of excitons (e^- & h^+ couples); (iii) segregation and transport of excitons to the surface; and (iv) the participation of excitons to redox reactions at surface [195]. Recent studies have concentrated on generating new photocatalysts that can capture solar energy over a broad spectrum of light, improving the population and quality of catalytic sites, and separating excitons at the interface and in bulk by employing a variety of photocatalyst designs and controls. Therefore, in order to make the most of solar light, it is necessary to simultaneously address broadening the producing reactive sites, optical response and developing routes for efficient separation of excitons.
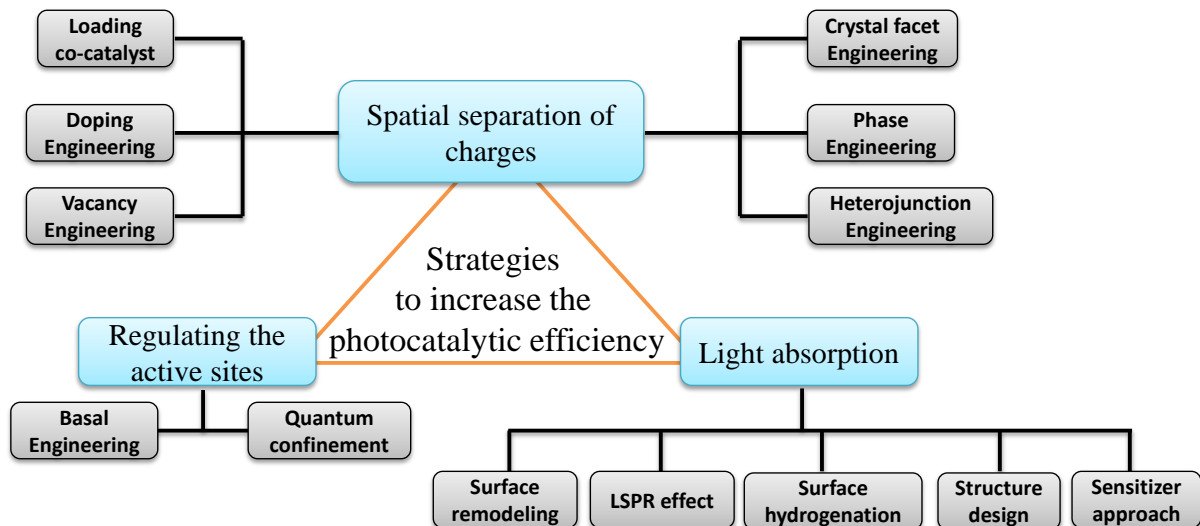
Fig.1.11 Schematic diagram of different strategies to increase the photocatalytic efficiency [196, 197]

- ➢ **Spatial separation of excitons**

- ➢ **Regulating the active sites**

- ➢ **Increased optical absorption**

1.5.1. Excitons are separated spatially

The rate of e^-/h^+ pair separation is crucial to the photocatalytic efficiency. The photocatalyst is excited by the energy of incident photon flux in femtoseconds (fs) to picoseconds (ps), and

the photo-induced carriers of charge travel to its respective bands in nanoseconds (ns) to microseconds (s) before arriving at the surface and participating in the redox reactions [198]. However, e^-/h^+ recombination with the bulk is likely to occur during transit or at the surface of catalyst, causing heat to be released. Excitons recombine considerably more quickly than they are transferred to the catalyst's surface, where they take part through reduction and oxidation reactions, on a time range of picoseconds to nanoseconds. Loading co-catalyst (i.e. doping, vacancy engineering, crystal facet engineering, phase engineering, as well as heterojunction), regulating the sites that are active (basal engineering, quantum confinement effect, single atom photocatalysts), and increasing optical absorption (surface remodelling, SPR effect, surface hydrogenation, and SPR) are the examples of methods that have been explored to increase the distance between the charge carrier and thus increase the photocatalyst efficiency [199]. This section will go into further detail about them.

1.5.1.1.Co-catalyst being loaded

The photocatalytic activity is enhanced by loaded the co-catalyst, which increase the separation and transmission of charge carrier. To avoid recombination with the VB holes, electrons produced by photosynthesis in the catalyst's CB can be efficiently transported to the co-catalyst [200]. It is important to note that strong carrier transportation requires close interaction with the catalyst and co-catalyst. The co-catalyst acts as an e^- sink to improve charge separation at the interface when charges are introduced. The co-catalyst part in kicking off electron and hole dissociation can be broken down into two parts: (i) by placing the metallic co-catalyst on top of the photocatalyst, a Schottky heterojunction is created, which generates an electric field and improves charge separation. To increase the quantity of electrons contributing to the process, the photocatalyst must generate a Schottky circuit, which prevents electrons from returning to the CB [201]; (ii) to accommodate the

photocatalyst's electrons, the semiconductor co-catalyst with narrower band gaps forms a heterostructure analogous to a type I heterojunction, which enhances charge separation. The unusual metallic and semiconductor structure of transition metal dichalcogenides has made them a promising candidate for use as co-catalysts to improve electron and hole separation. Previous studies have used several metal co-catalysts to enhance the photocatalytic efficiency of photocatalysts. Among these catalysts, silver (Ag) and platinum (Pt) have been the most often utilized co-catalysts. Zhu et al. investigated the effect of the Pt co-catalyst size on the produced H_2 by the g-C_3N_4 photocatalyst [202]. Under visible light irradiation, the photocatalytic findings revealed that the best samples contained 0.1 weight percent of Pt co-catalyst, which produced a maximum H_2 output of $473.82 \mu mol g^{-1} h^{-1}$. Increased light absorption, rapid exciton separation and transmission, and an abundance of active sites were all hypothesised to be responsible for the improved photo-activity. Camposeco et al. [203] looked at how adding an Rh co-catalyst improved the performance of Cu-doped TiO_2 photocatalysts for the production of H_2, using Pt as a co-catalyst, evolved 9260 $\mu mol g^{-1} h^{-1}$ of hydrogen from a H_2O-CH_3OH mixture when exposed to 254 nm light. Enhanced light absorption volume, a decreased photonic slit, and barrier to charge unification were cited as the reasons for the increase in H_2 evolution activity. To demonstrate its enhanced H_2 development ability under visible irridiation, CoP QDs loaded as co-catalyst onto CdS nanorods by Sun et al. [204]. The vast majority of the research done on co-catalysts focuses on those derived from transition metals rather than precious metals. Using NiO as a model, Liu and colleagues developed a highly effective g-C_3N_4 photocatalyst that has been altered with NiO as a co-catalyst. The photocatalytic evolution of hydrogen activity was increased accordingly of the creation of C-O-Ni bonds, which produced an abundance of active sites that facilitated absorption of light and the couples of electron-hole separation. Under visible light irradiation, a scavenger rummaged h$^+$ from the VB of g-C_3N_4, while

photo-generated in the CB of g-C$_3$N$_4$ migrated to the NiO to participate in the reduction reaction [205]. MXene and other transition metal carbides have gained popularity as co-catalysts due to their fast photoelectron extraction rates. For example, Li et al. ensure effectively produced MXene QDs and coupled them with g-C$_3$N$_4$ to serve as a supernumerary for costly metal co-catalysts. MXene QDs improved charge carrier transport by increasing density and surface area of active sites. MXene has been studied extensively for its potential equally a co-catalyst to improve photocatalytic enactment, but its inexpensive and limited synthetic ways, poor stability in acidic conditions and multifaceted experimental requirements prevent its wide-scale implementation [206].

1.5.1.2. Doping

Another useful strategy for enhancing e$^-$/h$^+$ pair separation is the introduction of extrinsic defects within the crystal structure of photocatalysts throughout their modification. Once elements are doped into a photocatalyst's framework, impurity states are often created in the optical band gap, hence decreasing charge recombination as shown in fig. 1.12. Some studies found that doping actually hinders photocatalytic activity by serving as a recombination centre for excitons. Doping elements can be introduced to photocatalysts in a few different ways: (i) in the synthetic process, when the dopant precursors and photocatalyst precursors are mixed together; (ii) by annealing the original catalysts in the presence of dopants vapour form; and (iii) by a method of ion implantation that permits precise regulation of the dopant concentration [207]. To sum up, the properties of host photocatalysts are highly sensitive to the amount and kind of dopant used. In order to increase the optical responsiveness and facilitate the separation of excitons, photocatalysts typically have metals and non-metal dopants inserted into their lattice. Here we shall discuss (i) doping with elements other than metals, (ii) doping with metals, and (iii) co-doping.
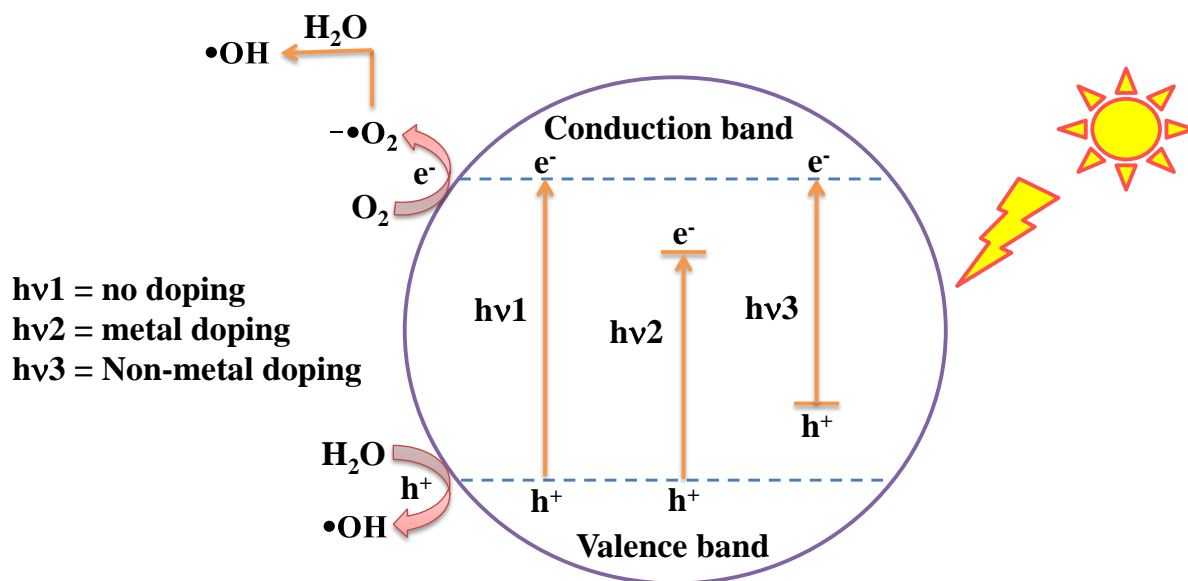
Fig. 1.12 Schematic representation of the photocatalyst without doping or doping with metals and non-metals [208]

1.5.1.2.1. Non-metal doping

Carbon C, oxygen N, nitrogen N, boron B, sulphur and fluorine F are just few of the non-metals that have been reported to be doped into photocatalysts in the extensive literature [209]. When non-metal ions are injected above the VB of the photocatalyst, the separation of e^- h^+ couples, optical harvesting, and electrical conductivity are all enhanced. Hydrothermal synthesis was used by Prabakaran et al. to create nitrogen-doped ZnO nanoparticles. An N-doped ZnO photocatalyst outperformed pure ZnO in terms of light capture efficiency and surface area [210]. The development of defects owing to N doping into the ZnO lattice was credited with the enhanced optical responsiveness. Bento et al. used the MOCVD method to successfully prepare S-doped TiO_2 thin films as a photocatalyst. X-ray photoelectron spectroscopy (XPS) demonstrated that oxygen vacancies were formed once Ti^{+4} ions were replaced with S^{+6} for modification the host TiO_2 electronic characteristics. Furthermore, S^{+6} ion doping into the TiO_2 lattice resulted in impurity amounts above the VB, which minimized

the band gap [211]. Doping of sulphur into TiO$_2$, then, suppressed charge recombination while simultaneously expanding the optical absorption spectrum of material. The photocatalytic capacity of TiO$_2$ was similarly enhanced through the addition of N dopant and Ti ions [212]. Similarly, ZnS can effectively limit the oxidation capacity of holes and restrict the recombination manner of charge carriers to diminish the photocorrosion of ZnS after the doping of N [213]. Since N-doped ZnS had a rather rough surface, it was able to offer an extensive amount of active sites to redox processes. Similarly, doping non-metals into metal oxides can increase the ability to separate of photoinduced excitons. In contrast to pure WO$_3$, the amount of electrons is reduced when the surface is doped with sulphur, as demonstrated by Li et al. [214]. The DRS findings recommended the structure of the charge relocation mechanism and quantum confinement process was responsible for the enhanced optical absorption in S-doped WO$_3$. In addition, the formation of highly charged oxygen vacancies improved the electron transport and oxidative capability, leading to greater e$^-$ h$^+$ pair separation and, ultimately, greater photocatalytic activity. To create S-doped hollow TiO$_2$ nanoparticles, Chaudhuri et al. took a unique approach, using a sacrificial core strategy where the outer layer gets doped with S by substituting O throughout the core removal procedure [215]. The newly created hollow doped nanoparticles have a narrow band gap (2.5 eV) and a better specific surface area (318.11 m^{-2} g^{-1}) than solid nanoparticles (3.2 eV and 130.94 m^{-2} g^{-1}, respectively). As a result, the particles have impressively high photocatalytic activity, superior photostability, and have a good potential for the environmental application. The reduction of band gap from 3.2 to 2.5 eV with sulphur doping of TiO$_2$ improves its performance as a solar-powered photocatalyst. Non-metal doping using S or N is commonly used in visible-range photocatalytic applications. Umebayashi et al. reported that, like in the case of TiO$_2$, a significant red-shift of the absorption edge is induced by replacing S for O (anionic doping). Ab initio band calculation reveals that the intercourse of S 3p states through

the valence band causes a rise in the VB, decreasing the band gap [216]. To generate a unique mid-gap level exceeding the valence band, a different, more hypothetical approach uses the orbitals of the dopant atoms.

1.5.1.2.2. Metal doping

Various lattice of photocatalyst has also been widely employed to incorporate other metal ions, including Ag^{+2}, Au^{+2}, Cu^{+2}, Fe^{+3}, V, Nb, etc., to control their electrical characteristics and boost the photocatalytic activity intended for various photocatalytic applications [217]. Photocatalytic activity used for hydrogen evolution, for example, Vaiano and team synthesised nanoparticles of Cu-doped ZnO. The results demonstrated that compared to pristine ZnO, the optical absorption range were greatly increased by Cu doping in the lattice, and the recombination of e^-/h^+ pairs was prevented [218]. In addition, ZnO doped with Cu photocatalysts showed remarkable photostability. Another common method for enhancing photocatalytic performance is to incorporate silver into the photocatalyst structure. For instance, Sumadevi and colleagues used a co-precipitation method to create Ag-doped ZnS nanoparticles. X-ray diffraction analysis revealed that Ag-doped ZnS had smaller crystallites than pure ZnS. Adding Ag to ZnS caused a change in blue shift in the optical absorption edge of the material outstanding to the confinement effect of excitons, resulting into better charge separation and change in the band gap energy [219]. Absorption of light is shifted toward the red because of Fe doping performances as trapping sites, which slow the recombination rate of e^-/h^+ pairs. To examine the effect of Fe doping on the optical and photocatalytic properties of $g-C_3N_4$ Ma et al. synthesized $g-C_3N_4$ doped with Fe photocatalyst. The DRS findings designated that the electrical characteristics of $g-C_3N_4$ are tuned to exhibit high light absorption once Fe is introduced into the lattice. In addition, PL analysis demonstrated that Fe^{+3} cations acted by way of charge trapping sites, postponing recombination of charges. Fe

doped g-C$_3$N$_4$ also demonstrated high stability after repeating the experiments upto five cycles [220]. In photocatalyst, doping with Au has been demonstrated to increase both the absorption of light capacity and the separation of charge carrier. Wang et al. used two simple methods to manufacture Au-doped CdS nanorods. Their photocatalytic activity was greatly improved, and they were extremely stable, thanks to the self-reduction of Au^{+3} and the surface plasmon resonance effect. Nanorods with typical dimensions of 0.5-3 m in length and 50-100 nm in diameter were successfully formed, as shown by SEM and TEM examinations. In comparison to the 14.2 ns average lifetime for charge carriers in pure CdS, 3 wt% Au doped sample had the lower recombination rate of charge carriers. It was further confirmed by EIS Nyquist plots that the CdS doped with 3% Au photocatalyst had the lowest interfacial charge transfer opposition [221]. The use of Nb as a dopant to boost photocatalytic activity has been found to have great potential. Since Nb can replace for Ti^{4+} cations in the TiO$_2$ lattice, it can effect the formation of Ti^{3+} cations and oxygen vacancies, which in turn boosts the photocatalytic activity of the TiO$_2$ by increasing its electron-hole split-up efficiency, internal quantum capacity, and charge transfer efficiency [222]. By introducing Nb dopant into the Ta$_3$N$_5$ lattice, Truc et al. were capable to increase the photocatalytic activity of the material by increasing the separation of electron-hole pair. This was achieved due to the fact that Nb dopant introduced into Ta$_3$N$_5$ lattice reduced the band gap energy of Ta$_3$N$_5$, which in turn improved the electron hole pair split-up efficiency, reduced the chance of recombination of the generated electrons and holes [223].

1.5.1.2.3. Co-doping

While investigating ways to boost the photocatalytic efficiency of photocatalysts, co-doping has received as much attention as single-element doping. Element types in co-doped compounds might be the same or different (one metal and another non-metal) [224]. In

general, doping photocatalysts with many elements is more effective than doping them with a single element since it allows them to circumvent more limitations. In the context of photocatalysts, co-doped elements serve two distinct purposes: (i) one element turns to manipulate the host band structure, and (ii) another element either facilitates the introduction of the exchanged element into the structure of the host, or recompenses for charge mismatching throughout aliovalent doping. Mid-gap impurity levels may be established by doping with S, Fe, P, C, etc., and may be their action as recombination centres to boost exciton recombination [225]. Phosphorus, sodium, chlorine, and other elements with large ionic radii tend to accumulate in the interstitial sites. Depending on the Mullekin electronegativity of the substituted dopants, the CB maxima of photocatalysts may be pushed up or down [226]. Co-doping with non-metal compounds has been widely studied in order to get a high synergistic influence on a photocatalyst. Farahdian et al. used sulphur and nitrogen co-doped elements to make N, S- doped TiO_2 and N, S- doped ZnO materials, in addition to compound photocatalysts. The photocatalytic effectiveness improved as a result in the reduction of the optical band gap brought about via the introduction of new intra-gap intensities above the VB, which expanded the photocatalyst's capacity to absorb visible light [227]. Similarly, Yao et al. revealed that co-doping g-C_3N_4 with metal cations Ag and B increases its photocatalytic efficiency. By creating faulty sites to serve as trap centres, B dopants enhanced charge carrier separation and conduction. Co-doping g-C_3N_4 with B and Ag increased its surface area, leading to a greater concentration of active sites, and pushed the wavelength range across which it could absorb light. Furthermore, the synergistic action of B and Ag was observed to cause a positive shift in CB maxima of g-C_3N_4, which successively enhanced the photocatalytic activity [228]. Extensive methods and research have shown that by mixing TiO_2 with non-metals and metals, an extremely efficient and visible light active photocatalyst may be produced. Co-doping a non-metal with a metal can boost

photocatalytic activity while keeping the structure as stable as possible. Introducing a cationic pair to bulk TiO_2 dopants has been found in recent studies to boost photocatalytic activity while decreasing structural variability [229].

1.5.2. Controlling the active sites

Redox reactions take place at specific areas known as active sites in photocatalysis. As a result, the amount of active sites is directly correlated with photocatalytic efficiency. In general, there are two basic methods to increase the quantity of active sites: the effect of quantum confinement and basal engineering [230]. In order to improve photocatalytic efficiency, we will discuss the use of these two methodologies in this section.

1.5.3. Improved photosensitive absorption

Although specific photocatalyst could control their optical sensitivity towards the visible area of the solar spectrum, designing a photocatalyst proficient of harvesting the solar light from the UV all the way through the visible and also the near infra-red part of the solar spectrum remains a significant challenge. A flat and uniform surface cannot show a better light absorption capability since most irradiation light will be reflected off. On the other hand, rough surfaces are able to scatter light effectively, that it is trapped for an enough long time [231-233]. In order to function as a photocatalyst, a photoactive material must be able to absorb light and transform it into usable chemical or electrical energy. Experiments with a wide range of typical photoactive materials have revealed that these materials are selective in the light they absorb, leading to a narrow spectrum of radiation. Decreased TiO_2 (in the presence of Ti^{3+} cations and oxygen vacancies), also acknowledged as black Titania, and has been used to increase optical absorption with a change in red shift in the absorption edge just before the IR region [234]. The bandgap of a semiconductor material is well-known to have a

significant impact on the absorption of incident photons. And by utilising cocatalysts, creating composites, and doping with appropriate materials, it is possible to modify the photoactive material bandgap. Its size can be altered by changing the intensity of the incident radiation. To supply charge carriers for photochemical processes, a catalyst needs to have the right redox potentials in addition to the optical qualities we've just covered. Because water reflects light and has an absorption coefficient that isn't zero (at wavelengths over 600 nm), photochemical reactions in aqueous media may result in substantial photon absorption, making it necessary to have the photo absorber or catalyst to grab the incoming photon [235]. While it is possible to tune the optical response of some photocatalysts such that they are more active in the visible portion of the lunar spectrum, it remains a formidable task to create a photocatalyst that could absorb all wavelengths of solar radiation. Since most irradiation light will be immediately reflected off of a smooth and uniform surface, such a surface cannot demonstrate a greater light absorption capability. On the other hand, rough surfaces are able to disperse light effectively, which leads to light being trapped for an extended amount of time. Therefore, the light utilisation capacity may be improved by extending the range of the scattering effect by altering the catalyst surface [236]. The optical absorption capability of photocatalysts could be enhanced using the subsequent methods:

1.5.3.1. Structure design

The photochemical process begins through adsorption of H_2O molecules on the photocatalyst surface. Most crucial is the rate at which water molecules are adsorbed on their surface nature, and wettability. The photocatalytic processes occur through the participation of free charges generated in the photocatalyst via quantum-mechanical transition of electrons into a mobile state by annihilation of the absorbed photons. As these free charges that diffuse toward the materials surface, they can then start the redox reaction between the adsorbed

reactants on the surface of photocatalyst [237, 238]. Adsorption on the catalyst surface is facilitated through lattice defects (vacanscies, interstitial defects, and antidefects) present in crystal. To improve a photocatalyst performance, current research has highlighted the significance of taking into account crystallinity, particle size, and surface-to-volume percentage. Maximum photocatalytic performance has been achieved by optimising the rational structural design such as photocatalyst size, band gap energy, and recombination of charge carrier. Additionally, the crystallinity of photocatalyst material was improved by reducing the density of structural defects through calcination improving the charge transfer [239]. In a similar vein, a greater concentration of active sites, as provided by a larger surface area, enhance the adsorption of reactants, speeding up the reaction. However, free electron-hole pair recombination is more likely to occur at sites with a greater surface area. As a result, large surface area increases the photocatalytic performance [240]. When a particle adsorbs on a solid surface it is going to alter the zeta potential (ZP) of the solid surface [241]. ZP is among the most accessible analytical techniques to report the surface net charge indirectly, however surface charge is the density of charge on the particle surface, whereas ZP is the strength of particles shear plane during electrophoresis. The photocatalyst adsorption property is affected by its zeta potential or surface charge [242, 243]. It is crucial to consider that the adsorption quality of a catalyst is enhanced when it has a porous surface area, which is created during the synthesis process, rather than having a smooth surface. Higher adsorption and photocatalytic activity have been suggested by numerous studies of pore volume and simultaneously increased the surface area [244]. Photoelectrochemical water splitting using mesoporous (pore size 9.0 nm) hematite (α-Fe$_2$O$_3$) has been shown by Sivula et al. to be more efficient than using a non-porous hematite electrode [245]. A large surface-volume ratio, distinct optical and carrier mobility characteristics, and a core-shell and hierarchical shape are all hallmarks of photocatalyst structures designed with these features in

mind. Therefore, in this part, we will examine how core-shell structures and hierarchical structures can improve photocatalytic performance.

1.5.3.1.1. Core-Shell design

When trying to create a highly effective photocatalyst, overall core-shell nanostructure is by far the most popular choice for the structure design method. Core-shell structures play an important part in improving photocatalytic efficiency by doing the following: (i) preventing corrosion or undesirable aggregation throughout photocatalytic reactions; (ii) activating distinct optical characteristics; (iii) the interaction between core and outer shell layers offers charge carriage channels and encourage localized surface plasmon resonance (LSPR) effect; (iv) constructing ploy-functional materials. Photocatalyst stability is much improved when it is prepared with a core-shell configuration. The shell, whether they are yolk-shell, dual-shell, core-shell, and hollow shell, could be constructed on photocatalytic material [246]. The possible shape for Cores may exist in the form of nanotubes, nanoparticles, or nanorods. Additionally, complicated core shell structures have been built due to its enormous surface area, high compacted diffusion pathways of carriers, density of catalytic sites, and improved accessibility to reactants, a photocatalyst having hollow spheres has been the subject of extensive research. There are two basic methods used to make hollow spheres: without a template and with the aid of a template. Several researchers have discussed the advantages of using a core-shell structure to create a high-performance photocatalyst [247]. Another significant hurdle that must be overcome in the photocatalytic process is maintaining the stability of the nanoparticles photocatalyst. During the synthesis and photocatalytic reaction, a particle with smaller in size has higher-surface-area with significant porosity and strong stability. The catalyst structure offers advantages, such as stabilising nanoparticles inside the shell to maintain the activity of the catalytic sites.

1.5.3.2. **Sensitizer methodology**

Introducing photocatalysts with a narrower photonic gap, such as quantum dots, is a key technique for increasing the photocatalyst optical response time. The optical absorption range can be efficiently expanded by constructing a heterojunction between the photocatalyst and the sensitizer. The band gaps of the photocatalyst and sensitizer, as well as their capacity to separate charges, affect the photocatalytic efficacy of the sensitised composite. One study showed that sensitising ZnO with CdS increased its ability to absorb light, which in turn improved its photocatalytic efficacy [248].

1.5.3.2.1. Sensitization/Protection with Polymer (PANI)

Several research studies have linked Ta_3N_5 with former semiconductors, like as Co_3O_4, Ag_3PO_4 and Bi_2O_3, to generate complexes with the goals of further increasing charge transfer productivity and preventing from own photocorrosion of Ta_3N_5 [249, 250]. The photogenerated charge carriers of Ta_3N_5 may be excited to its surface, where the connected semiconductor could function by way of a charge acceptor to boost the composite photocatalytic activity. In order to increase the photocatalyst efficiency and stability, photocatalysts such as carbon composite, CdS, TiO_2, and Fe_2O_3 sensitized with conducting polymers conjugated electron systems for example polypyrrole (PPy), polythiophene (PTs), and polyaniline (PANI) [251]. The polymers high mobility of charge carriers, great optical absorption characteristics, and superior environmental stability made them ideal for this application. To increase the photocatalytic activity of a photocatalyst, an outer layer of suitable conducting polymer can be placed on its surface.

1.6. Miscellaneous features (photo stability)

A catalyst chemical stability is essential for maintaining a constant rate of photocatalytic H_2 production. Photocatalyst can't undergo photocorrosion, wherein they break down under the exposed of light because of electron consumption during self-photo-oxidation or self-photoreduction. Despite the lack of hole scavengers (i.e., ethanol and Na_2SO_3), Toe et al. observed photocorrosion of Cu_2O converted into CuO due to self-oxidation (Cu_2O converted into CuO) [252]. Ning et al. reviewed the likely tactics implemented to improve the photostability of CdS for effective photocatalytic reactions and the relevant mechanisms of photocorrosion of CdS [253]. Following is a detailed discussion of the role of photon-induced holes, sulphide anion (S^{2-}/S or S^{2-}/SO_4^{2-}), and dissolved oxygen.

$$CdS + 2h^+ \rightarrow Cd^{2+} + S \tag{1.7}$$

$$CdS + 4h^+ + 2H_2O + O_2 \rightarrow Cd^{2+} + SO_4^{2-} + 4H^+ \tag{1.8}$$

$$CdS + 2O_2 \rightarrow Cd^{2+} + SO_4^{2-} \tag{1.9}$$

Both prolonged reaction time and numerous reaction cycles using the identical catalyst have been studied to learn more about its long-term stability. Shibli et al. have demonstrated that the rearrangement of Mn centers in $MnCo_2O_4$ nanoparticles during a photochemical reaction decreases their photocatalytic ability, which contradicts their effectiveness in splitting water in a single cycle. After each cycle, the powder catalyst was dried and re-heated to 470 °C to restore its previous level of activity [254]. Recently, Gogoi et al. used Ag-doped TiO_2 nanoparticles for photocatalytic H_2 generation and reported almost no efficiency reduction after three consecutive cycles [255].

Summary

Chapter 1 (page no. 1-65)

Introduction to current scenario of energy & environmental issues in the world, present remedial technologies used for taking care of these issues and importance of photocatalysis were discussed. The detailed mechanism of Photocatalytic hydrogen evolution and CO_2

reduction through water splitting were also explained. There are several semiconductors which have been reported as photocatalysts so far. However, uncontrolled charge recombination which reduces the quantity of active species is the major drawback for using these photocatalysts. As reported by Kanhere et al. 2014, this can be overcome by using complex oxide structures as photocatalysts [256]. The existing complex oxide/sulphides/nitrides type semiconductors photocatalyst and their drawbacks were listed and discussed. The importance of photocatalysts structures and their photocatalytic properties were reported. There are several strategy discussed above in regards to increase the efficiency of photocatalysts. Doping/codoping of elements with different ionic radii (metal/non-metals) has an adaptability to maintain the structure. The bandgap and band edge potentials can be altered without affecting its structure by doping with different elements. The defective sites after doping different elements can act as active centres to reduce charge recombination. In this form it reduces the recombination rate by separating the charges and also supplies additional charges to photocatalysts for enhancement of efficiency of photocatalytic properties. Another important issue is availability and cost-effectiveness. Vanadium (V), niobium (Nb), and tantalum (Ta) are transition metals from group fifth. Nb and V are extensively distributed in Earth crust, but there are few concentrated deposits of these elements. Tantalum is less abundant in the Earth crust it occurs in the same minerals as niobium. Complex tantalum nitride can be synthesized by facile hydrothermal methods by using tantalum oxide precursor. Most importantly they are visible light active materials due to their narrower bandgap and can be used under sunlight irradiation. Because of these factors, in this work tantalum nitride based composites photocatalysts are synthesised. They are modified to be visible light active by doping/codoping also by employing carbon as a supporting material to increase the surface area for the maximum absorptions of light irradiations. PANI was also used in this work to protect the synthesized materials from self-

photocorrosion which leads to advance the photocatalytic activity of materials. Finally the composite was used as photocatalysts for hydrogen generation and reduction of CO_2 through water splitting.

The main objective of this research work is to rationally design and fabricate an efficient novel co-doped Ta_3N_5 immobilized with carbon based materials for combination with a suitably sensitized with PANI based photocatalyst for effective visible-light-driven overall PC water splitting. This study finding might provide worthwhile information for future efforts to develop visible-light-driven photocatalysts for use in cleaning up polluted environments. The outcomes of the present investigations and its future prospects are presented in the subsequent chapters.

Chapter 2 (page no. 66-114)

This chapter provides an overview of research studies carried out on PC water dissociation systems. First, it introduces the basic concepts and operation of PC water splitting system that employs semiconductor-based photocatalyst. This chapter also ventures into the current development of metal nitride (Ta_3N_5) photocatalyst specifically, which includes insights into its synthesis and surface modification strategies. Furthermore, the literature review also addresses the research progress on Carbon based materials with a specific focus on the wide range of material improvement strategies used. This chapter also further scrutinises the development of the photocatalyst system and Photoreactor design, covering its fundamentals in system configuration. Photocatalytic water dissociation is a reliable alternative method to harvest renewable hydrogen to address the world energy crisis and environmental pollution. The state-of-the-art regarding water splitting and carbon dioxide reduction and recent research approaches are provided. Since the pioneering works by Fujishima, Honda on solar water splitting and carbon dioxide reduction by semiconductor photocatalysts several semiconductor photocatalysts have been developed to produce photocatalytic H_2 and CO_2

reduction.

Chapter 3 (page no. 115-132)

Chapter 3 deals with all the characterization techniques used and synthetic methodologies employed in the present investigation. The compounds reported in this study are synthesized by solid-state reaction method from precursor salts, such as, metal oxides, carbonates, or oxyhalides. This chapter also gives a detailed discussion about various synthetic procedures e.g. hydrothermal syntheses involved for the synthesis of photocatalysts. The entire course of synthesis and formation of products are monitored via X-ray diffraction (XRD) analysis. The morphological, compositional and fundamental details of the compounds are explored through energy dispersive X-ray spectroscopy (EDS), field emission scanning electron microscopy (FE-SEM), and UV-visible diffused reflectance spectroscopy (UV-Vis DRS) is used toward study the optical properties of the compounds. The detailed analysis of the recombination of charge carriers and their lifetimes are investigated by photoluminescence (PL), electrochemical impedance spectroscopy (EIS) techniques. The experimental details of photocatalytic water splitting of the compounds of interact under solar irradiation or 80 W bulbs (visible light) are given in this chapter. The details of all the techniques and instruments utilized with methods of sample preparation for the analyses are discussed in this section.

Chapter 4 (page no. 133)

This chapter includes the development of the nanocomposites photocatalysts Ta_3N_5/BSC@PANI, V@S-Ta_3N_5/PANI and Nb- Ta_3N_5/PANI via hydrothermal, sol-gel and chemisorption synthetic procedure, characterization of these nanocomposites and their use as an efficient catalyst for water splitting.

In Chapter 4 section A (page no. 133-150) the fabrication, characterization and photocatalytic movement studies of cost-effective, most stable and eco-friendly Ta_3N_5/BSC@PANI nanocomposites are described. The composite was synthesized by

utilising the waste/biomass of peanuts shell into useful carbon. FE-SEM and studies confirm morphology with homogeneous distribution of the constituent elements. The EIS and PL analysis suggest suppression of photogenerated electron-hole recombination. The photocatalytic bustle studies of the compounds for water electrolysis under visible-light irradiation. The reusability and stability of the photocatalysts are probed for six cycles of H_2 production.

Section 4 (B) (page no. 151-170) in this chapter, the development of a cost-effective, stable and eco-friendly co-doped V@S-Ta$_3$N$_5$/PANI nanocomposites and their photocatalytic applications for HER have been discussed. The enhancement of the activity of dealloyed V@S-Ta$_3$N$_5$/PANI towards water splitting reaction has been elaborated in this chapter. The compounds are synthesized by hydrothermal and chemisorption process. The UV-Vis DRS data confirm the visible band gaps of the compounds in the range 1.56 – 2.15 eV. The catalysts reveal exceptional photocatalytic activity for H_2 generation beneath visible-light irradiation. The photocatalytic cycle tests were done to confirm the stability and reusability of the photocatalyst amount of H_2 evolution of V@S-Ta$_3$N$_5$/PANI was almost unaffected even after five cycles.

Section 4 (C) (page no. 171-172) in this chapter, we have discussd about the design of photoreactor to carry out the experimental part. The efficiency of a photocatalytic process greatly depends on factors such as the extent of optical absorption and the adsorption of reactants on the catalyst surface. Therefore, the design of photoreactors holds significant importance, encompassing aspects such as the choice and positioning of light sources, reactor configuration, and the incorporation of reflectors. The photoreactor contents should be evenly in order to provide the greatest photocatalytic results. Due to its capacity to capture more photon, larger surface area, maximum light absorption, and improved photocatalytic effects, have been the subject of substantial research in photocatalyst technology.

Section 4 (D) (page no. 173-180) in this chapter, the development of a cost-effective, stable and eco-friendly Nb-Ta$_3$N$_5$/PANI nanocomposites and their photocatalytic applications for HER have been discussed. The enhancement of the activity of dealloyed Nb-Ta$_3$N$_5$/PANI towards water splitting reaction has been elaborated in this chapter. The compounds are synthesized by sol-gel and chemisorption process. The UV-Vis DRS data confirm the visible band gaps of the compounds in the range 1.94 – 2.15 eV. The catalysts reveal good photocatalytic activity for H$_2$ generation under visible-light irradiation. The photocatalytic cycle tests were done to confirm the stability and reusability of the photocatalyst amount of H$_2$ evolution of Nb-Ta$_3$N$_5$/PANI was almost unaffected even after three cycles.

Chapter 5 (page no. 182)

The overall conclusions and future prospects of the current investigation are presented in this chapter. The work has resulted in the synthesis of new photocatalyst materials with the core shell polymer structures. The role of carbon based materials and doping/codoping with metals and non-metals, especially PANI layered structure changing composition and their effect on the light absorption and subsequent interplay in the photocatalytic activity are highlighted. Moreover, the interplay among various parameters, such as, charge carrier recombination, absorption and charge-transfer resistance, which influence the photocatalytic activity of nanocomposites are elucidated. The present work has also demonstrated an improved photocatalytic activity under visible light driven by enhanced charge carrier transport. Co-doping by the metal/non-metal (V, S) incorporated Ta$_3$N$_5$ semiconductor V@S-Ta$_3$N$_5$, visible-light focused photocatalytic water splitting has been demonstrated. Because of slow recombination of photoinduced e$^-$-h$^+$ pairs, increased charge separation, and the excellent photocatalytic H$_2$ generation from water splitting under visible-light irradiation, the nanocomposite V@S-Ta$_3$N$_5$/PANI is shown to be a promising material.

The outcomes of the present work have significant research potential for the development of

various nanocomposites layered with polymer for the photocatalytic H_2 production via water splitting under visible-light irradiation. This present work contributes to new insights in the designing of semiconductors with visible band gaps and they offer wide applications in water splitting. The main objective of this research work is to rationally design and fabricate an efficient novel co-doped Ta_3N_5 immobilized with carbon based materials for combination with a suitably sensitized with PANI based photocatalyst for effective visible-light-driven overall PC water splitting. This study finding might provide worthwhile information for future efforts to develop visible-light-driven photocatalysts for use in cleaning up polluted environments.

Chapter 2

Literature Review

2.1 Principles of Solar-driven PC Water Electrolysis/Splitting

2.1.1 General Concept of Overall PC Water Electrolysis

Similar to electricity, H_2 is a secondary form of energy where energy input is always required to produce H_2. At present, approximately 5 % of the global H_2 is produced using renewable energy sources, while the rest is still derived from fossil fuels, such as coal gasification and steam methane reforming [257]. Despite the many different feedstocks that can be used to produce H_2, such as biomass, glycerol or urea, more intensified efforts are focused on the use of water as the starting feedstock. The ideology of overall water splitting has become immensely popular as most of the aforementioned production routes for H_2 generation are still rather costly and unsustainable [258]. In this regard, electrolysis is the most commonly performed process that splits pure water molecules using electricity/photon via an electrolyzer. Although H_2 of high purity can be obtained, the application of water electrolysis to produce H_2 only covers about 4 % of the world H_2 production. Its applications are often limited by the energy-intensive process and the inefficiency of electrolyze systems

2.1.2 PC water splitting

Photocatalytic water dissociation is an auspicious alternative system to harvest hydrogen to address the world energy crisis and environmental pollution [259]. The state-of-the-art regarding water splitting and carbon dioxide reduction and recent research approaches are provided. Since the pioneering works by Fujishima, Honda on solar water splitting and carbon dioxide reduction by semiconductor photocatalysts several semiconductor photocatalysts have been developed such as TiO_2, ZnO, WO_3, C_3N_4, TaON, $SrTiO_3$,

CeO$_2$, Fe$_2$O$_3$, LaFeO$_3$, GaN, Bi$_2$S$_3$, CdS, ZnS and Ta$_3$N$_5$, etc. (Band edge position of these the photocatalyst shown in Figure 2.1) to produce photocatalytic H$_2$ and CO$_2$ reduction [260, 261]. Among them, Ta$_3$N$_5$ is an auspicious material because of its suitable electronics band levels, availability, economic viability, non-toxicity, long-term stability and non-photo corrosiveness [262].
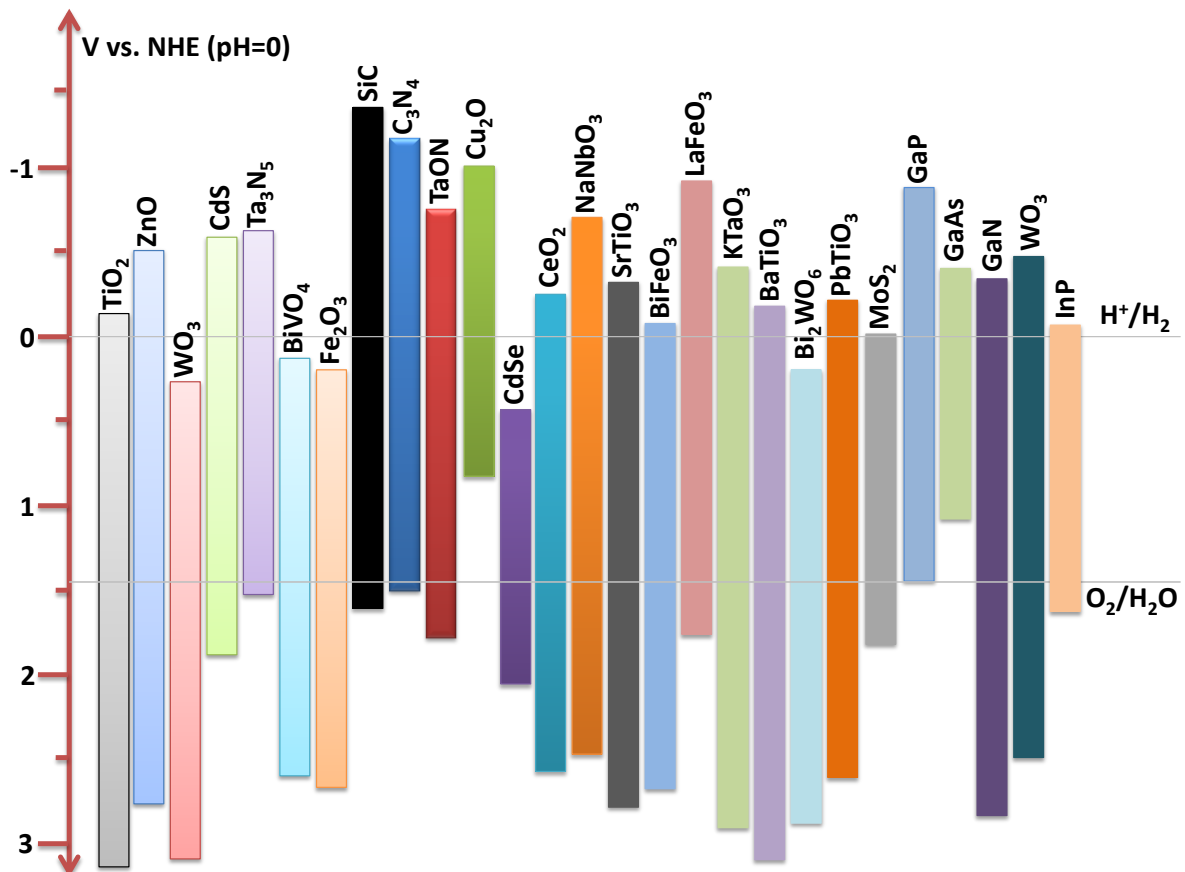
Fig. 2.1 Shows Band edge position of these photocatalyst [263]

2.2 The photocatalytic water electrolysis mechanism and associated characteristics

Figure 2.2 demonstrates a simplified representation of the water electrolysis by photocatalytic process. Absorption of light by photon energy higher than the photocatalyst's bandgap triggers the reaction. Through this mechanism, an electron gets excited to the CB from the VB, creating a VB hole in the manner. This initiation happens very quickly (on the femtosecond time scale), and it is followed by a correspondingly rapid moderation of the hole

to the base of the CB and then the peak of the VB. When charge transfer toward the surface from bulk (i.e., there is no recombination response), the photogenerated charges will perform an electrochemical reaction on the photocatalyst's surface. The oxidation and reduction reactions of H_2O are catalyzed via photogenerated holes and electrons on the photocatalyst surface.
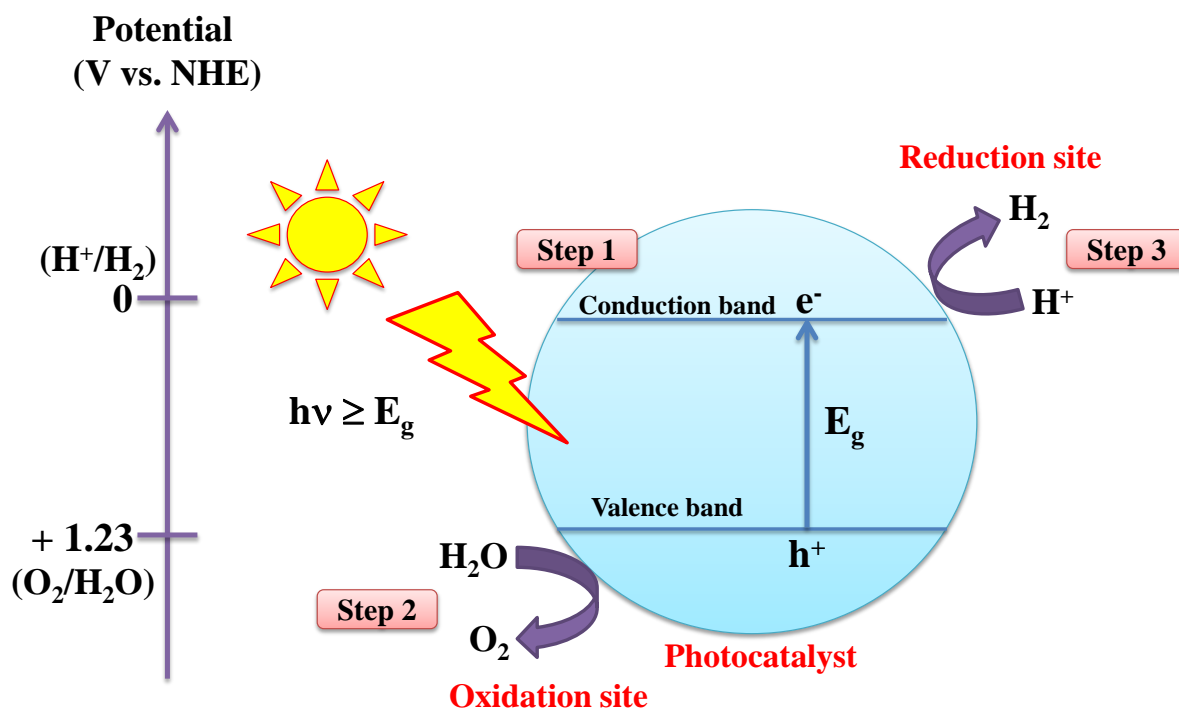
Fig. 2.2 Mechanism of water electrolysis by photocatalytic process [264]

Generally, water electrolysis by photocatalytic process undoubtedly entailed several intricate photophysical and chemical processes. Multiple steps associated with the reaction are discussed here for a comprehensive understanding of the mechanism. The following six processes classify the stages elaborate in photocatalysis for water splitting and define important factors [265].

2.2.1 Absorption of photon and generation of excitons

The development of excitons (excited electron and hole couples) is the result of the photocatalytic activity, which begins with the semiconductor absorbing a photon. Photons in a powder system will not only be absorbed, but will also be scattered, reflected, and

transmitted. Rayleigh and Mei scattering are useful for categorising light path through a particle, whereas the Fresnel equation provides a good description of light reflection off of a particle surface. Light absorption in a semiconductor sheet arrangement system is diminished by reflection and scattering [266]. As the varied semiconductor particles absorb the reflected and dispersed light, powder semiconductor systems provide further benefits in this area.

Absorption coefficient (α) is a quantitative definition of the absorption qualities of photocatalysts and is preferably measured for a semiconductor thin layer. The overall formula states as:

$$\alpha(cm^{-1}) = \ln(10) \times A/l(cm) \tag{2.1}$$

Wherever *A* is the absorbance and *l* is the path length of light passing over the sample [267].

2.2.2 Exciton split-up

After a semiconductor absorbs light, excitons are created as the following step in the process. Excitons are defined by their binding energy, which must be minimized to promote their easy dissociation [268]. The excitons, once separated, will become free charges that can be contributed to use in a photocatalytic activity.

Compared to the binding energy of a hydrogen atom, which is well-defined as the energy necessary to ionize the exciton in its lowest energy state, the gap between the series limit and the lowest bound state (n = 1) is substantially less for excitons [269]. The following equation provides a useful framework for describing it:

$$R = \frac{m^* e^4}{2h^2 \varepsilon_r^2} = \frac{E_1 m^*}{\varepsilon_r^2} \tag{2.2}$$

Wherein m^* is the abridged effective mass of the e^--h^+ system ($1/m^* = 1/m_e^* + 1/m_h^*$), *e* as essential charge, *h* as the Planck constant, and ε_r as dielectric constant.

2.2.3 Diffusion and recombination of charge carriers

After exciton separation, free carriers must go to the surface to initiate a photocatalytic process. Electron and hole mobility refers to the freedom with which electrons and holes can move within a material and transport charge [270]. The Einstein relation connects the mobility of carriers with the distribution coefficient D and the carrier lifetime [271]:

$$D = \frac{K_B T}{e} \mu \qquad (2.3)$$

$$\text{And, } \mu = e \frac{\tau}{m^*} \qquad (2.4)$$

This is the effective mass, m*, where e is the elemental charge and kB is the Boltzmann constant. Current is produced by the association of free carriers in a semiconductor. Diffusion current and drift current are typically added together to form the total current in semiconductors, as shown in the following equation [272].

$$\vec{J}_{total} = \vec{J}_{p,diffusion} + \vec{J}_{n,diffusion} + \vec{J}_{p,drift} + \vec{J}_{n,drift} \qquad (2.5)$$

$$= -qD_P \frac{dp_x}{dx} + qD_n \frac{dn_x}{dx} - pq\mu_p E_x + nq\mu_n E_x \qquad (2.6)$$

The concentration gradient of free carriers is the source of the current known as diffusion current. According to Fick's rule, the diffusion currents can be characterized by their respective diffusion coefficients (Dn for electrons and Dp for holes) and charges (q for holes and +q for electrons). Potential gradients, brought on by the electric field, lead to drift currents. Diffusion length and minority carrier lifetime are significantly correlated with the concentration and mobility of charge carriers. One of the characteristics that establish photocatalyst efficiency is the lesser carrier lifespan, or the regular duration a typical lesser carrier occurs before recombination [273]. Minority carrier is represented by n for n-type semiconductors, where holes are the lesser carrier, and by p for p-type semiconductors, where electrons are the minority carrier. Spectroscopic techniques allow for its optical or electronic measurement.

2.2.4 Charge carrier transport

After the carriers have been successfully separated and transferred, they should go to the semiconductor surface, where a redox reaction can take place. Since the main mechanism for carrier transfer in a complete semiconductor is diffusion, the carrier lifetime appears to be a powerful determinant of efficiency. When placed in contact with an electrolyte, metal, or another semiconductor, semiconductors exhibit an electric field or space charge. Band bending due to this intrinsic electric field is then used for efficient charge separation [274].

2.2.5 Efficiency of catalysis

Effective electrocatalytic processes are used to complete all of the photophysical processes on the semiconductor surface that were previously outlined. One of the most crucial factors in achieving successful photocatalytic electrolysis of water in visible light is the efficient catalyst. It is currently unclear how cocatalysts affect photocatalytic reactions whether they merely supply active sites for redox reactions or also speed up hole utilization [275]. The following is a general expression for the general redox reactions on the cocatalysts:

$$2H^+ + 2e^- \rightarrow H_2 \ (acid) \ or \ 2H_2O + 2e^- \rightarrow H_2 + 2OH - (base) \tag{2.8}$$

$E = 0 \ V$ vs. RHE

$$2H_2O \rightarrow O_2 + 4H^+ + 4e^- \ (acid) \ or \ 4OH^- \rightarrow 2H_2O + O_2 + 4e^- \ (base) \tag{2.9}$$
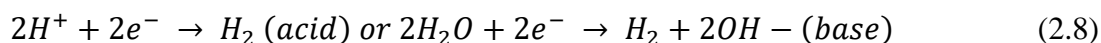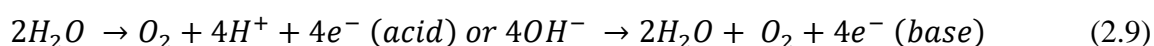
$E = 1.23 \ V \ vs. RHE$

On the surface of photocatalysts, electrochemical reactions take place at the electrocatalysts steady-state potential, which is dictated by all the previous photophysical and photochemical events. Whenever the possible shifting of the electrocatalyst immobilized on the surface of the semiconductor could be monitored, the rate of the electrocatalytic reaction itself could be evaluated distinctly by using an electrochemical technique electrocatalytic activity could be represented by the Tafel equation [276]. The following equations can be used to indicate the photoelectrochemical half reaction reaction rate, r (mol s^{-1});

$$r = \frac{i_0}{nF} exp \frac{\alpha nF(E_D - E^0)}{RT} \tag{2.10}$$

i_0 represents the exchange current density of the specified metal (in A cm^{-2}), is the transferal coefficient, n represents the number of electrons participating in the reaction, F represents the Faraday constant, ED and E0 represent the metal's Fermi level and its solution secure redox potential, respectively, R represents the universal gas constant, and T defined the absolute temperature.

Identification of diverse co-catalysts using an electrochemical method is crucial for effective photocatalytic reaction. The volcano plot of some metals for the formation of hydrogen in acidic conditions has been published by Trasatti and Norskov [277, 278]. It has been demonstrated that the free energy of H$_2$ adsorption on metals has an ideal value. For oxygen evolution catalysts, similar volcano charts have been described with a variety of thermodynamic descriptors. As a minimum scale back the usage of noble metals, current research is focused on creating the oxygen and hydrogen evolution catalyst. It has been originated that the islands of nickel (Ni) and cobalt (Co) sort on the surfaces of noble metals exhibit excellent results for both H$_2$ and O$_2$ evolution. Perovskites and other materials with assorted oxyhydroxides, such as nickel-iron, have similarly been found to function as minimal above-potential electrocatalysts.

2.3 Photocatalytic H$_2$ production and CO$_2$ reduction

2.3.1 Photocatalytic H$_2$ production

Hydrogen is produced photo-catalytically by a reduction process that ages photogenerated electrons and aqueous hydrogen ions. Photons from sunlight or artificial light are taken in by a photocatalyst. After this, electron migration after the VB to the CB is triggered, depleting the VB of its electrons and leaving behind positively charged holes. Some of the electrons at the surface might turn into a reductant to produce H$_2$, but the vast majority of them will recombine with the holes [279].

In a nutshell, here what goes on during photocatalytic hydrogen synthesis: Seven distinct

steps are involved in the transmission of excited photogenerated charges to water or other molecules or ions: (1) absorption of light on the photocatalyst; (2) creation of excited charge carriers; (3) recombination; (4) split-up; (5) migration; (6) trapping; and (7) transmission. With photocatalytic (PC) water splitting, solar energy is transformed into pure, usable hydrogen (H_2), which may then be stored for later use [280]. Several different types of photocatalysts for photocatalytic water dissociation have been studied. In the photocatalytic hydrogen evolution reaction (PCHER) system, semiconductors including metal oxides, metal nitrides, metal sulfides/metal chalcogenides, and etc. play a crucial role as photocatalysts.

By monitoring the volume of hydrogen gas over a predetermined amount of irradiation of light, the effectiveness of photocatalytic hydrogen generation may be ascertained. Hydrogen evolution is either $\mu mol h^{-1}$ or $\mu mol g^{-1} h^{-1}$, which is used to standardize the photocatalytic efficiency across different photocatalysts and setup configurations [281].

$$\text{Apparent quantum yield (AQY)} = \left(\frac{2 \times no. of\ produced\ Hydrogen}{no. of\ absorbed\ photons} \right) \times 100 \tag{2.11}$$

The efficiency is defined by the apparent quantum yield (Eq. 2.11), which, as the entire photons of the incident light are fewer than the photons that are absorbed, is an expected value that is lower than the entire quantum yield.

2.3.2 Photocatalytic CO_2 Reduction

2.3.2.1 CO_2 photocatalysis

The carbon dioxide (CO_2) emission is rising into the environment because the use of fossil fuel, there are now many concerns about global warming. In order to counteract climate change, by 2030, greenhouse gas emissions should be reduced in half, agreeing to the International Panel on Climate Change [282]. The global temperature may rise by 10-15 $^{\circ}$C and CO_2 altitudes taken in 2017 of 400 ppm (0.04%) may touch 750 ppm, according to predictions. Therefore, producing ecological renewable energy sources for managing carbon, oxidising it to release carbon dioxide, and reducing it to release valuable materials is

extremely difficult to offer clean energy. Because of its C-O bonds (C=O bond enthalpy in CO_2 is + 805 kJ/mol), linear geometry, D∞h symmetry, closed-shell electronic configuration, and Gibbs unrestricted energy of ΛG° = -394.4 kJmol^{-1}, CO_2 is a chemically steady linear molecule [283]. Therefore, endothermic processes, which demand a large amount of energy input, are the most reductive transformations from a thermodynamic perspective. In fact, considerable energy input is needed for bond cleavage during the conversion of carbon dioxide to carbon-based fuels. An increase in atmospheric CO_2 concentration and the major effects of environment change highlights the urgent need for renewable energy sources. It is acknowledged that one of the most interesting and promising study areas for solving environmental and energy issues is the solar energy convert into chemical energy by forming of methane, methanol, H_2, etc. One of the most promising solutions in this situation is the chemical reduction of CO_2. Dependent on the amount of transmitted electrons ($2e^-$, $4e^-$, $6e^-$, and $8e^-$), the reduction of CO_2 by chemically could result in a innumerable products, including carbon monoxide, HCHO, CH_3OH, and methane. From an economic perspective, CH_3OH and CH_4 are the most lucrative products. The energy needed to convert CO_2 can also come from a diversity of sources, leading to a variety of conversion processes, including either direct or catalyzed chemical, electrochemical, thermochemical, photochemical conversion and biological fixing. Surprisingly, heat or electricity is required for the operation of thermochemical and electrochemical conversion processes. Additionally, CO_2 can be converted into valuable chemicals through electrochemical processes, but doing so is expensive and impractical on a large scale due to the electrical energy needed. The process efficiency is constrained by lower efficiency and electrode stability. Photo catalytically reduction of carbon dioxide (PCCR) is superior to traditional methods of producing chemicals like CH_4, CO, CH_3OH, HCOOH, and HCHO because of its low-cost reactant (water), plentiful solar energy, eco-friendly byproducts, and nil carbon emission. Because

PCCR operates at ordinary pressure and doesn't require a lot of input energy, it is a feasible technology. Therefore, PCCR is the most effective way to address pollution-related environmental issues, control global warming, and resolve the energy crisis. One of the straightforward and practical methods that have sparked a lot of curiosity among scientists and researchers is the remarkable benefit of using photocatalysis to convert CO_2 into valuable compounds. PCCR, sometimes known as "artificial photosynthesis," is the use of a photocatalyst with reducing agents such water, hydrogen, and sunlight to reduce carbon dioxide into renewable compounds [284]. The chemical energy (energy detained in chemical bonds of molecule) in PCCR is simply converted using solar energy into useful compounds and fuels as shown in fig. 2.3.
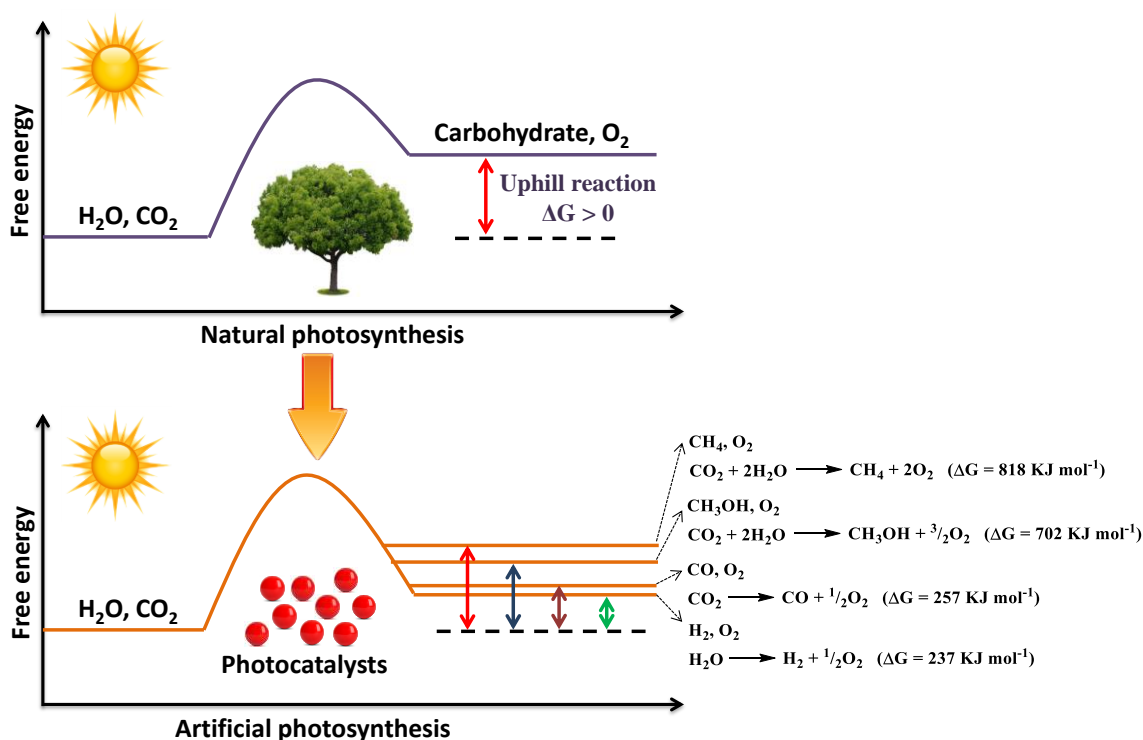
Fig. 2.3 Schematic representation of the natural and artificial photosynthetic processes [284]

The most cost-effective and environmentally beneficial method for sustainable development appears to be the creation of solar fuel through the artificial photosynthesis process from CO_2. Using semiconductor catalysts and light irradiation, CO_2 photocatalysis converts

75

collected CO_2 into chemicals and fuels. Therefore, there has been a meteoric rise in recent decades in the number of studies focusing on CO_2 photocatalytic reduction [285]. Energy for this conversion might potentially come from solar power, a sustainable and carbon-free source (see Fig. 2.4).
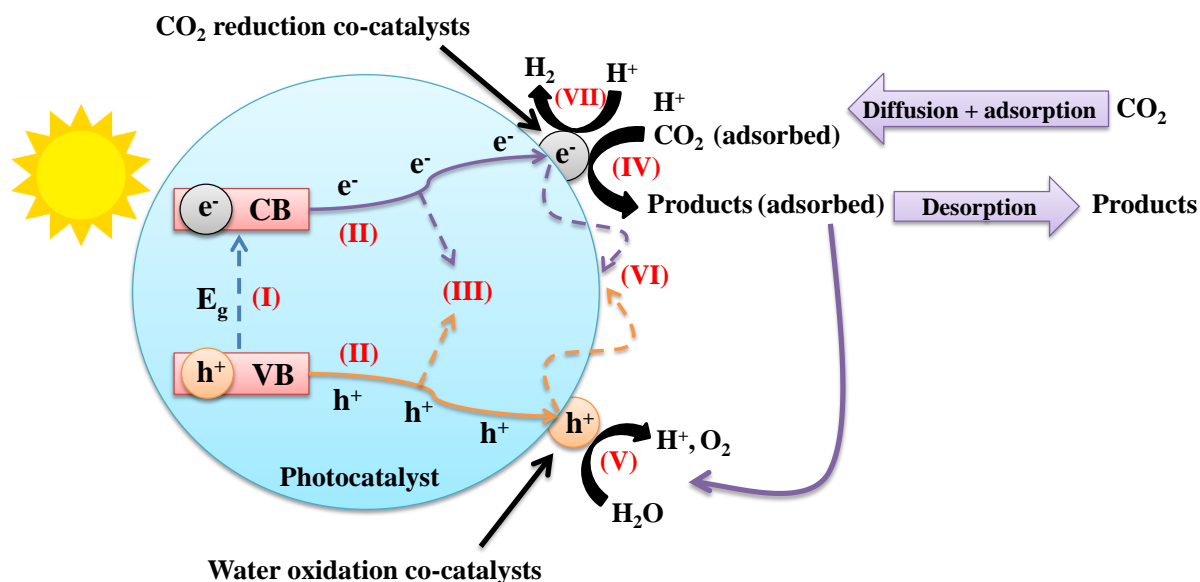
Fig. 2.4 Mechanism of photocatalytic reduction of CO_2 into valued products [285]

Energy-rich reactants, like metals or organometallic compounds, may be utilized via solar or other freely available light bases while also being better for the environment. Eq. (1) depicts a couple of electron-hole, where e^-, hv, and h^+ signify the conduction-band electron, photon energy, and valence-band hole, respectively. Eq. (2.15) expressions of the possibility of charge carriers recombining upon the surface or before the reaction with adsorbed sorts, releasing energy by way of heat or light, while Eq. (3) displays the energy of the band gap (Eg), which remains corresponding to the difference amid the energy of the conduction (Ec) and the valence (E_v) bands [286].

$$\text{Photocatalyst} \rightarrow h\nu \; e^- + h \qquad (2.12)$$

$$e^- + h^+ \rightarrow \text{heat} \qquad (2.13)$$
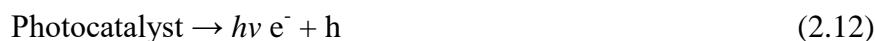
$$Eg = E_c - E_v \qquad (2.14)$$

The adsorbate species bandgap energy and potential redox levels impact the probabilities and

rates of electron and hole transfer procedures. Uncertainty the donor redox potential level is greater than the semiconductor VB site; an electron can be transferred into a vacant hole. The acceptors should be lower than the CB position at the same time. The reduction potentials for photoreduction of carbon dioxide with H_2O to various NHE-related compounds at pH 7 are shown in Table 2.1 [287].

Table 2.1 The different semiconductors reduction potentials in relation to NHE at pH 7.

Products	Product Reaction E0 (V)	E0 (V) pH = 7
–	$HO + 2\ h^+ \rightarrow 1/2O_2 + 2H^+$	+0.82
–	$CO_2 + e^- \rightarrow CO_2^-$	-1.9
CO	$CO_2 + 2H^+ + 2e^- \rightarrow CO + H_2O$	-0.53
HCOOH	$CO_2 + 2H^+ + 2e^- \rightarrow HCOOH$	- 0.61
HCHO	$CO_2 + 2H^+ + 4e^- \rightarrow HCHO + H_2O$	-0.48
CH$_3$OH	$CO_2 + 6H^+ + 6e^- \rightarrow CH_3OH + H_2O$	-0.38
CH$_4$	$CO_2 + 8H^+ + 8e^- \rightarrow CH_4 + 2H_2O$	-0.24
–	$2H^+ + 2e^- \rightarrow H_2$	-0.41

2.3.2.1.1 The chemical transformation

As mentioned above, the distribution of electron density over the photocatalyst determines whether reductants are oxidised or reduced during the photocatalytic transformation of CO_2. When the light irradiation falls on photocatalysts, carbon dioxide can be converted into CO, CH_4, CH_3OH, CH_3CH_2OH and other useful chemical compounds. Exciting a photocatalyst with light of the right wavelength causes it to produce a photogenerated hole-electron pair. Carbon dioxide may be converted into sustainable hydrocarbon fuel using photogenerated electrons under mild reaction conditions (room temperature and pressure) ($CO_2 + H_2O \rightarrow$ hydrocarbon + O_2). Particularly crucial in photo-catalytically reduction of CO_2 is the

construction of highly active photocatalysts. In general, photocatalysts are semiconductor materials containing a forbidden band, a conduction band, and a valence band. The forbidden band and conduction band are both essential to the catalytic activity of the catalyst. In contrast to the valence band, which is packed with electrons and has a lower energy level, the CB is frequently unoccupied and has a greater energy level. When the light energy is superior than or equal to the photocatalyst bandgap, positively charged photogenerated holes were produced in semiconductor VB, and electrons goes to the CB of semiconductor thus photogenerated charges are separated [288].

At present, metal oxides, metal nitrides, metal sulphides, layered double hydroxides (LDH), C_3N_4 composites, and other semiconductors are the most commonly reported photocatalysts [289]. In general, the following qualities make for a great photocatalyst: It is important that 1) the photocatalyst's production process is cost-effective and environmentally friendly, 2) photogenerated holes have a high enough oxidation potential in the valence band to oxidise the electron donors, and 3) photogenerated electrons have a low enough reduction potential in the conduction band to reduce the electron acceptor. In semiconductor aqueous suspensions, photochemical reduction of CO_2 results in CH_4 through two different reaction pathways [290, 291]:

$$CO_2 \rightarrow HCOOH \rightarrow HCHO \rightarrow CH_3OH \rightarrow CH_4 \tag{2.15}$$

Or else

$$CO_2 \rightarrow CO \rightarrow C^. \rightarrow CH_2 \rightarrow CH_4 \tag{2.16}$$

The particular pathways intended for converting CO_2 are unclear and instead be contingent substantially on the reaction parameters. The following is a description of the photocatalytic reduction of CO_2:

$$H_2O + h^+ \rightarrow OH + H^+ \tag{2.17}$$

$$2H_2O + 2\,h^+ \rightarrow H_2O_2 + 2H^+ \tag{2.18}$$

$$2H_2O + 4\,h^+ \rightarrow 4H^+ + O_2 \tag{2.19}$$

The creation of the hydrogen and carbon dioxide (CO_2) radicals, two essential forms of radicals, is caused by the transfer of electrons from the CB:

$$H^+ + e^- \rightarrow H \tag{2.20}$$

$$CO_2 + e^- \rightarrow CO_2^- \tag{2.21}$$

Furthermore, these radicals can combine with other hydrocarbons to produce the following stable compounds:

$$\text{Methane formation} + 8.H + 8\,h^+ \rightarrow CH_4 + 2H_2O \tag{2.22}$$

$$\text{Methanol formation} + 6.H + 6\,h^+ \rightarrow CH_3OH + H_2O \tag{2.23}$$

$$\text{Carbon monoxide formation} + 2.H + 2\,h^+ \rightarrow CO + H_2O \tag{2.24}$$

$$\text{Formic acid formation} + 2.H + 2\,h^+ \rightarrow HCOOH \tag{2.25}$$

$$\text{Formaldehyde formation} + 4.H + 4\,h^+ \rightarrow HCHO + H_2O \tag{2.26}$$

$$\text{Ethanol formation} + 12.H + 2\,h^+ \rightarrow C_2H_5OH + 3H_2O \tag{2.27}$$
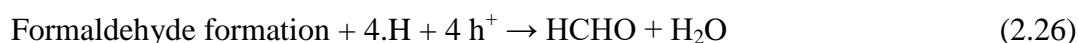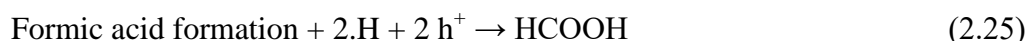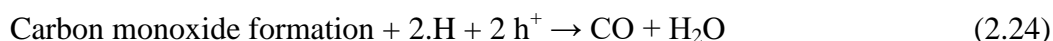
Excited electron-hole pairs have a sufficient lifetime of a few nanoseconds to stimulate redox processes. TiO_2, silver/TiO_2, iodine/TiO_2, platinum/TiO_2, palladium/TiO_2, CeO_2-TiO_2, $FeTiO_3$/TiO_2, ZnO, Fe_3O_4, WO_3, CdS, SnO_2, ZnS and many others have all been used as photocatalysts in this context [292].

2.4 Study of hydrogen production & CO_2 reduction with various reported photocatalyst

2.4.1 Reported Photocatalysts for Hydrogen evolution

Using rutile TiO_2 as the photocatalyst, Piotr J, Barczuk first showed the photocatalytic O_2 evolution process in 1968 [293]. Photoelectrochemical (PEC) water splitting with n-type TiO_2 as the photoanode and platinum as the counter electrode was first demonstrated by Fujishima and Honda in 1972 [294]. Hydrogen generation using TiO_2 as a photocatalyst under ultraviolet light was originally described in 1972. The results of Fujishima and Honda

inspired researchers to investigate photocatalysts and the potential of H_2 generation in the existence of solar light. Metal nitrides, metal oxides, metal chalcogenides, and other semiconductors were used in photocatalytic water dissociation throughout the last ten years. This is due to the fact that semiconductors like CdS, CdSe, MoS_2, etc. have CB and VB that are optimal for the photo-catalytically hydrogen evolution reaction and bandgap and band edge locations that are optimal aimed at the oxygen evolution reaction. Individual a small number of photocatalysts, including Ta_3N_5 and TaON, could demonstrate complete water dissociation when exposed to visible light [295]. TiO_2 is a semiconductor with an enormous band gap (3.2 eV), with a conduction band (CB) at 0.55 eV and a valence band (VB) at 2.65 eV. This allows H_2 and O_2 to be extracted from water. TiO_2 is the supreme studied photocatalyst owing to its low environmental impact, exceptional physicochemical stability and low cost of raw materials and synthesis method over the past 50 years. Nonetheless, it has been widely used in the last decade. As a result of the high recombination rate of photogenerated charges, researchers are looking into coupling a second semiconductor with TiO_2 to create heterojunctions, which facilitate the flow and separation of these charges at their interfaces. Doping TiO_2 with various elements including nitrogen [296], Zinc oxide (Alamelu K. ramasami et al., 2017) [297], tungsten trioxide (Wilson Erbs et al., 1984) [298], iron trioxide (Fe_2O_3) (Lingqiao Kong et al., 2018) [299], etc. have all been described as photocatalysts. However, these metal oxides have unfavourable band edge potentials, which reduce their overall efficiency at splitting water. The voltage near the band edges only encourages photo oxidation and not photo reduction in these materials. It has been found that sulfides and nitrides can exhibit photocatalytic activity as well as metal oxides. Their narrower bandgap (i.e. 1.9 eV-2.3 eV) and beneficial band edge potentials make them an excellent choice for water splitting applications. However, they exhibit photocorrosive properties [300]. Recently, numerous Z-scheme photocatalysts have been employed for water

splitting, with the aim of avoiding the aforementioned limitations (for example, TiO_2-CdS, ZnO-CdS, and WO_3-Cu_2O) [301]. Table 2.2 lists information about the various semiconductor photocatalysts that have been published. Among the many semiconducting oxides, only a select few have the narrow bandgap necessary to function as photocatalysts.

Table 2.2 Reported semiconductor photocatalysts for the evolution of hydrogen

Photocatalyst	Co-catalyst	Light source	PC H_2 activity	Ref.
TiO_2	Rh	UV light Irradiation	3.3 $\mu mol g^{-1} h^{-1}$	[302]
N doped TiO_2	Pt	300 W Xenon lamp Irradiation	205.8 $\mu mol g^{-1} h^{-1}$	[303]
S doped TiO_2	Pt	500 W Xenon lamp Irradiation	2356 $\mu mol g^{-1} h^{-1}$	[304]
N, S doped TiO_2	Pt	500 W Xenon lamp Irradiation	9.97 $\mu mol g^{-1} h^{-1}$	[305]
CdS	MoS_2	Visible light Irradiation	5400 $\mu mol g^{-1} h^{-1}$	[306]
TiO_2 nanotubes Pt/CdS	Pt	300 W Xenon lamp Irradiation	402 $\mu mol g^{-1} h^{-1}$	[307]
$Ti_3CN@TiO_2$/	Cds	300 W Xe lamp	3393.4 $\mu mol g^{-1} h^{-1}$	[308]

CdS				
Ta$_2$O$_5$	NiO	400 W Hg lamp Irradiation.	1154 $\mu molg^{-1}h^{-1}$	[309]

2.4.1.1 Complex oxide structures

A Combination of two or more metal oxides combined to form a definite structure is called complex oxide structure. There are several types of complex oxide structures namely Perovskites, Spinels, Brownmillerites, etc reported so far. In this section we are discussing about the perovskites. They are reported to be useful in several applications such as ionic conductors, dielectrics, piezoelectrics, thermoelectrics, magnetism, multiferroics, photocatalysis, etc.

2.4.1.1.1 Perovskites

Perovskites often have the chemical formula ABX$_3$, where A and B represent two distinct cations and X can be oxygen, halogen, nitrogen, etc. Perovskite oxides (ABO$_3$), which are amenable to modification by varying degrees of slanting in octahedral sites, remained one of the greatest promising materials for photocatalytic applications because of their ability to alter electron-hole transport characteristics, band structures, etc. Perovskites have superior photocatalytic properties to those of other binary oxides because (1) They feature a greater variety of band edge potentials that are ideal for photocatalytic processes (in particular, a larger conduction band potential), and (2) their band structures can be modified by incorporating different cations into the A and/or B sites of their lattice [310]. Hydrogen evolution via water splitting is a process for which numerous perovskites materials have been described as photocatalysts as shown in Table. 2.3).

Table 2.3 List of reported perovskites with different photocatalytic properties

Type	Photocatalyst	PC H_2 activity	Ref.
Titanates	$BaTiO_3$	$30.8\ \mu mol g^{-1} h^{-1}$	[311-313]
	$CaTiO_3$	$670\ \mu mol g^{-1} h^{-1}$	
	$SrTiO_3$	$28\ \mu mol g^{-1} h^{-1}$	
Tantalates	$NaTaO_3$	$0.86\ \mu mol g^{-1} h^{-1}$	[314, 315]
	$AgTaO_3$	$76\ \mu mol g^{-1} h^{-1}$	
Niobates	$KNbO_3$	$5.3\ \mu mol g^{-1} h^{-1}$	[316]
Ferrites	$LaFeO_3$	$3315\ \mu mol g^{-1} h^{-1}$	[317-319]
	$GaFeO_3$	$289\ \mu mol g^{-1} h^{-1}$	
	$PrFeO_3$	$2847\ \mu mol g^{-1} h^{-1}$	

2.4.1.1.2 Titanate perovskites

Titanate perovskites are highly reported photocatalysts due to their wider bandgap as well as improved conduction band potential than widely used photocatalyst TiO_2 [320]. They are more favorable for higher electron-hole recombination rates due to their wider bandgap. In order to reduce the recombination rate it is necessary to use co-catalysts along with these photocatalysts. Among several titanates, $CaTiO_3$ is reported to exhibit higher hydrogen evolution rate in presence of NiO as co-catalyst [321, 322]. It was enhanced by 8 times after Cu doping in its Ti site. $SrTiO_3$ is another important

photocatalyst having bandgap of > 3.2 eV. Several attempts were made to improve its photocatalytic activity by doping Mn, Ru, Rh & Ir in its Ti site and making it Z-scheme photocatalyst like Rh-SrTiO$_3$ with BiVO$_4$, AgNbO$_3$, WO$_3$, etc. [323, 324]. Ag-TiO$_2$ photocatalyst was successfully synthesized by D. Gogoi et al. via chemical reduction using ascorbic acid. The band gap of doped catalyst exists 2.5 eV, which is a decrease from the 3.0 eV of TiO$_2$. The EDX analysis verified that Ag was widely discrete over the top of the TiO$_2$ substrate. The operative interfacial transfer of charge from TiO$_2$ to Ag was demonstrated by PL and EIS, perhaps via the Ti-Ag-O bonds. Transient photocurrent densities of 1.16 mA cm^{-2} and 0.33 mA cm^{-2} were measured over 1.5Ag/TiO$_2$, respectively, demonstrating effective charge carrier separation. With the presence of 0.1 N Na$_2$SO$_3$ and 0.1 N Na$_2$S sacrificial reagents (SR), over 1.5Ag/TiO$_2$, the highest H$_2$ evolution rate of 23.5 $\mu mol g^{-1} h^{-1}$ was observed, with a superficial quantum yield of 19%. When compared to other alcohols used as SRs, ethanol produced the highest evolution of H$_2$ rate ($1251 \mu mol g^{-1} h^{-1}$) [325]. The detriments of these titanate perovskites are that they indicate higher photocatalytic efficiency under UV irradiation than visible light irradiation, expensive co-catalysts and preparation methods. Niobates and Tantalates are also highly reported wider bandgap photocatalysts. When exposed to UV light rather than visible light, they become more active. Recently, solid solution of KNbO$_3$-BaNiNbO$_3$ perovskites showed ferro electricity as well as photocatalytic properties. Doping several elements in NaTaO$_3$ such as La-N and La-Fe improved its photocatalytic activity. The disadvantages of these perovskites are expensive preparation methods, availability, and expensive co-catalysts. Among all, iron-based perovskites are earth-abundant, inexpensive photocatalysts having narrower bandgap. Several iron based perovskites such as LaFeO$_3$, BiFeO$_3$, GaFeO$_3$, etc are reported as photocatalysts for H$_2$ evolution as well as organic contaminants removal. LaFeO$_3$ is one of the highly reported

photocatalyst than other ferrite perovskites for hydrogen evolution and organic pollutants removal [326-330].

2.4.1.1.3 Lanthanum ferrite - LaFeO$_3$

LaFeO$_3$ Due to its lower bandgap and appropriate band-edge potentials, LaFeO$_3$ is a well-known perovskite photocatalyst. It degrades dyes in the presence of light and can even generate hydrogen. When compared to other complex oxide photocatalysts, however, its efficiency as a photocatalyst is found to be lower. Higher valence band potential and lower conduction band potential were discovered to be to blame for this phenomenon, along with the recombination of couples of e$^-$ and h$^+$ throughout the reaction. It was discovered that during photocatalytic processes, point defects in the parent crystal serve as recombination barriers. LaFeO$_3$, like other perovskites, can have desirable elements doped into it to improve its properties.

Doping LaFeO$_3$ with an aliovalent cation causes the creation of structural defects and the stabilization of various valence states of Fe. A similar charge imbalance can be produced by doping the Fe site with a cation of lower valence [331].

As the number of dopant ions increases, the valence state of Fe shifts from Fe^{3+} to Fe^{4+}, and oxygen vacancies form. Doping of LaFeO$_3$ with various elements has been tried on multiple occasions in an effort to boost its photocatalytic performance.

2.4.1.2 Heterojunction

A wide range of visible light active single photocatalysts are available, but they still lack better photocatalytic performance due to charge carrier recombination during surface redox reactions. This problem of charge recombination needed to be resolved for further improvement in performance of semiconductor photocatalysts. Various tactics have been envisioned by researchers for effective split-up of photoinduced e$^-$ h$^+$ pairs, such as metal nanoparticles loading or surface plasmon resonance (SPR) result, co-catalyst deposition

and/or introducing heterojunctions. Among these strategies, heterojunction formation in photocatalysts was found to be more promising for the spatial separation of charge carriers. This was clearly demonstrated by Yu et al. with the analogy of a guy being affected by gravity when he leaps from the ground as shown if fig. 2.5. The man (electron) will quickly drop back on the ground (merge back with the hole) because of the effect of gravitational pull (Coulombic strength between the electron and the hole) when he jumps from the ground (VB) into the air (CB). When a chair (the CB of semiconductor B) is made available, the man can repeatedly land on it without touching the floor, enabling photo-generated electron-hole pairs to be separated [332].
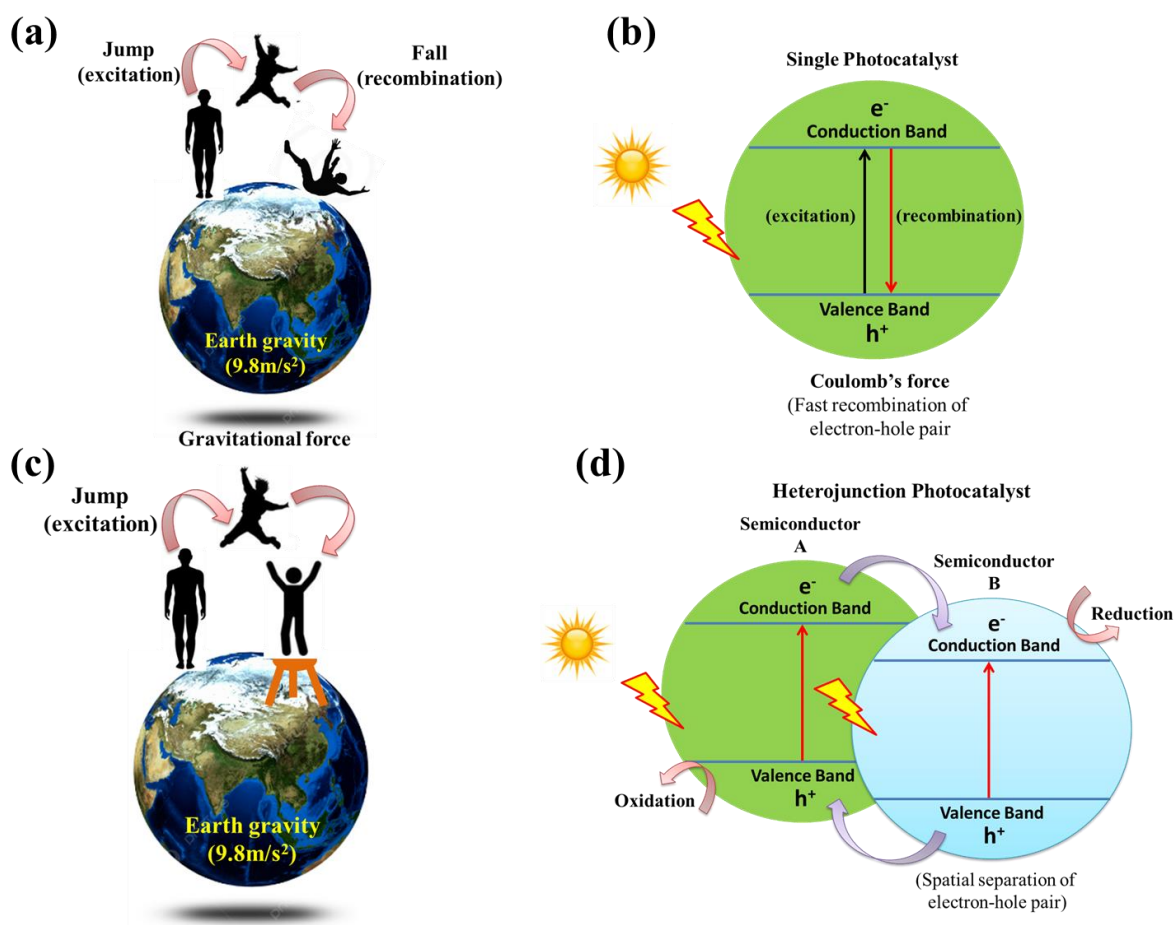
Fig. 2.5 Diagram depicting (a) the effect of gravity on a man who leaps off a building, (b) e⁻ h⁺ recombination on a single photocatalyst, (c) a man using a stool to hold himself

upright, and (d) e⁻ h⁺ separation on a heterojunction photocatalyst

Typically, following type of heterojunctions were extremely investigated for efficient suppression of $e^- h^+$ recombination to enrich the activity of photocatalysts. These stand direct Z-scheme heterojunctions, semiconductor–graphene/g-C_3N_4 heterojunctions and p–n heterojunctions. Recently, an Ag-bridged heterojunction of $Bi_5FeTi_3O_{15}$ with g-C_3N_4 was reported to exhibit enhanced photocatalysis for tetracycline degradation [333]. Semiconductors of p- and n-type are highly recommended for heterojunction creation as it was observed in photovoltaic cells that p-n diode structures had shown greatly enhanced photocatalytic performance.

2.4.1.2.1   The P-N Junction Construction Process

Charge separation can be improved by mixing p-type and n-type semiconductors to create a p-n junction. As "n" refers to the negative, and "e^-" is the primary electrical conductor, this makes sense. Donor impurities, which can supply conducting electrons, make up the bulk of N-type semiconductors. Semiconductors, also known as electronic semiconductors, rely heavily on electrons to conduct electricity; since "P" denotes a positive charge, the h^+ ions that play the most significant role in the conduction of electricity are the primary electron carriers in semiconductors. The acceptor impurities are the primary building blocks of P-type semiconductors. Semiconductors, often known as hole semiconductors, are characterized by the presence of numerous hollow hole carriers. There are only few electrons and holes at the p-n junction as shown in fig.2.6. The holes that exist will diffuse to the n-region from the p-region. In fact, electrons will flow to the p-region from the n-region via diffusion. As a result of the diffusion process, a coating of negatively charged particles forms in p field, while a coating of positively exciting particles forms in n field. Because of this, a strong local electric field is generated in the p-n junction, with the direction of the field being from n to p. It is simple to create n- or p-type semiconductors by combining the two. The p-type results from

an additional electron vacancy left over after the two elements combine, while the n-type results from a residual hole. Combinations of p-type elements include C, N, P, As, Sb, and Ge; n-type elements include B, Al, Ga, Si, and Ge. ZnO, TiO$_2$, PbS, etc. are all examples of n-type semiconductors, while NiO, Cu$_2$O, Co$_3$O$_4$, CdTe, etc. are all examples of p-type semiconductors. When n-type and p-type semiconductors are connected, p-n junctions are created. When exposed to light, electrons typically move from the p-type conductor base (CB) to the n-type conductor's base (VB), and holes travel in the opposite direction. The resulting photocatalytic activity is quite strong due to the p-n junction ability to further improve charge separation [334-336].
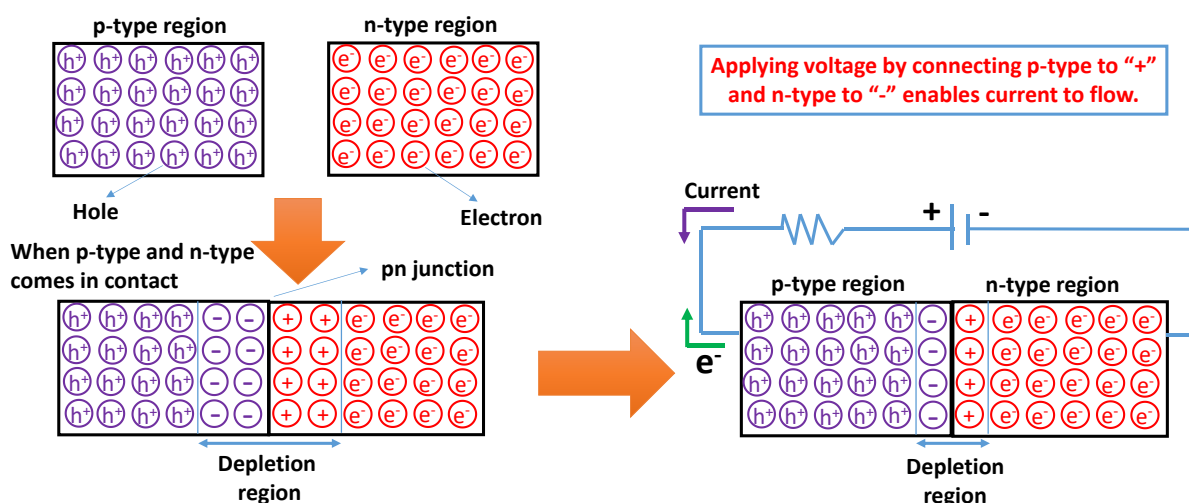
Fig.2.6 Diagrammatic representation of p-n junction construction process [336]

The Co(OH)$_2$/ZnCr LDH "p-n" heterojunction for H$_2$ and O$_2$ was created by using a water electrolysis application. The overall productivity of water splitting by photocatalysis is enhanced in this composite [337]. Wang et al. reported overall performance of Cu$_2$O@ZnCr-LDH in water splitting (H$_2$ and O$_2$). ZnCr-(LDH) was added to pure Cu$_2$O to boost its photocatalytic overall water splitting activity [338]. Since water splitting requires more energy, it is challenging for a single photocatalyst to accomplish it.

2.4.1.3 Bismuth-based semiconductors

Bismuth there is a new, promising family of photocatalysts that are bismuth based and driven

by visible light. Bismuth oxides, bismuth-containing bi-metal oxides, and bismuth-based sulphides are only a few of the bismuth-based compounds that have been synthesized and studied as photocatalysts. Such compounds include pentavalent bismuthates, $(BiO)_2CO_3$, $BiPO_4$, $BiVO_4$, Bi_2O_3, Bi_2S_3, BiOX (where X denotes I, Br and Cl), Bi_2MO_6 (M = Mo, W and Cr) [339]. Bi-based semiconductors have an additional complex electronic structure in the valence band due to the presence of hybrid orbitals of O 2p and Bi 6s, as opposed to merely the O 2p orbital found in metal oxides like WO_3, ZnO, TiO_2, etc. Band gaps should be smaller than 3.0 eV, equivalent to excitation energies of visible light with wavelengths larger than 415 nm; have been reported to be made possible by the well-dispersed Bi 6s orbital. Bismuth-based photocatalysts have received countless consideration over previous decades owing to its high efficiency in the incidence of visible light. The band gaps of the various polymorphs of Bi_2O_3 (monoclinic, tetragonal, gamma, delta, and omega tetragonal, cubic, face-centered cubic, and triclinic) lies in the series of 2.1 eV to 2.8 eV. It is possible to couple Bi_2O_3 to other semiconductors using a precipitation process, a hydrothermal process, or a solid-state reaction. Because of Bi_2O_3 high light-harvesting efficiency, the resulting composite materials reacted to visible light. Heterojunctions formed between Bi_2O_3 and other photocatalysts with higher CB locations, such as TiO_2, ZnO, AgI, and g-C_3N_4, showed markedly increased the generation of hydrogen by photocatalytic efficiency [340]. Increased photo-induced charge separation in the air-stable $MA_3Bi_2I_9$/DMA_3BiI_6 perovskite heterostructure has been found to have evolution of H_2 in aqueous hydrogen iodide solution under illumination of visible light via photocatalytic process. By applying 100 mW cm^{-2} of visible-light (420 nm) irradiation, MA_3Bi_2I9/DMA_3BiI_6 heterostructure composite (BBP-5) in powdered form exhibited the evolution of hydrogen rate of 198.2 $\mu mol g^{-1} h^{-1}$ [341]. For the evolution of hydrogen below visible-light irradiation (> 420 nm), an advanced catalyst of g-C_3N_4/Bi_4NbO_8Cl fabricated on a simple great-energies ball-milling technique, between the

two phases a close high efficiency Z-scheme interface is formed to evaluate hydrogen at a rate of 0.57 $\mu mol g^{-1} h^{-1}$ under illumination of visible light [342]. CdS nanoparticles evenly scattered on BiVO$_4$ nanosheet significantly enhanced photo-catalytically performance. The rate of evolution of hydrogen by photo catalytically can be raised to 1853.33 $\mu mol g^{-1} h^{-1}$ [343]. All of these heterojunctions involving bismuth-based photocatalysts follow the Z-scheme. In the presence of 500 W xenon lamp irradiation, Wang reported firstly that the rate of photo-catalytically splitting of water for the evolution of hydrogen over Pt loaded Bi$_{0.5}$Na$_{0.5}$TiO$_3$ had achieved 325.4 $\mu mol g^{-1} h^{-1}$ [344].

2.4.1.4 Hydrogen-generation heterojunction photocatalysts based on sulfide

Metal sulphides and bimetal sulphides predominate semiconductor photocatalysts mostly in sulfide-based. Metal sulphide semiconductors contain metal cations with electron configurations of d^0, d^5, and d^{10}. Metal sulphides have a considerable reduction capacity to water because their valence band locations are developed than those of metal oxides (S 3p orbit is greater than O 2p), and their CB fall into the negative potential range.

For photocatalytic hydrogen generation, CdS and ZnIn$_2$S$_4$ have been extensively explored owing to their highly visible light responsiveness and substantial electron reduction control, respectively. CdS and ZnIn$_2$S$_4$ have valence bands of 1.88 eV and conduction bands of 0.52 eV, while those of CdS and ZnIn$_2$S$_3$ are 1.45 eV and 0.52 eV, respectively. Heterojunction formation of these two semiconductors with other semiconductors is crucial for enhancing photocatalytic hydrogen generation. Under visible light irradiation, the evolution of hydrogen rate over CdS@CdxZn1-xS (5.17 $\mu mol g^{-1} h^{-1}$) is 12.3 folders of CdS core-shell, which could be assigned to the efficient charge separation [345]. In addition, CdS-based heterojunction photocatalyst worked effectively when paired with a precious metal and graphene in a single system. Hydrothermal annealing of CdS/ZnS heterostructure on rGO, monitored by in-situ installation of Au nanoparticles. The noteworthy photocatalytic

evolution of H$_2$ rate of 9.96 $\mu mol g^{-1} h^{-1}$ under visible-light illumination is achieved by the Au-CdS/ZnS-rGO composite due to the efficient split-up and transmission of photogenerated electrons and holes thanks to the strong electron capture ability of Au and the electron transfer ability of graphene [346].

Zinc indium sulfide composites with g-C$_3$N$_4$, MoS$_2$, and Cu$_3$P are the reported heterojunctions with the best photocatalytic evolution of hydrogen performance utilizing ZnIn$_2$S$_4$ as host, with productivities of 7740, 3891.6 and 2561.1 $\mu mol g^{-1} h^{-1}$, correspondingly. The extraordinary photocatalytic efficiency of such heterostructure to produce hydrogen may be ascribed to the increased segregation of photogenerated holes and electrons [347]. When a CuInS$_2$/ZnIn$_2$S$_4$ 2D/2D heterojunction composite photocatalyst is constructed with CuInS$_2$ wt% of 5, heterojunction apparent quantum efficiency extents 12.4% at 420 nm, resulting in the highest H$_2$ evolution rate of 3430.2 $\mu mol g^{-1} h^{-1}$ [348]. The MoSe$_2$/ZnIn$_2$S$_4$ hierarchical heterojunction had greater photocatalytic activity for the evolution of H$_2$ rate of 1226 $\mu mol g^{-1} h^{-1}$ [349]. The photoactivity remained traced back to a heterojunction between ZnIn$_2$S$_4$ and MoSe$_2$, with MoSe$_2$ playing both a catalytic role in the evolution of H$_2$ reaction and by way of an electron storage site.

Light irradiation with the wavelength of 420 nm, 3 wt% of MWCNTs/ZnIn$_2$S$_4$ composite touches its highest photocatalytic evolution of hydrogen efficiency of 684 $\mu mol g^{-1} h^{-1}$ [350]. This corresponds to an apparent quantum efficiency of 23.3%. This was achieved by adopting a facile hydrothermal procedure to prepare MWCNTs and ZnIn$_2$S$_4$ composites for hydrogen photocatalysis. ZnIn$_2$S$_4$ nanosheets with sulphur vacancies containing 0.9 wt% of Ni single atoms have a photocatalytic hydrogen generation rate 89.4 $\mu mol g^{-1} h^{-1}$ which is 5.7 times greater than that of pure ZnIn$_2$S$_4$ [351]. When the loading concentration was increased of single atom Ni (2.85 wt%) on CdS nanorods, the photo catalytically evolution of hydrogen rate was greatly increased up to 630.1 $\mu mol g^{-1} h^{-1}$ under the illumination of

visible light [352]. Akyuz et al. investigated the efficiency of RGO-$Cd_{0.60}Zn_{0.40}S$ composite as a photocatalyst and photoelectrocatalyst for hydrogen evolution [353]. Photocatalysts doped with heteroatom demonstrated higher visible-light photoactivity than undoped ones because of the effect of charge split-up and relocation in the PC and PEC system. The greatest photocurrent was found to be generated by the N-RGO-$Cd_{0.60}Zn_{0.40}S$ photocatalyst among the entire heteroatom doped nanocomposite in the absence of a bias voltage and the photocatalytic evolution of hydrogen rate ($1114 \ \mu mol g^{-1} h^{-11}$) with 17.8% QE [354]. Lin et al. studied full spectrum-active photocatalytic H_2 evolution of single photocatalyst $CuWO_4$ [355]. The results show an enhanced hydrogen evolution rate.

2.4.1.5 Reported metal nitrides based photocatalyst for H_2 production

Nitrides have attracted more attention in the photocatalytic research area and are seen as the best potential applicants for the conversion of solar energy because of their extensive visible light absorption, appropriate CB and VB spot, and exceptional photostability due to their much smaller bandgaps (e.g. Ta_3N_5 2.1 eV) than comparable oxides (e.g. Ta_2O_5 5.1 eV). Because of the appropriate fine band gap range lie around 2.1 eV, appropriate CB (0.7 eV in V VS. NHE), and VB (1.3 eV in V VS. NHE) sites, tantalum nitride (Ta_3N_5) have been the focus of widespread research in the field of photocatalysis or photocatalysis for the production of green renewable energy like evolution of hydrogen from solar energy.

N doping in Ta_2O_5 was investigated by W. S. Liu et al., and they found that annealing Ta_2O_5 powdered in NH_3 for 1 hour at 600-700 °C was the most effective method [356]. N-Ta_2O_5 (700) underwent partial transformation to Ta_3N_5 and underwent a complete transformation to Ta_3N_5 after being annealed at 800 °C for 6 hours. Raman spectroscopy, X-ray photoelectron spectroscopy, X-ray diffraction and X-ray absorption spectroscopy all point to a preferred surface substitution of nitrogen for oxygen in Ta_2O_5. H_2 production from H_2O splitting is increased by nitrogen doping in Ta_2O_5, which under sun irradiation causes oxygen vacancies

to develop and reduces the band gap. As a charge carrier recombination center, Ta_3N_5 reduces the photocatalytic activity of the material. $N-Ta_2O_5$ (650) has the highest H_2 evolution compared to other $N-Ta_2O_5$ samples due to its higher nitrogen doping and lack of Ta_3N_5 presence. For the first time, Xiao et al. have used a simple technique to produce a MoS_2/Ta_3N_5 heterostructure with a 2D hierarchical structure. The photocatalytic evolution of hydrogen from H_2O by using the MoS_2/Ta_3N_5 heterostructure existed be quite efficient, with an hydrogen rate of generation of 119.4 $\mu molg^{-1}h^{-1}$ with MoS_2 and wt% is 5.2, which is similarity with the performance nanosheets of Ta_3N_5 by using Pt as cocatalysts [357]. The excellent photocatalytic production of H_2 is due to the compatible band structure of MoS_2/Ta_3N_5, which reduces charge recombination and promotes charge transfer amid MoS_2 and Ta_3N_5. Towards highly efficient photocatalytic applications, we anticipate the fabrication of precious metal free photocatalytic systems with broad visible light absorption and 2D hierarchical nanostructures determination is productive.

Nanoparticles of Ta_3N_5 coupled with new functional semiconductors to produce multicomponent heterostructure have been demonstrated to considerably enhance charge carrier immigration and endorse photocatalytic activities in numerous studies. The $Ta_3N_5/W_{18}O_{49}$ nanocomposite fiber, for instance, has been shown to have exceptional photocatalytic performance, and Jones et al. published an ascendable Solvothermal process to synthesize this material [358]. A new $Ta_3N_5/g-C_3N_4$ heterojunction with enriched photocatalytic activity was produced by Jiang et al. [359]. $BaMg_{1/3}Ta_{2/3}O_{3-x}Ny/Ta_3N_5$ heterostructure photocatalysts with excellent charge migration and separation capacity were developed by Cui et al. by single-pot nitridation approach [360]. Taking cues from the research that has come before it, creating a core-shell heterojunction with a Ta_3N_5 core could be a workable method since it provides a larger contact area and more efficient charge transfer while also shielding Ta_3N_5 from photo-corrosion.

Because of its promising applications in photocatalysis particularly hydrogen generation, photodegradation, and photoreduction zinc indium sulphide ($ZnIn_2S_4$) has received attention from researchers all over the world. The favorable band edge potentials and exceptional photostability of $ZnIn_2S_4$ have led to its widespread acceptance as a promising shell material with a low bandgap (about 2.4 eV). Core-shell structures, such as carbon nanofiber@$ZnIn_2S_4$, TiO_2@$ZnIn_2S_4$, WO_3/$ZnIn_2S_4$, and $ZnIn_2S_4$/$In(OH)_3$, fall under this category [361, 362].

Using a one-pot environmentally friendly hydrothermal technique, Xiao et al. developed an innovative twofold-functional $ZnIn_2S_4$/Ta_3N_5 (ZIS/TN) nanocomposite with close connections. Increased visible light gathering capacity, advanced definite surface areas, further high-speed charge nanochannels, and quicker charge transmission and separation are all shown for a core/shell heterojunction composed of $ZnIn_2S_4$ nanosheets and Ta_3N_5 nanoparticles. As such, the ZIS/TN nanocomposite in its as-prepared state showed dramatically enhanced dual-functional photocatalytic efficiency in producing hydrogen and photodegrading tetracycline hydrochloride (TCH). The result was an increase in H_2 production activity from the pure $ZnIn_2S_4$ nanosheet sample by 6.07 times, to 834.86 $\mu mol g^{-1} h^{-1}$. In addition, ZIS/TN-3 sample is 1.90 folds as effective as bare $ZnIn_2S_4$ and 11.01 times as effective as bare Ta_3N_5 at photodegrading TCH. In addition, the exterior $ZnIn_2S_4$ coating prevents the photocorrosion of the Ta_3N_5 core, making core/shell heterojunction extremely photostability and reusability [363].

Jia et al. have developed a novel type II hetero-structured photocatalyst (designated as Ta_3N_5/STON) by nitriding 1D $Sr_2KTa_5O_{15}$ (SKTO) nanorods in a single step to create one dimensional of Ta_3N_5 nanorods and zero dimensional nanoparticles of $SrTaO_2N$ (STON). Under visible light irradiation, Ta_3N_5/STON (1D/0D) heterojunctions produce hydrogen at a rate (77.31 $\mu mol g^{-1} h^{-1}$) that is 386.6, 11.9 $\mu mol g^{-1} h^{-1}$ and 8.8 folds greater, respectively, as comparison to pure Ta_3N_5, STON, and a Ta_3N_5/STON (mix) composite [364].

Significantly increased hydrogen evolution rate may be attributed to the unusual one dimensional/zero dimensional structure in Ta_3N_5/STON heterojunction and the close interface contact among Ta_3N_5 and $SrTaO_2N$. Solar H_2 generation from water is already rather efficient, Ta_3N_5/$BaTaO_2N$ heterojunction using 1D Ta_3N_5 nanorods and $BaTaO_2N$ nanoparticles, which showed a substantial drop in the recombination rate of photogenerated carriers [365]. Zhao et al. showed that Mg doping Ta_3N_5 hollow spherical shape boosts electron mobility for easier charge transfer and minimizes the charge migration distance [366]. Double co-catalysts (Pt/CoOx) for redox reactions are placed onto the porous Ta_3N_5 structure to diminish surface recombination and accelerate the slothful surface reaction. Ta_3N_5 photocatalysts with a hollow structure, Mg^{2+} doping, an MgO interfacial coating, and double co-catalysts show remarkable improvement in charge separation and transfer. Zhan et al. designed two dimensional nanosheets of Ta_3N_5/ReS_2 van der Waals heterojunction photocatalysts by combining solution-adsorption and template-assisted techniques. The resulting heterojunctions have more reaction sites enabling hydrogen evolution, superior light absorption, and higher interfacial charge transmission. As such, they offer an extraordinary photocatalytic evolution of hydrogen yield of $615 \mu mol g^{-1} h^{-1}$, which was three to twelve times greater as compared to pristine nanosheet of Ta_3N_5 and ReS_2, respectively [367]. A novel nanocomposite photocatalyst $CdIn_2S_4$/Ta_3N_5 (CIS/TN) well successfully synthesised by utilising the straightforward in-situ hydrothermal method, in which the $CdIn_2S_4$ nano-octahedral are securely connected on the Ta_3N_5 nanoparticles surface for the formation of the core-shell heterostructure. Synthesized CIS/TN heterostructure exhibited excellent photocatalytic capabilities for both evolution of hydrogen and degradation of Methyl Orange. The CIS/TN heterostructure clearly outperformed pure $CdIn_2S_4$ in photocatalytic activities, by CIS/TN$_3$ sample containing 3 wt percentage of Ta_3N_5 producing 122.6 $\mu mol g^{-1} h^{-1}$, or nearly 2.43 fold as much H_2 like $CdIn_2S_4$ nanooctahedra [368]. In addition, its rate constant

was 2.79 times greater than that of pure $CdIn_2S_4$, making it the most efficient material for MO photodegradation. Higher quantum yield and efficiency may be attributable to the intimate heterogeneous interface and effective relocation of photoinduced charge carriers among the broad spectral adsorption region.

The photocatalytic water reduction activity of MgZr-co-doped single-crystalline Ta_3N_5 (Ta_3N_5: Mg+Zr) nanoparticles was 45 folds more than pristine Ta_3N_5 under visible light, as reported by Xiao et al. synthesized the nanoparticles using a fast NH_3 nitridation process [369]. Defect species like reduce Ta, oxygen impurities and nitrogen vacancies, were connected to surface features, transmission of charge carrier, and photo-catalytically performance. It is evident that the co-doping tuning of defects and the concurrent optimisation of surface features are responsible for the large concentrations of prolonged electrons in this material, as they permit proficient relocation of these electrons to evenly allocate on the surface of Pt sites. The photocatalytic activity was greatly enhanced by these modifications. The Z-scheme Ta_3N_5-$WO_{2.72}$ heterojunction film photo catalyst was fabricated for improved H_2 generation through atomic layer deposition and sol-gel procedures. Atomic layer deposition method used to deposit Ta_3N_5 onto a Si wafer with a $WO_{2.72}$ sol coating. Six hours of illumination with a cut-off filter (lambda > 420 nm) from a 150 W Xe lamp resulted in 13.2 $\mu mol g^{-1} h^{-1}$ evolution of hydrogen from a Ta_3N_5 layer deposited on a bare Si wafer. There was a notable growth in H_2 yield (31.9 $\mu mol g^{-1} h^{-1}$) from the straight Z-scheme Ta_3N_5-$WO_{2.72}$ heterojunction film compared to other films. Atomic layer deposition method used for Pt nanoparticles coating on the heterojunction sheet of Ta_3N_5-$WO_{2.72}$ increased its efficiency upto 46.4%. Furthermore, direct Z-scheme of Ta_3N_5-$WO_{2.72}$ heterojunction film produced 18 folds more hydrogen than a Ta_3N_5-WO_3 liquid-state system. Generating 3072.5 $\mu mol g^{-1} h^{-1}$ yield of hydrogen evolution was attained thru Pt nanoparticle-coated Ta_3N_5-$WO_{2.72}$ heterojunction film in the absence of the 420 nm cut-off filter [370]. A recent study,

Zhan et al. defined the rational design of one dimensional Ta_3N_5 or two dimensional $MoSe_2$ (TN/MS) heterojunction photocatalysts, in which $MoSe_2$ nanosheets, resembling silk, are firmly and consistently fastened to the surfaces of Ta_3N_5 nanofibers. The optimized nanocomposites outperform recently reported Ta_3N_5 based photocatalysts in terms of photocatalytic evolution of hydrogen activity ($811.74 \mu mol g^{-1} h^{-1}$), indicating their potential for real-world applications. Experiments and theoretical calculations confirm that heterojunction engineering among two dimensional $MoSe_2$ and one dimensional Ta_3N_5 is responsible for the enhanced photocatalytic activity compared to TN/MS heterojunction photocatalysts, and that this improvement is primarily attributable to enhanced increased reaction kinetics, light absorption, and promoted carrier separation [371].

The synthesis of a novel mixed cobalt nitrides and Ta_2N bifunction-modified Ta_3N_5 nanosheet photocatalyst by performing an ammonolysis of $Ta_3N_5@Ta_2O_5$ nanoparticles adsorbed on Co^{2+}/Co^{3+} at elevated temperatures. Ta_3N_5 structural, electrical, optical, and photoelectrochemical performances were studied in depth to determine the impact of Co_2 or/and Co_3 altering. The optical absorption of band gap at the amplified heterojunction edges of Ta_2N/Ta_3N_5 or $CoxN/Ta_3N_5$ was what allowed co-modifying to improve absorption over the whole visible spectrum. The crystallization of Ta_3N_5 was stymied by a twofold modification with Co^{2+} and Co^{3+}. Co elements were uniformly distributed on the surface of Ta_3N_5, prominent to a larger number of surface active sites. Co_3 was critical in determining the relative proportions of Ta_2N and $Co5.47N$ modifiers. Ta_3N_5 charge carrier separation, hydrogen evolution reaction overpotential, and oxygen evolution reaction overpotential were all successfully improved by the synergistic impact of Co_2/Co_3 dual-modifying, prominent to a development in the material photocatalytic evolution of H_2 activity. The photocatalytic evolution of H_2 activity of $1.5\%Co_2/1.5\%Co_3$-TN under irradiation of visible light was found to be 348% more than that of $Ta_3N_5@Ta_2O_5$ nanoparticles ($75.69 \ \mu mol g^{-1} h^{-1}$) [372]. Zeng

et al. reported the successful fabrication of a new $SrTaO_2N/Ta_3N_5$ hetero-structured photocatalyst by using a $Sr_2Ta_2O_7/Ta_2N_5$ precursor and flow of ammonia gas. Despite the optimized heterostructure $SrTaO_2N$ (0.1)/Ta_3N_5 photocatalytic hydrogen production being roughly 14.1 folds greater as comparison to that of individual $SrTaO_2N$, the synthesized $SrTaO_2N/Ta_3N_5$ heterojunction is type-II category with an close interface contact. The experimental evidence suggests that the increased hydrogen generation rate results from the construction of type-II heterostructure and close interface contact amid Ta_3N_5 and $SrTaO_2N$ under irradiation of visible light. Besides, we emphasize the potential of one-pot nitridation as a general technique for designing and constructing supplementary sorts of high-efficiency tantalum oxynitride-based hetero-structured photocatalysts. Visible light was castoff to implement the photocatalytic reaction. Pure $SrTaO_2N$ produced 1.26 $\mu mol g^{-1} h^{-1}$ of hydrogen, $SrTaO_2N$ (0.05)/Ta_3N_5 produced $11.82 \mu mol g^{-1} h^{-1}$, $SrTaO_2N$ (0.1)/Ta_3N_5 produced $19.07 \mu mol g^{-1} h^{-1}$, and $SrTaO_2N$ (0.2)/Ta_3N_5 produced $4.90 \mu mol g^{-1} h^{-1}$, whereas Ta_3N_5 produced negligible amounts of hydrogen. Since the performance of $SrTaO_2N$ (0.1)/Ta_3N_5 was nearly 15.1 folds that of pure $SrTaO_2N$, this suggests that the heterostructure has contributed significantly to the improvement of photocatalytic activity [373].

Two-dimensional mesoporous Ta_3N_5 was synthesized by using a straightforward sol-gel technique and a biological prototype of filter paper subjected to a series of vacuum nitriding processes. Ta_3N_5 has an extensive light response range, even the nearby infrared (NIR) region, because N_2 vacancies are produced when N^{3-} anions are exchanged for O^{2-} anions throughout vacuum nitridation. Despite its small bandgap (1.99 eV), water splitting can still be accomplished if the redox potential is met. Compared to Ta_2O_5 and partially nitride Ta_2O_5 (N-Ta_2O_5), the experimentally observed evolution of hydrogen rate of the Ta_3N_5 photocatalyst is 34.6 $\mu mol g^{-1} h^{-1}$ [374]. The material photocatalytic act is enriched, and its band structure is optimised by the replacement of N^{3-} for O^{2-} anions. Zhan et al. proposed

new core-shell nanofibers heterojunction photocatalyst Ta_3N_5/ZnO prepared through electro-spinning process and atomic layer deposition for enhancing photocatalytic evolution of H_2 activity. Incorporating nanostructure engineering and heterojunction led to the bigger reaction sites and increased charge transfer responsible for the superior photocatalytic bustle of the hybrid Ta_3N_5/ZnO sample. The optimized Ta_3N_5/ZnO-150 composite photocatalyst beat even the most Ta_3N_5 based photocatalysts reported to date with a photocatalytic evolution of hydrogen activity of 1193.75 $\mu mol g^{-1} h^{-1}$ [375].

2.4.1.6 Polymer

Truc et al. were able to boost the photocatalytic activity or separation proficiency of electron-hole by using PTh and PANI conducting polymers as sensitizers of Ta_3N_5 photocatalyst by decreasing the high recombination rates of photo-excited electrons and holes. This means that the Ta_3N_5/polymers exhibit a new photocatalytic bustle for complete electrolysis of water to create hydrogen and oxygen under irradiation of visible light. We also looked at whether or not the Ta_3N_5 photocatalysts were protected from self-photocorrosion by the polymers used. Because of the higher electric conductivity of the PANI, the Ta_3N_5/PANI produced more hydrogen and oxygen from H_2O electrolysis than the Ta_3N_5/PTh. Truc et al. also synthesised Nb-Ta_3N_5/PPy photocatalyst for overall photocatalytic electrolysis of water to produce hydrogen and oxygen and shown to have very great photocatalytic activity even under the irradiation of visible light. Narrowing the band gap energy of Ta_3N_5 thanks to the incorporation of Nb dopant boosted the separation efficacy of electron-hole pair, reduced the likelihood of recombination of produced electrons and holes, and lengthened the period of the latter. The π conjugated system of electron in PPy behaves as protector to increase the separation efficacy of electron hole of the modified Ta_3N_5 photocatalysts by encouraging the relocation of the produced electrons and holes on the surface and reducing their recombination. This was achieved by the combination of the valence and conduction bands of

Nb-Ta$_3$N$_5$, forming a hybrid system. Therefore, the synthesised Nb- Ta$_3$N$_5$/PPy produced abundance couples of electron-hole, even in the occurrence of visible light, which took part throughout the reaction with H$_2$O to generate sufficient amounts of hydrogen and oxygen [376, 377]. Core-shell structure of Ta$_3$N$_5$@polyaniline was fabricated by Niu et al. via a chemisorption technique. Photocatalytic bustle and properties such as optical, microstructure, and photoelectrochemical, were investigated as a function of PANI concentration. Subsequently the adsorption manners, PANI were efficiently coated on the surface of Ta$_3$N$_5$ with close contact, significantly enhancing its photocatalytic activity. The photocatalytic activity was very sensitive to the PANI shell thickness. Ta$_3$N$_5$@PANI2 outperformed Ta$_3$N$_5$ alone in both the visible light photocatalytic evolution of H$_2$ and the RhB degradation ratio, with the former being 3.2 and the latter being 16.6 times faster, respectively. Ta$_3$N$_5$@PANI showed remarkable results in terms of photostability and reusability [378].

Table 2.4 Carbon based photocatalyst for photocatalytic H$_2$ evolution (PCHE)

Photocatalysts	Method	Sacrificial Agent	Light intensity	PC parameters PCHE rate	Stability	AQE %	PEC system parameter Photocurrent	Electrolyte	Ref.
N-rGO600	Pyrolysis	Na$_2$S/Na$_2$SO$_3$	500 W Xe lamp	0.96 $\mu mol g^{-1} h^{-1}$	6 h		7 mAcm^{-2}	Na$_2$SO$_4$	[379]
B-rGO1000	Pyrolysis	Na$_2$S/Na$_2$SO$_3$	500 W Xe lamp	1.00 $\mu mol g^{-1} h^{-1}$	6 h		12 mAcm^{-2}	Na$_2$SO$_4$	[380]
P-doped	Pyrolysis	Trietha	1.3	3.96	23 h		-	-	[381]

graphene(Pt-(P)G-4)	is	nolamine (TEA)	W/m^2	$\mu molg^{-1}h^{-1}$					
C, P-doped g-C_3N_4	Hydrothermal	Triethanolamine TEOA	300 W Xe lamp	74.7 $\mu molg^{-1}h^{-1}$	10 h	2.14	9 mAcm^{-2}	Na_2SO_4/TEOA	[382]
GrapheneZn0.5Cd0.5S	Hydrothermal	Na_2S/Na_2SO_3	140 mWcm^{-2}	53 $\mu molg^{-1}h^{-1}$	12 h	19.8	0.08 mA cm^{-2}	Na_2SO_4	[383]
RGO-Cd0.60Zn0.40S	Solvothermal	Na_2S/Na_2SO_3	Solar Simulator (1000 Wm^{-2})	65 $\mu molg^{-1}h^{-1}$	72 h	8.50	0.35 mAcm^{-2}	Na_2S/Na_2SO_3	[384]
N-RGO-Cd0.60Zn0.40S	Solvothermal	Na_2S/Na_2SO_3	Solar Simulator (1000 Wm^{-2})	78 $\mu molg^{-1}h^{-1}$	72h	17.87	0.92 mAcm^{-2}	Na_2S/Na_2SO_3	[385]

2.4.2 Photocatalyst for PC CO$_2$ Reduction earlier study

2.4.2.1 Metal halide perovskites

Because of its cost-effective, production volume at large scale, widespread optical absorption range, and extended diffusion lengths of electron-hole pairs, MHPs have swiftly risen to

prominence as one of the most promising photovoltaic materials. Materials based on MHPs stand out from other semiconductor nanocrystals due to their extraordinary extinction coefficient, emission of narrow band gas, and elongated carrier diffusion length. In addition, the energy band of MHPs can be tuned to optimize light capture thanks to the wide diversity of MHP architectures. Interest in MHPs as semiconductor materials has expanded beyond solar cells to include applications in photocatalysis for the production of hydrogen (H_2), the reduction of carbon dioxide, the deprivation of organic pollutants and even chemical synthesis. Photocatalytic H_2 production by visible light stimulation has been achieved, for instance, with methylammonium lead iodide ($MAPbI_3$), as demonstrated by Park et al. [386]. Xu et al. synthesised $CsPbBr_3$/GO composite for photocatalytic reduction of CO_2, increasing attention has been given to MHP based photocatalysts for the reduction of CO_2 [387].

Wang et al. synthesised highly stable co-doped $CsPbBr_3$/Cs_4PbBr_6 nanocomposite in aqueous solution protected with hexafluorobutyl methacrylate (HFBMA). Photocatalytic CO_2 reduction with a yield of 11.95 $\mu mol g^{-1} h^{-1}$ in an aqueous medium was also achieved by Co doping $CsPbBr_3$/$Cs4PbBr_6$ to form surface trap positions and increase the separation of charge. The findings demonstrate the water-tolerant features of Co-doped MHPs, which may pave the way for their use as photocatalysts in real-world artificial photosynthesis. Afterwards, they built the co-doped $CsPbBr_3$/Cs_4PbBr_6 nanocomposites as photocatalysts to accomplish the photo-conversion of CO_2 and methanol oxidation into formic acid concurrently, with a high production of carbon monoxide at 122.3 $\mu mol g^{-1} h^{-1}$ [388].

The complexes of [Ni (terpy) $_2$]$^{2+}$ (Ni (tpy)) onto the perovskite to increase the number of active sites to internment electrons for the separation of electron-hole in nanocomposites of $CsPbBr_3$, optimized $CsPbBr_3$-Ni (tpy) photocatalysts demonstrated outstanding efficiency in converting CO_2 to CO and CH_4 at 431 $\mu mol g^{-1} h^{-1}$ [389]. Xiao et al. decorated $CsPbBr_3$ with MXene (Ti_3C_2Tx) nanosheet and it shown high efficiency of CO_2 photoreduction after a

Schottky heterojunction was formed between $CsPbBr_3$ nanocrystals (NCs) and MXene nanosheets using an in situ growth strategy. High production rates for CO and CH_4 were shown for the ideal composite of $CsPbBr_3$/MXene, with values of 26.32 and $7.25 \mu mol g^{-1} h^{-1}$, respectively, demonstrating that photoinduced electrons in $CsPbBr_3$ NCs could migrate electrons to MXene nanosheets. For photocatalytic CO_2 reduction, used a self-assembling technique to produce a Ti_3C_2/$CsPbBr_3$ quantum dot hybrid, with methane and carbon monoxide production rate of 19.31 and 17.98 $\mu mol g^{-1} h^{-1}$, correspondingly [390].

Quantum dots of Inorganic halide Perovskite ($FAPbBr_3$) above sheet-like Ti_3C obtain a yield of CO rate with the value of 283.41 $\mu mol g^{-1} h^{-1}$, thanks to the Schottky interaction of the $FAPbBr_3$/Ti_3C_2 composites improving photogenerated separation and migration of charge carrier [391]. Chen et al. employed a photocatalyst composed of $CsPbBr_3$@-g-C_3N_4 to reduce CO_2 in ethyl acetate. CO and CH_4 were produced at amounts of 22.08 and $2.83 \mu mol g^{-1} h^{-1}$, respectively, from the photoreduction of CO_2 [392].

Recently Wan et al. fabricated a heterojunction photocatalysts $CsPbBr_3$ QDs/UiO-66(NH_2) to advance the efficiency and selectivity of photocatalytic reduction of CO_2. The maximum yields of CH_4 ($3.08 \mu mol g^{-1} h^{-1}$) and CO ($98.57 \mu mol g^{-1} h^{-1}$) were achieved after 12 hours of processing an optimum sample [393]. Ding et al. developed a composite of $Cs_2AgBiBr_6$/Ce-UiO-66-H using an in situ assembly scheme; Cs_2-$AgBiBr_6$ was inserted in the framework of Ce-UiO-66-H and made fitted contact. This allowed them to obtain a greater conversion of CO_2 activity of 309.01 $\mu mol g^{-1} h^{-1}$ [394]. Sun et al. used a photo-deposition technique to synthesize a Cu_2O quantum dot (QD)/g-C_3N_4 foam hybrid material. The material was found to have excellent photocatalytic performance, with a CO yield 11 folds superior than that of g-C_3N_4 at 8.182 $\mu mol g^{-1} h^{-1}$ [395]. Loaded Cu_2O QDs, in particular, may function as an efficient electron storage layer by encouraging charge separation as well as offering active sites for CO_2 reduction. In 2011, Li et al. examined the

visible light catalyzed CO_2 into methanol conversion in the existence of alkali and sodium sulfite. According to the data analysis, it was discovered that SiC, Cu_2O, and Cu_2O/SiC catalysts produced 153, 104, and 191 $\mu mol g^{-1} h^{-1}$ of methanol, correspondingly. The photocatalytic efficiency of SiC NPs might be enhanced by Cu_2O treatment [396].

2.4.2.2 Metal oxides based photocatalyst

Different amount of Cu doped TiO_2 photocatalysts were synthesized by Olowoyo et al. using sonothermal and hydrothermal synthesis technique. Higher surface area was observed in the obtained photocatalysts, which had Cu species doped both on the surface and within the TiO_2 lattice. The Cu_2-TiO_2 photocatalyst was found to be the most effective of the produced materials when exposed to UV-A light under optimal reaction conditions. The reduction of CO_2 in KOH/H_2O medium under the irradiation upto 24 hours the product yield obtained for methane of 6.6 $\mu mol g^{-1} h^{-1}$, 472.5 $\mu mol g^{-1} h^{-1}$ of methanol, and most interestingly, 743.8 $\mu mol g^{-1} h^{-1}$ of acetone. The yields of methanol, acetone, methane and ethylene, while exposed to visible light were 74.17, 22.17, 6.18 and 0.53 $\mu mol g^{-1} h^{-1}$, correspondingly. It is possible that the photocatalyst's activity upon the irradiation of visible light is due to the copper content contained in the material [397]. The Ce doped TiO_2 photocatalyst (0.2 wt %) was synthesized by Ali et al. using the sol gel technique. Under the irradiation of fluorescent light the best photocatalytic activity shown by the composite of Ce/La/TiO_2, which is fabricated with the optimal doping of Ce with 1.5 wt% in TiO_2. The maximum production of CH_3OH was 317.7 $\mu mol g^{-1} h^{-1}$ in the liquid phase. Additionally, 119.4 and 262.8$\mu mol g^{-1} h^{-1}$, respectively, of CO and CH_4 were obtained as major products from the reaction in gas phase. Compared to La/TiO_2, the product yields of CH_3OH (1.8 times), CH_4 (1.9 times), and CO (2.1 times) for wt% of 1.5 Ce/La/TiO_2 were measured [398]. Under the irradiation of a 300 W Xe arc lamp for 9 hours, Huang et al. calculated the photocatalytic activity of nanoparticles of Eu-doped TiO_2 for CO_2 reduction. When using a Eu-TiO_2 catalyst

at a concentration of 0.25 percent, the highest yields of both CO ($42.91 \mu mol g^{-1} h^{-1}$) and CH$_4$ ($65.53 \mu mol g^{-1} h^{-1}$) were recorded. Compared to pure Titania photocatalysts, the optimal concentration of 0.25% of Eu doped TiO$_2$ photocatalyst produced much more products and this difference can be attributed to the reduced rate of charge carrier recombination in the doped photocatalyst. The photocatalytic reduction activity was shown to be reduced with increasing doping content [399]. Xiong et al. synthesized a codoped TiO$_2$ with V and W (V^{4+} and W^{6+}) cations arranged the honeycomb channel interior and V^{5+} (V$_2$O$_5$) on the surface as the dopants. When studying the photocatalytic productivity of such co-doped TiO$_2$ at reducing CO$_2$, researchers discovered that doping with V^{4+} increased the material's capacity to absorb visible light by producing a transitional state inside the material's band gap. Additionally, the W^{6+} cation encased into the lattice of TiO$_2$ structure may capture photogenerated e$^-$ and transmit them toward the surface-adsorbed CO$_2$ and H$_2$O molecules [400].

Table 2.5 List of several photocatalysts for the reduction of CO$_2$ by photocatalytic process

Photocatalysts	Co-catalysts	Conditions	Yield (%)	Main product	Remarks	Ref.
TaON and Ta/N-co-doped TiO$_2$ in conjunction with a binuclear Ru (II) complex, GaN:ZnO solid solutions	Ag	300 W xenon lamp; λ > 400 & 365 nm; 15 h; pH:6.4	-	Hydrogen and formate	It emphasises the tremendous potential of band-tunable mixed-anion semiconductors in Z-scheme based hybrid photocatalysts for the CO$_2$ reduction in visible light.	[401]
Copolymerized	polymer	300 W	98	Formic	In contrast to the common	[402]

carbon nitride paired with Ru (II) complex		xenon lamp; $\lambda > 500$ nm; 5 h		acid	practice of requiring time-consuming post-synthesis modifications to increase electron density, this study showed that a simple modification of a bulk semiconductor by using the copolymerization approach becomes a further successful method to boost the photocatalytic activity of the hybrid photocatalyst.	
Ru-complex Ta_2O_2(N-Ta_2O_5: nitrogen doped Ta_2O_5) hybrid	NH_3	500 W xenon lamp; $\lambda > 390$–750 nm; 15 h; pH:5–6		Carbon monoxide and formic acid	According to the study, NH_3 adsorption on the surface of the Ta_2O_5 aids in the transit of electrons to the Ru-complex. In addition, this work's calculations suggest that replacing some of the Ta_2O_5 surface oxygen atoms with NH groups causes a red shift in the absorption band edge and a little upward shift in the CBM.	[403]
Macrocyclic Co(III) on three different semiconductor surfaces	No	mercury lamp; $\lambda > 420$ nm; 5 h			Since N-Ta_2O_5-based hybrid photocatalysts lack surface functionalities (such as hydroxyl groups) necessary for the molecular deposition of	[404]

					cobalt complexes, their performance is subpar.	
Mesoporous carbon nitride with polymeric cobalt phthalocyanine catalyst	Polymer	300 W xenon lamp; $\lambda > 500$ nm; 5 h	60	Carbon monoxide	Photocatalytic CO_2 conversion relies on precise control over catalyst loading, which can only be achieved through in situ polymerization of the phthalocyanine.	[405]
Mn-immobilized TiO_2 hybrid (OrgD-TiO_2-MnP)	Dye	300 W xenon lamp; $\lambda > 500$ nm; 5 h	> 99	Formate and carbon monoxide	It was shown that the amount of MnP applied to the surface of TiO_2 greatly affected the product selectivity (HCOO-/CO).	[406]

The yields of the CO, CH_4, and H_2 of the V_3W_3T photocatalyst were 1.91, 0.22, and $0.27 \mu mol g^{-1}h^{-1}$, correspondingly, when compared to individuals of particular metal doped TiO_2 catalysts [407]. Wang et al. examined the usage of lead sulfide quantum dots (PbS-QDs) sensitized with copper doped-TiO_2 catalysts for the photo-catalytically reduction of carbon dioxide. The CO_2 conversion yield for the synthesized Cu/TiO_2 catalyst with 4 nm PbS-QD was 1.71 $\mu mol g^{-1}h^{-1}$ for CO, 0.58 $\mu mol g^{-1}h^{-1}$ for CH_4, and 0.31 $\mu mol g^{-1}h^{-1}$ for C_2H_6. Researchers discovered that adding photosensitizers to Cu/TiO_2 increased yield by almost a factor of 5. In addition, the product yield of a PbS-QD sensitized Cu/TiO_2 photocatalyst was greater at 4 nm than at 3 and 5 nm [408].

2.4.2.3. Carbon based material used as sensitizer

Researcher all around the world are currently inspired by carbon-based photocatalysts because of low environmental impact, cost effective and lack of toxicity. A conjugated system is more in the carbon-based materials facilitates the transit of photo excited e⁻s by

facilitating the split-up of excitons. In addition, the photocatalyst is more uniformly distributed across the carbon matrix, making it easier for molecules reactant to be adsorbed. Together, the photocatalyst and the carbon material create a synergistic effect that greatly boosts production rates. Therefore, the requirement of an effective photocatalyst for CO_2 reduction is met by any photocatalyst united with carbon-based materials. Many problems in real life have been resolved with the support of carbon materials like activated carbon, carbon quantum dots, graphene, carbon nanotubes (CNTs), and carbon fibers, etc.

For instance, two dimensional graphene oxides are intended for its chemical stability, great specific surface area and high charge carrier movement. Because of a number of benefits, GO is a great addition to the MHPs system for photo-reducing CO_2. Wang et al. also produced methyl ammonium lead bromide (MAPbBr$_3$) wrapped in GO [409]. The photo lumniscence decline periods of CsPbBr$_3$ anchored on MWCNT were shorter than those of simple MAPbBr$_3$ (0.268 lmol cm^{-2}h^{-1}) thanks to a self-assembly method used by Shu et al. The shorter photo luminescence decline times definite the existence of a transmission of charge channel in the composites of MWCNT/CsPbBr$_3$, by which the photogenerated carriers were quickly relocated, leading to a 3.14 and 2.13-fold increase in CO and CH$_4$ yields, respectively, over pristine CsPbBr$_3$ QDs in the CO_2 photo reduction route. The yields of CH$_4$ and CO are shown in the figure to be 27.3 and $71.3 \mu mol g^{-1} h^{-1}$, respectively, when CsPbBr$_3$ was treated with fullerenes (C$_{60}$) to enhance charge separation for photocatalysis [410].

2.4.2.3.1 Photocatalysts based on activated carbon

Activated carbons have been used in the production of photocatalytic materials due to their large surface areas, high adsorption capabilities, and high porosity. ZnO composites with activated carbons have been synthesized and published in several publications. However, high price of commercially available activated carbon is the chief barrier to their widespread use. Therefore, in recent time, there has been a lot of attention on synthesizing activated

carbons economically using agricultural byproducts and low-cost wastes. In addition to guava seeds, black stone cherries, peanut shell, apricots stones, peach stones, sugarcane bagasse, almond shell, and orange peels have all been reported as sources of activated carbons.

Zinc oxide (ZnO) is a semiconductor metal oxide with a deep violet absorbance at room temperature a binding energy of 60 meV and a band gap of 3.37 eV. This metal oxide exhibits great photocatalytic activity in addition to its excellent electrical, mechanical, antibacterial, optical, and antifouling properties [411]. ZnO has been used in the literature for photocatalytic organic waste degradation, metal ion reduction, and carbon dioxide (CO_2) sequestration. The CO_2 photoreduction property of ZnO/activated carbon composites has been reported on only infrequently, even though several publications have revealed their synthesis and their use in photocatalysis [412]. Carbon fiber, among carbon materials, is considered a useful component for making composites because of its ability to prevent nanocrystal aggregation and photo- corrosion as well as its high electron mobility. One study describes an in-situ controlled procedure for producing composites of ZnO nanorod arrays and carbon fibres [413]. The maximal yield of 430.2 under UV irradiation for as-synthesized composites was 7.15 times greater than that of pure zinc oxide (ZnO) (60.2 UNIT), demonstrating remarkable activity in CO_2 to CH_3OH photoreduction. A precedent for the carbon materials and functional cross-linking of TiO_2 was first reported to have been established by the Uchida team in Japan in 1993 when degrading propionamide by photocatalysis, they combined activated carbon with TiO_2. The mineralization efficiency was raised by more than a factor of three when activated carbon was added to the TiO_2 catalyst, which greatly boosted the adsorption rate of propionamide on the TiO_2 catalyst [414]. The photocatalytic degradation ability of TiO_2 when exposed to visible light was found to be enhanced by the upconversion effect of carbon QDs, as proven by Pan et al. in 2014 [415]. The formation of a photocatalytic heterojunction enhances the adsorption effectiveness,

prevents the recombination of photogenerated carriers, and makes CO_2 reduction more efficient. More studies on photocatalytic degradation and reduction using carbon materials-TiO_2 functionalized materials have been conducted in recent years. Research has shifted its focus to improving photocatalytic efficiency by modifying carbon-based materials and employing numerous catalysts. In the presence of a graphene-TiO_2 composite, Zhang et al. found that CO_2 could be reduced photo-catalytically, leading to the production of 160 $\mu mol g^{-1} h^{-1}$ CH_3OH and 150 $\mu mol g^{-1} h^{-1}$ of formic acid [416]. It was discovered that increasing the graphene loading enhanced photocatalytic activity. In their study on the nanostructure of composite hollow carbon nitride spheres (HCNS)@TiO_2, Dehkordi et al. discovered that the composite produced 11.3 $\mu mol g^{-1} h^{-1}$ CH_3OH products on exposing to CO_2 photoreduction. As a result, the yield obtained was approximately five times higher than that achieved with pure g-C_3N_4 and ten times more efficient compared to the P-25 TiO_2 photocatalyst [417]. Wang et al. achieved the highest yields of CH_4 and CO after 4 hours of irradiation using g-C_3N_4 modified TiO_2. The highest yields obtained of CH_4 and CO are of 72.2 and 56.2 $\mu mol g^{-1} h^{-1}$ [418].

2.4.2.4 Polymer based photocatalyst

Furthermore, Polyaniline (PANI) and other linear conjugated polymers have been explored for formation of conjugates having inorganic semiconductors. The photocatalytic reduction of CO_2 in the presence of H_2O was significantly enhanced by a polyaniline/TiO_2 hybrid. The production rates of methane (CH_4), carbon monoxide (CO), and hydrogen (H_2) were 3.8%, 2.8%, and 2.7% higher, respectively, in a 0.85% PANI-TiO_2 hybrid photocatalyst compared to a pure TiO_2 photocatalyst [419]. The yolk-shell (YS) structure is another significant class of carbon-based nanostructures with fascinating chemical and physical properties. The typical YS structure has a solid inner core surrounded by a hollow shell, which increases light scattering in the shell interior while also providing a wide surface area from which to

generate many active sites. In this context, hollow heterostructure g-C_3N_4@CeO_2 photocatalysts were shown to improve photocatalytic reduction of CO_2 by Liang et al. The highest yields were found to be 3.5%, 5.2%, and 16.8% $\mu mol g^{-1}h^{-1}$ for CH_4, CH_3OH, and CO [420].

2.4.2.5 Tantalum nitride based photocatalyst for CO_2 reduction

Due to their characteristics as narrow band active visible light absorbers, several Ta-based materials, like as tantalum nitrides (Ta_3N_5) and tantalum oxynitrides (TaON), have lately emerged as leading contenders for effective solar light water splitting. Due to their low band gap of 2.4 and 2.1 eV, correspondingly, TaON and Ta_3N_5 are ideally suited to begin photocatalysis through visible light absorption (low energy consumption). As a result of its probable use in water splitting and the photocatalytic destruction of organic contaminants, several research endeavors have been dedicated to investigating Ta_3N_5. Based on the data, Ta_3N_5 appears to be a strong contender for use as a photocatalyst driven by visible light. Ta_3N_5 was modified by Wang et al. by using the low-work-function metal Bi. Due to the lower work function of Bi (4.2 eV) compared to Ta_3N_5 (4.5 eV), it is expected that a surface band bending will occur at the interface junction region between these two materials, with a downward direction. This improved photocatalytic activity is due to increased electron transport from Ta_3N_5 to Bi as well as efficient separation of the redox sites. $BiTaO_4$ was effectively synthesized as a Ta_3N_5/Bi composite catalyst by heating it in an ammonia environment, and the observed photocatalytic activity demonstrated remarkable efficiency in converting CO_2 to CH_4. The addition of bi metal particles clearly increased the Ta_3N_5 carrier-separation efficiency. The values for total CH_4 production vary from 0.89 for Ta_3N_5 to 1.14 for M-Ta_3N_5/Bi to 4.52 $\mu mol g^{-1}h^{-1}$ for Ta_3N_5/Bi. The Ta_3N_5 value falls in the middle of this range. The rate of CH_4 synthesis is $\mu mol g^{-1}h^{-1}$ over Ta_3N_5/Bi, that is 5.2 and 4.1 times more than it is over Ta_3N_5 ($\mu mol g^{-1}h^{-1}$) and M-Ta_3N_5/Bi $\mu mol g^{-1}h^{-1}$) [421]. Nguyen et

al. synthesized V doped Ta_3N_5 and results demonstrated much greater absorption of visible light in addition to reduced band gap energy in comparison to Ta_2O_5. The CO_2 was transformed into CO and CH_4 by the synthesized Ta_3N_5 and Ta_3N_5 photo catalytic materials even in the presence of visible light. The photocatalyst electron-hole separation efficiency was improved because to the presence of V dopants in the lattice of Ta_3N_5, which served as intermediary band (V 3d) between the Ta_3N_5 VB (N 2p) and CB (Ta 5d). Therefore, V-Ta_3N_5 had significantly better photocatalytic activity than Ta_3N_5. Photocatalytic CO_2 reduction 2 wt. % of V-Ta_3N_5 on exposure to visible light resulted in 1003, 425, 236 and 56 $\mu mol g^{-1} h^{-1}$ of O_2, CH_4, CO and H_2, respectively [422].

2.5.   Scope and Objectives of Research

A significant amount of time and effort has been invested in the quest for an energy source that is ecologically responsible and renewable. To achieve zero-carbon fuel, water splitting is considered as key, therefore, the investigation of catalysts for the water splitting reaction remains a significant challenge. For the removal of noble-metal catalysts, transition metal based catalysts are considered as very important class of catalysts. These catalysts are highly abundant, highly stable, reactive under diverse operational conditions and helpful to cut the cost. Numerous advance articles supported that transition metal based catalysts will be very essential in near future.

There are several semiconductors which have been reported as photocatalysts so far as mentioned in above section. However, uncontrolled charge recombination, this leads to a decrease in the quantity of active species, that is the major drawback for using these photocatalysts. The aim of this thesis is to develop some promising and stable transition metal based photo-catalysts for water splitting reactions. It is vital to solve future energy and environmental concerns that need the synthesis of photocatalysts that are both efficient and driven by visible light.

2.6. The objective of this present work is as follows:

1. Synthesis of solar catalytic system metal (V, Nb) and non-metal (S) co-doped Ta_3N_5 solar catalyst efficient for photo-catalysis immobilized with biomass-soot carbon followed with carbonization and activation to increase the surface area

2. Development of nanocomposite co-doped Ta_3N_5 immobilized BSC with conducting polymer PANI as an efficient solar catalytic system

3. Production of H_2 using efficient photo-catalytic system under solar irradiation

4. Reduction of CO_2 using novel photo-catalytic system under solar irradiation for conversion renewable energy (methanol, methane) production

5. Characteristic analysis of novel photo-catalytic system for renewable energy production

2.7. Methodology in brief

Figure shows the methodology used in this work. The Ta_3N_5 composites were synthesised by carbonization, hydrothermal and electrochemical-polymerization methods. The preliminary characterizations like structural, morphological, compositional and optical analysis were performed. Photocatalytic water splitting experiment was carried out for all composites materials to check if they are photocatalytically active. The composites materials which showed appropriate band gap and band edge potentials are tested for H_2 evolution and CO_2 reduction through photocatalytic water splitting experiments.
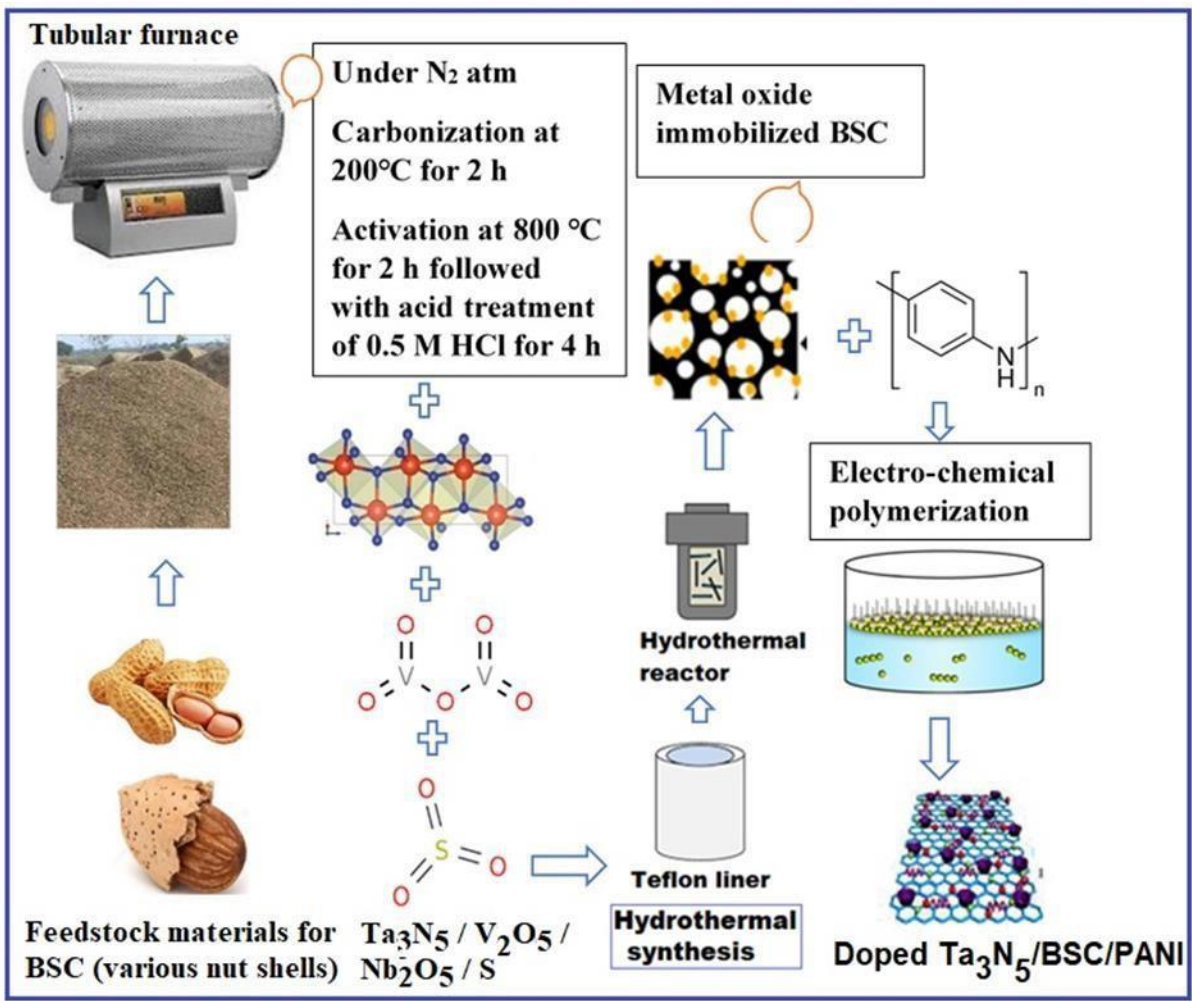
Fig. 2.7 Schematic design for the fabrication route of the composites materials

<center>**Chapter 3**</center>

3.1 Materials and Characterization studies

3.2. Materials

Biomass of Dulcis (almond) Shell and Arachishypogaea (peanut) Shell, Ta_2O_5 and $TaCl_5$ (99% Sigma-Aldrich), vanadium pentaoxide (V_2O_5), niobium ethoxide, Thiourea, Ethanol, Hydrochloric acid (HCl), Aniline (Lobachemie), Ammonium peroxydisulfate (($NH_4)_2S_2O_8$ from CDH), Potassium hydroxide (KOH), Sodium hydroxide (NH_4OH), Acetone, and Methanol (99%, LiChrosolv Merck) used as sacrificial agent. The entirely chemicals utilized as procured. As a substrate to manufacture photoelectrodes (PEs) ITO (Merck) glass plates were used. Sulphuric acid (99%), sodium sulphate, potassium hydroxide, purchased from CDH Pvt. Ltd. was used to carry out electrochemical and photoelectrochemcial (PEC) studies. All reagents were synthesized by using ultrapure deionized water obtained from Millipore, and glassware was cleaned by using ethanol and distilled water.

3.3. Synthesis Process for the preparation of photocatalyst materials

A wide range of chemical methods are documented for the synthesis of different metal-nitride based composites. The following are some of the commonly used approaches.

- ➢ **Hydrothermal**
- ➢ **Solvothermal**
- ➢ **Deposition–precipitation method**
- ➢ **Calcination method**
- ➢ **Electrostatic self-assembly method**
- ➢ **Thermal decomposition**
- ➢ **Carbothermal synthesis**
- ➢ **Sol-gel**

> **Electrochemical synthesis**

> **Mechanochemical synthesis (MCS)**

> **Direct element combination**

> **Solid-solid separation method**

> **Post-synthesis heat treatment of carbides and nitrides**

3.3.1. Hydrothermal Method

The British geologist Sir Roderick Murchison invented the word "hydrothermal" in 1792 [423]. Tuning the reaction conditions allows for more size and form control in the solution-based methods of synthesis known as hydrothermal and solvothermal synthesis, respectively. Hydrothermal chemistry refers to the use of heat to bring about a chemical reaction in aqueous solution, while solvothermal chemistry refers to the use of non-aqueous solution. The hydrothermal technique creates a reaction environment with high pressure and temperature by dissolving, heating, and recrystallizing compounds that were previously insoluble or sparingly soluble. This process takes place in a sealed autoclave, enabling the synthesis of nanomaterials through the separation and subsequent heat treatment of the dissolved components. Hydrothermal synthesis is appealing because it can create both homogeneous and monodispersed nanoparticles and nano-hybrids. This technique is best suited for the manufacture of monodisperse nanoparticles. The hydrothermal process, in which nanomaterials are formed, requires a closed steel autoclave, a temperature range from mild to the broad and high pressure. The main benefit of this technique is the ability to create nicely crystals [424].

3.3.2. Solvothermal method

Hydrothermal processing is typically reserved for materials that are not affected by water. Solvothermal reactions often involve water; however for chemicals that may react or

hydrolyze in water, organic solvents are typically used instead. Insoluble or poorly soluble compounds can be dissolved and recrystallized into pure, homogeneous crystals using the solvothermal process. Parameters like reaction time allow control over nano product shape and composition. The solvothermal approach not only promotes the formation of nanoparticles on specified crystal planes, but it also stops reduced nanoparticles from aggregating with one another, ensuring that the appropriate shape is achieved [425].

3.3.3. Deposition–precipitation method

The deposition-precipitation method enables the preparation of a catalyst containing desired metal nanoparticles [426]. This technique involves combining a solution of the target metal (usually a noble metal) with a suspension of the carrier material. The mixture is then stirred at a specific temperature and pH to facilitate the deposition and precipitation process. Many composites, including g-C_3N_4/Bi_2WO_6/AgI, PANI/Ag_3PO_4/$NiFe_2O_4$, AgBr@Bi_2WO_6/WO_3, and MIL-53 (Fe)/a-Bi_2O_3/g-C_3N_4, have been prepared using the deposition-precipitation method. This technique increases the surface area in contact between the parts and creates enough pathways to segregate and transport photogenerated carriers. The deposition-precipitation process allows for the distribution of most loaded components primarily on the carrier material's surface, which results in low consumption and a high utilization rate. This is especially important for noble metal assisted catalysts like platinum, iridium, and others that can conserve a great deal of their respective precious metals. The second benefit is the immediate availability of uniform; instead, shaped support materials. It is simple to select a suitable catalyst due to the fact that its form, specific surface area, and porosity are all determined by the support.

3.3.4. Calcination method

In order to create solid catalysts, calcination is one of the processes that can be used. Catalysts are normally produced by bringing an aqueous solution of metal salts into contact

with a carrier, adsorbing or storing the solution in the capillary of the carrier, draining off any surplus solution, and then calcining and activating the material in a chamber furnace. This is the standard method for producing catalysts. The dual Z-scheme composite of Co_3O_4@CoO/g-C_3N_4 was produced by combining the previously obtained g-C_3N_4 dispersion with CoO in methanol solution, stirring the mixture evenly until the methanol evaporated, drying the mixture at 60 ^{o}C, and then calcining it at 200 ^{o}C [427]. By selecting a carrier with suitable specific surface area and porosity during the calcination process, it is possible to obtain an ideal composite material with the desired physical and structural characteristics of the catalyst, thereby altering the morphology of the carrier. This is possible because of the fact that the calcination process. There is a wide range of degrees of heat resistance among the various substances. Changing the calcination temperature may vary the amount of certain chemicals present in a compound or the crystal shape of the compound, both of which are necessary for the production of a composite material having stable features and the ideal form [428]. Waste gas contamination during the calcination process, however, is unavoidable and could limit its widespread practical applicability.

3.3.5. Electrostatic self-assembly method

Electrostatic self-assembly is a spontaneous process in which fundamental structural units, ranging from molecules to nanomaterials or larger entities, assemble themselves into ordered structures. The spontaneous arrangement or aggregation of essential structural components into a sturdy form with a regular geometric appearance is what we mean when we talk about self-assembly. In order to construct heterogeneous structures, electrostatic self-assembly has become a widely used and practical method [429]. Self-assembly guarantees a limited granularity distribution for precise control over the resulting morphology and system.

3.3.6. Thermal decomposition

A chemical reaction known as thermal decomposition takes place when heat is applied to a

single component, causing it to split into two or more substances. This synthesis process, which was performed at temperatures between 400 and 1000°C, is one of the earliest ways to create monodispersed nanoparticles. The muffle furnace was used to heat the alumina or silica crucible containing the precursor to a high temperature, yielding the desired product [430].

3.3.7. Carbothermal synthesis

At high temperatures (usually 1350-1400°C for 3 hours), activated carbon can be used to reduce metal oxides, a process known as carbothermal synthesis. Similar to the reduction procedure used to refine metals from their ores, carbothermal synthesis generates carbon monoxide and, in some cases, carbon dioxide. Intriguingly, the technique could potentially create a hydrophobic carbon support for the nanoparticles of metal carbide if too much carbon is used [431]. The several steps (chemical processes) involved in this method make it time-consuming and not very practical for synthesizing nanoparticles, despite the fact that it is scalable and has been industrialized in the past. Furthermore, this process is linked to high energy consumption, high production costs, and undesirable by-products. However, due to their properties, carbides synthesized in this way have found a number of intriguing applications. For example, phase-pure Fe_3C nanoparticles have been reported to have superior values to iron for both particle diameter (20 nm) and saturated magnetization (~130 emu/g). Recent studies have reported the use of organic gelators, this technique involves dispersing soluble metal precursors (metal oxides) within a homogeneous gel network using various substances, including small molecules like urea and polymers like chitosan, as an alternative to the conventional carbothermal approach.

3.3.8. Sol-gel synthesis

The transition of a gel intermediate is an essential step in the sol-gel synthesis process, which may be used to produce a nano-material or a solid product starting from a solution. This

method of synthesis allows for rapid reactions by mixing the reactants at the molecular level, and it also produces more uniform products with a larger effective surface area. In particular, metal alkoxides that are amenable to hydrolysis, nucleophilic attack and condensation on the way to polymerization are commonly used in a sol-gel method. Regulating reaction conditions and/or employing suitable supports or templates allows for regulation of the end products' size, morphology, and porosity [432]. It is fascinating that this technique has been utilized to synthesize materials like metal carbide and nitride nanoparticles. Designing new layered hybrid materials with magnetic characteristics often involves the Complexation of metallic center. However, this method requires a number of chemical processing stages, which can be time-consuming and laborious. If you want to slow down or speed up the condensation processes, all you have to do is add a polymeric network or suitable catalyst. The origins of sol-gel techniques can be traced back to the synthesis of metal nitrides, which involved the utilization of metal-organic compounds containing the metal element and di alkyl amine. The intermediate product undergoes a transformation to become the final product by a series of reactions with sodium acetylide and subsequently with an aqueous solution of ammonia that take place at a temperature of $50^{o}C$ for an hour. The final product also undergoes an at-room-temperature ammonia evacuation process. Since many achievements have been accomplished in the oxide material's synthesis, there has been a significant amount of interest in the non-oxide material's synthesis. Since the sol-gel process allows for precise control over the resulting material's morphology, it can be used to manufacture a wide range of substances. In order to synthesize metal carbides with a high surface area, such as titanium carbide, the hybrid approach of combining the sol-gel method with the carbothermal reduction process is employed, despite its more prevalent use in the creation of silicates and common metal oxides.

3.3.9. Electrochemical synthesis

In electrochemical synthesis, metals and non-metals undergo charge transfer from ionic melts at high temperatures by multi-electron reactions. This technique has not seen widespread use in industry because of the high temperatures (1023-1473 k) and extended times (say, 2 hours or more) required for electron electro-reduction of numerous system components. It's worth noting that this synthetic route to metal carbide has advantages such as (i) fewer byproducts, (ii) the ability to keep an eye on the temperature during production, and (iii) the potential for meso or nano-scale product development. But there are drawbacks to this technique as well: (i) Purification of the cathodic products is essential, and (ii) It is not easy to produce a chemical with perfect stoichiometric ratios. The electro-chemical reduction of solid metal oxides to metals in melted salts is an intriguing issue that has gained a great deal of interest recently. Many reactive metals, including titanium, chromium, and others, have been extracted using electrochemical techniques, and these techniques have also been applied to the creation of numerous functional alloys and inorganic composite materials [433].

3.3.10. Mechanochemical synthesis (MCS)

Mechanochemical synthesis (MCS), a solvent-free and top-down approach that involves the milling or grinding of their precursors, has emerged as a viable route for the creation of MHPs in recent years [434]. It has various benefits over the traditional solution-based approach, such as reduced organic solvent consumption and improved stoichiometric control of the end products. In order to create the required MHPs at kilograms scales, Hong et al. used the MCS technique to synthesize a variety of metal halide (M-X) perovskites, including trigonal $FAPbI_3$ cubic $CsPbI_3$, and cubic $CsSnCl_3$ [435]. In a similar manner, Kumar et al. conducted a study on the fabrication of gas-phase photocatalytic CO_2 reduction using Cu-RGO and Pb-free $Cs_2AgBiBr_6$ double perovskite nanoplates [436]. The morphology of the $CsPbBr_3$ was tunable by adjusting milling conditions such as cesium salt precursor ball

milling time, and ball size.

3.3.11. Synthetic methods for metal carbide and nitride

3.3.11.1.   Direct element combination

In this synthetic technique, non-metal and metal are immediately reacted together at high temperatures. There are a number of drawbacks to this method, however, including the need for a very high temperature, the creation of nanoparticles with uneven grain sizes, an incomplete reaction, a lengthy reaction time, and the absence of a mesoporous structure [437]. Lie et al. note that due to the absence of auspicious features of the final product, long reaction time and high energy consumption, this strategy has not received much interest from researcher [438].

3.3.11.2.   Solid-solid separation method

A recent research looked at the process of producing metal nitrides using the solid-solid separation technique. This synthetic method involves ammonolysis of bulk ternary oxides in the presence of ammonia gas at temperatures between 600 and 800 degrees Celsius. This approach is both economical and ecologically friendly, allowing for the synthesis of a wide range of metal nitrides with desirable properties such as small pore size ($\sim$10-40 nm) and high surface area [439].

3.3.12. Post-synthesis heat treatment of carbides and nitrides

Most of the nitrides and carbides mentioned earlier are typically manufactured in the form of powders, but they need to be cast into precise forms before they can be used in applications. Consolidation can be achieved through two methods: cold pressing followed by heating (also known as cold compaction) or simultaneous hot pressing [440]. Cold compaction involves applying pressures in the range of a few hundred megapascals to the powders, followed by heating to around 0.5-0.6 times the melting point (Tm) of the material. Hot pressing, on the

other hand, combines both pressing and heating steps simultaneously. The transformation of powder compacts into a solid, brittle ceramic is accomplished through a process called sintering. During sintering, the powder particles interact with each other, resulting in the formation of the final microstructure. This microstructure plays a vital role in determining the material's properties, including its dielectric response, mechanical strength, and other characteristics. It should be noted that a higher sintering temperature (above 0.8 Tm) increases the likelihood of oxidation. In addition, the lattice diffusion process will take precedence at these temperatures, which will result in the growth of bigger particles or grains. This coarsening works against densification (i.e. pore reduction) mechanisms, leading to the trapping of small pores and thus altering the material's structural and functional properties. This is especially true of cemented carbides based on Tungsten (WC), which are currently undergoing extensive research for their potential use in the manufacturing industry, specifically as drilling and cutting tips. They exhibit a thermal expansion coefficient comparable to that of glass and possess a high hot hardness, measured at 15 GPa on the Knoop hardness scale. Sintering tungsten requires either a high temperature for an extended period of time or the inclusion of secondary particles known as additives, to achieve maximal densification (approx. 95%) due to tungsten's poor diffusion coefficient. On the other hand, high temperatures pose a threat of grain coarsening and the appearance of second phase particles, both of which can negatively affect fracture characteristics. Recent years have seen a shift away from traditional heat treatment and sintering in favor of more modern alternatives such as microwave sintering and spark plasma sintering (SPS). Due to its shorter processing time (total time of 5-10 minutes) and the ability to achieve near theoretical density (100%) at lower temperatures (below 0.4 times the melting point), it offers advantages over traditional sintering methods SPS has attracted considerable attention. In spark plasma sintering (SPS), particles are compacted using the heat created by the passage of current,

which is supplied as a high direct current over graphite dies. Since the heat is being produced on the inside of the material, the sintering process can proceed at a high cooling/heat (100 °C/min) [441].

3.4. Characterization Techniques

The synthesised photocatalysts were studied using a number of different analytical methods. X-ray diffraction (XRD) analysis was employed to observe the entire synthesis and product production process. Once XRD confirmed the formation of a pure phase, additional analyses were conducted using UV-visible diffused reflectance spectroscopy (UV-Vis DRS), field emission-scanning electron microscopy (FE-SEM), and energy dispersive X-ray spectroscopy (EDS) to further examine the photocatalysts. For a comprehensive investigation of the charge carriers, photoluminescence spectroscopy (PLS) and electrochemical impedance spectroscopy (EIS) were utilized. This chapter provides a concise overview of all the tools, techniques, and instruments used, as well as the procedures for the sample analyses.

3.4.1. X-ray Diffraction (XRD)

Powder samples can be analysed nondestructively using XRD, a well-established characterization technique. It can be used to find out information about solid materials, such as their crystallinity, crystallite size, crystallographic group, and phase purity. The XRD pattern, which is the result of incident X-rays being diffraction-recorded at 2θ angles, is specific to a given crystal structure. Since every compound leads to a set of diffraction peaks at explicit d-spacings, the XRD pattern is analysed to determine the lattice system. According to Bragg's law, the monochromatic incident X-ray of wavelength is related to the path difference, d as follows:

$$n\lambda = 2d \sin\theta \qquad (3.1)$$

where, n represent order of diffraction, λ is referred as incident X-ray's wavelength, θ is referred as incidence angle of the X-rays and d stands for interplanar distance in the crystal

structure [442].

In this research, XRD analysis was employed extensively. All of the XRD readings were taken using a graphite monochromatized CuKα (1.5406 Å) radiation source powered by a Bruker AXS D8 Advance diffractometer at 40 kV and 40 mA. Powder X-ray diffraction measurements of the solids were taken at a rate of 1°/min throughout an angular range (2θ) of 5−90°. For consistent diffraction, a powder sample of ~ 0.5g is put onto the groove of the sample holder for scanning and then pressed with a glass slide. Figure 3.1 depicts the high-level configuration diagram.
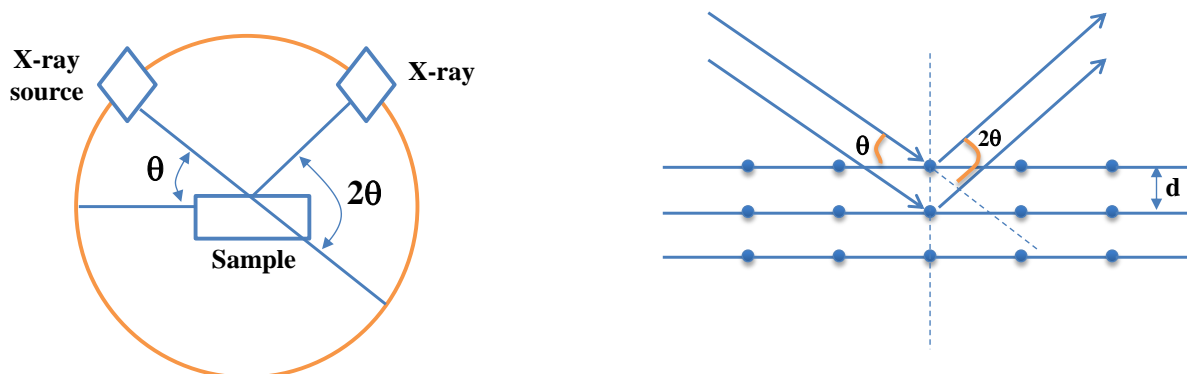
Fig. 3.1 Schematic representation of XRD setup and Bragg's constructive diffraction

Bragg's constructive diffraction, as depicted in Figure 3.1, elucidates the X-ray diffraction diffraction condition. If the x-ray path difference, $\Delta = \Delta1 + \Delta2$ is equal to an integer multiple of the wavelength, then we have evidence of constructive interference. Bragg's law is the result of the following trigonometric mathematical computation. The interplanar distance is determined by applying Bragg's law (Equation 3.1) [443].

3.4.2. Fourier Transform Infrared Spectroscopy

The chemical bonds of substances have their own unique vibrational frequencies. When IR radiation hits on a material, it is absorbed at the frequencies that correspond to those of the material. Materials' functional groups can be determined from their distinctive frequencies' absorbance profiles [444]. Figure 3.2 is a diagram showing how the FTIR machine is

typically constructed.
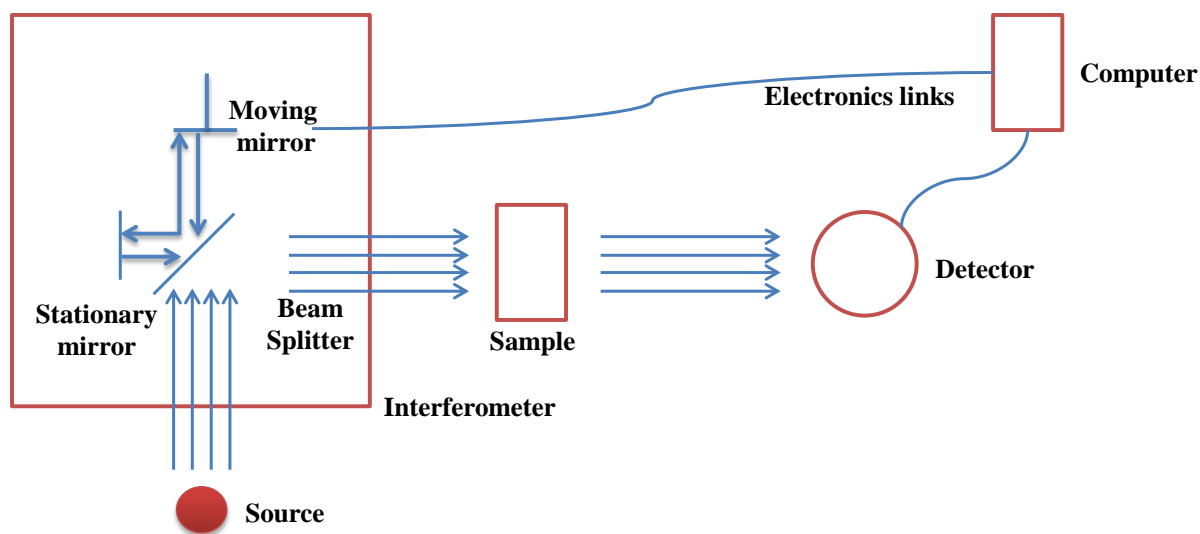
Fig. 3.2 Schematic diagram of FTIR spectrometer

The working of FTIR is explained below:

1. Source: IR beam generated by black body source. These generated beams pass through the aperture and incident on the sample.

2. The interferometer: In the interferometer beam entered are encoded and directed towards the sample.

3. The sample: The beam entered from the interferometer falls on the samples; depending on the frequency of the beam sample may absorb, transmit or reflect

4. The detector: The beam from the sample is detected by the detector.

5. Reflection gratings: Used to avoid stray beams.

6. Mirror: Mirrors focus and redirect the IR beam

7. The computer: Finally, in the computer Fourier transform, decodes the signal to display the graph.

3.4.3. Field Emission Scanning Electron Microscopy (FESEM)

The scanning electron microscope (SEM) is a popular technique to study morphology of surface and topology through a raster scan of high-energy electrons.

Principle

Backscattered electrons, secondary electrons, photons, x-rays, and heat were just a few of the signals produced when accelerated electrons strike materials. Images can be created by accumulating secondary and backscattered electrons. The secondary electrons provide as a visual representation of the matter structure and architecture. Backscattered electrons are critical to picture contrast [445].

3.4.3.1. Energy-Dispersive Spectroscopy (EDS)

Energy dispersive spectroscopy is used to measure the relative amount of elements present in the samples.

Principle

A moderately energetic X-ray photon excites a photoelectron crystal, which then propagates through the crystal and excites further exciton (electron-hole pair). This process repeats itself until the total electron kinetic energy falls below the bandgap. This energy is picked up by the detector.

3.4.4. UV-visible Diffused Reflectance Spectroscopy

The lamp used in a UV-Visible setup emits radiation in the region of the ultra-violet (UV) to the near infra-red (NIR) and is focused onto the sample by a monochromator. The qualities of the sample determine which wavelengths are reflected or absorbed, while the other ones are transmitted. A photodetector measures the amount of light that is transmitted (or reflected) and sends that information to a recorder or computer. When working with fluids in which colloids are suspended, it is best practise to employ a reference to eliminate the route

travelled by photons in the sample holder. As a result, a beam emanating from the radiation source is divided in half. The sample's reference compartment is traversed by one section. This substrate is used as a standard for comparison. Finally, the signal attributable only to the sample is determined by comparing the reference and sample light intensities. The spectrometer outline is depicted in Figure 3.3 [446].
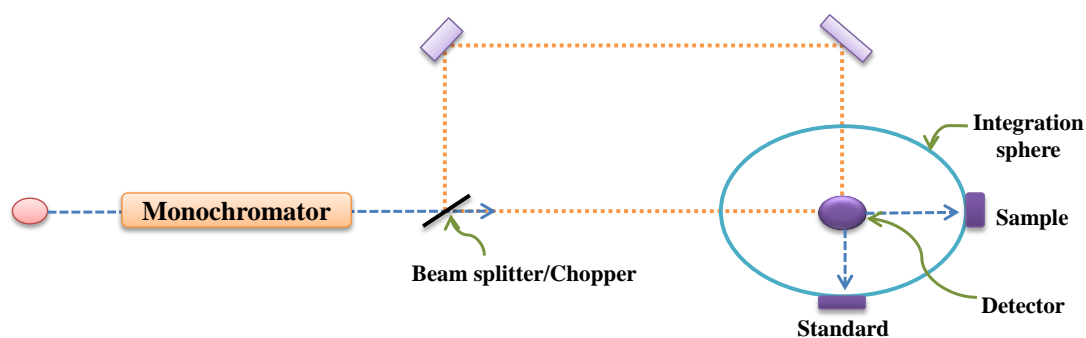
Fig. 3.3 Schematic representation of the UV-Visible spectrometer

3.4.5. Photoluminescence Spectroscopy (PL)

The emitted light is measured as a function of wavelength by a process called photoluminescence. This method involves using light with a maximum wavelength to stimulate the material, and then monitoring the resulting emission. This method can provide a relative charge recombination rate among the materials under consideration. In photocatalysis especially, a decrease in PL intensity is linked to less charge carrier recombination [447].

3.4.6. Photoelectrochemical Studies

Using an electrochemical workstation (Metrohm) and A solar simulator with an intensity equivalent to 1.5 AM (Air Mass) was used for the experiment. The solar simulator model used was a 300 W SSEM (Photo Emission Tech, USA), the photoelectrochemical characteristics of the produced photocatalysts were determined. The following procedure was used to prepare the working electrodes. Ultrasonication was used for 45 minutes to provide a homogeneous dispersion of 0.25 g photocatalyst and 0.023 g methyl cellulose in a 1:1 ethanol

and water combination, and after that, the compound was dried at 120 °C for 60 minutes to make the working electrode. To investigate the photoelectrochemical characteristics of photocatalysts, electrochemical impedance techniques were used. We used a counter electrode made of pure Pt wire and a reference electrode of Ag/AgCl. Furthermore, throughout all laboratory experiments, a solution of Na_2SO_4 with a concentration of 0.1 M was used as the electrolyte.

3.4.6.1. Electrochemical Impedance Spectroscopy

The determination of electrochemical impedance involves the generation of an electric current through the application of a sinusoidal (AC) voltage to the working electrode. The sinusoidal (AC) voltage controls the amplitude and phase of the generated current. After then, impedance can be determined with the help of Ohm's law. Schematic illustration of impedance spectra is presented in Figure 3.4 [448]; this measurement involves calculating electrolyte resistance, charge transfer resistance, and Warburg resistance.
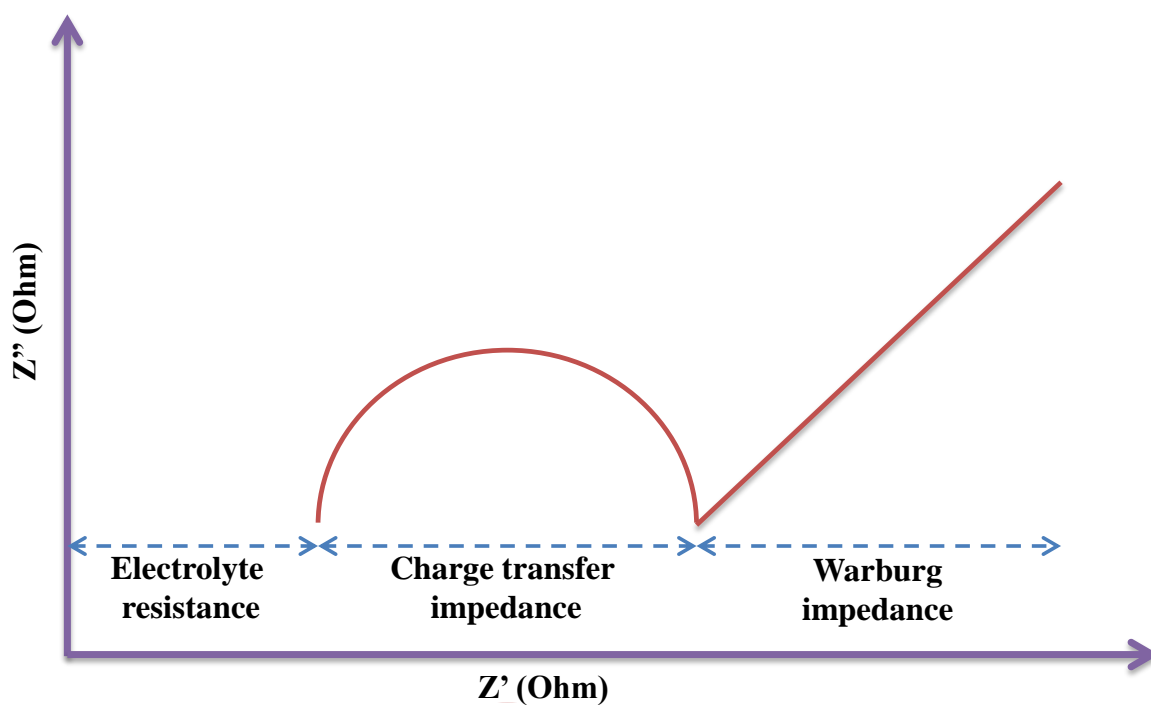
Fig. 3.4 Schematic representation of Impedance graph

3.4.6.2. Mott-Schottky Measurement

Mott-Schottky plot is (1/C$_2$) vs. the potential difference between the material and electrolyte. If the slope is negative, then the semiconductor is n-type; otherwise, it is p type. This technique helps in finding the nature of the semiconductor, carrier density, and semiconductor's flat band potential. The carrier density of the semiconductor can be calculated by using equation (3.2).

$$\frac{1}{C^2} = \frac{2}{qA^2 \, \varepsilon N_D} \, (V + V_{bi}) \qquad (3.2)$$

Where 1/C$_2$ is the slope from the Mott-Schottky plot, A is electrode area, ND is the charge density, and ε is dielectric constant, and V$_{bi}$ is built-in potential.

3.4.7. BET (Brunauer-Emmett-Teller)

Surface property measurement has become more essential for a wide range of materials. One of the most fundamental of these characteristics is the surface area accessible for gas molecule adsorption. Surface area is the way a solid interacts with its surroundings, particularly liquids and gases. Surface area can be created by reducing particle size, such as grinding and milling, as well as making materials porous. Brunauer-Emmett-Teller is a surface area analysis technique, which is used to define the specific surface area of powders, granules and solids the values are expressed in m^2/g. The principle of BET surface area testing is that at lower pressures gas adsorbs to solids in a monolayer. The surface area covered by this layer is calculated by physical adsorption of a gas on the solid's surface and estimating the amount of adsorbate gas equivalent to a monomolecular layer on the surface. The porous characteristics for example pore size distribution and pore volume of the materials was analysed by principle of capillary condensation. BET analysis provides a precise specific surface area evaluation of materials via nitrogen multilayer adsorption evaluated as a function of relative pressure utilising a fully automated analyzer [449]. Barrett-

Joyner-Halenda (BJH) analysis can also be used to determine pore area and specific pore volume utilizing adsorption and desorption techniques.

3.4.8. TGA/DSC

Thermogravimetry analysis/differential scanning calorimetry (TG/DSC) can evaluate thermal parameters such as weight loss and reaction nature (exothermic or endothermic) at different temperature intervals [450]. The intermediate phases obtained during chemical synthesis in the form of dried gel and ball-milled precursors obtained during solid state synthesis were analyzed by using a thermal analyser in a static air atmosphere in the temperature range 26-1200 °C at a heating rate of 20 °C min^{-1}. The thermal analysis results of the intermediary phases indicate the temperature range of the final phase production and its thermal stability.

3.4.9. High-Resolution Transmission Electron Microscopy (HR-TEM)

Electron microscopes are used as a powerful technique to observe the morphology of the prepared samples. Scanning electron microscopy (SEM) and Transmission electron microscopy (TEM) provide the information about 3D-structural morphology and 2D-micro structure of prepared photocatalyst. High resolution transmission electron microscopy (HR-TEM) imaging is identical to TEM imaging except that the magnifications used are high enough to see the lattice spacing of inorganic materials (typically on the order of several) [451]. Although such lattice spacings can be easily recorded onto film at moderate magnifications (the 3.4 Å spacing between graphite layers can be recorded onto film at magnifications as low as 15,000-20,000x), CCD cameras and much higher magnifications (usually above 200,000 or 300,000x at the plane of the imaging device) allow the user to control the defocus much more easily and produce the best HRTEM images.

3.4.10. PC H$_2$ production

A sealed quartz reactor was used to perform the photocatalytic H$_2$ production experiment

which contains a catalyst (0.25 g) and water for an overall reaction volume of 10 ml to evaluate photocatalytic activity (H_2 evolution) of the synthesized materials. In order to get rid of the dissolved oxygen, we first degassed the reactor with Ar gas for 15 minutes before exposing it to visible light (80 W LED). Throughout the experiment, constant stirring was used to ensure that the reaction mixture remained uniform. Flowing cold water linked to the reactor was used to control the reaction temperature. The evolved gas was collected and analyzed at regular intervals using an off-line gas chromatograph. The gas chromatograph was equipped with a TCD (Thermal Conductivity Detector) and utilized a molecular sieve 5 Å column, with Ar serving as the carrier gas.

3.4.10.1. Catalyst Stability and Reusability Test

The recyclability and stability of photocatalysts are confirmed by repeating the same experiments upto 6 cycles. After the first cycle of PC water splitting, the solution was decanted and the catalyst was separated. Catalyst was dry after each run and then use in the next cycle. Again, the same experiments were repeated and irradiated with visible light. The aforementioned procedure was replicated many times, and the photocatalytic activity remained nearly unaffected even after repeating many cycles, indicating the outstanding stability of the sample due to the presence of polymer (polymer prevents the metal nitrides from self-photo corrosion during the reaction).

Chapter 4

Section (A)

Characterization studies of Ta$_3$N$_5$/BSC@PANI nanocomposites for hydrogen production via water-electrolysis under visible light irradiation

4.1.Introduction

As the global population continues to grow and industrialization expands on a daily basis, human society faces two major and unsolved issues: energy crisis and environmental damage [452]. Currently, our energy system depends on traditional fossil fuels, which causes climate change and is on the verge of diminution. Recently, researchers have been looking forward to solving these issues; there is an urgent need to develop a green and sustainable energy source to replace fossil fuels [453]. An additional greater than 14 Terawatts of power society would need by 2050 [454]. The latest studies revealed that only solar energy has the potential to meet that need [455]. Due to the discrepancy between the intermittent nature of solar energy and economic/domestic demand, this additional energy input must be stored reliably. Producing fuels from abundant resources like water may be the only viable option in such a scenario. Nowadays, developing an effective and sustainable method for producing H$_2$ gas is the most attractive area of research for scientists. Hydrogen (H$_2$) is considered the ideal long-term fuel for the future because it produces zero carbon emissions, only water as a byproduct, and has a higher chemical energy density (142 MJkg^{-1}) [456]. In 1972, Japanese scholars named Fujishima and Honda discovered photocatalytic (PC) and photoelectrochemical (PEC) water splitting by semiconductor TiO$_2$ act as a photocatalyst for the production of H$_2$ in sunlight irradiation [457]. Thus, the evolution of H$_2$ through H$_2$O splitting appears to be a desirable option for storing the copious amounts of sunshine that fall upon the Earth. Water is the most common substance on earth, and the sun is the greatest source of

energy [458]. In recent years, semiconductor photocatalysis has expanded interest as a possible answer to the world's pressing energy problems.

In this regard, there has been extensive research into the morphological changes of semiconductor materials comprising metal oxides and metal nitrides for efficient photocatalytic water electrolysis [459, 460]. The quantum yield is relatively modest, despite numerous materials and methodological efforts to boost it. Photocatalytic water electrolysis has been the subject of extensive research regarding various types of photocatalysts, including carbon-based materials, metal nitrides, metal oxides and conducting polymers. Carbonaceous nanostructures like CNTs, graphene, GO, and many more ensure widely adopted due to their atmosphere compatibility and abundant and substantial electron transport mechanism [461, 462]. Aimed at photocatalytic H_2 production, Kang et al. showed that amorphous carbon nitride photocatalysts have an astonishingly broad visible-light-responsive range [463]. As an analogous example, Silva et al. created a carbon nanotubes-TiO_2 catalyst to produce H_2 from saccharides and methanol [464]. Numerous studies reveal that carbonaceous materials play an important role in increasing photocatalytic H_2 production. Recently, carbon dots have emerged as promising candidates for water splitting due to their capacity to efficiently absorb visible light, tunability in excitation/emission, and excellent photostability. Carbon nanocomposites containing TiO_2 were produced by Yu et al. and used to split water using ultraviolet (UV) or visible light [465]. An efficient semiconductor photocatalyst is crucial for this type of solar H_2 generator because it must fulfill many criteria, including (i) a lesser band gap near absorbing a broad spectrum of solar light, (ii) proper band alignment for the production of H_2 from water, (iii) glib charge transport to enable faradaic reaction, (iv) strength in aqueous solutions [466]. Among them, carbon-based materials present excellent life cycles/stability [467]. The present work select BSC as the carbon-based

material, a low-cost and commercially available material. Soot carbon is a strong absorber of UV light. Ta_3N_5 is a visible light photocatalyst immobilized with biomass soot carbon to increase the absorption of UV light also. Physiochemical structures of activated carbons and extensive specific surface area can enhance the photocatalytic process. This is typically due to the rise in contact surface area. While conducting polymers have a substantially larger capacitance, their cycle stability is low because of the pseudocapacitance of the redox reaction [468]. In recent years researchers have been focusing on metal nitride carbon conducting polymer as photocatalyst materials to combat these issues. These materials are exposed to a significant increase in photocatalytic activity, resulting in a high yield of H_2 evolution. The BSC acts as the backbone to sustain and provide a dependable electrical connection to polyaniline (PANI) and as an active material to offer the necessary double-layer capacity [469]. Tantalum nitride (Ta_3N_5), characterized by its favorable band positions and an appropriate band gap of 2.1 eV, exhibits exceptional potential as the leading visible-light photocatalyst for efficient water splitting. However, Ta_3N_5 has many limitations that prevent it from being widely used, for example, due to its high charge recombination rate, tantalum nitride (Ta_3N_5) suffers from low photocatalytic activity and poor photostability. Numerous methods, including manufacturing of shape/size, doping of metal, and pairing with other catalysts, are used to advance Ta_3N_5 the photocatalytic performance. It has been shown that merging Ta_3N_5 with other cocatalysts to construct composites is the most operative strategy [470]. Recent research efforts have focused on photocatalysis techniques to mitigate these drawbacks. Over the past few years, the exponential development of publications demonstrates the growing interest in immobilizing photocatalysts in porous carbon materials [471, 472]. Zhong et al. constructed a GaN/Ta_3N_5 composite and found that GaN dramatically improves the stability of Ta_3N_5 water-splitting capability [473]. Hou et al. used chemical

in situ phase-induced etching to fabricate core-shell Ta_3N_5@NaTaON heterojunctions with excellent photocatalytic activity [474]. However, in the Ta_3N_5 system modification, it is pretty of considerable awareness to discover further proficient materials aimed at enhancing photocatalytic activity and stability of Ta_3N_5 photocatalyst. Given these considerations, the present research was planned to optimize H_2 production using Ta_3N_5/BSC core-shell structure with PANI composite photocatalyst. BSC supports Ta_3N_5 outstanding, distinctive surface properties, such as superior electrical conductivity, easily tunable functional groups and chemical stability. Also, BSC has an electron-conductive nature that can help to reduce the quick recombination of the electron-hole pair [475]. Here, PANI is used as the conductive polymer known for many intriguing qualities, including high conductivity, exceptional environmental constancy, and ease of manufacture. PANI (polyaniline), known for its affordability, exhibits a high absorption coefficient for visible light and excellent charge transport capabilities. Furthermore, PANI effectively serves as a hole acceptor and an electron donor when exposed to visible light [476]. PANI is a good material for improving photocatalyst performance and charge transfer efficiency due to its distinct properties. Ta_3N_5/BSC@PANI is obtained via facile synthesis, and its optical, morphological, structural, and photoelectrochemical properties are all well-characterized. It has also been effectively used in photocatalytic and PEC measurements to create hydrogen.

4.2. Experimental Section

4.2.1. Materials

Biomass of peanut shells, Ta_2O_5 (99% Sigma-Aldrich), Ethanol, Hydrochloric acid (HCl), Aniline (Lobachemie), ammonium peroxydisulfate ((NH_4)$_2S_2O_8$ from CDH), Acetone, and Methanol (99%, LiChrosolv Merck) used as sacrificial agent. Entirely chemical was readily accessible and directly utilized without pretreatment. Glass

plates were cast off as a substrate to manufacture photoelectrodes (PEs) ITO (Merck). Sulphuric acid (99%), sodium sulphate, potassium hydroxide, purchased from CDH PVT Ltd. was used to examine electrochemical and photoelectrochemical (PEC) studies. All reagents were synthesized using ultrapure deionized water from Millipore, and the glassware was cleaned.

4.2.2. Instrumentation

The electronic excitation of Ta_3N_5 and Ta_3N_5/BSC@PANI composite is examined by Analytik Jena, Specord UV-Vis spectrophotometer. The infrared absorption spectrum was obtained using a Fourier transform infrared (Perkin Elmer) spectrophotometer to identify structural characteristics of the synthesized materials in the 1000-4000 cm^{-1} range. At ambient temperature, the excitation wavelength of 390 nm was used using a photoluminescence (PL) spectrophotometer (Perkin Elmer) to record light emission. The phase empathy was performed with an X-ray diffractometer (Bruker) using Cu kα (λ=1.540 Å) as the radiation basis. The morphology of Ta_3N_5 as-synthesized and Ta_3N_5/BSC/PANI was studied using a field emission scanning electron microscope (FE-SEM, JEOL). The electrochemical characteristics of Ta_3N_5 and Ta_3N_5/BSC@PANI were dignified by fabricating PEs discussed below. Three-electrode configurations were used to examine the impedance performance of the PEs, where PEs existed as working electrodes, Pt and Ag/AgCl as counter electrodes, and as reference electrodes.

4.2.3. Preparation of photocatalyst

4.2.3.1. Synthesis of biomass soot carbon

The biomass soot carbon is synthesized by carbonization using biomass of Arachis hypogaea (peanut) shells at 200 °C temperature for 3 h in the presence of inert atmosphere to eradicate volatile organics and moistness. Further, to carbonise solid

biomass into biomass carbon, heat it to 800°C for 3 hours. Once the reaction cooled down gained biomass carbon chunks were drenched in 0.5 M HCl for 5 h and washed with deionized water and ethanol and, finally dried at 100 °C in air. Finally, biomass soot carbon was formed. A product similar to charcoal produced by biomass pyrolysis, biomass soot carbon is composed mainly of carbon. Pyrolysis is a thermochemical conversion of biomass in the absence of O_2 to produce energy products, in which biomass is heated at high temperature (frequently 450°-750°C). Biomass soot carbon preserves the novel structure of the feedstock, but the porosity has increased.

4.2.3.2. Synthesis of Ta_3N_5

Ta_3N_5 was synthesized via ammonolysis. Here amorphous tantalum pentaoxide (Ta_2O_5) was used as a precursor. Initially, a solution of Ta_2O_5 in 150 ml of ethanol was prepared and subjected to magnetic stirring for a duration of 45 minutes. Subsequently, the reaction mixture was transferred to a Teflon-based autoclave hydrothermal reactor and maintained at a temperature of 150°C for a period of 7 hours. After cooling to room temperature, the resulting white precipitates were collected, filtered, purified, and then dried at 100°C for 2 hours. Ammonolysis was carried out in a muffle tube furnace by exposing the precipitates to an ammonia flow rate of 30 ml/min at a high temperature of 850°C for 8 hours. Finally, Ta_3N_5 nanoparticles were received.

4.2.3.3. Synthesis of PANI by in-situ chemical oxidative polymerization process

The chemical techniques through which PANI can be synthesized bring their benefits. PANI, for instance, can be fabricated in large quantities and powder form via a chemical procedure. Solution #A was made by adding 2.61 ml of aniline monomer

($C_6H_5NH_2$) and 14.94 ml of hydrochloric acid (HCl) (37% w/v) to 144 ml of deionized water and stirring the mixture constantly for 15 minutes. To make a transparent solution (labeled solution #B) of ammonium persulfate (APS) ((NH_4)$_2S_2O_8$, 98%), 1.641 g of APS was liquified in 36 ml of DI water and the mixture was agitated continuously for 15 minutes. Then, solution B was added rapidly to solution A, and the mixture was agitated vigorously for the next 50 min. After that, the entire solution was left aside for 24 h in a cool, dark environment. After being centrifuged at 3000 rpm for 5 min in deionized water, the product was filtered by collecting the precipitate. Washing with DI water and centrifugation operations were repeated twice to eliminate any lingering oxidants and oligomers from the products (each time 15 min of centrifugation at 3000 rpm). Another 24 h were spent storing the final collected product in the dark at ambient temperature. The dark green solution was then dried at 60 °C for 12 h, and the resulting powder was saved for further analysis.

4.2.3.4. Synthesis of Ta_3N_5/BSC and Ta_3N_5/BSC@PANI composites

The prepared Ta_3N_5 and 10 wt% BSC were mixed mechanically in a vibration mill for 10-15 min to get a uniform mixture of Ta_3N_5/BSC composite. Using the chemisorption technique, Ta_3N_5/BSC core-missile structure with PANI was fabricated. In 50 ml of tetrahydrofuran, 0.3 g of Ta_3N_5/BSC nanoparticles and a known quantity of PANI were combined, sonication for duration of 1 hour, followed by continuous stirring for a period of 24 hours and the reaction temperature was fixed at 60 °C. The mixture was kept in oven and dried for 3 h at 80 °C. Finally, Ta_3N_5/BSC/PANI composite was synthesized. Ta_3N_5/BSC core-missile structure with PANI was fabricated via the chemisorption method. In 50 ml of tetrahydrofuran, 0.3 g of Ta_3N_5/BSC nanoparticles and a known quantity of PANI were combined, sonicated

for one hour followed by swirling for 24 hours. After removing the solvent, the mixture was dried at a temperature of 80 °C for a duration of 3 hours. Finally, a Ta_3N_5/BSC/PANI composite was prepared.

4.2.4. Photoelectrochemical study

To prepare the working electrode, a slurry consisting of 0.2 g of photocatalyst and 0.02 g of methyl cellulose in ethanol was coated onto an indium-tin-oxide (ITO) glass. The coated electrode was then dried at a temperature of 110 °C for a duration of 50 minutes. For the experiment, an electrochemical workstation (Metrohm) with a three-electrode system was employed. The reference electrode used was SCE, the counter electrode was Pt flake, and the electrolyte was a 0.1 M Na_2SO_4 aqueous solution. To maintain a pH of 3 and eliminate dissolved oxygen, nitrogen gas was continuously poured into the system. The experimental setup included a 300W Xe lamp with a 410 nm cutoff filter to provide illumination. A 10-mV perturbation signal was applied, and the frequency range for measurement was set from 100 kHz to 0.01 Hz, as indicated by the Nyquist plots. The applied potential during these photoelectrochemical studies was 0.5 V relative to Ag/AgCl.

4.2.5. Photocatalytic activity

Tests were performed in a sealed quartz reactor containing a catalyst (0.2 g) and water/methanol (used as sacrificial agents) mixture (50:50) for an overall reaction volume of 10 ml to evaluate photocatalytic activity (H_2 generation) of the synthesized materials. In order to get rid of the dissolved oxygen, we first degassed the reactor with Ar gas for 15 minutes before exposing it to UV (120 W Hg arc) and visible light (80 W LED). Flowing cold water linked to the reactor was used to control the reaction temperature. Then, substances were put into the quartz-covered reactor. The experiment proceeded with continuous stirring. The amount of H_2 evolution was

analyzed using gas chromatography with a thermal conductivity detector (GC-TCD). The temperature was sustained at 30°C for the column, injector, and detector. In addition, material photocatalytic activity recycling experiments were carried out, with the photocatalyst being centrifuged back into its original form after each use.

4.3. Results and discussion

4.3.1. Characteristics analysis of the synthesized materials Ta₃N₅ and Ta₃N₅/BSC@PANI

Fig. 4.1 (A) illustrates the UV-visible absorption spectrum of Ta_3N_5 and Ta_3N_5@PANI composites. Ta_3N_5 bare photoabsorption capacity in visible light range around 600 nm, as mentioned previously [477]. Ta_3N_5@PANI absorption intensity in visible light areas steadily improved after assortment with PANI. It has been known for quite some time that PANI absorbs visible light (This can be attributed to the propensity of Ta_3N_5 to facilitate electron transitions in polyaniline, specifically to the π^* band from the polaron band) [478]. In order to boost its photocatalytic activity, the Ta_3N_5@PANI composite achieved a higher light harvesting ability. Fig. 4.1(B) confirms FT-IR spectra analysis of Ta_3N_5, Ta_3N_5/PANI and Ta_3N_5/BSC@PANI composites. The presence of Ta_3N_5 was verified by the presence of a peak at $918 cm^{-1}$, corresponding to the stretching mode of the Ta-N bond [479]. Peak achieved at $1057\ cm^{-1}$, $1220\ cm^{-1}$ and $1300\ cm^{-1}$ were ascribed toward plane bending vibration of C-O-C, C-N stretching mode in the benzenoid unit [480]. Band at $1472\ cm^{-1}$ accredited to C-H bending mode on behalf of the benzenoid unit, and band at $1560\ cm^{-1}$ were ascribed to the C=C stretching. The band observed at $1698\ cm^{-1}$ was assigned to the stretching vibration of the C=O bond in the conjugated system. The chemical structure of the PANI deposit and biomass soot carbon powder is characterized. Characteristic peaks at $3742\ cm^{-1}$ are observed in the FTIR spectrum of N-H stretching; and $3649\ cm^{-1}$ these peaks can be ascribed to –OH stretching (free molecule) and C–H ($2975 cm^{-1}$) stretching modes.

The characteristic peaks at 1698 cm^{-1} of C=O and 1649 cm^{-1} of C=C stretching correspond toward the benzene ring, respectively, C–C–O (1057 cm^{-1}) stretching modes [481]. The band at 1510 cm^{-1} was allocated to the C=N mode of stretching in a secondary aromatic amine [482]. Consequently, these FTIR spectrum results validated that PANI was prepared in our experiment. To examine the migration, trapping, and pairing of photogenerated charge carriers, this study employs the PL emission spectra of synthetic materials stimulated at 390 nm, as illustrated in Figure 4.1(C), PL emission peaks traced roughly 675 nm confirms the presence of Ta_3N_5, which match with the previous study [483]. When Ta_3N_5 was aggregated with polyaniline, have smaller emission intensities than that of pure Ta_3N_5 at the same position. Theoretically, more photocatalytic activity can be achieved with lower PL intensity because it suggests a lower recombination rate of photogenerated charge carriers [484]. XRD shows (fig.4.1 (D) crystallinity structures of the synthesized materials (Ta_2O_5, synthesized Ta_3N_5, BSC, PANI, and Ta_3N_5/PANI/BSC). The foremost diffraction peaks detected at 2θ values of 23.8°, 28.3°, 28.8°, 36.7°, 38.3°, 46.9°, and 49.9° designate that the synthesized Ta_3N_5 occurred in the form of orthorhombic [485, 486]. The XRD graph exhibited no contamination peaks, indicating the complete conversion of Ta_2O_5 to Ta_3N_5 [487]. PANI and BSC don't show any effect on the crystalline structure of the Ta_3N_5 because the peak obtained in XRD patterns of Ta_3N_5/BSC and Ta_3N_5/BSC/PANI was similar to those of Ta_3N_5, correspondingly.
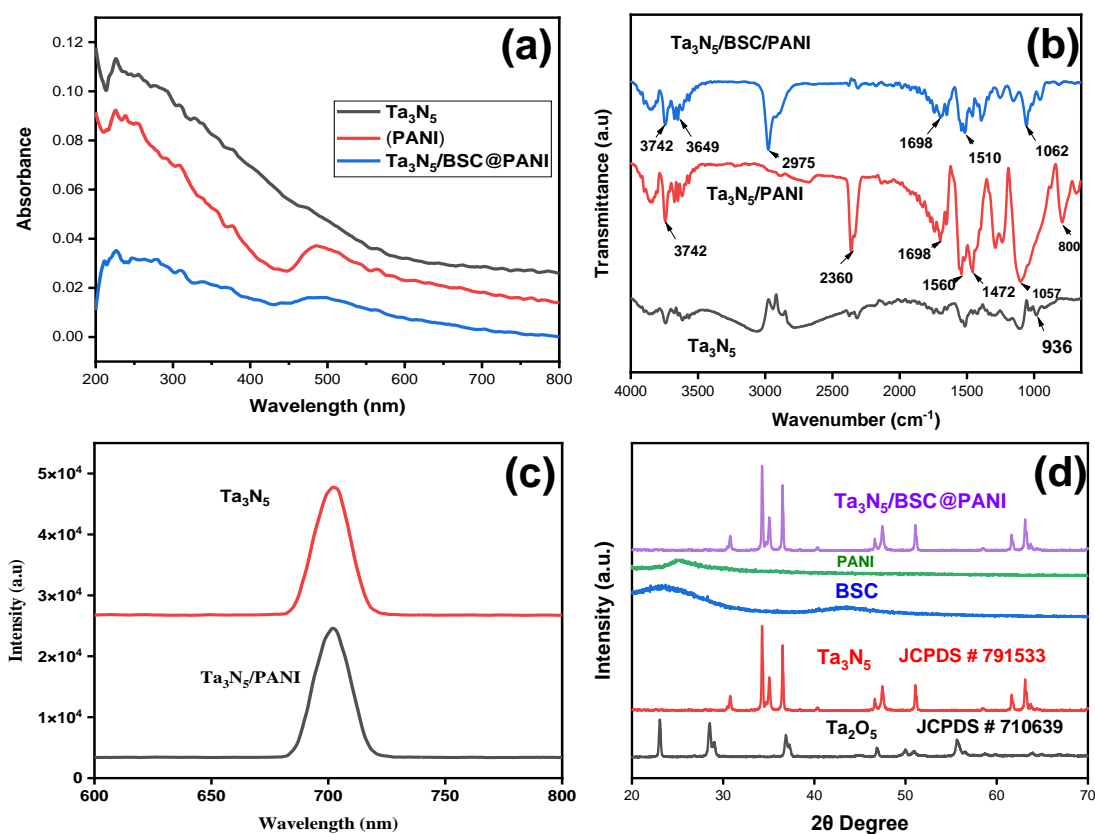
Fig. 4.1 (A) UV-visible absorptions spectra, (B) FTIR-Spectrum, (C) Photoluminescence (PL) Spectra and (D) XRD patterns of the synthesized materials.

Fig. 4.2 (a-d) displays the results of Surface analyses of all the fabricated materials characterized via FE-SEM. SEM shows the morphology and microstructure of pure Ta_3N_5, Ta_3N_5/PANI. Fig. 4.2 (a) shows the pristine Ta_3N_5 appearance, looking like a massive layered particle with a flocculent lamellar structure [488]. (b) The SEM images of Ta_3N_5/PANI fibrous morphology show that as a nanocomposite PANI covering the Ta_3N_5 surface. (c) Shows SEM images of BSC block-like structures are obtained. Moreover, (d) Ta_3N_5/BSC/PANI shows the neurons-like surface morphology with high porosity, which clearly indicates the presence of carbon [489, 490].
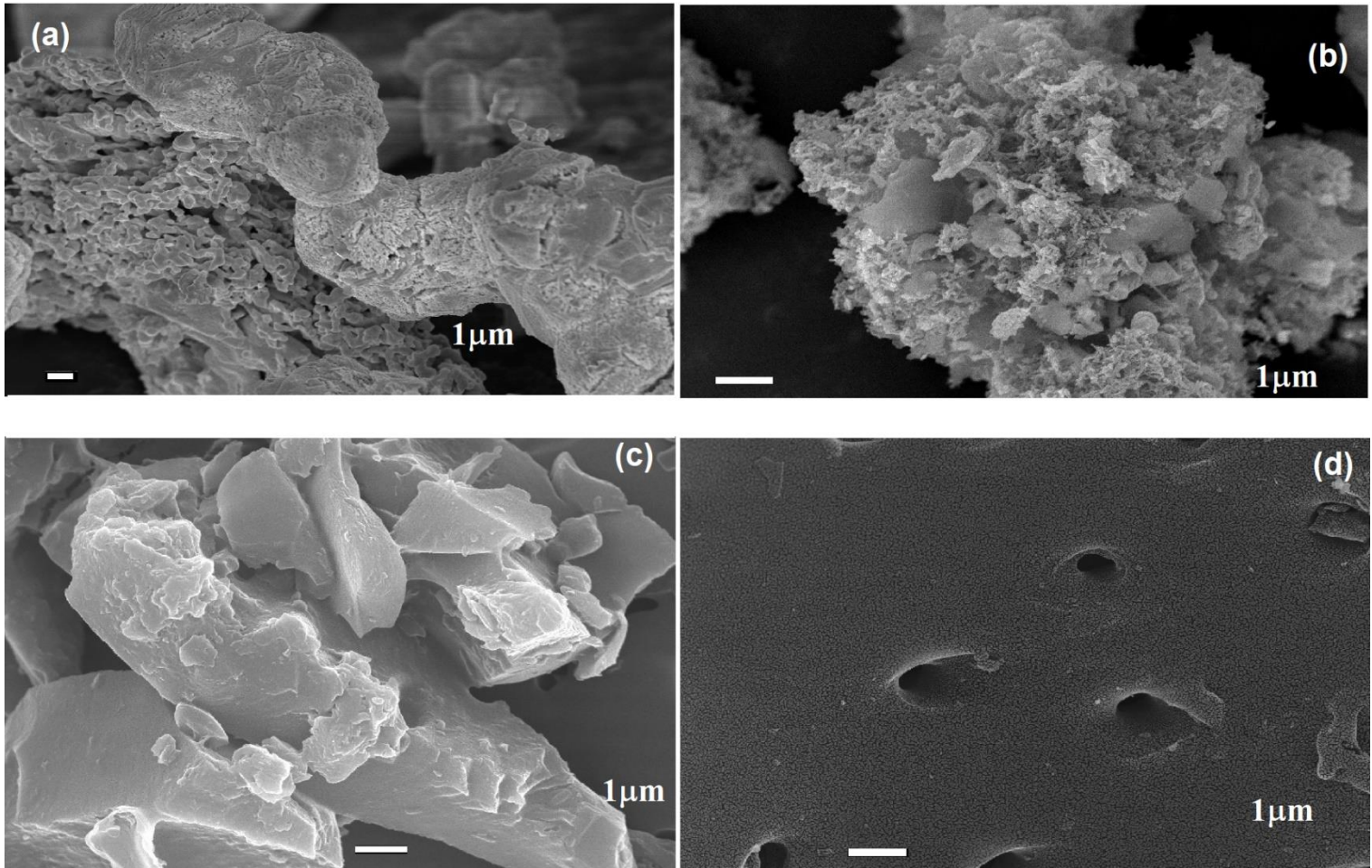
Fig. 4.2 FE-SEM morphology: (a) Ta$_3$N$_5$, (b) Ta$_3$N$_5$/PANI, (c) BSC, and (d) Ta$_3$N$_5$/BSC/PANI

The High-Resolution Transmission Electron Microscopy was used to analyse the structure of the nanocomposite. The transparent spherical shape of the Ta$_3$N$_5$ particles, and mixed spherical and rod like shape of the BSC on the surface of Ta$_3$N$_5$ were observed in the microscopy. The formation of composite between Ta$_3$N$_5$ and BSC and the core shell layer of PANI wrapping the Ta$_3$N$_5$/BSC were clearly visible in Fig.4.3 results indicates the formation of Ta$_3$N$_5$/BSC@PANI core shell structure was successfully synthesize.
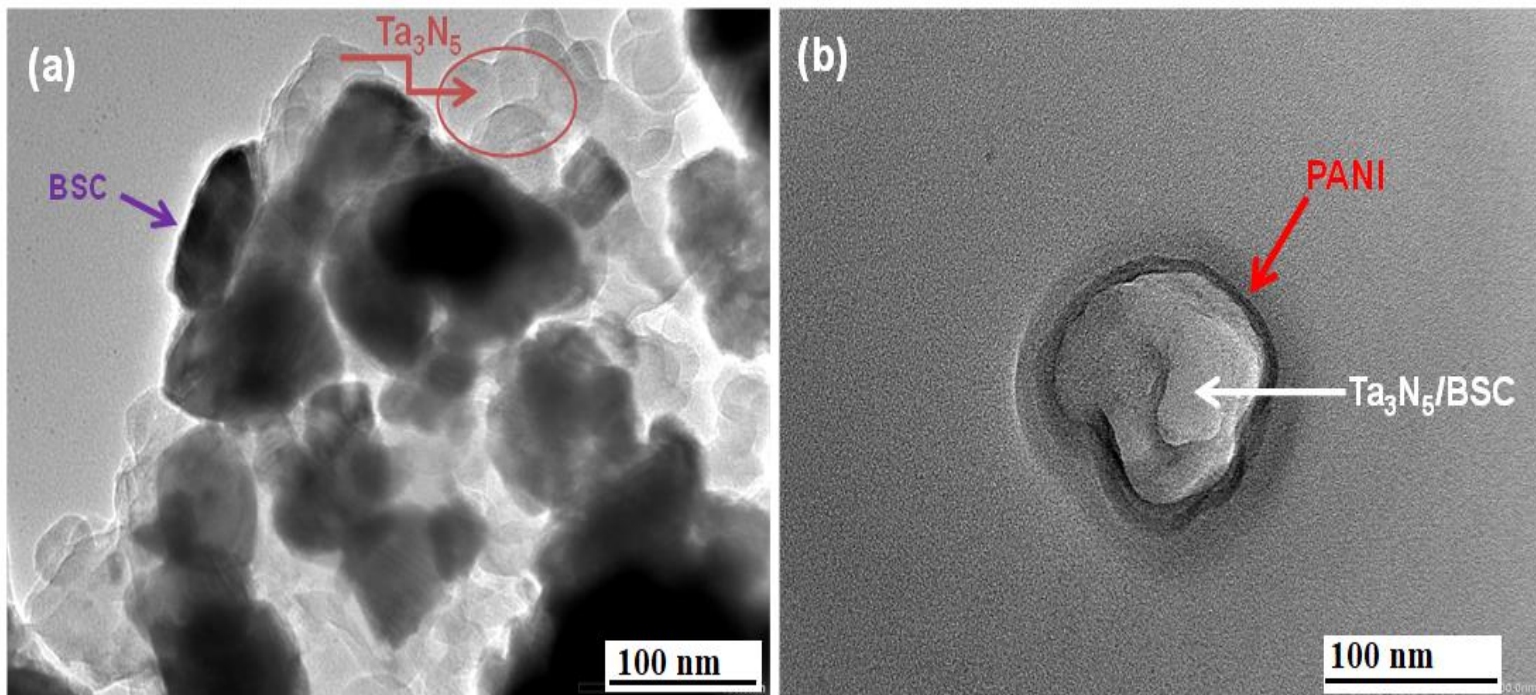
Fig.4.3. HRTEM imaging of (a) Ta_3N_5/BSC and (b) Ta_3N_5/BSC@PANI nanocomposites

Nyquist plots of electrochemical impedance spectra (EIS) are presented in Fig. 4.4. Ta_3N_5, and Ta_3N_5/BSC@PANI composites were tested to understand their transfer resistance and interfacial charge separation. In general, photogenerated e^--h^+ pairs are separated more efficiently, and charge transfer resistance is reduced at a smaller arc radius [491]. Ta_3N_5/BSC@PANI composites have a lower arc radius than primeval Ta_3N_5, indicating advanced photocatalytic activity due to decreased charge transfer resistance in the photocatalyst composite.
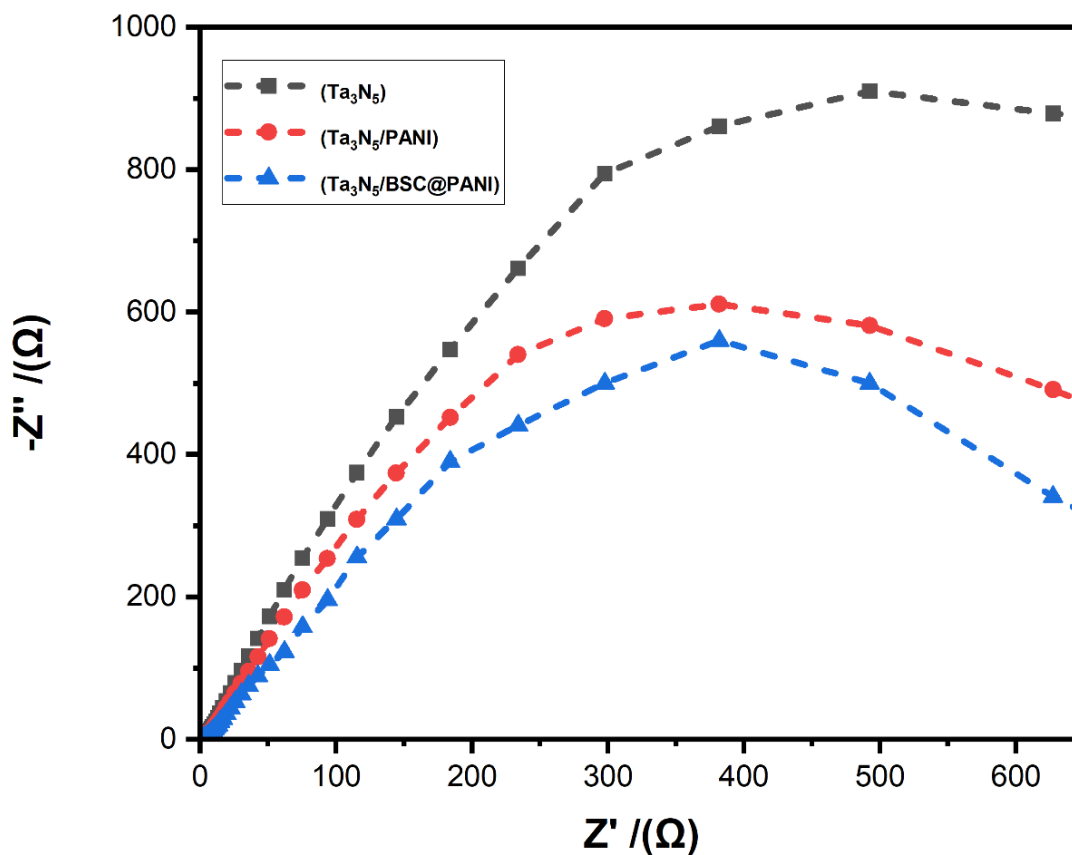
Fig. 4.4 The EIS Nyquist plots of synthesized materials

4.3.2. Experimental yield of photocatalyst

Fig. 4.5 demonstrate H_2 production of photocatalytic bustle of fabricated Ta_3N_5, and Ta_3N_5/BSC/PANI composites in visible light radiation ($\lambda > 410$ nm). As demonstrated in Fig. 4.5. (A), upon the irradiation of visible light the H_2 production ratio of Ta_3N_5 with 22.5 $\mu mol g^{-1}h^{-1}$. H_2 Evolution enactment of Ta_3N_5 was considerably superior to later alteration with BSC and PANI. The Ta_3N_5/BSC@PANI composite demonstrates the highest photocatalytic H_2 production rate, with a value of 76.9 $\mu mol g^{-1}h^{-1}$. This value is 3.42 times greater than that of pristine Ta_3N_5. Moreover, we observed good photocatalytic stability of Ta_3N_5 and Ta_3N_5/BSC/PANI composite for H_2 production by photocatalysis when exposed to visible light. The quantity of H_2 production of Ta_3N_5/BSC/PANI was almost unaffected even

after six cycles, according to the evidence in fig 4.5. (B), indicating the brilliant stability of the sample due to the presence of carbon and polymer (polymer prevents the metal nitrides from self-photo corrosion during the reaction). Nevertheless, the photocatalytic H_2 ratio of Ta_3N_5 was apparently shrunk, mainly recognized to the self-photo corrosion. Throughout the reaction process, According to the following equation, Ta_3N_5 might be converted to Ta_2O_5 if photogenerated holes oxidised the nitrogen anions [492].

$$2Ta_3N_5 + 30h^+ + 30OH^- \rightarrow Ta_2O_5 + 5N_2 + 15H_2O \qquad (4.1)$$
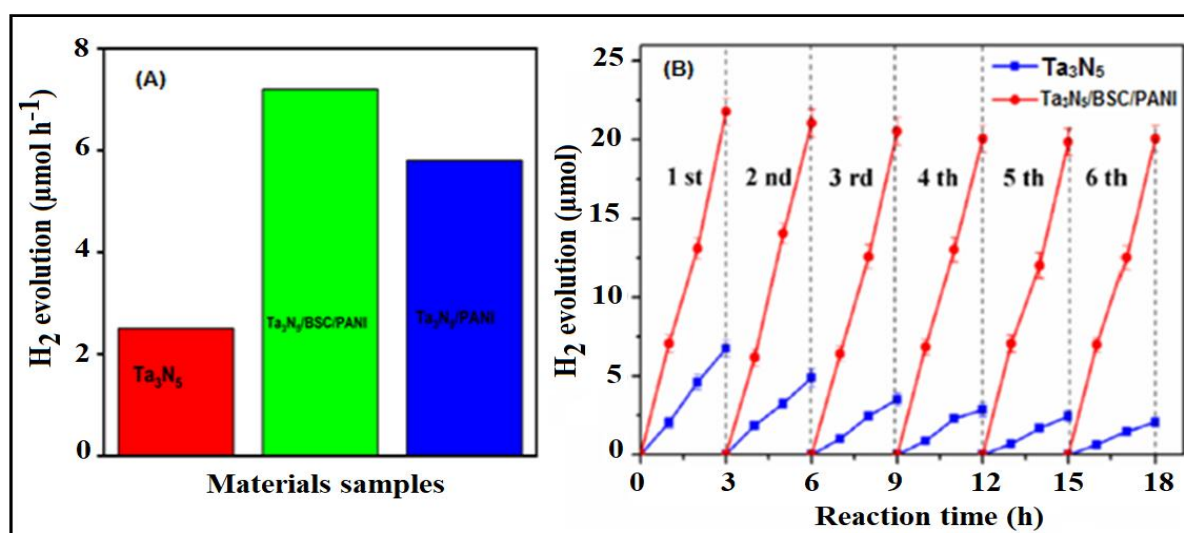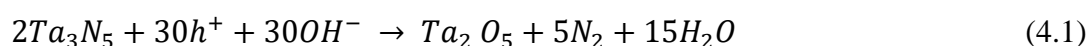
Fig. 4.5 (A) The photocatalytic H$_2$ evolution rate after being exposed to visible light for 3 h of reaction and (B) Reusable photocatalytic activity of Ta$_3$N$_5$, Ta$_3$N$_5$/BSC/PANI

4.3.3. Boosted photocatalytic mechanism

Based on the foregoing experiment, Fig. 4.6 proposes a mechanism for improved photocatalytic H_2 production by Ta_3N_5/BSC@PANI nanocomposite under solar light (UV & visible). Under visible light irradiation, Ta_3N_5/BSC and PANI create electrons and holes. PANI Photogenerated electrons directly relocate to Ta_3N_5 CB because of the synergic impact of their relative energy levels (LUMO and HOMO). On the Ta_3N_5 surface, hydrogen is

formed through photogenerated electrons. Excited holes go from Ta_3N_5 VB to PANI HOMO simultaneously. PANI easily transports holes toward the surface and captures them with the sacrificial regent. The steady interfacial contact between Ta_3N_5 and PANI may help interfacial charge carriers migrate [493]. Moreover, the holes deposited on the PANI surface further develop the photostability of Ta_3N_5 (hole-induced photocorrosion). Charge transfer inhibited photogenerated electron-hole pair recombination, improving photocatalytic efficacy. Ta_3N_5/BSC@PANI photocatalyst is appealing enough to use the complete spectrum of sunlight efficiently.
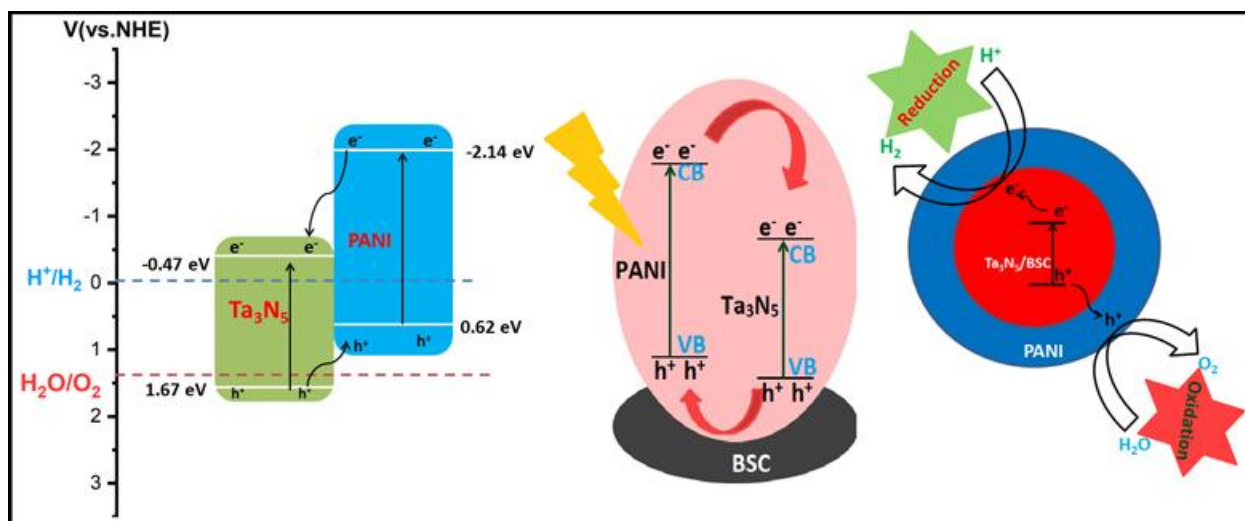
Fig. 4.6 The mechanism of Ta_3N_5/BSC@PANI composite photocatalyst for H_2 evolution

A list of several carbons based and protected with polymer composites photocatalysts (UV and visible light driven) is mentioned in Table 4.1.as well as their photocatalytic application on water splitting for H_2 evolution rate with different reaction conditions.

Table 4.1 Comparison data of different types of carbon and polymers with conjugated pair-based photocatalysts triggered by UV and visible light for HER.

Photocatalyst	Light Source	Reaction Temp.	Vulture	Reactant Medium	H_2 production Yield ($\mu molg^{-1}h^{-1}$)	Ref.
CdS/Au/ZnO	UV Xe Lamp	RT	Na_2S/Na_2SO_3	$Na_2S/Na_2SO_3/H_2O$	60.8	[494]

BiTaO$_4$ nanoplates	UV Xe Lamp	5 °C	TEA	TEA/H$_2$O	70	[495]
CoxN/Ta$_3$N$_5$	300 W Xeon Lamp	RT	Methanol	CH$_3$OH/H$_2$O	75.69	[496]
Ta$_3$N$_5$	UV Mercury Lamp and visible light (LED bulb)	RT	Methanol	CH$_3$OH/H$_2$O	22.5	This study
Ta$_3$N$_5$/BSC@PANI	UV Mercury Lamp and visible light (LED bulb)	RT	Methanol	CH$_3$OH/H$_2$O	76.9	This study

4.4. Conclusions

The novel work described here improves and expands the use of carbon-based (biomass utilised to make the useful carbon) metal nitride as a potentially cost-effective, stable, and eco-friendly material for H$_2$ production. This research utilized a chemisorption process to fabricate Ta$_3$N$_5$/BSC core-shell composite with PANI Photocatalysts. The results suggested that incorporating carbon and PANI into Ta$_3$N$_5$ could significantly improve the material photocatalytic activity. Ta$_3$N$_5$/BSC@PANI had a maximum visible light photocatalytic production amount of H$_2$ is 76.9 $\mu mol g^{-1} h^{-1}$. This obtained yield in case of composite photocatalyst Ta$_3$N$_5$/BSC@PANI is 3.42 times greater than pure Ta$_3$N$_5$ ($22.5 \mu mol g^{-1} h^{-1}$). Ta$_3N_5$/BSC@PANI nanocomposite showed remarkable photostability and reusability. A synergistic effect, consisting of strong interfacial interaction, which increased visible, and absorption of UV light, effective split-up of pairs of electron-hole, and acidic holes relocated from the Ta$_3$N$_5$ surface to the PANI surface (to inhibit the self-photocorrosion), was found to be accountable for the better photocatalytic activity. The results indicate that the Ta$_3$N$_5$/BSC@PANI nanocomposite shows potential UV and visible light photocatalyst aimed at H$_2$ photocatalytic production. Due to carbon excellent availability, low toxicity, good

stability and photocatalytic and PEC capability, it can compete with and even exceed other reported materials (mentioned in Table 4.1). The research also paves the way for this novel supporting/sensitizer to be used in several solar-powered applications.

Section 4 (B)

Fabrication & characterization of V, S co-doped Ta$_3$N$_5$ protected with PANI Photocatalyst for water splitting process

4.1. Introduction

The rising global need for energy and the associated with environmental problems it is essential to the development of renewable and eco-friendly energy systems [497, 498]. Due to its properties as a carbon-free and sustainable energy source, Hydrogen is currently recognized as the most promising alternative to conventional fossil fuels [499]. As a result, there has been significant research focus on developing strategies for the direct conversion of abundant solar energy into hydrogen. The concept of utilizing particulate semiconductor photocatalysts for solar-driven water splitting, enabling the production of hydrogen through a single-step photoexcitation process, is widely acknowledged. TiO$_2$, NaTaO$_3$, Ge$_3$N$_4$, GaN, K$_2$La$_2$Ti$_3$O$_{10}$, CdS, NaNbO$_3$, ZnO$_2$, g-C$_3$N$_4$, and SrTiO$_3$ are only some of the photocatalysts that have been investigated for photocatalytic water splitting [500]. Because of its versatility, long-term stability, and non-toxicity, tantalum nitride (Ta$_3$N$_5$) has garnered significant attention as a photocatalyst for photochemical applications [501]. At last, it all comes down to how much you value your time. If you're like most people, you probably don't have a lot of time to waste on things like reading lengthy articles. Several photocatalytic systems have been reported, however most of them merely create H$_2$ or O$_2$ by half-splitting water. Solar water splitting devices rely on photocatalysts with band gaps of approximately 2.0 eV, reflecting the minimal energy required to excite one electron from the VB to the CB [502]. In recent times, there has been a growing focus on tantalum nitride (Ta$_3$N$_5$) as a highly promising photocatalyst for water splitting. This can be attributed to its favorable band gap energy of approximately 2.1 eV, enabling efficient absorption of visible light up to 600 nm.

Ta_3N_5 theoretical efficiency in converting solar energy is close to 16%, suggesting the photo catalyst will find widespread use in the future [503]. In a nutshell, the Ta_3N_5 gadget demonstrates the capability to simultaneously split H_2O into H_2 and O_2. Ta_3N_5 is more stable and less hazardous than materials with a narrower band gap, like as CdSe and CdS.

Although, as a single photocatalyst, the water splitting method using Ta_3N_5 has been confronted with several obstacles such as quick recombination, small charge transfer capacity, and self-photo corrosion (reduced stability), In an electrolyte solution, the generated holes have the potential to oxidize the nitrides present in Ta_3N_5 [504]. Numerous strategies have been employed to overcome these challenges such as doping with metals (Cr, Fe, Mn, Pd, etc.,), non- metals (C, N and S) etc., of the Ta_3N_5 lattice will improve internal quantum transmission, electrons trapping, and to extend the light absorption in the visible region thereby decreasing the recombination of the photo generated electrons and holes, thus enhance the photocatalytic activity of the photocatalysts [505]. The band gap can be greatly reduced by the combination of V, S-doped Ta_3N_5, leading to improved photocatalytic activity. Consequently, a novel composite of V@S-Ta_3N_5/PANI was synthesized in this study through mechanical and in-situ polymerization method using vanadium pentaoxide and thiourea as a precursor for doping vanadium and sulfur.

The vanadium-sulfur codopant into Ta_3N_5 has not been employed in any previous research to the best of our knowledge. Earlier, vanadium used as a dopant into TiO_2 lattice [506]. Ti^{3+} and V^{4+} were created when the migration of V dopant into the lattice of TiO_2, which increased the photocatalyst's capacity for generating electron-hole pairs and decreasing their chances of recombining. To enhance the photocatalytic activity of Ta_3N_5 for efficient solar light-driven water splitting, we utilized V as a dopant due to its capability to migrate to the Ta_3N_5 lattice, similar to the function performed by the V dopant in the TiO_2 lattice. Visible-range photocatalytic applications also frequently employ nonmetal doping using S [507] or N

[508]. In a similar manner to Ta_3N_5, Umebayashi et al. reported that substituting oxygen with sulfur (anionic doping) causes a significant red-shift in the absorption edge [509]. Ab initio band calculations reveal that this narrowing of the band gap is attributed to the increase in the VB through the mixing of the valence band with the S 3p states. A different, more speculative method relies on the orbitals of the dopant atoms to create a distinct mid-gap level above the VB.

With the flexibility to combine the mechanical and chemical characteristics of polymers including the electronic capabilities of semiconductors and metals, conducting polymers provide intriguing potential for technological applications [510]. Modern research is focused on improving the mechanical strength and chemical stability of such polymers by introducing metals or metal oxides through electrochemical or chemical processes, hence adjusting their electrical characteristics [511]. These hybrid systems, known as organic-inorganic hybrids or composites, have emonstrated immense potential as versatile materials for a range of applications, including super capacitors, solar cells, photocatalysis and sensors [512]. Conducting polymers (polyaniline (PANI), polythiophene, polypyrrole and their derivatives) having extended π-conjugated electron systems, have recently emerged as promising sensitizers for enhancing response of photocatalysts to visible light like TiO_2, CdSe and ZnO [513, 514]. This study expands the usefulness of such hybrids by using PANI, a well-known conducting polymer, as an organic component due to PANI adjustable electrical and chemical characteristics, simplicity of production, and high efficiency [515].

The second goal of our research is to improve the photocatalytic activity of the synthesised materials to achieve efficient solar light-driven water splitting by sensitising the V [516]. In order to enhance charge transfer efficiency and inhibit recombination of photogenerated electrons and holes in the V and S-doped Ta_3N_5 photocatalyst, PANI was employed [517]. This approach helps prevent the oxidation of nitrides in Ta_3N_5, thereby avoiding self-

photocorrosion of Ta_3N_5 in the electrolyte solution and increasing its stability. The holes generated by the V and S-doped Ta_3N_5 system can be efficiently transported to the PANI surface.

4.2. Materials and methods

4.2.1. Materials

Tantalum nitride (nanoshell 99.9%), Vanadium pentaoxide (Loba Chemie), thiourea (CDH), Aniline (Merck), Ammonium persulfate (CDH), Ferric chloride (CDH), Hydrochloric acid (Loba Chemie), Acetone (Merck) and methanol (99%, LiChrosolv Merck), Deionized water. Entirely chemical was readily accessible and directly utilized without pretreatment. Glass plates were cast off as a substrate to manufacture photoelectrodes (PEs) ITO (Merck). Sulphuric acid (99%), sodium sulphate, potassium hydroxide, purchased from CDH PVT Ltd. was used to examine electrochemical and photoelectrochemical (PEC) studies. All reagents were synthesized using ultrapure deionized water from Millipore, and the glassware was cleaned**.**

4.2.2. Instrumentation

Powder X-ray diffraction (XRD) using a Rigaku diffractometer with Cu kα (=1.540) radiation was utilised to assess the crystallinity and purity of the generated samples. Analytik Jena, Specord UV-Vis diffuse reflectance spectroscopy (DRS) is used to analyse the electronic excitation of synthetic materials and derive band gap energy. FTIR spectra were collected from 400 to 4000 cm^{-1} using a Perkin Elmer IR instrument. The images were captured using a Hitachi FE-SEM scanning electron microscope (SEM) (SU-4800). Our EIS experiments were performed on an electrochemical workstation (CHI VMP3B-20) with a conventional three-electrode set-up (an Ag/AgCl reference electrode, a platinum wire auxiliary electrode and a working electrode). The Perkin-Elmer (LS55) Fluorescence spectrometer was used to record the results of the photoluminescence (PL) experiments.

4.2.3. Synthesis of Photocatalyst Materials

4.2.3.1. Synthesis of the doped and co-doped Photocatalyst

V-doped Ta_3N_5 were prepared by mechanically in a vibration ball milling mixing method after grind for 15 min, Ta_3N_5 (2g) and V_2O_5 (0.05g) were added in 150 mL of deionized water under stirring to obtain a homogeneous mixture. After the reaction, the mixture was stirred continuously at room temperature for 24 hours. Following this, the reaction mixture was filtered and dried. The resulting powder was subjected in a tubular muffle furnace to calcination at 900 °C for 8 hours, resulting in the formation of the final product, $V-Ta_3N_5$. Similar experiment was repeated for the synthesis of S-doped Ta_3N_5. Here thiourea was used as a precursor for the S dopant. $V@S-Ta_3N_5$ were prepared by ball milling mechanical mixing method after grind in ball milling for 15 min, Ta_3N_5 (2g), V_2O_5 (0.05g) and thiourea (0.15g) were added in 250 mL of deionized water under stirring to obtain a homogeneous mixture. The reaction mixture was continuously swirled at ambient temperature for 24 h. Subsequently, this reaction mixture was filter and dry. The obtained powder was calcinated at 900 °C for 8 h in a tubular furnace to get the final product $V@S-Ta_3N_5$.

4.2.3.2. Preparation of PANI

A [HCl]/[aniline] ratio of 6 was used to dissolve 35 wt% HCl (20 mL) and aniline (2.0 g) in distilled water (200 mL), yielding pure PANI. Over the course of three hours, of ammonium persulfate (($NH_4)_2S_2O_8$, 4.8 g) and ferric chloride ($FeCl_3$, 3.75 g) were added while being constantly agitated. After that, we let the mixture at least 10 hours to polymerize while sitting at room temperature. The resulting reaction product was separated through centrifugation and subsequently washed with HCl (1M), deionized water, and acetone until the filtrate became colorless. It was then dried under vacuum conditions at 60 °C for 24 hours, resulting in the formation of a dark green powder of PANI.

4.2.3.3. Synthesized materials protected with PANI

Synthesis of V@S-Ta$_3$N$_5$/PANI using the chemisorption technique, V@S-Ta$_3$N$_5$ core-missile structure with PANI was fabricated. In 50 ml of tetrahydrofuran, 0.32 g of V@S-Ta$_3$N$_5$ nanoparticles and a known quantity of PANI were combined, sonicated for 1 h followed stirring for 24 h. The mixture was placed in an oven and subjected to drying at 80 °C for a duration of 3 hours. Finally, V@S-Ta$_3$N$_5$/PANI composite was fabricated.

4.2.4. Photoelectrochemical study

The working electrode was fabricated by applying a slurry of 0.25 g photocatalyst and 0.023 g methyl cellulose in ethanol onto an indium-tin-oxide (ITO) glass substrate, which was then dried at 120 °C for 60 minutes. The experiment was carried out using an electrochemical workstation (Metrohm) equipped with a three-electrode system (Na$_2$SO$_4$ (0.1 M, aq.) serving as the electrolyte, SCE serving as reference electrode, and Pt flake serving as the auxiliary electrode). Also, maintain the pH at 3 and pour nitrogen gas to eradicate the dissolved oxygen. The scene was illuminated by a 300W Xe lamp, which had a 410 nm cutoff filter. A measurement was conducted using a 10 mV perturbation signal within a frequency range of 100 kHz to 0.01 Hz, as indicated by the Nyquist plots. These photoelectrochemical studies employed an applied potential of 0.5 V relative to Ag/AgCl.

4.2.5. Photocatalytic activity

Tests were performed in a sealed quartz reactor containing the catalyst (0.25 g) and water for an overall reaction volume of 10 ml to evaluate photocatalytic activity (H_2 evolution) of the synthesized materials. In order to get rid of the dissolved oxygen, we first degassed the reactor with Ar gas for 15 minutes before exposing it to visible light (80 W LED). Flowing cold water linked to the reactor was used to control the reaction temperature. Then, substances were put into the quartz-covered reactor. The experiment proceeded with continuous swirling. The quantity of H_2 evolution was scrutinized by gas chromatograph

(GC-TCD). The temperature was fixed at 30°C for the column, injector, and detector. In addition, material photocatalytic activity recycling experiments were carried out, with the photocatalyst being centrifuged and dry in oven back into its original form after each use.

4.3. Results and discussion

4.3.1. Characteristics analysis of the synthesized materials

4.3.1.1. Photoluminescence (PL) study

To determine the recombining ability, migration, and excitons transfer, experts perform photoluminescence spectroscopy (PL). A decrease in PL intensity suggests that the rate of reintegration of charge carriers is slower, resulting in improved photocatalytic efficacy in the composites [518]. The PL spectra of the produced composites were examined with an excitation wavelength of 370 nm. As seen in Fig. (4.1), [519] all of the photocatalysts exhibited an emission peak about 545 nm.

Fig. 4.1 shows PL spectra of the pure Ta₃N₅, V and S doped- Ta₃N₅, V@S-codoped Ta₃N₅ and V@S-Ta₃N₅/PANI composite materials

We found that the intensity orders of photocatalysts were in the following sequence: V@S-Ta₃N₅/PANI < V@S-Ta₃N₅ < S-Ta₃N₅ < V-Ta₃N₅ < Ta₃N₅. In comparison to the other samples, the PL intensity of the V@S-Ta₃N₅/PANI composite is the lowest, whereas that of pure Ta₃N₅ is the greatest. Due to the fact that the emission intensities of Ta₃N₅ aggregated with polyaniline are lower than those of pure Ta₃N₅ in the same position, these findings demonstrated that V@S-Ta₃N₅/PANI has good charge separation, allowing for a notable improvement in the Photocatalytic or electrocatalytic activity. As a result, V@S-Ta₃N₅/PANI excels as a photo (electro) catalyzer when exposed to sunlight light.

4.3.1.2. Fourier transform infrared (FTIR) study

Fig. (4.2) Confirms FT-IR spectra of pristine Ta₃N₅ doped and co-doped Ta₃N₅ and the

synthesized materials sensitized with PANI composite. Ta_3N_5 existence was confirmed by the pinnacle observed at 918 cm^{-1} because of the stretching mode of the Ta-N bond [520]. In the quinone unit, the stretching vibrations of C=N bonds produce the 1576 cm^{-1} band. C=C stretching vibrations are represented by the pinnacle at 1496 cm^{-1}, and C-H bond stretching vibrations in the phenyl ring are represented by the peak at 825 cm^{-1} [521]. Peak achieved at $1057\ cm^{-1}$, $1220\ cm^{-1}$ and $1300\ cm^{-1}$ were ascribed toward plane bending vibration of C-O-C, C-N stretching vibrations in the benzenoid unit [522, 523]. The band at $1698\ cm^{-1}$ were accredited to C=O stretch for the conjugated system [524]. The chemical structure of the PANI deposit is characterized. Characteristic peaks at $3742\ cm^{-1}$ are observed in the FTIR spectrum of N-H stretching; and $3649\ cm^{-1}$ these peaks can be ascribed to –OH stretching (free molecule) [525] and C–H ($2975 cm^{-1}$) stretching modes. The characteristic peaks at $1698\ cm^{-1}$ of C=O and $1649\ cm^{-1}$ of C=C stretching correspond toward the benzene ring, respectively [526]. Peaks at 2361 cm^{-1} are associated with carbon (IV) oxide vibrations caused by CO_2 in the atmosphere [527]. Consequently, these FTIR spectrum results validated that co-doped Ta_3N_5/PANI composite was prepared in our experiment.
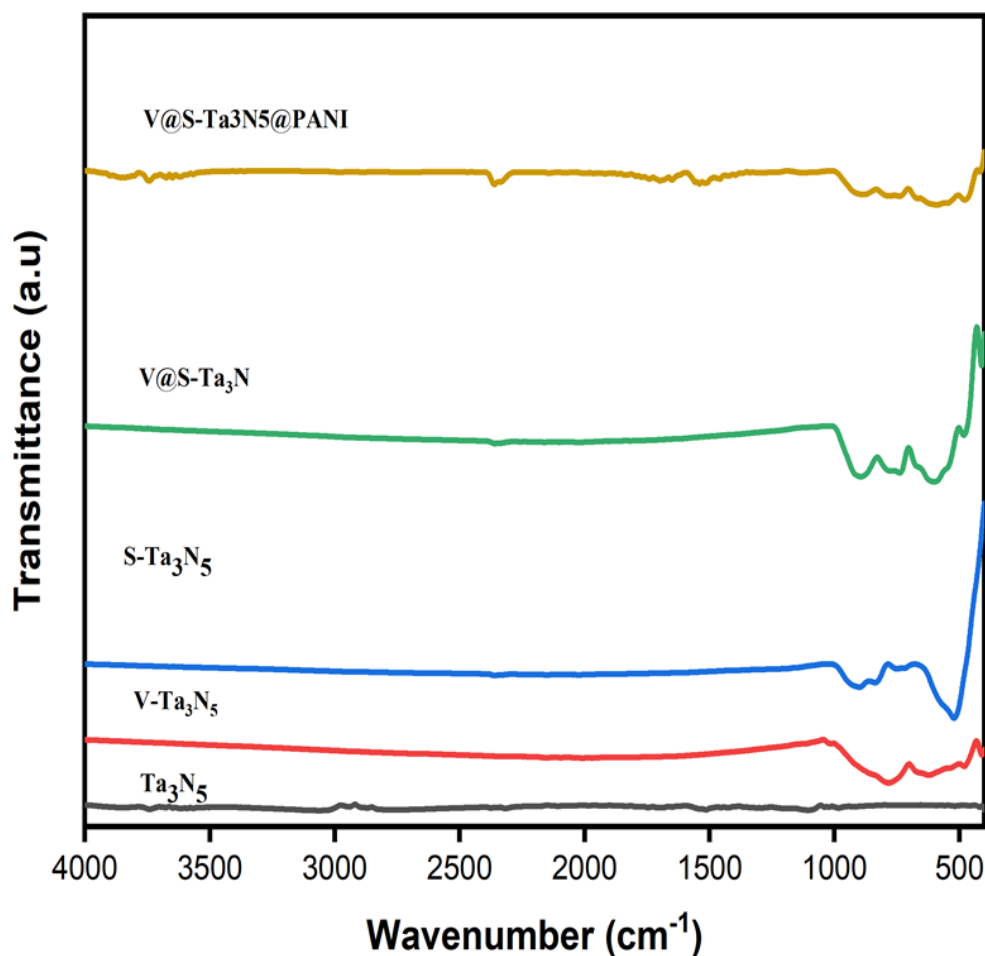
Fig. 4.2 demonstrations of FTIR spectrum of the pure Ta₃N₅, V and S doped- Ta₃N₅, V@S-codoped Ta₃N₅ and V@S-Ta₃N₅/PANI composite materials.

4.3.1.3. UV–visible diffuse reflectance spectroscopy (DRS) study

Fig. (4.3) illustrates the UV-visible absorption spectra of undoped Ta_3N_5 doped, co-doped and composites photocatalysts. An efficient photocatalyst has several characteristics, including a narrow band gap, high migration rate, low recombination, strong segregation of the photogenerated excitons, and maximum optical absorption. Ultraviolet-visible diffuse reflectance spectroscopy was employed to investigate the band-gap and absorption spectrum of nano-composite.
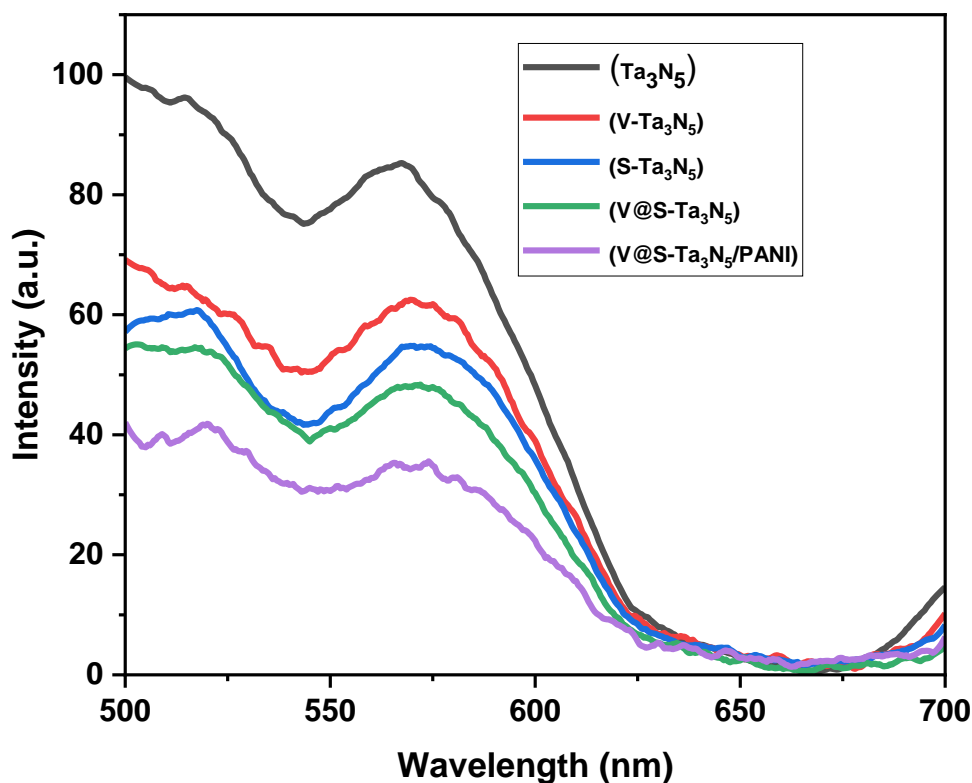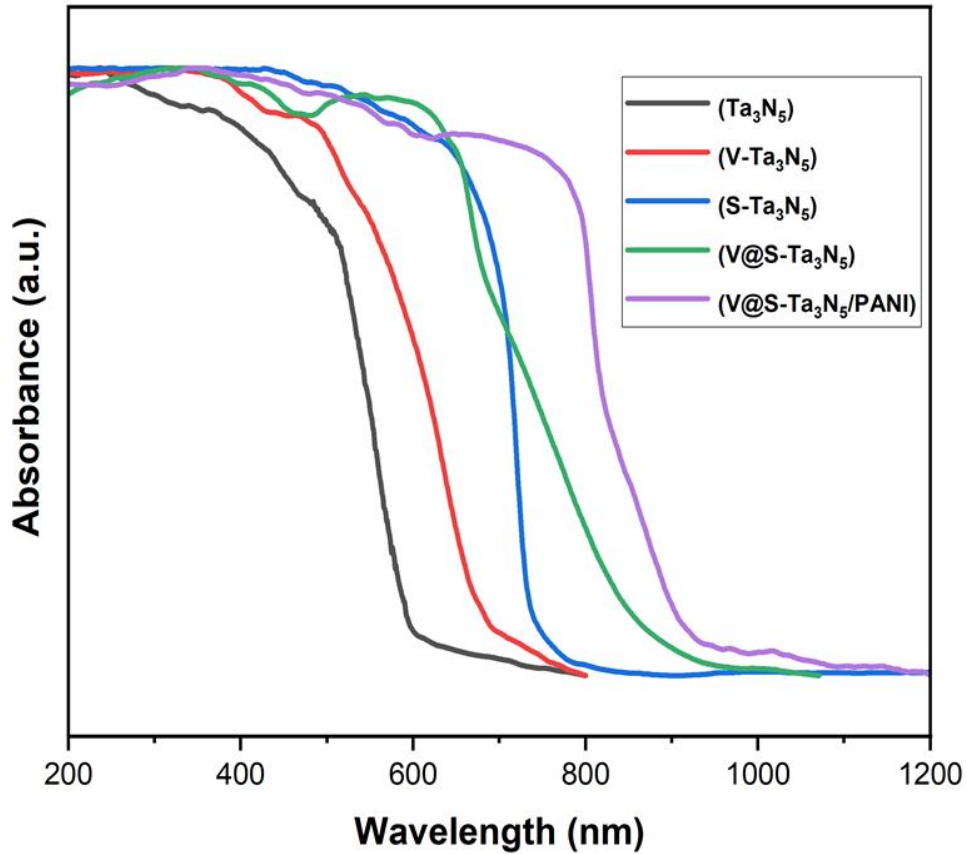
Fig. 4.3 shows the UV-Vis spectra of the pure Ta_3N_5, V and S doped- Ta_3N_5, V@S-codoped Ta_3N_5 and V@S-Ta_3N_5/PANI composite materials.

The band gap energies of Ta_3N_5, V-Ta_3N_5, S-Ta_3N_5, V@S-Ta_3N_5, and V@S-Ta_3N_5/PANI were calculated using the Tauc's relation shown in Eqs. (4.1 & 4. 2) [528].

$$(\alpha h v)^{1/2} = h v - E_g \tag{4.1}$$

$$(\alpha h v) = h v - E_g \tag{4.2}$$

v stand for frequency of light

α stand for the absorption coefficient

h stand for Planck's constant and

Eg stand for band gap energy

As shown in Fig. 4.4(A-D) and mentioned in Table 4.1, the band gaps of undoped Ta_3N_5, doped V-Ta_3N_5, S-Ta_3N_5, and co-doped V@S-Ta_3N_5 were evaluated to be 2.15, 1.90, 1.70, and 1.56 eV, correspondingly, according to the Tauc formula. It is the optimal photocatalyst

since the band gap range is in the visible area (600 nm) [529]. Ta_3N_5@PANI absorption intensity in visible light areas steadily improved after assortment with PANI. It has been known for quite some time that PANI absorbs visible light (due to its affinity for electron transitions in polyaniline to π^* band from the polaron band) [530]. In order to boost its photocatalytic activity, the V@S-Ta_3N_5@PANI composite achieved a higher light harvesting ability.
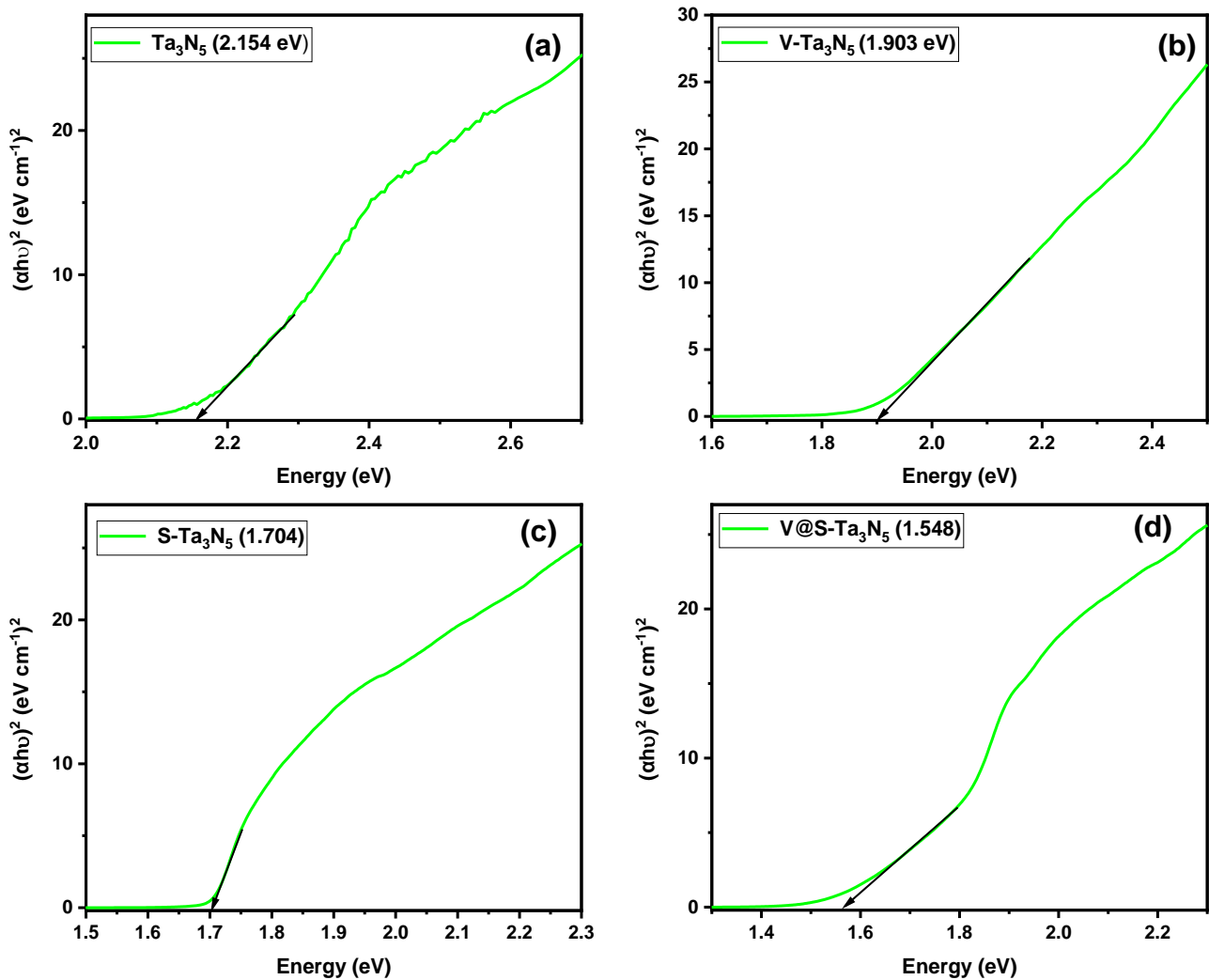
Fig. 4.4 shows the band gap energies of the (A) pristine Ta_3N_5, (B) V-doped Ta_3N_5, (C) S-doped Ta_3N_5 and (D) V@S co-doped Ta_3N_5 calculated by Tauc plot.

Table 4.1 Band gap Energy of undoped, doped and co-doped Ta₃N₅ calculated by tauc plots.

Photocatalyst	Bandgap energy (eV)
Undoped-Ta$_3$N$_5$	2.15
V-doped- Ta$_3$N$_5$	1.90
S-doped- Ta$_3$N$_5$	1.70
V@S codoped- Ta$_3$N$_5$	1.56

4.3.1.4. X-ray diffraction (XRD) study

The crystalline structures of the synthesized materials Ta$_3$N$_5$, V-Ta$_3$N$_5$, S-Ta$_3$N$_5$, V@S-Ta$_3$N$_5$, and V@S-Ta$_3$N$_5$/PANI were analyzed by XRD (fig. (4.5). The foremost diffraction peaks detected at 2θ values of 28.8°, 35.8°, 36.7°, 38.8°, 43.9°, 46.9°, and 49.9° designate that the synthesized Ta$_3$N$_5$ occurred in the form of orthorhombic [531]. The XRD patterns of the synthetically produced doped V-Ta$_3$N$_5$ and S-Ta$_3$N$_5$ photocatalysts exhibit a change in the peak location towards a narrower diffraction angle together with peak widening when compared to the Ta$_3$N$_5$ sample. This occurred as a result of dopants V and sulphur defecting into the Ta$_3$N$_5$ lattice [532]. By swapping out a number of Ta atoms in the lattice, V and S may readily integrate into the Ta$_3$N$_5$ structure. In the XRD pattern, there was no sign of a contamination peak. Because the peak observed in the XRD patterns of V@S-Ta$_3$N$_5$/PANI was comparable to V@S-Ta$_3$N$_5$, PANI had no effect on the crystalline structure of Ta$_3$N$_5$ [533].
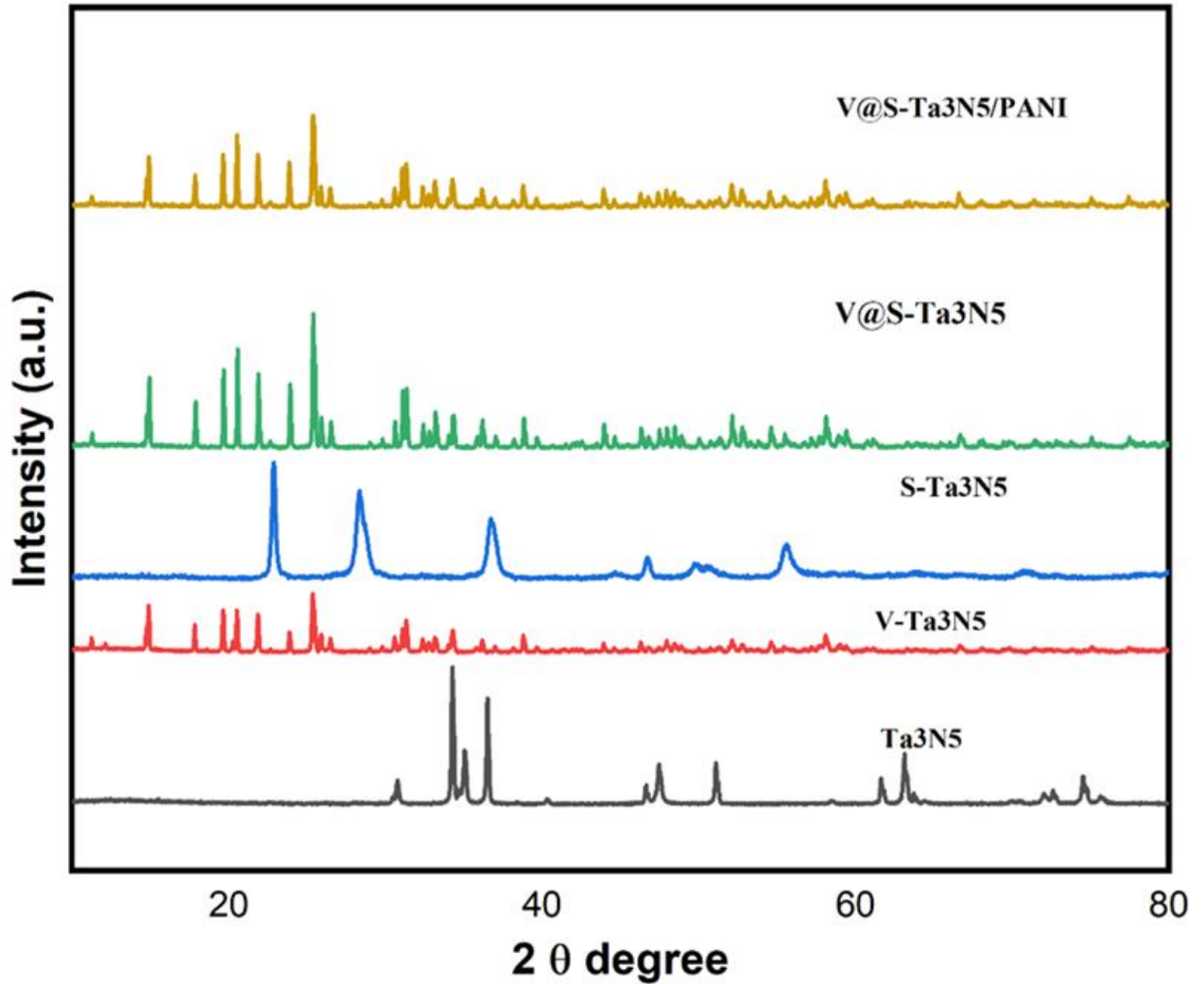
Fig. 4.5 displays XRD data of the pure Ta₃N₅, V and S doped-Ta₃N₅, V@S-codoped Ta₃N₅ and V@S-Ta₃N₅/PANI composite materials.

4.3.1.5.FE-SEM analysis

Fig. 4.6 (A-D) displays the results of Surface analyses of all the fabricated materials characterized via FE-SEM. SEM divulges the morphology and microstructure of pure Ta₃N₅, doped and co-doped Ta₃N₅/PANI composite. Fig. 4.6 (A) shows the pristine Ta₃N₅ appearance, looking like a massive layered particle with a flocculent lamellar structure [534]. Fig. 4.6 (B&C) showed that the SEM morphology of all V and S doped -Ta₃N₅ samples have spherical shapes. Moreover, Fig. 4.6 (D) depicted fibrous/neurons-like surface morphology with high porosity shows that as a nanocomposite PANI covering the Ta₃N₅ surface, which

clearly indicates the presence of PANI [535].
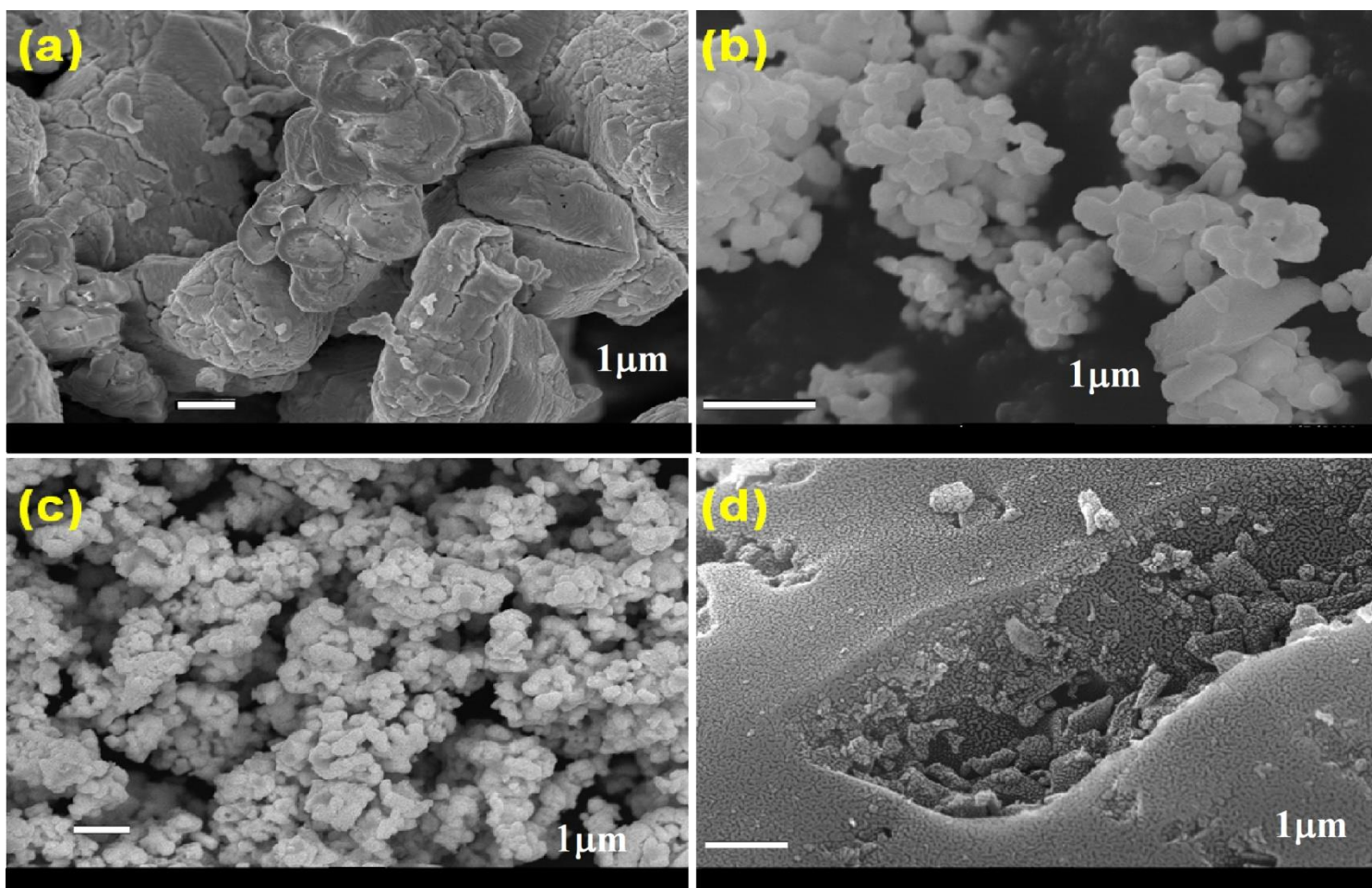
Fig. 4.6 Shows the FE-SEM morphology of the synthesized (A) undoped Ta₃N₅; (B) V doped Ta₃N₅, (C) V@S codoped-Ta₃N₅ and (D) V@S-Ta₃N₅/PANI composite.

4.3.1.6. PEC measurement

The electrochemical impedance spectroscopy (EIS) measurements produced Nyquist plots, as depicted in Figure 4.7(A) that were also carried out for better understanding the charge transfer processes at the electrode/electrolyte interface of the manufactured electrodes. The V@S-Ta₃N₅/PANI electrode exhibits greater charge transfer than other electrodes because it possesses the charge transfer resistance (Rct) shortest semi-circle. This may be attributed to the heterostructure of Ta₃N₅ and PANI, which allows for superior charge generation, separation, and channelling, and thus enhanced photocatalytic activity [536].

4.3.1.7. Experimental yield of photocatalyst

Fig. 4.7 (B & C) demonstrate H_2 evolution of photocatalytic bustle of fabricated doped, co-doped-Ta_3N_5, and V@S-Ta_3N_5/PANI composites in visible light radiation ($\lambda > 410$ nm). As demonstrated in Fig. 4.7(B), H_2 production ratio of Ta_3N_5, V-Ta_3N_5, S-Ta_3N_5, V@S-Ta_3N_5 and V@S-Ta_3N_5/PANI with 22.8, 50.3, 58.6, 72.9 and 98.4 $\mu mol g^{-1} h^{-1}$ in 5 hours exposed to visible light irradiation. H_2 Evolution enactment of Ta_3N_5 was considerably superior to later alteration with PANI. The photocatalytic production rate of H_2 for the V@S-Ta_3N_5/PANI composite reached its maximum value at $98.4 \mu mol g^{-1} h^{-1}$, which is around four times (4) higher than that of pristine Ta_3N_5. Fig. 4.7 (C) shows H_2 yield of all synthesized catalyst increase with time. Moreover, we observed good photocatalytic stability of V@S-Ta_3N_5/PANI composite for H_2 generation by photocatalysis on exposure to visible light. The amount of H_2 generation of V@S-Ta_3N_5/PANI was almost unaffected even after five cycles, according to the evidence in fig 4.7(D), the presence of the polymer in the sample contributed to its excellent stability, as evidenced by the results (polymer prevents the metal nitrides from self-photo corrosion during the reaction). Nevertheless, the photocatalytic H_2 ratio of Ta_3N_5 was apparently shrunk, mainly recognized to the self-photo corrosion. Throughout the reaction process, according to the following equation, the photogenerated holes had the capability to oxidize nitrogen anions in Ta_3N_5, leading to the formation of Ta_2O_5 [537].

$$2Ta_3N_5 + 30h^+ + 30OH^- \rightarrow Ta_2O_5 + 5N_2 + 15H_2O \qquad (4.3)$$
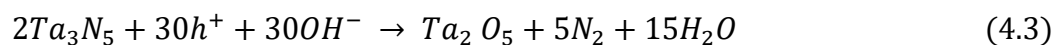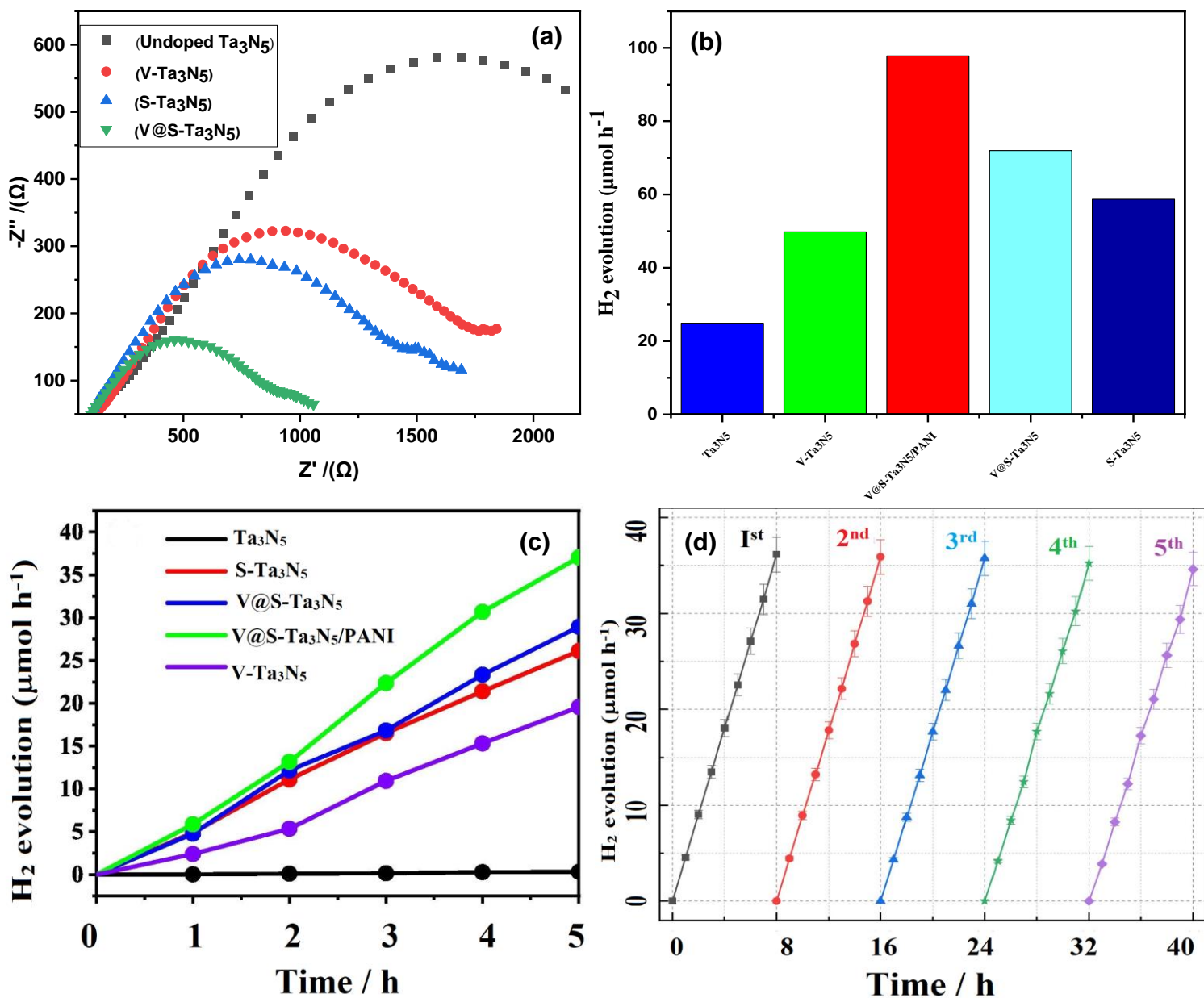
Fig. 4.7 shows the (A) Nyquist plot of undoped Ta₃N₅, V-doped Ta₃N₅, S-Ta₃N₅, and V@S codoped-Ta₃N₅, (B) shows the H_2 evolution activity of the of undoped Ta₃N₅, V-doped Ta₃N₅, S-Ta₃N₅, and V@S codoped-Ta₃N₅ synthesized materials, (C) H_2 evolution activity of the synthesized materials with time and (D) displays the recyclability of the Photocatalyst to check the stability up to 5 cycles.

4.3.2. Proposed photo catalytic mechanism

Based on the foregoing experiment, Fig. 4.8 proposes a mechanism for improved photocatalytic H_2 production by V@S-Ta$_3$N$_5$/PANI nanocomposite under solar light (visible). Under visible light irradiation, doped and co-doped Ta$_3$N$_5$ and PANI create electrons and holes. PANI's photogenerated electrons directly relocate to Ta$_3$N$_5$ CB because of the synergic impact of their relative energy levels (LUMO and HOMO). Doped, co-doped and composites among them V@S-Ta$_3$N$_5$/PANI composite has the lower band gap energy and much higher absorption of visible light than undoped Ta$_3$N$_5$. This was due to the fact that the Ta$_3$N$_5$ lattice V and S dopants may function as an intermediary band (V 3d) and (S 3p) between the VB (N 2p) and conduction band (Ta 5d) for the transfer of electrons from the valence band to the Ta$_3$N$_5$ conduction band [538, 539]. On the Ta$_3$N$_5$ surface, hydrogen is formed through photogenerated electrons. Excited holes go from Ta$_3$N$_5$ VB to PANI HOMO simultaneously. PANI easily transports holes toward the surface and captures them. The steady interfacial contact between Ta$_3$N$_5$ and PANI may help interfacial charge carriers migrate [540]. Moreover, the holes deposited on the PANI surface further develop the photostability of Ta$_3$N$_5$ (hole induced photocorrosion). Charge transfer inhibited photogenerated electron-hole pair recombination, improving photocatalytic efficacy. V@S-Ta$_3$N$_5$/PANI photocatalyst is appealing enough to use the spectrum of sunlight efficiently. A list of several photocatalysts protected with polymer composites (visible light driven) is mentioned in Table 4.2 as well as their photocatalytic application on water splitting for H_2 evolution rate with different reaction conditions.
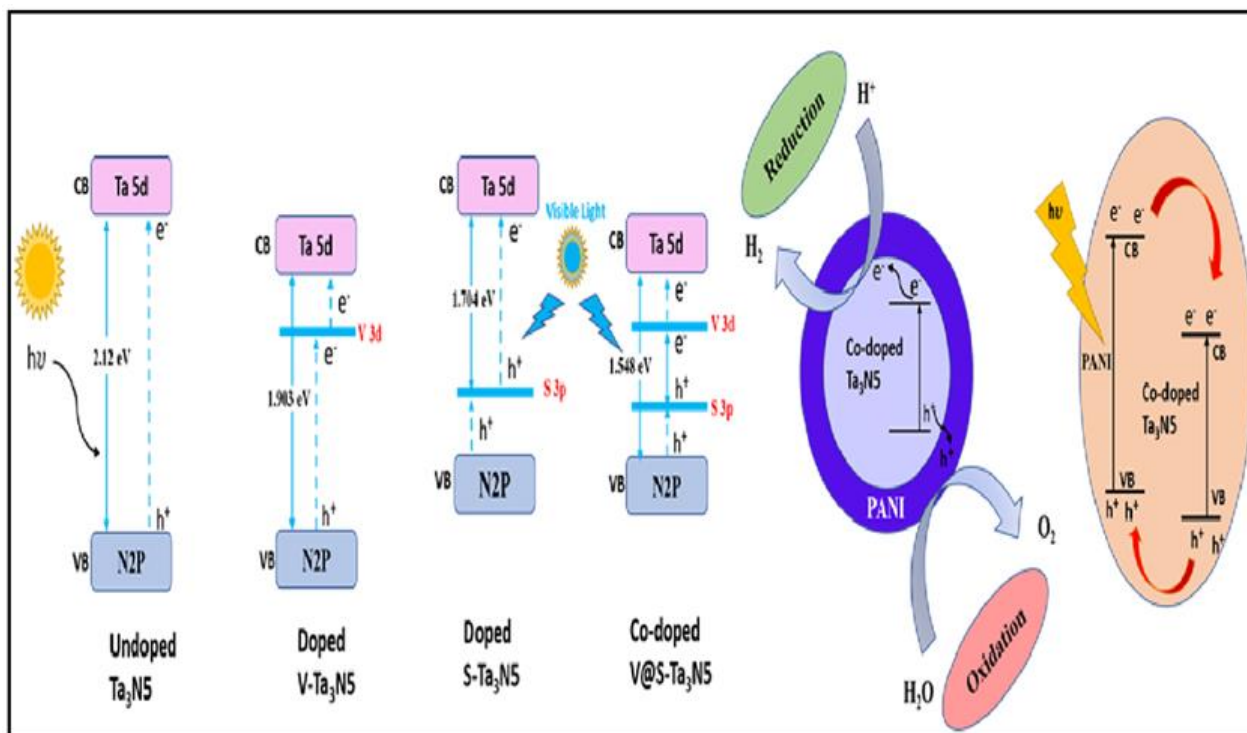
Fig. 4.8 shows schematic diagram of photocatalytic mechanism for the evolution of H_2.

Table 4.2 Shown comparison study of different types of Ta₃N₅-dependent photocatalyst triggered by visible light for H_2 evolution reaction

Photocatalyst	Source of Light	Reaction medium	Sacrificial agents/cocatalysts	H₂ production Yield $(\mu mol g^{-1} h^{-1})$	Ref.
SrTaO₂N/Ta₃N₅	300 W Xe lamp (λ > 420 nm)	Na₂SO₃/H₂O	4 wt% Pt as a cocatalysts	19.07	[541]
Au@Cu₂O-Ta₃N₅	300 W Xe lamp (λ > 410 nm)	Cu₂SO₄/TEOA	-	65.78	[542]
Ta₃N₅/PANI	300 W Xe lamp (λ > 410 nm)	TEOA/H₂O	TEOA as a sacrificial agent	72.6	[543]
Ta₃N₅	Visible light bulb (400-700 nm)	Water	-	22.8	Present work
V@S-Ta₃N₅/PANI	Visible light bulb (400-700 nm)	Water	-	98.4	Present work

4.4. Conclusions

In summary, the mechanical mixing method was used to prepare doped (V, S), co-doped (V@S), and composite (V@S-Ta$_3$N$_5$/PANI) materials. The synthesized composite shows stable and higher photocatalytic H$_2$ production performance of 98.4 $\mu mol g^{-1} h^{-1}$ which is around 4 folds of pure Ta$_3$N$_5$. The photostability and reusability of the V@S-Ta$_3$N$_5$/PANI nanocomposite were extremely remarkable. The obtained results suggest that, given optimal growth conditions, doping with (V), (S), and (V, S) codoping is energetically optimal. V or S doping leads to band gap narrowing and improved optical absorption in the visible region of the spectrum. Additionally, (V, S) codoping of Ta$_3$N$_5$ further enhances the band gap narrowing and extends the visible-light absorption edge up to approximately 700 nm, surpassing the effects of V-doping or S-doping alone. The superior photocatalytic activity can be attributed to a synergistic effect resulting from strong interfacial interaction, which enhances visible light absorption, facilitates efficient separation of electron-hole pairs, and promotes the transfer of acidic holes from the Ta$_3$N$_5$ surface to the PANI surface, thereby inhibiting self-photocorrosion. Our research demonstrates that mechanical mixing can streamline the composite preparation process and boost photocatalytic property, offering a practical roadmap for the catalyst's future synthesis and design.

Chapter 4

Section (C)

4. Photoreactor design

4.1. Introduction

The exploration of a photoreactor is a forefront strategy currently under investigation to identify an appropriate system that facilitates photocatalytic activity. The efficiency of a photocatalytic process greatly depends on factors such as the extent of optical absorption and the adsorption of reactants on the catalyst surface. Therefore, the design of photoreactors holds significant importance, encompassing aspects such as the choice and positioning of light sources, reactor configuration, and the incorporation of reflectors. The photoreactor contents should be evenly lit in order to provide the greatest photocatalytic results. Due to its capacity to capture more photon flux, bigger light absorption surface area, and improved photocatalytic effects, monolith reactors, which have equivalent straight channels, have been the subject of substantial research in photocatalyst technology. With a monolith photoreactor, Tahir and colleagues found that the photocatalytic production of H_2 activity from H_2O splitting with CH_3OH as an oblational reagent and $NiO-In_2O_3/TiO_2$ serving as a catalyst could be accomplished with a greater efficiency than with a cell reactor [544]. Gao et al. successfully synthesised a $V-W/TiO_2$ catalyst and investigated its photocatalytic performance in honeycomb and conventional reactors for H_2 evolution [545]. In comparison to the typical reactor, they discovered an H_2 production of roughly 0.27 $\mu mol g^{-1} h^{-1}$. This improved photocatalytic activity possibly will be credited to the large amount of available surface area. In our research we have designed the two similar setup of photocatalytic reactor as shown in fig (4.1 and 4.2) to carry out the experimental work for H_2 generation and CO_2 reduction through water splitting reaction.
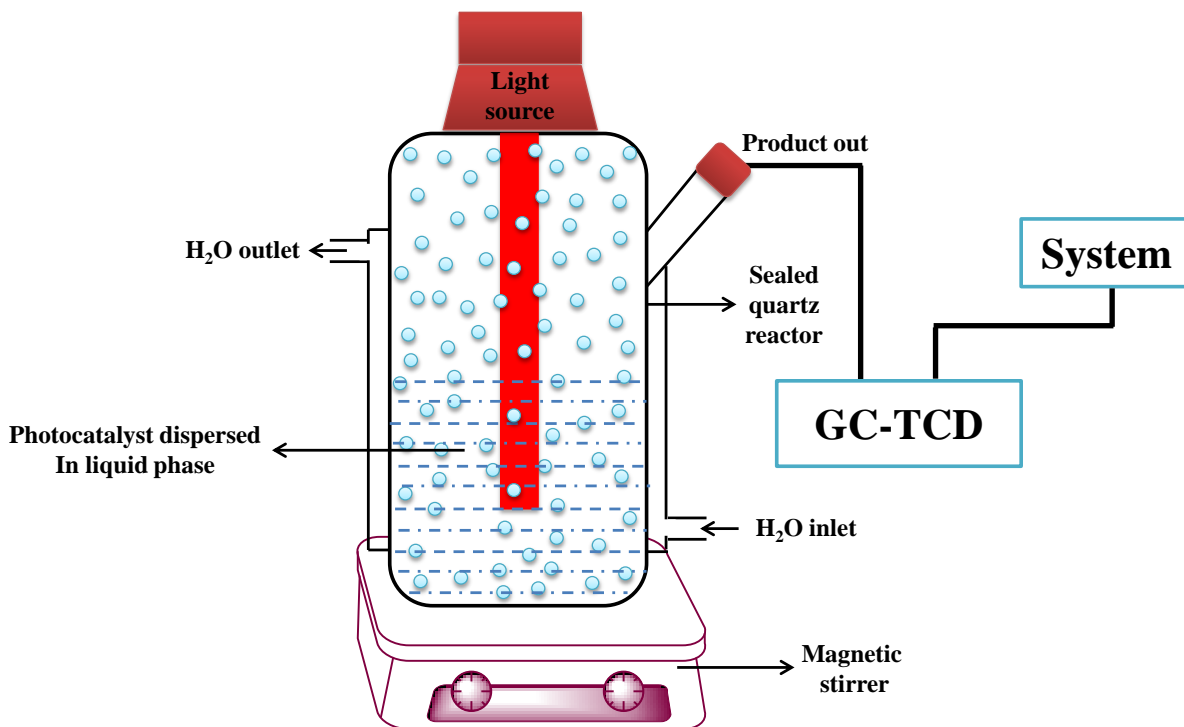
Fig. 4.1 Design photoreactor set-up for photocatalytic water splitting for the evolution of H_2
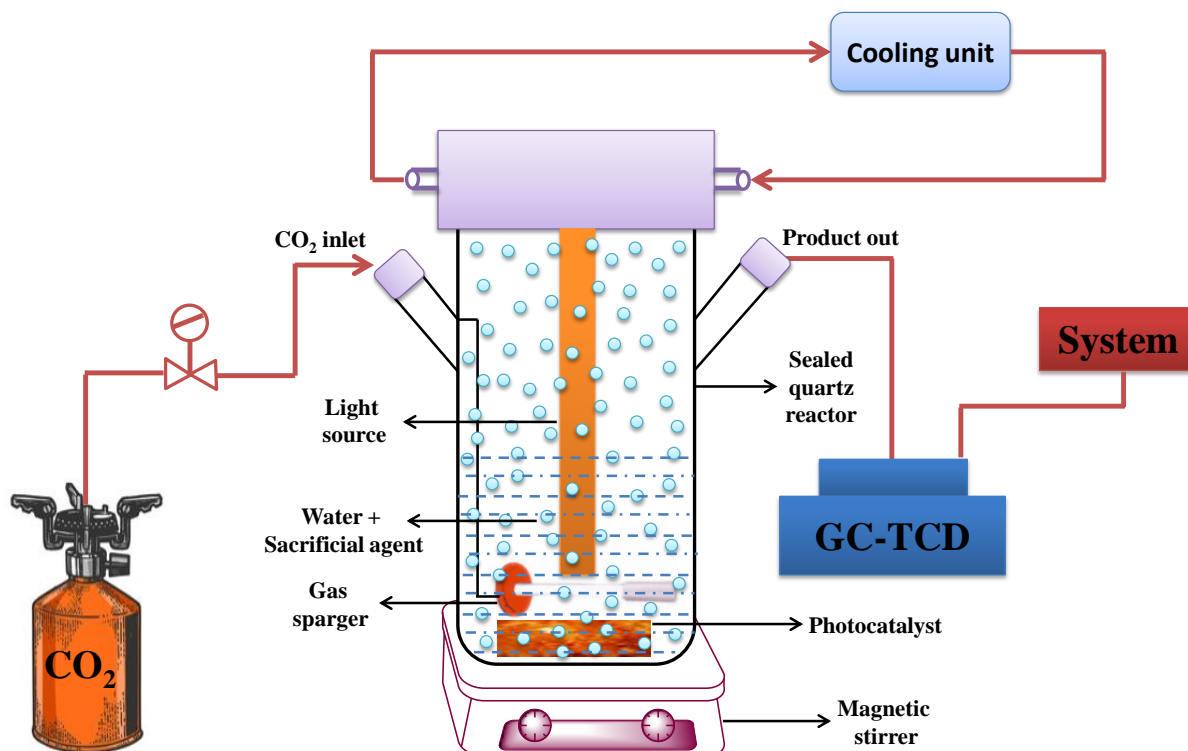
Fig.4.2. Design photoreactor set-up for photocatalytic water splitting for the reduction of CO_2 into valuable fuels

Nb-Ta$_3$N$_5$ protected with PANI nanocomposite for promoted water-splitting under visible light irradiation

4.1 Introduction

To date, issues relating to energy shortages and environmental pollution are among the most difficult challenges confronting humans. Global energy demand is expanding faster than fossil fuel capacity, generating an energy deficit. Recently, hydrogen (H$_2$) has been a promising alternative energy source as a next-generation energy carrier [546].

Over the past decades, many studies have focused on splitting pure water into H$_2$ and O$_2$ (2H$_2$O → 2H$_2$ + O$_2$, $\Delta G° = 238$ kJ·mol^{-1}) by different approaches. Heterogeneous photocatalytic water-splitting using sustainable solar energy has been recognized as a practical approach for H$_2$ production. This approach does not require an external electrical potential and can make hydrogen an abundant energy source [547]. However, their performance is still low and needs further effort. Various strategies have been reported to develop and prepare efficient, inexpensive photoactive materials. To date, many promising candidates, such as TiO$_2$ (Lin et al., 2009), α-Fe$_2$O$_3$ (Sivula et al., 2011), WO$_3$ (Pesci et al., 2011), BiVO$_4$ (Kim et al., 2015), and others are UV and visible light-efficient photocatalysts, have been successfully reported [548]. Interestingly, tantalum nitride (Ta$_3$N$_5$) is one of the few ideal photocatalysts for overall solar water-splitting (He et al., 2016) [549]. However, it has low photovoltage and poor stability, which remain critical challenges that limit its application.

To do with this challenge, this study used Nb as a dopant increases e$^-$-h$^+$ pair separation by acting as an intermediate band between the valence band (VB) and conduction band (CB) of Ta$_3$N$_5$. Also, PANI, a conducting polymer, was protected by photogenerated e$^-$ and h$^+$ charge

transfer. The prepared samples were characterized by X-ray powder diffraction (XRD), UV-visible diffuse reflectance spectroscopy (UV-vis DRS), and field emission scanning electron microscopy (FE-SEM), etc., whose photocatalytic water-splitting for H_2 production activities were tested under visible light irradiation.

4.2 Materials and methods

4.2.1 Synthesis of photocatalysts

The doped-photocatalyst was synthesized by diluting $Nb(OCH_2CH_3)_5$ (Sigma-Aldrich, 99.9%) in 1M CH_3CO_2H (Sigma-Aldrich, ≥99%) and adding Ta_2O_5 (Sigma-Aldrich, 99.9%). To achieve 2wt.% Nb/Ta ratio, $Nb(OCH_2CH_3)_5$ volume and Ta_2O_5 weight were estimated. Ultrasonication for 2 h and stirring for 8 h produced a homogeneous suspension, oven-dried at 160°C for 10 h. $Nb\text{-}Ta_3N_5$ was produced by calcining at 850°C under NH_3 gas.

Pure PANI was synthesized by dispersing 20 mL of 35wt.% HCl (Loba Chemie) and 2.0 g of aniline (Merck) in 200 mL of distilled water at a [HCl]/[aniline] ratio of 6. While stirring for 3 h, 4.8 g of $(NH_4)_2S_2O_8$ (Sigma-Aldrich, ≥98%) and 3.75g of $FeCl_3$ (CDH) were added drop by drop. Polymerization took at least 10 h at room temperature. After centrifugation and washing with 1M HCl, deionized water, and CH_3COCH_3 (LiChrosolv Merck, 99%) in that order until the filtrate became colorless, a dark green PANI powder was produced and dried in a vacuum at 60°C for 24 h.

Following, $Nb\text{-}Ta_3N_5$ core-missile structure with PANI ($Nb\text{-}Ta_3N_5@PANI$) was prepared by the chemisorption technique. In 50 ml of C_4H_8O (Merck), 0.32 g of $Nb\text{-}Ta_3N_5$ nanoparticles and a known quantity of PANI were combined, sonicated for 1 h, and then stirred for 24 h. The mixture was kept from the solvent and dried for 3 h at 80 °C. Finally, the $Nb\text{-}Ta_3N_5@PANI$ composite was fabricated.

4.2.2 Characterizations

Powder XRD with Cu k_α (λ=1.540 Å) radiation on a Rigaku diffractometer assessed the

sample crystallinity and purity. Analytik Jena, Specord UV-vis diffuse reflectance spectroscopy (DRS) analyses synthesized material electronic excitation and band gap energy. FE-SEM images were taken with Hitachi FE-SEM (SU-4800).

4.2.3 Photocatalytic water-splitting

As shown in Fig. 4.1, water-splitting for H_2 evolution tests used powdered photocatalysts suspended in water. We must send Ar/N_2 gas through photoreactors before starting water-splitting studies to avoid contamination. For product evaluation, an online GC-TCD was set up. Photocatalytic activity (H_2 evolution) of synthesized materials was tested in our sealed quartz reactor with 0.25 g of catalyst and 10 mL of water. Before exposing the reactor to visible light (80 W LED), we degassed it with Ar gas for 15 min to remove dissolved oxygen. Cold water from the reactor-controlled reaction temperature. Substances were added to the quartz-covered reactor. Magnetic stirring continued throughout the experiment. The detector, injector, and column were kept at 30°C. After each usage in material photocatalytic activity recycling studies, the photocatalyst was centrifuged and oven-dried.
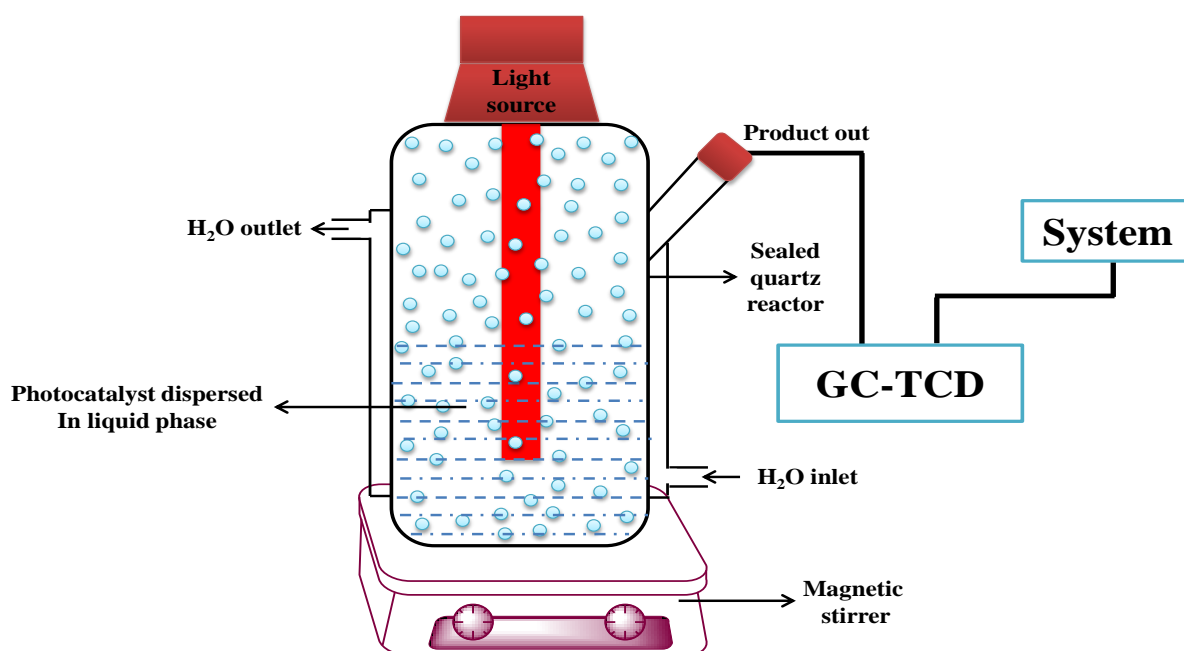
Fig. 4.1. Designed experimental setup for water-splitting toward photocatalytic H_2 evolution.

4.3 Results and discussion

4.3.1 Characteristics materials

Fig. 4.2(a) shows the UV-vis absorption spectrum of Ta_3N_5 and its composite photocatalysts. Ta_3N_5 has a broader absorption edge (600 nm) [550] and a small energy gap (2.15 eV, as seen in Fig. 4.2(b)). After doping by Nb, the Nb-Ta_3N_5 exhibited apparently enhanced visible-light absorption in comparison to that of pristine Ta_3N_5, evidencing that the Nb-Ta_3N_5 would have a strong absorptive ability in the visible-light region (band gap: 1.94 eV, Fig. 4.2(c)). Interestingly, Nb-Ta_3N_5@PANI absorption intensity in visible light areas progressively increased after combination with PANI due to its affinity for π-polaron transitions [551]. Both Nb-Ta_3N_5 Nb-Ta_3N_5@PANI samples could effectively harvest lighter irradiation and can be expected to possess robust photocatalytic properties. XRD patterns of Ta_3N_5, Nb-Ta_3N_5, and Nb-Ta_3N_5@PANI are shown in Fig. 4.2(d). The main diffraction peaks at 2θ values of 22.9°, 28.8°, 35.8°, 43.9°, and 49.9° indicate orthorhombic Ta_3N_5 [552]. Compared to Ta_3N_5, synthesized Nb- doped Ta_3N_5 photocatalysts have a peak shift towards a smaller diffraction angle and peak broadening. Which indicate Nb dopants defected into the Ta_3N_5 lattice and easily replaced numerous Ta atoms [553]. In case of Nb-Ta_3N_5@PANI XRD pattern were similar to Nb-Ta_3N_5 which indicate the amorphous nature of PANI. FE-SEM was conducted to investigate the morphology and microstructure of materials. Fig. 4.2(e) depicts virgin Ta_3N_5 as a large layered particle with a flocculent lamellar structure [554], offering favorable conditions to combine the merits of both PANI and Nb. Fig. 4.2(f) shows a nanocomposite with fibrous/clusters of particles covering the surface of Ta_3N_5, indicating PANI.
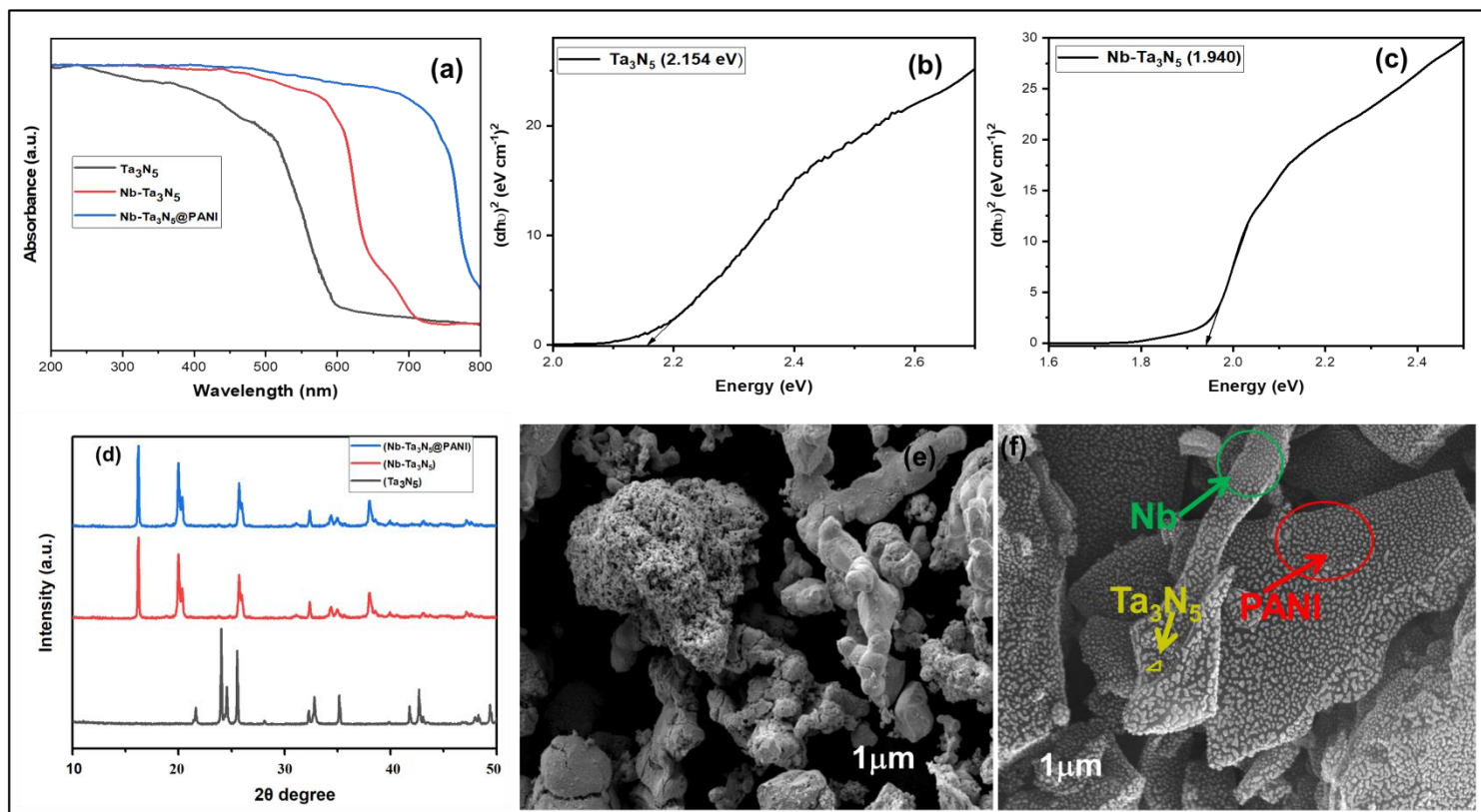
Fig. 4.2. (a) UV-Vis spectra of the Ta₃N₅, Nb-Ta₃N₅, and Nb-Ta₃N₅@PANI composite materials, (b-c) band gap energies of the Ta₃N₅ and Nb-Ta₃N₅ calculated by Tauc plot, (d) XRD data of the Ta₃N₅; Nb-Ta₃N₅, Nb-Ta₃N₅@PANI composite materials and (e-f) FE-SEM of Ta₃N₅ and Nb-Ta₃N₅@PANI.

4.4 Photocatalytic H_2 production

Fig. 4.3(a) shows the photocatalytic activity of synthesized materials in visible light radiation (λ > 410 nm). In 4 h under visible light, Ta_3N_5, Nb-Ta_3N_5, and Nb-Ta_3N_5@PANI produced 22.5, 46.8, and 71.3 mmol/g of H_2, respectively. Ta_3N_5 evolution outperformed PANI modification. The maximal photocatalytic H_2 generation rate of Nb-Ta_3N_5@PANI composite is 71.3 mmol/g, 3.17 times that of Ta_3N_5. The stability and recyclability of photocatalyst is also crucial qualification for practical application.
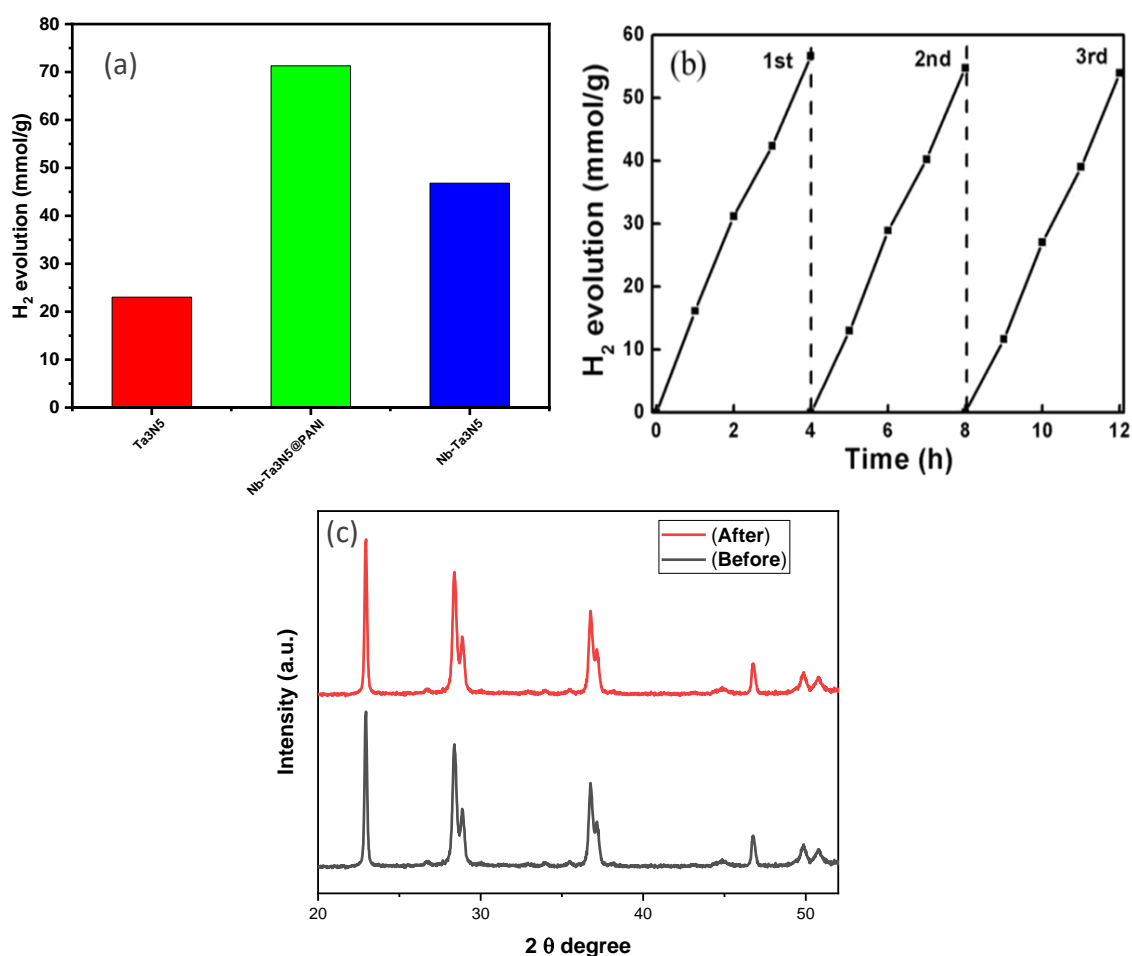
Fig. 4.3. (a) H$_2$ evolution activity of Ta$_3$N$_5$, Nb-Ta$_3$N$_5$, and Nb-Ta$_3$N$_5$@PANI synthesized materials, (b) Recyclability of the photocatalyst to check the stability up to 3 cycles and (c) XRD image of synthesized photocatalyst before and after the reaction.

As shown in Fig. 4(b), no apparent inactivation in the H$_2$ evolution could be found for Nb-Ta$_3$N$_5$@PANI even after three consecutive cycles, indicating that the photocatalyst has excellent stability. XRD of fresh and spent samples was also employed to reveal their crystal structures. To check out the stability of the synthesized composite the XRD pattern were taken before and after use as shown in fig. 4.3(c). As the XRD patterns of synthesized materials before and after were similar indicate the crystal structures did not change significantly from that before the test after the long-term photocatalytic experiments, indicating that the prepared catalysts have good stability.

4.5 Proposed photocatalytic mechanism

The feasible carrier-transfer process and the related photocatalytic mechanism of Nb-Ta$_3$N$_5$@PANI composite for photocatalytic H$_2$ production reaction under visible-light irradiation was exhibited in Fig.4.4. In the Ta$_3$N$_5$ lattice, Nb dopants can act as an electron-transfer band (Nb 4d) between the valence (N 2p) and conduction (Ta 5d) bands. On Ta$_3$N$_5$, photogenerated electrons can potentially form H$_2$, and PANI can easily catch holes. Maintaining contact between Ta$_3$N$_5$ and PANI could facilitate charge carrier mobility. Holes on the surface of PANI exacerbate the photocorrosion of Ta$_3$N$_5$. A list of several photocatalysts protected with polymer composites (visible light driven) is mentioned in Table 4.1 as well as their photocatalytic application on water splitting for H_2 evolution rate with different reaction conditions.
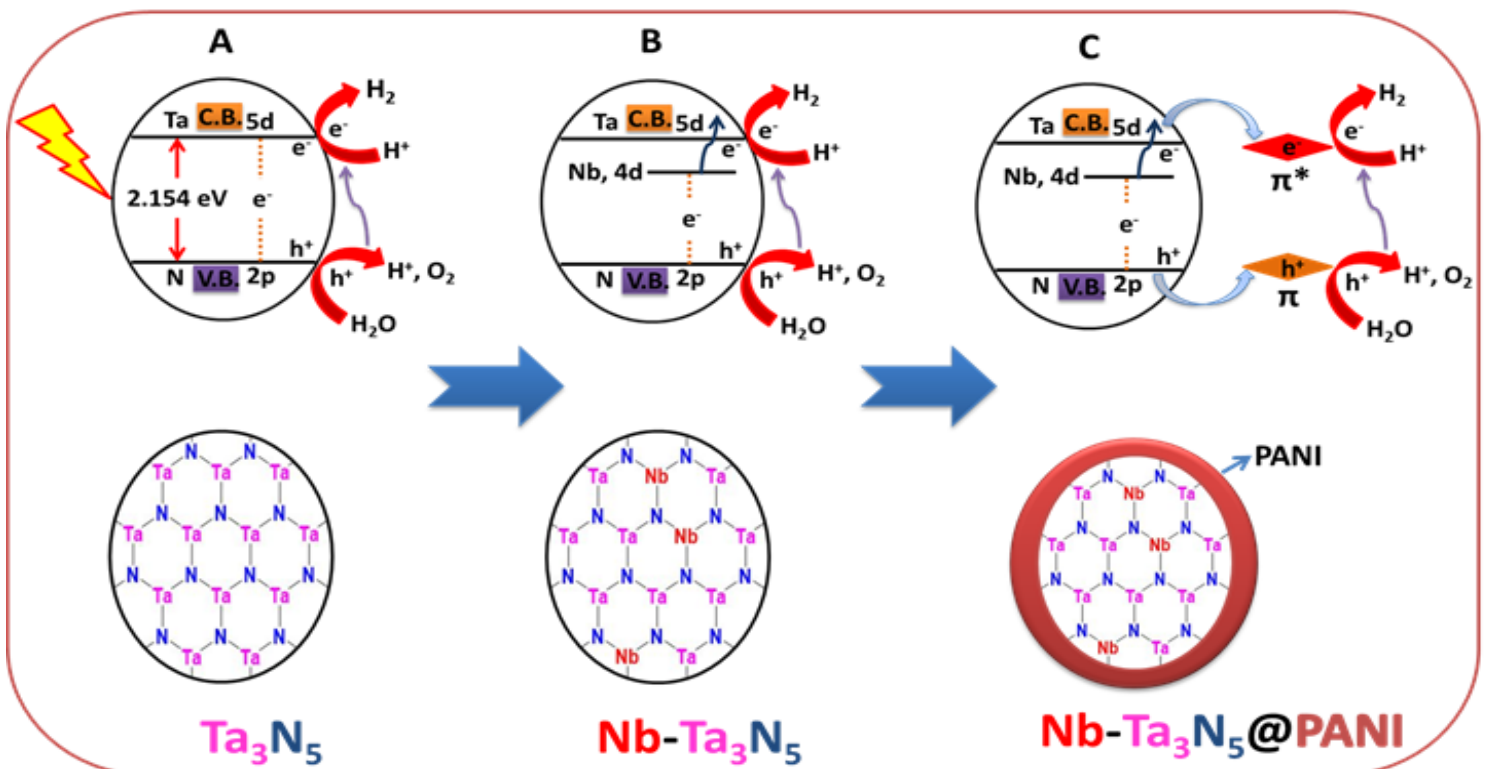
Fig.4.4. Schematic representation of the photocatalytic mechanism for all photocatalysts

Table 4.1 Shown comparison study of different types of Ta₃N₅-dependent photocatalyst triggered by visible light for H_2 evolution reaction

Photocatalyst	Source of Light	Reaction medium	Sacrificial agents/cocatalysts	H_2 production Yield ($\mu mol g^{-1} h^{-1}$)	Ref.
Pt/MgO–Ta₃N₅	300 W xenon lamp	Methanol/ H₂O	Pt as a cocatalysts	22.4	[555]
2-D mesoporous Ta₃N₅	500 W Xe lamp ($\lambda > 420$ nm)	TEOA/H₂O	2 wt% Pt as a cocatalysts	34.6	[556]
Nb-Ta₃N₅/PPy	Visible light bulbs (400-700 nm)	25 °C	Without any sacrificial agent and cocatalysts H₂O	65.1	[557]
Ta₃N₅	Visible light bulb (400-700 nm)	Water	-	22.5	Present work
Nb-Ta₃N₅/PANI	Visible light bulb (400-700 nm)	Water	-	71.3	Present work

4.6 Conclusions

In this study, Nb-Ta₃N₅@PANI nanocomposite was successfully synthesized via chemisorption. UV-Vis, XRD, and FE-SEM analysis reveal the preservation of Nb, Ta₃N₅, and PANI structures with improved interfacial contact in Nb-Ta₃N₅@PANI nanocomposite. The strong interfacial contact boosted visible light absorption; effective split-up of electron-hole pairs, and hole relocation from the Ta₃N₅ surface to the PANI surface to limit self-photocorrosion, improving photocatalytic activity. Our simple, cost-effective photoreactors boost photocatalytic activity for efficient water-splitting processes for H₂ evolution. The H₂ yield of Nb-Ta₃N₅@PANI composites photocatalyst is 71.3 $\mu mol g^{-1} h^{-1}$, which is 3.17 folds greater than Ta₃N₅ value. Therefore, the photocatalytic improvement of this hybrid

photocatalyst could be a promising candidate for high application potential water splitting toward environmental sustainability.

Chapter 5

Conclusion and future prospects

In conclusion, this work has introduced reasonable, promising and novel holistic design approaches to synthesize highly efficient carbon based metal nitride photocatalyst, as confirmed by a series of analytical characterizations. The new findings in this work can provide methodological contributions, especially in the building of a solid basis for future work in the rational development and design of semiconductor photocatalyst. It is anticipated that the outcomes of this thesis can offer new insights and drive intensified research efforts to meet the commercialization expectations of PC technology and improve the readiness of solar H_2, paving the way for envisioned long-term energy sustainability.

In this study, cost-effective, stable and eco-friendly Ta_3N_5 based metal nitride photocatalysts, such as $Ta_3N_5/BSC@PANI$, $V@S-Ta_3N_5/PANI$ and $Nb-Ta_3N_5/PANI$ were prepared and used for photocatalytic H_2O splitting for H_2 production. These are the key contributions made to this PhD study. Ta_3N_5 was prepared by two different methods, including hydrothermal, sol-gel. The Ta_3N_5 prepared by hydrothermal method has shown higher photocatalytic hydrogen production due to quantum confinement effect.

• The cost-effective, stable and eco-friendly Ta_3N_5/BSC core shell structure with PANI composite photocatalyst was prepared by simple hydrothermal and chemisorption method for photocatalytic hydrogen production. The composite photocatalyst was synthesized by using waste/biomass of peanuts and almonds shells (under the mission of utilizing waste into wealth). The synthesized composite photocatalyst shows superior photocatalytic activity for enhanced hydrogen production ($76.9\ \mu mol g^{-1} h^{-1}$) ~ 3.42 fold to the pure Ta_3N_5. Among all the synthesized photocatalyst $Ta_3N_5/BSC@PANI$ composite photocatalyst exhibit excellent photostability due to the presence of BSC even after the 6 cycles upto a time interval of 18 h. PANI was utilised as a conducting polymer having extended π-π^* transition conjugated

electron system to cover the Ta_3N_5 particles in order to increase the efficiency of charge separation and corrosive holes transfer from Ta_3N_5 to PANI surface its prevents the photocatalyst from self-photocorrosion.

• The Nb-doped Ta_3N_5@PANI hybrid photocatalyst H_2 yield is 71.3 $\mu mol g^{-1} h^{-1}$, which is 3.17 fold greater than pure Ta_3N_5. Consequently, the photocatalytic improvement of this cost-effective, stable and eco-friendly hybrid photocatalyst could be a promising candidate for high application potential water splitting toward environmental sustainability.

• The co-doped V@S-Ta_3N_5/PANI pn-junction photocatalyst was constructed by simple hydrothermal and chemisorption processes. The V@S-Ta_3N_5/PANI photocatalyst was exhibited the highest photocatalytic activity among all the synthesized materials ~ 4.32 fold enhanced hydrogen production (98.4 $\mu mol g^{-1} h^{-1}$) than that of Ta_3N_5. The inbuilt potential developed by the formation of pn-junction facilitates the raid separation and transport of photogenerated charge carriers, resulting in efficient hydrogen production.

The future work will be focused on the overall photocatalytic water splitting and by natural solar light with a high efficiency. Besides, the mechanistic pathway of the sacrificial agent in photocatalytic water splitting will be studied thoroughly by analytical techniques, such as nuclear magnetic resonance (NMR) spectroscopy, gas chromatography, liquid chromatography-mass spectroscopy (GC-MS).

References

1. Allwood, Julian M., Michael F. Ashby, Timothy G. Gutowski, and Ernst Worrell. "Material efficiency: providing material services with less material production." Philosophical transactions of the royal society a: mathematical, physical and engineering sciences 371, no. 1986 (2013): 20120496.

2. What Is Energy? A Deep Dive Into Understanding Energy Just Energy Website: https://justenergy.com/blog/what-is-energy-understanding.

3. Bartoletto, Silvana, and Md Mar Rubio. "Energy transition and CO_2 emissions in Southern Europe: Italy and Spain (1861-2000)." Global Environment 1, no. 2 (2008): 46-81.

4. Moss, R.H., Edmonds, J.A., Hibbard, K.A., Manning, M.R., Rose, S.K., Van Vuuren, D.P., Carter, T.R., Emori, S., Kainuma, M., Kram, T. and Meehl, G.A., 2010. The next generation of scenarios for climate change research and assessment. Nature, 463(7282), pp.747-756.

5. Tripathi, Lata, A. K. Mishra, Anil Kumar Dubey, C. B. Tripathi, and Prashant Baredar. "Renewable energy: An overview on its contribution in current energy scenario of India." Renewable and Sustainable Energy Reviews 60 (2016): 226-233.

6. UNDP, UNDESA. "WEC–"World Energy Assessment–Energy and the Challenge of Sustainability"–UNDP." New York, NY, USA (2000).

7. Dincer, Ibrahim. "Environmental issues: I-energy utilization." Energy Sources 23, no. 1 (2001): 69-81.

8. Dincer, Ibrahim. "Environmental issues: Ii-potential solutions." Energy sources 23, no. 1 (2001): 83-92.

9. Zohuri, Bahman, and Patrick J. McDaniel. Introduction to energy essentials: insight into nuclear, renewable, and non-renewable energies. Academic Press, 2021.

10. Rehm, Thomas E. "Advanced nuclear energy: the safest and most renewable clean energy." Current Opinion in Chemical Engineering 39 (2023): 100878.

11. Jacobson, Mark Z., and Mark A. Delucchi. "Providing all global energy with wind, water, and solar power, Part I: Technologies, energy resources, quantities and areas of infrastructure, and materials." Energy policy 39, no. 3 (2011): 1154-1169.

12. Williams, A. "Role of fossil fuels in electricity generation and their environmental impact." IEE Proceedings A (Science, Measurement and Technology) 140, no. 1 (1993): 8-12.

13. Lizunkov, Vladislav, Ekaterina Politsinskaya, Elena Malushko, Alexandr Kindaev, and Mikhail Minin. "Population of the world and regions as the principal energy consumer." International journal of energy economics and policy 8, no. 3 (2018): 250-257.

14. Béné, Christophe, Manuel Barange, Rohana Subasinghe, Per Pinstrup-Andersen, Gorka Merino, Gro-Ingunn Hemre, and Meryl Williams. "Feeding 9 billion by 2050–Putting fish back on the menu." Food Security 7 (2015): 261-274.

15. Lockwood, Matthew. "Right-wing populism and the climate change agenda: exploring the linkages." Environmental Politics 27, no. 4 (2018): 712-732.

16. Warner, Kevin J., and Glenn A. Jones. "The climate-independent need for renewable energy in the 21st century." Energies 10, no. 8 (2017): 1197.

17. Güney, Taner. "Renewable energy, non-renewable energy and sustainable development." International Journal of Sustainable Development & World Ecology 26, no. 5 (2019): 389-397.

18. Kaygusuz, Kamil. "Energy for sustainable development: A case of developing countries." Renewable and sustainable energy reviews 16, no. 2 (2012): 1116-1126.

19. Arutyunov, Vladimir S., and Georgiy V. Lisichkin. "Energy resources of the 21st century: Problems and forecasts. Can renewable energy sources replace fossil fuels." Russian Chemical Reviews 86, no. 8 (2017): 777.

20. Krapivin, Vladimir F., Costas A. Varotsos, and Vladimir Yu Soldatov. "The Earth's population can reach 14 billion in the 23rd century without significant adverse effects on survivability." International Journal of Environmental Research and Public Health 14, no. 8 (2017): 885.

21. Nejat, Payam, Fatemeh Jomehzadeh, Mohammad Mahdi Taheri, Mohammad Gohari, and Muhd Zaimi Abd Majid. "A global review of energy consumption, CO2 emissions and policy in the residential sector (with an overview of the top ten CO2 emitting countries)." Renewable and sustainable energy reviews 43 (2015): 843-862.

22. Wójcik-Gront, Elżbieta. "Analysis of sources and trends in agricultural GHG emissions from annex I countries." Atmosphere 11, no. 4 (2020): 392.

23. International Energy Agency Technical Report, 2012 Key World Energy Statistics. Website: http://www.iea.org/publications/freepublications/publication/kwes.pdf; 2012 [accessed 10.01.13].

24. Yuksel, Yunus Emre, and Murat Ozturk. "Thermodynamic and thermo economic analyses of a geothermal energy based integrated system for hydrogen production." International Journal of Hydrogen Energy 42, no. 4 (2017): 2530-2546.

25. Shi, Chen, Zhi-Hong Jiang, Wei-Lin Chen, and Laurent Li. "Changes in temperature extremes over China under 1.5 C and 2 C global warming targets." Advances in Climate Change Research 9, no. 2 (2018): 120-129.

26. New, Mark, Diana Liverman, Heike Schroder, and Kevin Anderson. "Four degrees and beyond: the potential for a global temperature increase of four degrees and its

implications." Philosophical Transactions of the Royal Society A: Mathematical, Physical and Engineering Sciences 369, no. 1934 (2011): 6-19.

27. Preethi, V. "Solar hydrogen production in India." Environment, Development and Sustainability 25, no. 3 (2023): 2105-2135.

28. Waheed, Rida, Dongfeng Chang, Suleman Sarwar, and Wei Chen. "Forest, agriculture, renewable energy, and CO_2 emission." Journal of Cleaner Production 172 (2018): 4231-4238.

29. Mohtasham, Javid. "Renewable energies." Energy Procedia 74 (2015): 1289-1297.

30. Omer, Abdeen Mustafa. "Energy, environment and sustainable development." Renewable and sustainable energy reviews 12, no. 9 (2008): 2265-2300.

31. Meinshausen, Malte, Jared Lewis, Christophe McGlade, Johannes Gütschow, Zebedee Nicholls, Rebecca Burdon, Laura Cozzi, and Bernd Hackmann. "Realization of Paris Agreement pledges may limit warming just below 2 C." Nature 604, no. 7905 (2022): 304-309.

32. Brockway, Paul E., Anne Owen, Lina I. Brand-Correa, and Lukas Hardt. "Estimation of global final-stage energy-return-on-investment for fossil fuels with comparison to renewable energy sources." Nature Energy 4, no. 7 (2019): 612-621.

33. Abbasi, Tasneem, M. Premalatha, and S. A. Abbasi. "The return to renewables: Will it help in global warming control?." Renewable and Sustainable Energy Reviews 15, no. 1 (2011): 891-894.

34. Sharma, Atul, Jaya Srivastava, Sanjay Kumar Kar, and Anil Kumar. "Wind energy status in India: A short review." Renewable and sustainable energy reviews 16, no. 2 (2012): 1157-1164.

35. Stober, Ingrid, and Kurt Bucher. "Geothermal energy." Germany: Springer-Verlag Berlin Heidelberg. doi 10 (2013): 978-3.

36. Kumar, Sunil, Sanjeev Kumar Gupta, and Manish Rawat. "Resources and utilization of geothermal energy in India: An eco–friendly approach towards sustainability." Materials Today: Proceedings 26 (2020): 1660-1665.

37. Lund, John W., and Aniko N. Toth. "Direct utilization of geothermal energy 2020 worldwide review." Geothermics 90 (2021): 101915.

38. Abbasi, Tasneem, and S. A. Abbasi. "Biomass energy and the environmental impacts associated with its production and utilization." Renewable and sustainable energy reviews 14, no. 3 (2010): 919-937.

39. Sansaniwal, S. K., M. A. Rosen, and S. K. Tyagi. "Global challenges in the sustainable development of biomass gasification: An overview." Renewable and Sustainable Energy Reviews 80 (2017): 23-43.

40. Kannan, Nadarajah, and Divagar Vakeesan. "Solar energy for future world:-A review." Renewable and sustainable energy reviews 62 (2016): 1092-1105.

41. Shaqsi, Ahmed Zayed AL, Kamaruzzaman Sopian, and Amer Al-Hinai. "Review of energy storage services, applications, limitations, and benefits." Energy Reports 6 (2020): 288-306.

42. Shahzad, Umair. "The need for renewable energy sources." energy 2 (2012): 16-18.

43. Solaun, Kepa, and Emilio Cerdá. "Climate change impacts on renewable energy generation. A review of quantitative projections." Renewable and sustainable energy Reviews 116 (2019): 109415.

44. Singh, Vishal, Ina Rayal, Himani Sharma, Charu Dwivedi, and Bharti Singh. "Solar radiation and light materials interaction." In Energy Saving Coating Materials, Elsevier, (2020): 1-32.

45. Hassanalieragh, Moeen, Tolga Soyata, Andrew Nadeau, and Gaurav Sharma. "UR-SolarCap: An open source intelligent auto-wakeup solar energy harvesting system for supercapacitor-based energy buffering." IEEE Access 4 (2016): 542-557.

46. Grimm, Alexa, Wouter A. de Jong, and Gert Jan Kramer. "Renewable hydrogen production: A techno-economic comparison of photoelectrochemical cells and photovoltaic-electrolysis." International Journal of Hydrogen Energy 45, no. 43 (2020): 22545-22555.

47. Rothwarf, A., and K. W. Böer. "Direct conversion of solar energy through photovoltaic cells." Progress in Solid State Chemistry 10 (1975): 71-102.

48. Lewis, Nathan S. "Research opportunities to advance solar energy utilization." Science 351, no. 6271 (2016): 1920.

49. Sayed, Enas Taha, Tabbi Wilberforce, Khaled Elsaid, Malek Kamal Hussien Rabaia, Mohammad Ali Abdelkareem, Kyu-Jung Chae, and A. G. Olabi. "A critical review on environmental impacts of renewable energy systems and mitigation strategies: Wind, hydro, biomass and geothermal." Science of the total environment 766 (2021): 144505.

50. Azarpour, Abbas, Suardi Suhaimi, Gholamreza Zahedi, and Alireza Bahadori. "A review on the drawbacks of renewable energy as a promising energy source of the future." Arabian Journal for Science and Engineering 38 (2013): 317-328.

51. Halkos, George E., and Eleni-Christina Gkampoura. "Reviewing usage, potentials, and limitations of renewable energy sources." Energies 13, no. 11 (2020): 2906.

52. Kirmani, Fahim, Anubhav Pal, Anurag Mudgal, Anvesh Shrestha, and Arafat Siddiqui. "Advantages and disadvantages of hydroelectric power plant." International Journal of Innovative Science and Research Technology (2021).

53. Wang, Shifeng, and Sicong Wang. "Impacts of wind energy on environment: A review." Renewable and Sustainable Energy Reviews 49 (2015): 437-443.

54. Kanoglu, Mehmet, Abdulkadir Ayanoglu, and Aysegul Abusoglu. "Exergoeconomic assessment of a geothermal assisted high temperature steam electrolysis system." Energy 36, no. 7 (2011): 4422-4433.

55. Sivabalan, K., Suhaimi Hassan, Hamdan Ya, and Jagadeesh Pasupuleti. "A review on the characteristic of biomass and classification of bioenergy through direct combustion and gasification as an alternative power supply." In Journal of Physics: Conference Series, vol. 1831, no. 1 (2021): 012033.

56. Khan, Jibran, and Mudassar H. Arsalan. "Solar power technologies for sustainable electricity generation–A review." Renewable and Sustainable Energy Reviews 55 (2016): 414-425.

57. Hosseini, Seyed Ehsan, and Mazlan Abdul Wahid. "Hydrogen production from renewable and sustainable energy resources: Promising green energy carrier for clean development." Renewable and Sustainable Energy Reviews 57 (2016): 850-866.

58. Christopher, Koroneos, and Rovas Dimitrios. "A review on exergy comparison of hydrogen production methods from renewable energy sources." Energy & Environmental Science 5, no. 5 (2012): 6640-6651.

59. Abdin, Zainul, Ali Zafaranloo, Ahmad Rafiee, Walter Mérida, Wojciech Lipiński, and Kaveh R. Khalilpour. "Hydrogen as an energy vector." Renewable and sustainable energy reviews 120 (2020): 109620.

60. Valenzuela, Miguel A., and Beatriz Zapata. "11 Hydrogen Production." Hydroprocessing of Heavy Oils and Residua (2007): 313.

61. Dincer, Ibrahim. "Green methods for hydrogen production." International journal of hydrogen energy 37, no. 2 (2012): 1954-1971.

62. Wang, Yishuang, Chunsheng Wang, Mingqiang Chen, Zhiyuan Tang, Zhonglian Yang, Jiaxin Hu, and Han Zhang. "Hydrogen production from steam reforming ethanol over Ni/attapulgite catalysts-Part I: Effect of nickel content." Fuel Processing Technology 192 (2019): 227-238.

63. Castonguay, S. "Green Technologies: Electric Cars with Hydrogen Fuel Cells." WIPO Magazine (2009).

64. Baykara, Sema Z. "Hydrogen: A brief overview on its sources, production and environmental impact." International Journal of Hydrogen Energy 43, no. 23 (2018): 10605-10614.

65. Cassir, Michel, Armelle Ringuedé, and Virginie Lair. "Molten carbonates from fuel cells to new energy devices." In Molten Salts Chemistry, pp. 355-371. Elsevier, 2013.

66. Verhaert, Ivan, Grietus Mulder, and Michel De Paepe. "Evaluation of an alkaline fuel cell system as a micro-CHP." Energy conversion and management 126 (2016): 434-445.

67. Wilberforce, Tabbi, A. G. Olabi, Imran Muhammad, Abed Alaswad, Enas Taha Sayed, Ahmed G. Abo-Khalil, Hussein M. Maghrabie, Khaled Elsaid, and Mohammad Ali Abdelkareem. "Recovery of waste heat from proton exchange membrane fuel cells–A review." International Journal of Hydrogen Energy (2022).

68. Solomon, Leera, and Moses Tonubari Bakpo. "Hydrogen and microbial fuel cells as alternate sources of clean energy." Journal of American Science 14, no. 11 (2018): 20-27.

69. Tashie-Lewis, Bernard Chukwudi, and Somtochukwu Godfrey Nnabuife. "Hydrogen production, distribution, storage and power conversion in a hydrogen economy-a technology review." Chemical Engineering Journal Advances 8 (2021): 100172.

70. Dunn, Seth. "Hydrogen futures: toward a sustainable energy system." International journal of hydrogen energy 27, no. 3 (2002): 235-264.

71. Momirlan, Magdalena, and T. N. Veziroglu. "Current status of hydrogen energy." Renewable and sustainable energy reviews 6, no. 1-2 (2002): 141-179.

72. Veziroğlu, T. Nejat, and Sümer Şahi. "21st Century's energy: Hydrogen energy system." Energy conversion and management 49, no. 7 (2008): 1820-1831.

73. Dufour, Javier, David P. Serrano, José L. Gálvez, Antonio González, Enrique Soria, and José LG Fierro. "Life cycle assessment of alternatives for hydrogen production from renewable and fossil sources." International Journal of Hydrogen Energy 37, no. 2 (2012): 1173-1183.

74. Hermesmann, M., and T. E. Müller. "Green, turquoise, blue, or grey? Environmentally friendly hydrogen production in transforming energy systems." Progress in Energy and Combustion Science 90 (2022): 100996.

75. Ursua, Alfredo, Luis M. Gandia, and Pablo Sanchis. "Hydrogen production from water electrolysis: current status and future trends." Proceedings of the IEEE 100, no. 2 (2011): 410-426.

76. Rao, C. N. R., and Sunita Dey. "Solar thermochemical splitting of water to generate hydrogen." Proceedings of the national academy of sciences 114, no. 51 (2017): 13385-13393.

77. Das, Soumya. "Critical review of water radiolysis processes, dissociation products, and possible impacts on the local environment: a geochemist's perspective." Australian Journal of Chemistry 66, no. 5 (2013): 522-529.

78. Acar, Canan, and Ibrahim Dincer. "Comparative assessment of hydrogen production methods from renewable and non-renewable sources." International journal of hydrogen energy 39, no. 1 (2014): 1-12.

79. Van Mierlo, Joeri, and Gaston Maggetto. "Hydrogen as an energy carrier." In KVAB (Koninklijke Vlaamse Academie van België voor Wetenschappen en Kunsten)–BACAS (Royal Belgian Academy Council of Applied Sciences)–CAWET (Comité van de Academie voor Wetenschappen en Techniek), 42pgs. KVAB (Koninklijke Vlaamse Academie van België voor Wetenschappen en Kunsten) BACAS (Royal Belgian Academy Council of Applied Sciences) CAWET (Comité van de Academie voor Wetenschappen en Techniek), 42pgs, 2006.

80. Fujishima, Akira, and Kenichi Honda. "Electrochemical photolysis of water at a semiconductor electrode." nature 238, no. 5358 (1972): 37-38.

81. Voldsund, Mari, Kristin Jordal, and Rahul Anantharaman. "Hydrogen production with CO_2 capture." International Journal of hydrogen energy 41, no. 9 (2016): 4969-4992.

82. Andrews, John W. "Hydrogen production and carbon sequestration by steam methane reforming and fracking with carbon dioxide." International Journal of Hydrogen Energy 45, no. 16 (2020): 9279-9284.

83. Midilli, Adnan, Haydar Kucuk, Muhammed Emin Topal, Ugur Akbulut, and Ibrahim Dincer. "A comprehensive review on hydrogen production from coal gasification: Challenges and Opportunities." International Journal of Hydrogen Energy 46, no. 50 (2021): 25385-25412.

84. Seyitoglu, S. S., I. Dincer, and A. J. I. J. O. H. E. Kilicarslan. "Energy and exergy analyses of hydrogen production by coal gasification." International Journal of Hydrogen Energy 42, no. 4 (2017): 2592-2600.

85. Pinsky, Roxanne, Piyush Sabharwall, Jeremy Hartvigsen, and James O'Brien. "Comparative review of hydrogen production technologies for nuclear hybrid energy systems." Progress in Nuclear Energy 123 (2020): 103317.

86. Safari, Farid, and Ibrahim Dincer. "A review and comparative evaluation of thermochemical water splitting cycles for hydrogen production." Energy Conversion and Management 205 (2020): 112182.

87. El-Emam, Rami S., Hasan Ozcan, and Calin Zamfirescu. "Updates on promising thermochemical cycles for clean hydrogen production using nuclear energy." Journal of Cleaner Production 262 (2020): 121424.

88. Orhan, Mehmet F., Ibrahim Dincer, and Marc A. Rosen. "Energy and exergy assessments of the hydrogen production step of a copper–chlorine thermochemical water splitting cycle driven by nuclear-based heat." International Journal of Hydrogen Energy 33, no. 22 (2008): 6456-6466.

89. Kowalczyk, Tomasz, Janusz Badur, and Mateusz Bryk. "Energy and exergy analysis of hydrogen production combined with electric energy generation in a nuclear cogeneration cycle." Energy Conversion and Management 198 (2019): 111805.

90. Ji, Guozhao, Joseph G. Yao, Peter T. Clough, João C. Diniz Da Costa, Edward J. Anthony, Paul S. Fennell, Wei Wang, and Ming Zhao. "Enhanced hydrogen production from thermochemical processes." Energy & Environmental Science 11, no. 10 (2018): 2647-2672.

91. Muritala, Ibrahim Kolawole, Dorottya Guban, Martin Roeb, and Christian Sattler. "High temperature production of hydrogen: Assessment of non-renewable resources technologies and emerging trends." international journal of hydrogen energy 45, no. 49 (2020): 26022-26035.

92. Forsberg, C. "Meeting Low-Carbon Industrial Heat Demand with High-Temperature Reactors Using Co-Generation and Heat Storage, Vol. 120." Transactions of the American Nuclear Society (2019).

93. Manna, Joydev, Prakash Jha, Rudranath Sarkhel, Chandan Banerjee, A. K. Tripathi, and M. R. Nouni. "Opportunities for green hydrogen production in petroleum refining and ammonia synthesis industries in India." international journal of hydrogen energy 46, no. 77 (2021): 38212-38231.

94. Sharma, Vijay Paul, and Hrima Thaker. "Economic policy reforms and Indian fertilizer industry." (No Title) (2011).

95. Bhandari, Ramchandra, Clemens A. Trudewind, and Petra Zapp. "Life cycle assessment of hydrogen production via electrolysis–a review." Journal of cleaner production 85 (2014): 151-163.

96. Reuß, Markus, Julian Reul, Thomas Grube, Manuel Langemann, Sonya Calnan, Martin Robinius, Rutger Schlatmann, Uwe Rau, and Detlef Stolten. "Solar hydrogen production: a bottom-up analysis of different photovoltaic–electrolysis pathways." Sustainable energy & fuels 3, no. 3 (2019): 801-813.

97. Li, Zheng, Peng Guo, Ruihua Han, and Hexu Sun. "Current status and development trend of wind power generation-based hydrogen production technology." Energy Exploration & Exploitation 37, no. 1 (2019): 5-25.

98. Correa, Catalina Rodriguez, and Andrea Kruse. "Supercritical water gasification of biomass for hydrogen production–Review." The Journal of Supercritical Fluids 133 (2018): 573-590.

99. Koponen, Joonas. "Review of water electrolysis technologies and design of renewable hydrogen production systems." (2015).

100. Zoulias, Emmanuel, Elli Varkaraki, Nicolaos Lymberopoulos, Christodoulos N. Christodoulou, and George N. Karagiorgis. "A review on water electrolysis." Tcjst 4, no. 2 (2004): 41-71.

101.   Kumar, S. Shiva, and Hankwon Lim. "An overview of water electrolysis technologies for green hydrogen production." Energy Reports 8 (2022): 13793-13813.

102.   Veeramani, Krishnan, Gnanaprakasam Janani, Joonyoung Kim, Subramani Surendran, Jaehyoung Lim, Sebastian Cyril Jesudass, Shivraj Mahadik, Tae-Hoon Kim, Jung Kyu Kim, and Uk Sim. "Hydrogen and value-added products yield from hybrid water electrolysis: A critical review on recent developments." Renewable and Sustainable Energy Reviews 177 (2023): 113227.

103.   Xu, You, and Bin Zhang. "Recent advances in electrochemical hydrogen production from water assisted by alternative oxidation reactions." ChemElectroChem 6, no. 13 (2019): 3214-3226.

104.   Gupta, Aayush, Blaž Likozar, Runia Jana, Wairakpam Chinglembi Chanu, and Mahesh Kumar Singh. "A review of hydrogen production processes by photocatalytic water splitting–From atomistic catalysis design to optimal reactor engineering." International Journal of Hydrogen Energy 47, no. 78 (2022): 33282-33307.

105.   Gong, Yixuan, Jiasai Yao, Ping Wang, Zhenxing Li, Hongjun Zhou, and Chunming Xu. "Perspective of hydrogen energy and recent progress in electrocatalytic water splitting." Chinese Journal of Chemical Engineering (2022).

106.   Koponen, Joonas. "Review of water electrolysis technologies and design of renewable hydrogen production systems." (2015).

107.   Alciaturi, C. E., J. Márquez, O. P. De Márquez, and C. M. Marschoff. "Partial oxidation of butadiene on platinized Pt and Au anodes in acid aqueous solutions." Electrochimica Acta 25, no. 3 (1980): 357-363.

108.   Bockris, JO'M., H. Wroblowa, E. Gileadi, and B. J. Piersma. "Anodic oxidation of unsaturated hydrocarbons on platinized electrodes." Transactions of the Faraday Society 61 (1965): 2531-2545.

109.   De Chialvo, MR Gennero, and A. C. Chialvo. "Hydrogen evolution reaction: Analysis of the Volmer-Heyrovsky-Tafel mechanism with a generalized adsorption model." Journal of Electroanalytical Chemistry 372, no. 1-2 (1994): 209-223.

110.   Azizi, O., M. Jafarian, F. Gobal, H. Heli, and M. G. Mahjani. "The investigation of the kinetics and mechanism of hydrogen evolution reaction on tin." International Journal of Hydrogen Energy 32, no. 12 (2007): 1755-1761.

111.   Fernandez-Ibanez, Pilar, Stuart McMichael, Adriana Rioja Cabanillas, Salem Alkharabsheh, Alvaro Tolosana Moranchel, and John A. Byrne. "New trends on photoelectrocatalysis (PEC): nanomaterials, wastewater treatment and hydrogen generation." Current Opinion in Chemical Engineering 34 (2021): 100725.

112.   Sun, Yu, Ran Li, Xiaoxuan Chen, Jing Wu, Yong Xie, Xin Wang, Kaikai Ma et al. "A-site management prompts the dynamic reconstructed active phase of perovskite oxide OER catalysts." Advanced Energy Materials 11, no. 12 (2021): 2003755.

113.   Villa, Katherine, José Ramón Galán-Mascarós, Núria López, and Emilio Palomares. "Photocatalytic water splitting: advantages and challenges." Sustainable Energy & Fuels 5, no. 18 (2021): 4560-4569.

114.   Wang, Qian, and Kazunari Domen. "Particulate photocatalysts for light-driven water splitting: mechanisms, challenges, and design strategies." Chemical Reviews 120, no. 2 (2019): 919-985.

115.   Cao, Shuang, Lingyu Piao, and Xiaobo Chen. "Emerging photocatalysts for hydrogen evolution." Trends in Chemistry 2, no. 1 (2020): 57-70.

116.   Rafique, Muhammad, Rikza Mubashar, Muneeb Irshad, S. S. A. Gillani, M. Bilal Tahir, N. R. Khalid, Aqsa Yasmin, and M. Aamir Shehzad. "A comprehensive study on methods and materials for photocatalytic water splitting and hydrogen

production as a renewable energy resource." Journal of Inorganic and Organometallic Polymers and Materials 30 (2020): 3837-3861.

117.   Zhu, Jiefang, and Michael Zäch. "Nanostructured materials for photocatalytic hydrogen production." Current Opinion in Colloid & Interface Science 14, no. 4 (2009): 260-269.

118.   Gupta, Aayush, Blaž Likozar, Runia Jana, Wairakpam Chinglembi Chanu, and Mahesh Kumar Singh. "A review of hydrogen production processes by photocatalytic water splitting–From atomistic catalysis design to optimal reactor engineering." International Journal of Hydrogen Energy 47, no. 78 (2022): 33282-33307.

119.   Lewis, Nathan S., and Daniel G. Nocera. "Powering the planet: Chemical challenges in solar energy utilization." Proceedings of the National Academy of Sciences 103, no. 43 (2006): 15729-15735.

120.   Ng, Boon-Junn, Lutfi Kurnianditia Putri, Xin Ying Kong, Yee Wen Teh, Pooria Pasbakhsh, and Siang-Piao Chai. "Z-scheme photocatalytic systems for solar water splitting." Advanced Science 7, no. 7 (2020): 1903171.

121.   Sakthivel, Shankar, M. V. Shankar, M. Palanichamy, Banumathi Arabindoo, D. W. Bahnemann, and V. Murugesan. "Enhancement of photocatalytic activity by metal deposition: characterisation and photonic efficiency of Pt, Au and Pd deposited on TiO_2 catalyst." Water research 38, no. 13 (2004): 3001-3008.

122.   Acar, Canan, Ibrahim Dincer, and Greg F. Naterer. "Review of photocatalytic water-splitting methods for sustainable hydrogen production." International Journal of Energy Research 40, no. 11 (2016): 1449-1473.

123.   Ismail, Adel A., and Detlef W. Bahnemann. "Photochemical splitting of water for hydrogen production by photocatalysis: A review." Solar energy materials and solar cells 128 (2014): 85-101.

124.   Li, Jiangtian, and Nianqiang Wu. "Semiconductor-based photocatalysts and photoelectrochemical cells for solar fuel generation: a review." Catalysis Science & Technology 5, no. 3 (2015): 1360-1384.

125.   Ngoh, Simon Koumi, and Donatien Njomo. "An overview of hydrogen gas production from solar energy." Renewable and Sustainable Energy Reviews 16, no. 9 (2012): 6782-6792.

126.   Luo, Jinming, Shuqu Zhang, Meng Sun, Lixia Yang, Shenglian Luo, and John C. Crittenden. "A critical review on energy conversion and environmental remediation of photocatalysts with remodeling crystal lattice, surface, and interface." ACS nano 13, no. 9 (2019): 9811-9840.

127.   Zhu, Shasha, and Dunwei Wang. "Photocatalysis: basic principles, diverse forms of implementations and emerging scientific opportunities." Advanced Energy Materials 7, no. 23 (2017): 1700841.

128.   Cao, Shuang, Lingyu Piao, and Xiaobo Chen. "Emerging photocatalysts for hydrogen evolution." Trends in Chemistry 2, no. 1 (2020): 57-70.

129.   Yang, H., W-Y. Lin, and K. Rajeshwar. "Homogeneous and heterogeneous photocatalytic reactions involving As (III) and As (V) species in aqueous media." Journal of Photochemistry and Photobiology A: Chemistry 123, no. 1-3 (1999): 137-143.

130.   Ibhadon, Alex Omo, and Paul Fitzpatrick. "Heterogeneous photocatalysis: recent advances and applications." Catalysts 3, no. 1 (2013): 189-218.

131.   Coronado, Juan M., Fernando Fresno, María D. Hernández-Alonso, and Raquel Portela, eds. Design of advanced photocatalytic materials for energy and environmental applications. Vol. 71. London: Springer, (2013).

132. Meng, Sugang, Cheng Chen, Xiaomeng Gu, Huihui Wu, Qiangqiang Meng, Jinfeng Zhang, Shifu Chen, Xianliang Fu, Dan Liu, and Weiwei Lei. "Efficient photocatalytic H_2 evolution, CO_2 reduction and N_2 fixation coupled with organic synthesis by cocatalyst and vacancies engineering." Applied Catalysis B: Environmental 285 (2021): 119789.

133. Guo, Jianping, and Ping Chen. "Catalyst: NH_3 as an energy carrier." Chem 3, no. 5 (2017): 709-712.

134. Roux, Yoann, Carole Duboc, and Marcello Gennari. "Molecular catalysts for N_2 reduction: state of the art, mechanism, and challenges." ChemPhysChem 18, no. 19 (2017): 2606-2617.

135. Li, Mengqiao, Hao Huang, Jingxiang Low, Chao Gao, Ran Long, and Yujie Xiong. "Recent progress on electrocatalyst and photocatalyst design for nitrogen reduction." Small Methods 3, no. 6 (2019): 1800388.

136. Hu, Shaozheng, Weidong Zhang, Jin Bai, Guang Lu, Lei Zhang, and Guang Wu. "Construction of a 2D/2D gC 3 N 4/rGO hybrid heterojunction catalyst with outstanding charge separation ability and nitrogen photofixation performance via a surface protonation process." RSC advances 6, no. 31 (2016): 25695-25702.

137. Chen, Dongjie, Yanling Cheng, Nan Zhou, Paul Chen, Yunpu Wang, Kun Li, Shuhao Huo et al. "Photocatalytic degradation of organic pollutants using TiO_2-based photocatalysts: A review." Journal of Cleaner Production 268 (2020): 121725.

138. Hu, Jundie, Dongyun Chen, Zhao Mo, Najun Li, Qingfeng Xu, Hua Li, Jinghui He, Hui Xu, and Jianmei Lu. "Z-Scheme 2D/2D heterojunction of black phosphorus/monolayer Bi_2WO_6 nanosheets with enhanced photocatalytic activities." Angewandte Chemie International Edition 58, no. 7 (2019): 2073-2077.

139.   Saqib, Najm Us, Irfan Shah, and Rohana Adnan. "An emerging photocatalyst for wastewater remediation: a mini-review on $CaCu_3Ti_4O_{12}$ photocatalysis." Environmental Science and Pollution Research 29, no. 27 (2022): 40403-40414.

140.   Ming, Tingzhen, Wei Liu, and Sylvain Caillol. "Fighting global warming by climate engineering: Is the Earth radiation management and the solar radiation management any option for fighting climate change?." Renewable and Sustainable Energy Reviews 31 (2014): 792-834.

141.   Chakrabortty, Sankha, Jayato Nayak, Biswajit Ruj, Parimal Pal, Ramesh Kumar, Shirsendu Banerjee, Moumita Sardar, and Prasenjit Chakraborty. "Photocatalytic conversion of CO_2 to methanol using membrane-integrated green approach: a review on capture, conversion and purification." Journal of Environmental Chemical Engineering 8, no. 4 (2020): 103935.

142.   Freund, H-J., and Meirion Wynn Roberts. "Surface chemistry of carbon dioxide." Surface Science Reports 25, no. 8 (1996): 225-273.

143.   Wu, Jinghua, Yang Huang, Wen Ye, and Yanguang Li. "CO_2 reduction: from the electrochemical to photochemical approach." Advanced Science 4, no. 11 (2017): 1700194.

144.   Mustafa, Azeem, Bachirou Guene Lougou, Yong Shuai, Zhijiang Wang, and Heping Tan. "Current technology development for CO_2 utilization into solar fuels and chemicals: A review." Journal of Energy Chemistry 49 (2020): 96-123.

145.   Rehman, Adeela, Ghazanfar Nazir, Kyong Yop Rhee, and Soo-Jin Park. "Electrocatalytic and photocatalytic sustainable conversion of carbon dioxide to value-added chemicals: State-of-the-art progress, challenges, and future directions." Journal of Environmental Chemical Engineering (2022): 108219.

146. Alli, Yakubu Adekunle, Peter Olusakin Oladoye, Onome Ejeromedoghene, Owolabi Mutolib Bankole, Oyekunle Azeez Alimi, Elizabeth Oyinkansola Omotola, Clement Ajibade Olanrewaju, Karine Philippot, Adeyemi S. Adeleye, and Adeniyi Sunday Ogunlaja. "Nanomaterials as catalysts for CO_2 transformation into value-added products: A review." Science of the Total Environment 868 (2023): 161547.

147. Kovacic, Zan, Blaz Likozar, and Matej Hus. "Photocatalytic CO2 reduction: A review of ab initio mechanism, kinetics, and multiscale modeling simulations." ACS catalysis 10, no. 24 (2020): 14984-15007.

148. Rehman, Adeela, Ghazanfar Nazir, Kyong Yop Rhee, and Soo-Jin Park. "Electrocatalytic and photocatalytic sustainable conversion of carbon dioxide to value-added chemicals: State-of-the-art progress, challenges, and future directions." Journal of Environmental Chemical Engineering (2022): 108219.

149. Sahoo, Prakash Chandra, Satyabadi Martha, and Kulamani Parida. "Solar fuels from CO2 photoreduction over nano-structured catalysts." In Materials Science Forum, vol. 855, pp. 1-19. Trans Tech Publications Ltd, 2016.

150. Houghton, R. A. "Carbon emissions and the drivers of deforestation and forest degradation in the tropics." Current Opinion in Environmental Sustainability 4, no. 6 (2012): 597-603.

151. Yan, Xuecheng, Han Guo, Dongjiang Yang, Shilun Qiu, and Xiangdong Yao. "Catalytic hydrogenation of carbon dioxide to fuels." Current Organic Chemistry 18, no. 10 (2014): 1335-1345.

152. Humayun, Muhammad, Lei Xu, Ling Zhou, Zhiping Zheng, Qiuyun Fu, and Wei Luo. "Exceptional co-catalyst free photocatalytic activities of B and Fe co-doped $SrTiO_3$ for CO_2 conversion and H_2 evolution." Nano Research 11 (2018): 6391-6404.

153. Gupta, Aayush, Blaž Likozar, Runia Jana, Wairakpam Chinglembi Chanu, and Mahesh Kumar Singh. "A review of hydrogen production processes by photocatalytic water splitting–From atomistic catalysis design to optimal reactor engineering." International Journal of Hydrogen Energy (2022).

154. Viswanathan, B. "Photocatalytic processes–selection criteria for the choice of materials." Bulletin of the Catalysis Society of India 2 (2003): 71.

155. Wang, Xiaonong, Mahmoud Sayed, Olim Ruzimuradov, Jingyan Zhang, Yisong Fan, Xiaoxia Li, Xiujun Bai, and Jingxiang Low. "A review of step-scheme photocatalysts." Applied Materials Today 29 (2022): 101609.

156. Acar, Canan, Ibrahim Dincer, and Calin Zamfirescu. "A review on selected heterogeneous photocatalysts for hydrogen production." International Journal of Energy Research 38, no. 15 (2014): 1903-1920.

157. Spasiano, Danilo, Raffaele Marotta, Sixto Malato, Pilar Fernandez-Ibanez, and Ilaria Di Somma. "Solar photocatalysis: Materials, reactors, some commercial, and pre-industrialized applications. A comprehensive approach." Applied Catalysis B: Environmental 170 (2015): 90-123.

158. Zhang, Hefeng, Jiaqi Liu, Ting Xu, Wenqian Ji, and Xu Zong. "Recent Advances on Small Band Gap Semiconductor Materials (≤ 2.1 eV) for Solar Water Splitting." Catalysts 13, no. 4 (2023): 728.

159. Navarro, Rufino M., M. Consuelo Alvarez-Galvan, Jose A. Villoria de la Mano, Saeed M. Al-Zahrani, and Jose Luis G. Fierro. "A framework for visible-light water splitting." Energy & Environmental Science 3, no. 12 (2010): 1865-1882.

160. Sakar, M., Chinh-Chien Nguyen, Manh-Hiep Vu, and Trong-On Do. "Materials and mechanisms of photo-assisted chemical reactions under light and dark

conditions: can day–night photocatalysis be achieved?." ChemSusChem 11, no. 5 (2018): 809-820.

161.   Xu, You, Yi Huang, and Bin Zhang. "Rational design of semiconductor-based photocatalysts for advanced photocatalytic hydrogen production: the case of cadmium chalcogenides." Inorganic Chemistry Frontiers 3, no. 5 (2016): 591-615.

162.   Kalanur, Shankara S., Il-Han Yoo, In-Sun Cho, and Hyungtak Seo. "Effect of oxygen vacancies on the band edge properties of WO3 producing enhanced photocurrents." Electrochimica Acta 296 (2019): 517-527.

163.   Kato, Hideki, Kiyotaka Asakura, and Akihiko Kudo. "Highly efficient water splitting into H_2 and O_2 over lanthanum-doped $NaTaO_3$ photocatalysts with high crystallinity and surface nanostructure." Journal of the American Chemical Society 125, no. 10 (2003): 3082-3089.

164.   Inoue, Yasunobu. "Photocatalytic water splitting by RuO 2-loaded metal oxides and nitrides with d^0-and d^{10}-related electronic configurations." Energy & Environmental Science 2, no. 4 (2009): 364-386.

165.   Kudo, Akihiko, Hideki Kato, and Seira Nakagawa. "Water splitting into H2 and O2 on new Sr2M2O7 (M= Nb and Ta) photocatalysts with layered perovskite structures: factors affecting the photocatalytic activity." The Journal of Physical Chemistry B 104, no. 3 (2000): 571-575.

166.   Kato, Hideki, and Akihiko Kudo. "Water splitting into H2 and O2 on alkali tantalate photocatalysts ATaO3 (A= Li, Na, and K)." The Journal of Physical Chemistry B 105, no. 19 (2001): 4285-4292.

167.   Huang, Langhuan, C. H. A. N. Qizhong, Bin Zhang, W. U. Xiaojing, G. A. O. Peng, J. I. A. O. Zibin, and L. I. U. Yingliang. "Preparation of sodium tantalate with

different tructures and its photocatalytic activity for H2 evolution from water splitting." Chinese Journal of Catalysis 32, no. 11-12 (2011): 1822-1830.

168. Opoku, Francis, Krishna Kuben Govender, Cornelia Gertina Catharina Elizabeth van Sittert, and Penny Poomani Govender. "Recent progress in the development of semiconductor-based photocatalyst materials for applications in photocatalytic water splitting and degradation of pollutants." Advanced Sustainable Systems 1, no. 7 (2017): 1700006.

169. Martha, Satyabadi, Prakash Chandra Sahoo, and K. M. Parida. "An overview on visible light responsive metal oxide based photocatalysts for hydrogen energy production." Rsc Advances 5, no. 76 (2015): 61535-61553.

170. Maeda, Kazuhiko, Tsuyoshi Takata, and Kazunari Domen. "(Oxy) nitrides and oxysulfides as visible-light-driven photocatalysts for overall water splitting." Energy Efficiency and Renewable Energy Through Nanotechnology (2011): 487-529.

171. Hojamberdiev, Mirabbos, Hajime Wagata, Kunio Yubuta, Kenta Kawashima, Junie Jhon M. Vequizo, Akira Yamakata, Shuji Oishi, Kazunari Domen, and Katsuya Teshima. "KCl flux-induced growth of isometric crystals of cadmium-containing early transition-metal (Ti4+, Nb5+, and Ta5+) oxides and nitridability to form their (oxy) nitride derivatives under an NH3 atmosphere for water splitting application." Applied Catalysis B: Environmental 182 (2016): 626-635.

172. Moniz, Savio JA. "Recent Developments in Heterostructure-Based Catalysts for Water Splitting." Visible Light-Active Photocatalysis: Nanostructured Catalyst Design, Mechanisms, and Applications (2018): 191-226.

173. Di, Tingmin, Quanlong Xu, WingKei Ho, Hua Tang, Quanjun Xiang, and Jiaguo Yu. "Review on metal sulphide-based Z-scheme photocatalysts." ChemCatChem 11, no. 5 (2019): 1394-1411.

174.   Mishra, Amit, Akansha Mehta, Soumen Basu, Nagaraj P. Shetti, Kakarla Raghava Reddy, and Tejraj M. Aminabhavi. "Graphitic carbon nitride (g–C₃N₄)–based metal-free photocatalysts for water splitting: a review." Carbon 149 (2019): 693-721.

175.   Singh, Pooja Dharni Dhar, Z. V. P. Murthy, and Suresh Kumar Kailasa. "Metal nitrides nanostructures: Properties, synthesis and conceptualization in analytical methods developments for chemical analysis and separation, and in energy storage applications." Coordination Chemistry Reviews 481 (2023): 215046.

176.   Han, Ning, Pengyun Liu, Jing Jiang, Lunhong Ai, Zongping Shao, and Shaomin Liu. "Recent advances in nanostructured metal nitrides for water splitting." Journal of Materials Chemistry A 6, no. 41 (2018): 19912-19933.

177.   Tareen, Ayesha Khan, G. Sudha Priyanga, Santosh Behara, Tiju Thomas, and Minghui Yang. "Mixed ternary transition metal nitrides: a comprehensive review of synthesis, electronic structure, and properties of engineering relevance." Progress in Solid State Chemistry 53 (2019): 1-26.

178.   Joshi, Siddharth, Qi Wang, Ajinkya Puntambekar, and Vidhya Chakrapani. "Facile synthesis of large area two-dimensional layers of transition-metal nitride and their use as insertion electrodes." ACS Energy Letters 2, no. 6 (2017): 1257-1262.

179.   Cheng, Zhixing, Weiliang Qi, Cheng Heng Pang, Tiju Thomas, Tao Wu, Siqi Liu, and Minghui Yang. "Recent advances in transition metal nitride-based materials for photocatalytic applications." Advanced Functional Materials 31, no. 26 (2021): 2100553.

180.   Wang, Hao, Jianmin Li, Ke Li, Yanping Lin, Jianmei Chen, Lijun Gao, Valeria Nicolosi, Xu Xiao, and Jong-Min Lee. "Transition metal nitrides for

electrochemical energy applications." Chemical Society Reviews 50, no. 2 (2021): 1354-1390.

181.   Gujral, Harpreet Singh, Gurwinder Singh, Arun V. Baskar, Xinwei Guan, Xun Geng, Abhay V. Kotkondawar, Sadhana Rayalu, Prashant Kumar, Ajay Karakoti, and Ajayan Vinu. "Metal nitride-based nanostructures for electrochemical and photocatalytic hydrogen production." Science and Technology of Advanced Materials 23, no. 1 (2022): 76-119.

182.   Chun, Wang-Jae, Akio Ishikawa, Hideki Fujisawa, Tsuyoshi Takata, Junko N. Kondo, Michikazu Hara, Maki Kawai, Yasumichi Matsumoto, and Kazunari Domen. "Conduction and valence band positions of Ta_2O_5, TaON, and Ta_3N_5 by UPS and electrochemical methods." The Journal of Physical Chemistry B 107, no. 8 (2003): 1798-1803.

183.   Kerlau, Marie, Odile Merdrignac-Conanec, Maryline Guilloux-Viry, and André Perrin. "Synthesis of crystallized TaON and Ta_3N_5 by nitridation of Ta_2O_5 thin films grown by pulsed laser deposition." Solid State Sciences 6, no. 1 (2004): 101-107.

184.   Harb, Moussab, Philippe Sautet, Ela Nurlaela, Pascal Raybaud, Luigi Cavallo, Kazunari Domen, Jean-Marie Basset, and Kazuhiro Takanabe. "Tuning the properties of visible-light-responsive tantalum (oxy) nitride photocatalysts by non-stoichiometric compositions: a first-principles viewpoint." Physical Chemistry Chemical Physics 16, no. 38 (2014): 20548-20560.

185.   Hara, Michikazu, Go Hitoki, Tsuyoshi Takata, Junko N. Kondo, Hisayoshi Kobayashi, and Kazunari Domen. "TaON and Ta_3N_5 as new visible light driven photocatalysts." Catalysis Today 78, no. 1-4 (2003): 555-560.

186.   Hara, Michikazu, Jun Nunoshige, Tsuyoshi Takata, Junko N. Kondo, and Kazunari Domen. "Unusual enhancement of H_2 evolution by Ru on TaON photocatalyst under visible light irradiation." Chemical Communications 24 (2003): 3000-3001.

187.   Chen, Shanshan, Yu Qi, Qian Ding, Zheng Li, Junyan Cui, Fuxiang Zhang, and Can Li. "Magnesia interface nanolayer modification of Pt/Ta_3N_5 for promoted photocatalytic hydrogen production under visible light irradiation." Journal of Catalysis 339 (2016): 77-83.

188.   Maeda, Kazuhiko. "(Oxy) nitrides with d 0-electronic configuration as photocatalysts and photoanodes that operate under a wide range of visible light for overall water splitting." Physical Chemistry Chemical Physics 15, no. 26 (2013): 10537-10548.

189.   He, Yumin, JamesáE Thorne, ChengáHao Wu, Peiyan Ma, Chun Du, Qi Dong, Jinghua Guo, and Dunwei Wang. "What limits the performance of Ta_3N_5 for solar water splitting?." Chem 1, no. 4 (2016): 640-655.

190.   Curie, Marie. "Hydrogen production from water splitting using photo-semiconductor catalysts." Renewable Hydrogen Technologies: Production, Purification, Storage, Applications and Safety 43 (2013).

191.   Jiang, Zhi, Zhen Ye, and Wenfeng Shangguan. "Recent advances of hydrogen production through particulate semiconductor photocatalytic overall water splitting." Frontiers in Energy 16, no. 1 (2022): 49-63.

192.   Wang, Zheng, Yasunobu Inoue, Takashi Hisatomi, Ryo Ishikawa, Qian Wang, Tsuyoshi Takata, Shanshan Chen, Naoya Shibata, Yuichi Ikuhara, and Kazunari Domen. "Overall water splitting by Ta_3N_5 nanorod single crystals grown on the edges of $KTaO_3$ particles." Nature Catalysis 1, no. 10 (2018): 756-763.

193. Ma, Su Su Khine, Takashi Hisatomi, Kazuhiko Maeda, Yosuke Moriya, and Kazunari Domen. "Enhanced water oxidation on Ta_3N_5 photocatalysts by modification with alkaline metal salts." Journal of the American Chemical Society 134, no. 49 (2012): 19993-19996.

194. Pinaud, Blaise A., Peter CK Vesborg, and Thomas F. Jaramillo. "Effect of film morphology and thickness on charge transport in Ta_3N_5/Ta photoanodes for solar water splitting." The Journal of Physical Chemistry C 116, no. 30 (2012): 15918-15924.

195. Su, Hui, Wei Che, Fumin Tang, Weiren Cheng, Xu Zhao, Hui Zhang, and Qinghua Liu. "Valence band engineering via PtII single-atom confinement realizing photocatalytic water splitting." The Journal of Physical Chemistry C 122, no. 37 (2018): 21108-21114.

196. Ahmad, Irshad, Yanhong Zou, Jiaying Yan, Yuyu Liu, Shazia Shukrullah, Muhammad Yasin Naz, Humaira Hussain, Waheed Qamar Khan, and N. R. Khalid. "Semiconductor photocatalysts: A critical review highlighting the various strategies to boost the photocatalytic performances for diverse applications." Advances in Colloid and Interface Science (2022): 102830.

197. Ahmad, Irshad, Yanhong Zou, Jiaying Yan, Yuyu Liu, Shazia Shukrullah, Muhammad Yasin Naz, Humaira Hussain, Waheed Qamar Khan, and N. R. Khalid. "Semiconductor photocatalysts: A critical review highlighting the various strategies to boost the photocatalytic performances for diverse applications." Advances in Colloid and Interface Science (2022): 102830.

198. Ahmed, Ghada H. "Tracking Ultrafast Charge Carrier Dynamics at the Interface of Semiconductor Nanocrystals." PhD diss., 2020.

199.   Gao, Chao, Jingxiang Low, Ran Long, Tingting Kong, Junfa Zhu, and Yujie Xiong. "Heterogeneous single-atom photocatalysts: fundamentals and applications." Chemical reviews 120, no. 21 (2020): 12175-12216.

200.   Bi, Wentuan, Xiaogang Li, Lei Zhang, Tao Jin, Lidong Zhang, Qun Zhang, Yi Luo, Changzheng Wu, and Yi Xie. "Molecular co-catalyst accelerating hole transfer for enhanced photocatalytic H2 evolution." Nature communications 6, no. 1 (2015): 8647.

201.   Chen, Huan, Shuo Chen, Xie Quan, and Yaobin Zhang. "Structuring a TiO2-based photonic crystal photocatalyst with Schottky junction for efficient photocatalysis." Environmental science & technology 44, no. 1 (2010): 451-455.

202.   Zhu, Yunqing, Tian Wang, Tao Xu, Yingxuan Li, and Chuanyi Wang. "Size effect of Pt co-catalyst on photocatalytic efficiency of g-C3N4 for hydrogen evolution." Applied Surface Science 464 (2019): 36-42.

203.   Camposeco, R., M. Hinojosa-Reyes, and R. J. I. J. O. H. E. Zanella. "Highly efficient photocatalytic hydrogen evolution by using Rh as co-catalyst in the Cu/TiO2 system." International Journal of Hydrogen Energy 46, no. 51 (2021): 26074-26086.

204.   Sun, Qianqian, Zebin Yu, Ronghua Jiang, Yanping Hou, Lei Sun, Lun Qian, Fengyuan Li, Mingjie Li, Qi Ran, and Heqing Zhang. "CoP QD anchored carbon skeleton modified CdS nanorods as a co-catalyst for photocatalytic hydrogen production." Nanoscale 12, no. 37 (2020): 19203-19212.

205.   Liu, Jianni, Qiaohui Jia, Jinlin Long, Xuxu Wang, Ziwei Gao, and Quan Gu. "Amorphous NiO as co-catalyst for enhanced visible-light-driven hydrogen generation over g-C$_3$N$_4$ photocatalyst." Applied Catalysis B: Environmental 222 (2018): 35-43.

206.   Li, Yujie, Lei Ding, Yichen Guo, Zhangqian Liang, Hongzhi Cui, and Jian Tian. "Boosting the photocatalytic ability of g-C3N4 for hydrogen production by Ti3C2 MXene quantum dots." ACS applied materials & interfaces 11, no. 44 (2019): 41440-41447.

207.   Mohtar, Safia Syazana, Farhana Aziz, Ahmad Fauzi Ismail, Nonni Soraya Sambudi, Hamidah Abdullah, Ahmad Nazrul Rosli, and Bunsho Ohtani. "Impact of doping and additive applications on photocatalyst textural properties in removing organic pollutants: A review." Catalysts 11, no. 10 (2021): 1160.

208.   Zaleska, Adriana. "Doped-TiO2: a review." Recent patents on engineering 2, no. 3 (2008): 157-164.

209.   Jyothi, M. S., Vignesh Nayak, Kakarla Raghava Reddy, S. Naveen, and A. V. Raghu. "Non-metal (oxygen, sulphur, nitrogen, boron and phosphorus)-doped metal oxide hybrid nanostructures as highly efficient photocatalysts for water treatment and hydrogen generation." Nanophotocatalysis and Environmental Applications: Materials and Technology (2019): 83-105.

210.   Prabakaran, Eswaran, and Kriveshini Pillay. "Synthesis of N-doped ZnO nanoparticles with cabbage morphology as a catalyst for the efficient photocatalytic degradation of methylene blue under UV and visible light." RSC advances 9, no. 13 (2019): 7509-7535.

211.   Bento, Rodrigo T., Olandir V. Correa, and Marina F. Pillis. "Photocatalytic activity of undoped and sulfur-doped TiO$_2$ films grown by MOCVD for water treatment under visible light." Journal of the European Ceramic Society 39, no. 12 (2019): 3498-3504.

212.   Ansari, Sajid Ali, Mohammad Mansoob Khan, Mohd Omaish Ansari, and Moo Hwan Cho. "Nitrogen-doped titanium dioxide (N-doped TiO2) for visible light photocatalysis." New Journal of Chemistry 40, no. 4 (2016): 3000-3009.

213.   Tie, Luna, Ruya Sun, Han Jiang, Yanmei Liu, Yu Xia, Ya-Yun Li, Hui Chen et al. "Facile fabrication of N-doped ZnS nanomaterials for efficient photocatalytic performance of organic pollutant removal and H2 production." Journal of Alloys and Compounds 807 (2019): 151670.

214.   Li, Wenzhang, Jie Li, Xuan Wang, and Qiyuan Chen. "Preparation and water-splitting photocatalytic behavior of S-doped WO3." Applied surface science 263 (2012): 157-162.

215.   Chaudhuri, Rajib Ghosh, and Santanu Paria. "Visible light induced photocatalytic activity of sulfur doped hollow TiO_2 nanoparticles, synthesized via a novel route." Dalton Transactions 43, no. 14 (2014): 5526-5534.

216.   Umebayashi, T., T. Yamaki, H. Itoh, and K. Asai. "Band gap narrowing of titanium dioxide by sulfur doping." Applied physics letters 81, no. 3 (2002): 454-456.

217.   Kamruzzaman, M., J. Antonio Zapien, M. Rahman, R. Afrose, T. Khairul Anam, M. Nurul Huda Liton, M. Al-Helal, and M. Khalilur Rahman Khan. "Effects of p-type (Ag, Cu) dopant on the electronic, optical and photocatalytic properties of MoS2, and impact on Au/Mo100-x-yAgxCuyS2 performance." Journal of Alloys and Compounds 863 (2021): 158366.

218.   Vaiano, Vincenzo, and Giuseppina Iervolino. "Photocatalytic hydrogen production from glycerol aqueous solution using Cu-doped ZnO under visible light irradiation." Applied Sciences 9, no. 13 (2019): 2741.

219.   Sumadevi, K. R., G. Krishnamurthy, Prabhaker Walmik, RS Priya Rani, Satish Naik, HS Bhojya Naik, and Nagaraja Naik. "Photocatalytic degradation of eriochrome

black-T and evan's blue dyes under the visible light using PVA capped and uncapped Ag doped Zns nanoparticles." Emergent Materials 4 (2021): 447-456.

220.   Ma, Tao, Qianqian Shen, Bin Zhaoa, Jinbo Xue, Rongfeng Guan, Xuguang Liu, Husheng Jia, and Bingshe Xu. "Facile synthesis of Fe-doped g-C_3N_4 for enhanced visible-light photocatalytic activity." Inorganic Chemistry Communications 107 (2019): 107451.

221.   Wang, Xulin, Xiuzhen Zheng, Huijuan Han, You Fan, Sujuan Zhang, Sugang Meng, and Shifu Chen. "Photocatalytic hydrogen evolution from biomass (glucose solution) on Au/CdS nanorods with Au^{3+} self-reduction." Journal Of Solid State Chemistry 289 (2020): 121495.

222.   Kubacka, A., G. Colón, and M. Fernández-García. "Cationic (V, Mo, Nb, W) doping of TiO_2–anatase: A real alternative for visible light-driven photocatalysts." Catalysis Today 143, no. 3-4 (2009): 286-292.

223.   Truc, Nguyen Thi Thanh, Dinh Trinh Tran, Nguyen Thi Hanh, and Thanh-Dong Pham. "Novel visible light-driven Nb-doped Ta_3N_5 sensitized/protected by PPy for efficient overall water splitting." International Journal of Hydrogen Energy 43, no. 33 (2018): 15898-15906.

224.   Zhuang, Huaqiang, Yingguang Zhang, Zhenwei Chu, Jinlin Long, Xiaohan An, Hongwen Zhang, Huaxiang Lin, Zizhong Zhang, and Xuxu Wang. "Synergy of metal and nonmetal dopants for visible-light photocatalysis: a case-study of Sn and N co-doped TiO 2." Physical Chemistry Chemical Physics 18, no. 14 (2016): 9636-9644.

225.   Acharya, Rashmi, and Prativa Pani. "Visible light susceptible doped TiO2 photocatalytic systems: an overview." Materials Today: Proceedings (2022).

226.   Chong, Wei-Kean, Boon-Junn Ng, Xin Ying Kong, Lling-Lling Tan, Lutfi Kurnianditia Putri, and Siang-Piao Chai. "Non-metal doping induced dual pn charge properties in a single ZnIn2S4 crystal structure provoking charge transfer behaviors and boosting photocatalytic hydrogen generation." Applied Catalysis B: Environmental 325 (2023): 122372.

227.   Farhadian, Negin, Rokhsareh Akbarzadeh, Meghdad Pirsaheb, Tien-Chien Jen, Yadolah Fakhri, and Anvar Asadi. "Chitosan modified N, S-doped TiO_2 and N, S-doped ZnO for visible light photocatalytic degradation of tetracycline." International journal of biological macromolecules 132 (2019): 360-373.

228.   Yao, Xiaxi, Wenjun Zhang, Jialei Huang, Zhongwei Du, Xuekun Hong, Xuefeng Chen, Xiuli Hu, and Xuhong Wang. "Enhanced photocatalytic nitrogen fixation of Ag/B-doped g-C_3N_4 nanosheets by one-step in-situ decomposition-thermal polymerization method." Applied Catalysis A: General 601 (2020): 117647.

229.   Kunnamareddy, Mehala, Sivarasan Ganesan, Ashraf Atef Hatamleh, Bassam Khalid Alnafisi, Ranjith Rajendran, Ragavendran Chinnasamy, Priyadharsan Arumugam, Barathi Diravidamani, and Huang-Mu Lo. "Enhancement in the visible light induced photocatalytic and antibacterial properties of titanium dioxide codoped with cobalt and sulfur." Environmental Research 216 (2023): 114705.

230.   Li, Yang, Xin Li, Huaiwu Zhang, Jiajie Fan, and Quanjun Xiang. "Design and application of active sites in g-C3N4-based photocatalysts." Journal of Materials Science & Technology 56 (2020): 69-88.

231.   Moskovits, Martin. "Surface-enhanced spectroscopy." Reviews of modern physics 57, no. 3 (1985): 783.

232.   Zada, Amir, Pir Muhammad, Waqas Ahmad, Zahid Hussain, Sharafat Ali, Maaz Khan, Qasim Khan, and Muhammad Maqbool. "Surface plasmonic-assisted

photocatalysis and optoelectronic devices with noble metal nanocrystals: design, synthesis, and applications." Advanced Functional Materials 30, no. 7 (2020): 1906744.

233.   Li, Jun, Fan Zhou, Hua-Ping Lin, Wen-Qing Zhu, Jian-Hua Zhang, Xue-Yin Jiang, and Zhi-Lin Zhang. "Enhanced photosensitivity of InGaZnO-TFT with a CuPc light absorption layer." Superlattices and Microstructures 51, no. 4 (2012): 538-543.

234.   Chen, Shihao, Yang Xiao, Yinhai Wang, Zhengfa Hu, Hui Zhao, and Wei Xie. "A facile approach to prepare black TiO_2 with oxygen vacancy for enhancing photocatalytic activity." Nanomaterials 8, no. 4 (2018): 245.

235.   Balzani, Vincenzo, Alberto Credi, and Margherita Venturi. "Photochemical conversion of solar energy." ChemSusChem: Chemistry & Sustainability Energy & Materials 1, no. 1-2 (2008): 26-58.

236.   Melchionna, Michele, and Paolo Fornasiero. "Updates on the Roadmap for Photocatalysis." Acs Catalysis 10, no. 10 (2020): 5493-5501.

237.   Xue, Sikang, Chuchu Zhou, Xiaocong Liang, Min Shen, Xiaoyuan Ye, Can Yang, Jinshui Zhang et al. "A versatile Topology Optimization Strategy for Devising Low-Dimensional Architectures with Boosted Photocatalytic Activity." Advanced Functional Materials (2023): 2213612.

238.   Yan, Hui, Xudong Wang, Man Yao, and Xiaojie Yao. "Band structure design of semiconductors for enhanced photocatalytic activity: The case of TiO2." Progress in Natural Science: Materials International 23, no. 4 (2013): 402-407.

239.   Li, Yuan-Yuan, Bing-Xin Zhou, Hua-Wei Zhang, Shao-Fang Ma, Wei-Qing Huang, Wei Peng, Wangyu Hu, and Gui-Fang Huang. "Doping-induced enhancement of crystallinity in polymeric carbon nitride nanosheets to improve their visible-light photocatalytic activity." Nanoscale 11, no. 14 (2019): 6876-6885.

240. Kim, Dong Suk, and Seung-Yeop Kwak. "The hydrothermal synthesis of mesoporous TiO2 with high crystallinity, thermal stability, large surface area, and enhanced photocatalytic activity." Applied Catalysis A: General 323 (2007): 110-118.

241. Hunter, Robert J. Zeta potential in colloid science: principles and applications. Vol. 2. Academic press, 2013.

242. Lunardi, Claure N., Anderson J. Gomes, Fellipy S. Rocha, Jacopo De Tommaso, and Gregory S. Patience. "Experimental methods in chemical engineering: Zeta potential." The Canadian Journal of Chemical Engineering 99, no. 3 (2021): 627-639.

243. Miyauchi, Masahiro, Ayako Ikezawa, Hiroki Tobimatsu, Hiroshi Irie, and Kazuhito Hashimoto. "Zeta potential and photocatalytic activity of nitrogen doped TiO 2 thin films." Physical Chemistry Chemical Physics 6, no. 4 (2004): 865-870.

244. Tian, Guohui, Honggang Fu, Liqiang Jing, and Chungui Tian. "Synthesis and photocatalytic activity of stable nanocrystalline TiO2 with high crystallinity and large surface area." Journal of Hazardous Materials 161, no. 2-3 (2009): 1122-1130.

245. Sivula, Kevin, Florian Le Formal, and Michael Grätzel. "Solar water splitting: progress using hematite (α-Fe2O3) photoelectrodes." ChemSusChem 4, no. 4 (2011): 432-449.

246. Zhang, Yanqiu, Yuqing Mei, Shouchun Ma, Yang Yang, Xianhe Deng, Yina Guan, Tingting Zhao et al. "A simple and green method to prepare non-typical yolk/shell nanoreactor with dual-shells and multiple-cores: Enhanced catalytic activity and stability in Fenton-like reaction." Journal of Hazardous Materials 436 (2022): 129234.

247.   Zhang, Qiao, Ilkeun Lee, Ji Bong Joo, Francisco Zaera, and Yadong Yin. "Core–shell nanostructured catalysts." Accounts of Chemical Research 46, no. 8 (2013): 1816-1824.

248.   Biswas, Indranil, Piyali Roy, Prasanta Kumar Sinha, Moumita Kanu, and Ashim Kumar Chakraborty. "Activating ZnO nanorods photoanodes in visible light by CdS surface sensitiser." Micro & Nano Letters 14, no. 9 (2019): 941-946.

249.   Adhikari, Shiba P., Zachary D. Hood, Karren L. More, Ilia Ivanov, Lifeng Zhang, Michael Gross, and Abdou Lachgar. "Visible light assisted photocatalytic hydrogen generation by Ta2O5/Bi2O3, TaON/Bi2O3, and Ta3N5/Bi2O3 composites." RSC Advances 5, no. 68 (2015): 54998-55005.

250.   Wang, Wen, Hua-Bin Fang, Yan-Zhen Zheng, Yanke Che, Xia Tao, and Jian-Feng Chen. "In situ template-free synthesis of a novel 3D p–n heteroarchitecture Ag3 PO4/Ta3N5 photocatalyst with high activity and stability under visible radiation." Rsc Advances 5, no. 77 (2015): 62519-62526.

251.   Pragada, Sarath Chandra, and Arun Kumar Thalla. "Polymer-based immobilized Fe2O3–TiO2/PVP catalyst preparation method and the degradation of triclosan in treated greywater effluent by solar photocatalysis." Journal of Environmental Management 296 (2021): 113305.

252.   Toe, Cui Ying, Zhaoke Zheng, Hao Wu, Jason Scott, Rose Amal, and Yun Hau Ng. "Photocorrosion of cuprous oxide in hydrogen production: rationalising self-oxidation or self-reduction." Angewandte Chemie International Edition 57, no. 41 (2018): 13613-13617.

253.   Ning, Xiaofeng, and Gongxuan Lu. "Photocorrosion inhibition of CdS-based catalysts for photocatalytic overall water splitting." Nanoscale 12, no. 3 (2020): 1213-1223.

254.   Shibli, S. M. A., P. S. Arun, and Anupama V. Raj. "Exploration of octahedrally shaped MnCo2O4 catalyst particles for visible light driven photocatalytic water splitting reaction." RSC Advances 5, no. 25 (2015): 19393-19399.

255.   Gogoi, Devipriya, Ashutosh Namdeo, Animes Kumar Golder, and Nageswara Rao Peela. "Ag-doped TiO2 photocatalysts with effective charge transfer for highly efficient hydrogen production through water splitting." International Journal of Hydrogen Energy 45, no. 4 (2020): 2729-2744.

256.   Kanhere, Pushkar, and Zhong Chen. "A review on visible light active perovskite-based photocatalysts." Molecules 19, no. 12 (2014): 19995-20022.

257.   Mehta, A., A. Mishra, S. Basu, N. P. Shetti, K. R. Reddy, and T. A. Saleh. "Band gap tuning and surface modification of carbon dots for sustainable environmental remediation and photocatalytic hydrogen production–a review." TIDEE: TERI Information Digest on Energy and Environment 19, no. 1 (2020): 47-47.

258.   Balat, Havva, and Elif Kırtay. "Hydrogen from biomass–present scenario and future   prospects." International journal of hydrogen energy 35, no. 14 (2010): 7416-7426.

259.   Su, Tongming, Qian Shao, Zuzeng Qin, Zhanhu Guo, and Zili Wu. "Role of interfaces in two-dimensional photocatalyst for water splitting." Acs Catalysis 8, no. 3 (2018): 2253-2276.

260.   Takanabe, Kazuhiro. "Photocatalytic water splitting: quantitative approaches toward photocatalyst by design." ACS Catalysis 7, no. 11 (2017): 8006-8022.

261.   Liu, Qiaoran. "Photocatalytic performance of nanocatalysts." PhD diss., Curtin University, 2021.

262. Nurlaela, Ela, Ahmed Ziani, and Kazuhiro Takanabe. "Tantalum nitride for photocatalytic water splitting: concept and applications." Materials for Renewable and Sustainable Energy 5 (2016): 1-21.

263. Chowdhury, Faqrul A., Zetian Mi, Md G. Kibria, and Michel L. Trudeau. "Group III-nitride nanowire structures for photocatalytic hydrogen evolution under visible light irradiation." APL Materials 3, no. 10 (2015).

264. Kumaravel, Vignesh, Snehamol Mathew, John Bartlett, and Suresh C. Pillai. "Photocatalytic hydrogen production using metal doped TiO2: A review of recent advances." Applied Catalysis B: Environmental 244 (2019): 1021-1064.

265. Takanabe, Kazuhiro. "Solar water splitting using semiconductor photocatalyst powders." Solar Energy for Fuels (2016): 73-103.

266. Hahn, David W. "Light scattering theory." Department of Mechanical and Aerospace Engineering, University of Florida (2009): 18.

267. Takanabe, Kazuhiro. "Solar water splitting using semiconductor photocatalyst powders." Solar Energy for Fuels (2016): 73-103.

268. Beard, Matthew C., and Randy J. Ellingson. "Multiple exciton generation in semiconductor nanocrystals: Toward efficient solar energy conversion." Laser & Photonics Reviews 2, no. 5 (2008): 377-399.

269. Karl, Norbert. "Charge carrier transport in organic semiconductors." Synthetic metals 133 (2003): 649-657.

270. Zhang, Jie, Kaiyu Wang, Qing Yao, Ye Yuan, Jianxu Ding, Weiwei Zhang, Haiqing Sun et al. "Carrier Diffusion and Recombination Anisotropy in the MAPbI$_3$ Single Crystal." ACS Applied Materials & Interfaces 13, no. 25 (2021): 29827-29834.

271. Baranovskii, S. D., T. Faber, F. Hensel, and P. Thomas. "On the Einstein relation for hopping electrons." Journal of non-crystalline solids 227 (1998): 158-161.

272. De Falco, Carlo, Emilio Gatti, Andrea L. Lacaita, and Riccardo Sacco. "Quantum-corrected drift-diffusion models for transport in semiconductor devices." Journal of Computational Physics 204, no. 2 (2005): 533-561.

273. Johnston, Michael B., and Laura M. Herz. "Hybrid perovskites for photovoltaics: charge-carrier recombination, diffusion, and radiative efficiencies." Accounts of chemical research 49, no. 1 (2016): 146-154.

274. Shirota, Yasuhiko, and Hiroshi Kageyama. "Charge carrier transporting molecular materials and their applications in devices." Chemical reviews 107, no. 4 (2007): 953-1010.

275. Navarro, R. M., F. Del Valle, JA Villoria De La Mano, M. C. Álvarez-Galván, and J. L. G. Fierro. "Photocatalytic water splitting under visible light: concept and catalysts development." Advances in chemical engineering 36 (2009): 111-143.

276. Ju, Hua, Zhihu Li, and Yanhui Xu. "Electro-catalytic activity of Ni–Co-based catalysts for oxygen evolution reaction." Materials Research Bulletin 64 (2015): 171-174.

277. Trasatti, Sergio. "Work function, electronegativity, and electrochemical behaviour of metals: III. Electrolytic hydrogen evolution in acid solutions." Journal of Electroanalytical Chemistry and Interfacial Electrochemistry 39, no. 1 (1972): 163-184.

278. Nørskov, Jens Kehlet, Thomas Bligaard, Ashildur Logadottir, J. R. Kitchin, Jingguang G. Chen, S. Pandelov, and U. Stimming. "Trends in the exchange current for hydrogen evolution." Journal of The Electrochemical Society 152, no. 3 (2005): J23.

279.   Li, Zhen, Mengqing Hu, Yanqi Xu, Di Zhao, Shuaiyu Jiang, Kaicai Fan, Meng Zu et al. "Photocatalytic Hydrogen Production." Photo-and Electro-Catalytic Processes: Water Splitting, N_2 Fixing, CO_2 Reduction (2022): 415-483.

280.   Zhu, Shasha, and Dunwei Wang. "Photocatalysis: basic principles, diverse forms of implementations and emerging scientific opportunities." Advanced Energy Materials 7, no. 23 (2017): 1700841.

281.   Kapoor, Atul, and Jaspreet Kaur Rajput. "Nanostructured materials for the visible-light driven hydrogen evolution by water splitting: A review." International Journal of Hydrogen Energy 47, no. 40 (2022): 17544-17582.

282.   Kumar, Ashwani. "Global warming, climate change and greenhouse gas mitigation." Biofuels: greenhouse gas mitigation and global warming: next generation biofuels and role of biotechnology (2018): 1-16.

283.   Fu, Zhiyan, Qi Yang, Zhan Liu, Fei Chen, Fubing Yao, Ting Xie, Yu Zhong et al. "Photocatalytic conversion of carbon dioxide: From products to design the catalysts." Journal of CO2 Utilization 34 (2019): 63-73.

284.   Wang, Qian, and Kazunari Domen. "Particulate photocatalysts for light-driven water splitting: mechanisms, challenges, and design strategies." Chemical Reviews 120, no. 2 (2019): 919-985.

285.   Behroozi, Amir Hossein, and Rong Xu. "Photocatalytic CO2 reduction: Photocatalysts, membrane reactors, and hybrid processes." Chem Catalysis 3, no. 3 (2023).

286.   Bard, Allen J. "Design of semiconductor photoelectrochemical systems for solar energy conversion." The Journal of Physical Chemistry 86, no. 2 (1982): 172-177.

287. Ouyang, Ting, Sheng Huang, Xiao-Tong Wang, and Zhao-Qing Liu. "Nanostructures for electrocatalytic CO2 reduction." Chemistry–A European Journal 26, no. 62 (2020): 14024-14035.

288. Wang, Huanli, Lisha Zhang, Zhigang Chen, Junqing Hu, Shijie Li, Zhaohui Wang, Jianshe Liu, and Xinchen Wang. "Semiconductor heterojunction photocatalysts: design, construction, and photocatalytic performances." Chemical Society Reviews 43, no. 15 (2014): 5234-5244.

289. Yang, Zhong-zhu, Chang Zhang, Guang-ming Zeng, Xiao-fei Tan, Dan-lian Huang, Jun-wu Zhou, Qian-zhen Fang et al. "State-of-the-art progress in the rational design of layered double hydroxide based photocatalysts for photocatalytic and photoelectrochemical H2/O2 production." Coordination Chemistry Reviews 446 (2021): 214103.

290. Fan, Wenqing, Qinghong Zhang, and Ye Wang. "Semiconductor-based nanocomposites for photocatalytic H 2 production and CO 2 conversion." Physical Chemistry Chemical Physics 15, no. 8 (2013): 2632-2649.

291. Wang, Yiou, Enqi Chen, and Junwang Tang. "Insight on reaction pathways of photocatalytic CO2 conversion." ACS catalysis 12, no. 12 (2022): 7300-7316.

292. Domínguez-Espindola, Ruth Belinda, Dulce M. Arias, Claramaria Rodríguez-González, and Pathiyamattom Sebastian. "Advances in Tio2-Based Photocatalytic Systems for Co2 Reduction Using Solar Energy." Available at SSRN 4057325.

293. Barczuk, Piotr J., Krzysztof R. Noworyta, Miroslaw Dolata, Katarzyna Jakubow-Piotrowska, and Jan Augustynski. "Visible-light activation of low-cost rutile TiO2 photoanodes for photoelectrochemical water splitting." Solar Energy Materials and Solar Cells 208 (2020): 110424.

294.   Fujishima, Akira, and Kenichi Honda. "Electrochemical photolysis of water at a semiconductor electrode." nature 238, no. 5358 (1972): 37-38.

295.   Li, Zhaosheng, Wenjun Luo, Minglong Zhang, Jianyong Feng, and Zhigang Zou. "Photoelectrochemical cells for solar hydrogen production: current state of promising photoelectrodes, methods to improve their properties, and outlook." Energy & Environmental Science 6, no. 2 (2013): 347-370.

296.   Bakar, Shahzad Abu, and Caue Ribeiro. "Nitrogen-doped titanium dioxide: An overview of material design and dimensionality effect over modern applications." Journal of Photochemistry and Photobiology C: Photochemistry Reviews 27 (2016): 1-29.

297.   Ramasami, Alamelu K., Thammadihalli Nanjundaiah Ravishankar, Ganganagappa Nagaraju, Thippeswamy Ramakrishnappa, Sergio Ribeiro Teixeira, and R. Geetha Balakrishna. "Gel-combustion-synthesized ZnO nanoparticles for visible light-assisted photocatalytic hydrogen generation." Bulletin of Materials Science 40 (2017): 345-354.

298.   Erbs, Wilson, Jean Desilvestro, Enrico Borgarello, and Michael Graetzel. "Visible-light-induced oxygen generation from aqueous dispersions of tungsten (VI) oxide." The Journal of Physical Chemistry 88, no. 18 (1984): 4001-4006.

299.   Kong, Lingqiao, Junqing Yan, Ping Li, and Shengzhong Frank Liu. "Fe2O3/C–C3N4-based tight heterojunction for boosting visible-light-driven photocatalytic water oxidation." ACS Sustainable Chemistry & Engineering 6, no. 8 (2018): 10436-10444.

300.   Kumar, Amit, Priya Rittika Thakur, Gaurav Sharma, Mu Naushad, Anamika Rana, Genene Tessema Mola, and Florian J. Stadler. "Carbon nitride, metal nitrides,

phosphides, chalcogenides, perovskites and carbides nanophotocatalysts for environmental applications." Environmental Chemistry Letters 17 (2019): 655-682.

301.   Vijayaraghavan, T., and Anuradha Ashok. "Oxide based Nanocomposites for Photocatalytic Applications." In Applications of Nanocomposites, pp. 55-89. CRC Press, 2022.

302.   Berdyugin, Semen, Ekaterina Kozlova, Anna Kurenkova, Evgeny Gerasimov, Andrey Bukhtiyarov, Boris Kolesov, Irina Yushina, Danila Vasilchenko, and Sergey Korenev. "Hydrogarnet-derived Rh/TiO2 catalysts with a low rhodium content for a photocatalytic hydrogen production." Materials Letters 307 (2022): 130997.

303.   Naik, Brundabana, Song Yi Moon, Sang Hoon Kim, and Jeong Young Park. "Enhanced photocatalytic generation of hydrogen by Pt-deposited nitrogen-doped TiO2 hierarchical nanostructures." Applied Surface Science 354 (2015): 347-352.

304.   Chen, Ximeng, Christian H. Gierlich, Simon Schötz, Dominik Blaumeiser, Tanja Bauer, Jörg Libuda, and Regina Palkovits. "Hydrogen production based on liquid organic hydrogen carriers through sulfur doped platinum catalysts supported on TiO2." ACS Sustainable Chemistry & Engineering 9, no. 19 (2021): 6561-6573.

305.   Nishijima, Kazumoto, Takaaki Kamai, Naoya Murakami, Toshiki Tsubota, and Teruhisa Ohno. "Photocatalytic hydrogen or oxygen evolution from water over S- or N-doped TiO 2 under visible light." International Journal of Photoenergy 2008 (2007).

306.   Zong, Xu, Hongjian Yan, Guopeng Wu, Guijun Ma, Fuyu Wen, Lu Wang, and Can Li. "Enhancement of photocatalytic H2 evolution on CdS by loading MoS2 as cocatalyst under visible light irradiation." Journal of the American Chemical Society 130, no. 23 (2008): 7176-7177.

307. Gao, Huazhen, Honge Wang, Youlai Jin, Jun Lv, Guangqing Xu, Dongmei Wang, Xinyi Zhang, Zhong Chen, Zhixiang Zheng, and Yucheng Wu. "Controllable fabrication of immobilized ternary CdS/Pt–TiO2 heteronanostructures toward high-performance visible-light driven photocatalysis." Physical Chemistry Chemical Physics 17, no. 27 (2015): 17755-17761.

308. Li, Dingyu, Chengwu Yang, Saravanan Rajendran, Jiaqian Qin, and Xinyu Zhang. "Nanoflower-like Ti3CN@TiO2/CdS heterojunction photocatalyst for efficient photocatalytic water splitting." International Journal of Hydrogen Energy 47, no. 45 (2022): 19580-19589.

309. Parida, K. M., Saroj Ku Mahanta, Satyabadi Martha, and Amtul Nashim. "Fabrication of NiO/Ta2O5 composite photocatalyst for hydrogen production under visible light." International journal of energy research 37, no. 2 (2013): 161-170.

310. Shimakawa, Yuichi. "Perovskite structure compounds." Handbook of Solid State Chemistry, 6 Volume Set (2017).

311. Maeda, Kazuhiko. "Rhodium-doped barium titanate perovskite as a stable p-type semiconductor photocatalyst for hydrogen evolution under visible light." ACS applied materials & interfaces 6, no. 3 (2014): 2167-2173.

312. Zhang, Hongjie, Gang Chen, Yingxuan Li, and Yujie Teng. "Electronic structure and photocatalytic properties of copper-doped $CaTiO_3$." International journal of hydrogen energy 35, no. 7 (2010): 2713-2716.

313. Townsend, Troy K., Nigel D. Browning, and Frank E. Osterloh. "Overall photocatalytic water splitting with NiO_x–$SrTiO_3$–a revised mechanism." Energy & Environmental Science 5, no. 11 (2012): 9543-9550.

314.   Kanhere, Pushkar, Jianwei Zheng, and Zhong Chen. "Visible light driven photocatalytic hydrogen evolution and photophysical properties of Bi3+ doped NaTaO3." international journal of hydrogen energy 37, no. 6 (2012): 4889-4896.

315.   Ni, Xin-Long, Xin Xiao, Hang Cong, Li-Li Liang, Kai Cheng, Xiao-Jie Cheng, Ning-Ning Ji, Qian-Jiang Zhu, Sai-Feng Xue, and Zhu Tao. "Cucurbit [n] uril-based coordination chemistry: from simple coordination complexes to novel poly-dimensional coordination polymers." Chemical Society Reviews 42, no. 24 (2013): 9480-9508.

316.   Wang, Ruwei, Yufeng Zhu, Yongfu Qiu, Chi-Fai Leung, Jun He, Guijian Liu, and Tai-Chu Lau. "Synthesis of nitrogen-doped KNbO3 nanocubes with high photocatalytic activity for water splitting and degradation of organic pollutants under visible light." Chemical engineering journal 226 (2013): 123-130.

317.   Tijare, Saumitra N., Meenal V. Joshi, Priyanka S. Padole, Priti A. Mangrulkar, Sadhana S. Rayalu, and Nitin K. Labhsetwar. "Photocatalytic hydrogen generation through water splitting on nano-crystalline LaFeO3 perovskite." International journal of hydrogen energy 37, no. 13 (2012): 10451-10456.

318.   Dhanasekaran, P., and N. M. Gupta. "Factors affecting the production of H2 by water splitting over a novel visible-light-driven photocatalyst GaFeO3." International Journal of Hydrogen Energy 37, no. 6 (2012): 4897-4907.

319.   Tijare, S. N., S. Bakardjieva, J. Subrt, M. V. Joshi, S. S. Rayalu, S. Hishita, and Nitin Labhsetwar. "Synthesis and visible light photocatalytic activity of nanocrystalline PrFeO3 perovskite for hydrogen generation in ethanol–water system." Journal of Chemical Sciences 126 (2014): 517-525.

320. Kavan, L., M. Grätzel, J. Rathouský, and A. Zukalb. "Nanocrystalline TiO2 (anatase) electrodes: surface morphology, adsorption, and electrochemical properties." Journal of the electrochemical society 143, no. 2 (1996): 394.

321. Passi, Manjusha, and Bonamali Pal. "A review on CaTiO3 photocatalyst: Activity enhancement methods and photocatalytic applications." Powder Technology 388 (2021): 274-304.

322. Zhang, Hongjie, Gang Chen, Yingxuan Li, and Yujie Teng. "Electronic structure and photocatalytic properties of copper-doped CaTiO3." International journal of hydrogen energy 35, no. 7 (2010): 2713-2716.

323. Niishiro, Ryo, and Akihiko Kudo. "Development of visible-light-driven TiO2 and SrTiO3 photocatalysts doped with metal cations for H2 or O2 evolution." Solid State Phenomena 162 (2010): 29-40.

324. Xu, Yisheng, Yaoheng Liang, Qingqing He, Ruoling Xu, Dongchu Chen, Xuejun Xu, and Huawen Hu. "Review of doping SrTiO3 for photocatalytic applications." Bulletin of Materials Science 46, no. 1 (2022): 6.

325. Gogoi, Devipriya, Ashutosh Namdeo, Animes Kumar Golder, and Nageswara Rao Peela. "Ag-doped TiO2 photocatalysts with effective charge transfer for highly efficient hydrogen production through water splitting." International Journal of Hydrogen Energy 45, no. 4 (2020): 2729-2744.

326. Tijare, Saumitra N., Meenal V. Joshi, Priyanka S. Padole, Priti A. Mangrulkar, Sadhana S. Rayalu, and Nitin K. Labhsetwar. "Photocatalytic hydrogen generation through water splitting on nano-crystalline $LaFeO_3$ perovskite." International journal of hydrogen energy 37, no. 13 (2012): 10451-10456.

327.   Dhanasekaran, P., and N. M. Gupta. "Factors affecting the production of H_2 by water splitting over a novel visible-light-driven photocatalyst $GaFeO_3$." International Journal of Hydrogen Energy 37, no. 6 (2012): 4897-4907.

328.   Tijare, S. N., S. Bakardjieva, J. Subrt, M. V. Joshi, S. S. Rayalu, S. Hishita, and Nitin Labhsetwar. "Synthesis and visible light photocatalytic activity of nanocrystalline $PrFeO_3$ perovskite for hydrogen generation in ethanol–water system." Journal of Chemical Sciences 126 (2014): 517-525.

329.   Jia, Qingxin, Akihide Iwase, and Akihiko Kudo. "$BiVO_4$–$Ru/SrTiO_3$: Rh composite Z-scheme photocatalyst for solar water splitting." Chemical Science 5, no. 4 (2014): 1513-1519.

330.   Xiao, Hongbo, Pengyun Liu, Wei Wang, Ran Ran, Wei Zhou, and Zongping Shao. "Ruddlesden–Popper perovskite oxides for photocatalysis-based water splitting and wastewater treatment." Energy & Fuels 34, no. 8 (2020): 9208-9221.

331.   Srinatha, N., S. Satyanarayana Reddy, M. Al-Dossari, K. Gurushantha, NS Abd EL Gawaad, S. O. Manjunatha, KJ Rudresh Kumar, MR Suresh Kumar, Vadiraj B. Tangod, and A. Madhu. "Effect of aliovalent substitution in the band structure engineered Ca2+-doped LaFeO3 nanoparticles for visible light-induced photocatalytic studies." Ceramics International (2023).

332.   Low, Jingxiang, Jiaguo Yu, Mietek Jaroniec, Swelm Wageh, and Ahmed A. Al-Ghamdi. "Heterojunction photocatalysts." Advanced materials 29, no. 20 (2017): 1601694.

333.   Wang, Kai, Jun Li, and Gaoke Zhang. "Ag-bridged Z-scheme 2D/2D Bi5FeTi3O15/g-C3N4 heterojunction for enhanced photocatalysis: mediator-induced interfacial charge transfer and mechanism insights." ACS Applied Materials & Interfaces 11, no. 31 (2019): 27686-27696.

334.   Sah, Chih-Tang, Robert N. Noyce, and William Shockley. "Carrier generation and recombination in pn junctions and pn junction characteristics." Proceedings of the IRE 45, no. 9 (1957): 1228-1243.

335.   Sproul, Alistair. "Understanding the pn Junction." Solar Cells: Resource for the Secondary Science Teacher 73 (2003).

336.   Lin, Min, Hui Chen, Zizhong Zhang, and Xuxu Wang. "Engineering interface structures for heterojunction photocatalysts." Physical Chemistry Chemical Physics 25, no. 6 (2023): 4388-4407.

337.   Sahoo, Dipti Prava, Susanginee Nayak, K. Hemalata Reddy, Satyabadi Martha, and Kulamani Parida. "Fabrication of a $Co(OH)_2$/ZnCr LDH "p–n" heterojunction photocatalyst with enhanced separation of charge carriers for efficient visible-light-driven H_2 and O_2 evolution." Inorganic chemistry 57, no. 7 (2018): 3840-3854.

338.   Wang, Chong, Bin Ma, Xingzhong Cao, Shan He, Jingbin Han, Min Wei, David G. Evans, and Xue Duan. "Bridge-type interface optimization on a dual-semiconductor heterostructure toward high performance overall water splitting." Journal of Materials Chemistry A 6, no. 17 (2018): 7871-7876.

339.   Chen, Lei, Bin Guan, Jiangfeng Guo, Yujun Chen, Zeren Ma, Junyan Chen, Shunyu Yao et al. "Review on the preparation and performance improvement methods of bismuth photocatalyst materials." Catalysis Science & Technology 13, no. 19 (2023): 5478-5529.

340.   Zhang, Tongtong, Yuqi Wang, Xin Xie, Yanning Shao, Yuhao Zeng, Siyu Zhang, Qishe Yan, and Zhongjun Li. "Dual Z-scheme 2D/3D carbon-bridging modified g-C3N4/BiOI-Bi2O3 composite photocatalysts for effective boosting

visible-light-driven photocatalytic performance." Separation and Purification Technology 277 (2021): 119443.

341.   Tang, Yunqi, Chun Hong Mak, Rugeng Liu, Zuankai Wang, Li Ji, Haisheng Song, Chunyan Tan, Frédéric Barrière, and Hsien-Yi Hsu. "In situ formation of bismuth-based perovskite heterostructures for high-performance cocatalyst-free photocatalytic hydrogen evolution." Advanced Functional Materials 30, no. 52 (2020): 2006919.

342.   You, Yong, Shuobo Wang, Ke Xiao, Tianyi Ma, Yihe Zhang, and Hongwei Huang. "Z-Scheme g-C3N4/Bi4NbO8Cl heterojunction for enhanced photocatalytic hydrogen production." ACS Sustainable Chemistry & Engineering 6, no. 12 (2018): 16219-16227.

343.   Zou, Lei, Haoran Wang, and Xiong Wang. "High efficient photodegradation and photocatalytic hydrogen production of CdS/BiVO4 heterostructure through Z-scheme process." ACS Sustainable Chemistry & Engineering 5, no. 1 (2017): 303-309.

344.   Wang, Lu, and Wenzhong Wang. "Photocatalytic hydrogen production from aqueous solutions over novel Bi0.5Na0.5TiO3 microspheres." International journal of hydrogen energy 37, no. 4 (2012): 3041-3047.

345.   Kai, Shuangshuang, Baojuan Xi, Yifeng Wang, and Shenglin Xiong. "One-Pot Synthesis of Size-Controllable Core–Shell CdS and Derived CdS@ ZnxCd1− xS Structures for Photocatalytic Hydrogen Production." Chemistry–A European Journal 23, no. 65 (2017): 16653-16659.

346.   Kai, Shuangshuang, Baojuan Xi, Xiaolei Liu, Lin Ju, Peng Wang, Zhenyu Feng, Xiaojian Ma, and Shenglin Xiong. "An innovative Au-CdS/ZnS-RGO

architecture for efficient photocatalytic hydrogen evolution." Journal of Materials Chemistry A 6, no. 7 (2018): 2895-2899.

347.   Liu, Xiaoming, Suqing Wang, Fang Yang, Yinchu Zhang, Liushui Yan, Kexin Li, Huiqin Guo, Jiajun Yan, and Jun Lin. "Construction of Au/g-C3N4/ZnIn2S4 plasma photocatalyst heterojunction composite with 3D hierarchical microarchitecture for visible-light-driven hydrogen production." International Journal of Hydrogen Energy 47, no. 5 (2022): 2900-2913.

348.   Guan, Zhongjie, Jingwen Pan, Qiuye Li, Guoqiang Li, and Jianjun Yang. "Boosting visible-light photocatalytic hydrogen evolution with an efficient CuInS2/ZnIn2S4 2D/2D heterojunction." ACS Sustainable Chemistry & Engineering 7, no. 8 (2019): 7736-7742.

349.   Feng, Ting, Kaili Zhao, Haiyan Li, Wei Wang, Bohua Dong, and Lixin Cao. "Constructing a 2D/2D heterojunction of MoSe2/ZnIn2S4 nanosheets for enhanced photocatalytic hydrogen evolution." CrystEngComm 23, no. 13 (2021): 2547-2555.

350.   Chai, Bo, Tianyou Peng, Peng Zeng, and Xiaohu Zhang. "Preparation of a MWCNTs/ZnIn2S4 composite and its enhanced photocatalytic hydrogen production under visible-light irradiation." Dalton Transactions 41, no. 4 (2012): 1179-1186.

351.   Pan, Jingwen, Gongxin Zhang, Zhongjie Guan, Qianyu Zhao, Guoqiang Li, Jianjun Yang, Qiuye Li, and Zhigang Zou. "Anchoring Ni single atoms on sulfur-vacancy-enriched ZnIn2S4 nanosheets for boosting photocatalytic hydrogen evolution." Journal of Energy Chemistry 58 (2021): 408-414.

352.   Zhang, Huizhen, Yuming Dong, Shuang Zhao, Guangli Wang, Pingping Jiang, Jun Zhong, and Yongfa Zhu. "Photochemical preparation of atomically dispersed nickel on cadmium sulfide for superior photocatalytic hydrogen evolution." Applied Catalysis B: Environmental 261 (2020): 118233.

353.   Akyüz, Duygu, Ali Rıza Özkaya, and Atıf Koca. "Enhanced hydrogen production with photo-induced phase transformation and cocatalyst loading." International Journal of Energy Research 43, no. 14 (2019): 8299-8313.

354.   ÖZKAYA, ALİ RIZA. "Metal chalcogenide based photocatalysts decorated with heteroatom doped reduced graphene oxide for photocatalytic and photoelectrochemical hydrogen production." (2019).

355.   Lin, Zhaoyong, Weijia Li, and Guowei Yang. "Hydrogen-interstitial CuWO4 nanomesh: a single-component full spectrum-active photocatalyst for hydrogen evolution." Applied Catalysis B: Environmental 227 (2018): 35-43.

356.   Liu, Wei-Szu, Sheng-Hsin Huang, Chia-Fen Liu, Chih-Wei Hu, Tsan-Yao Chen, and Tsong-Pyng Perng. "Nitrogen doping in Ta2O5 and its implication for photocatalytic H2 production." Applied Surface Science 459 (2018): 477-482.

357.   Xiao, M. U., Bin Luo, Supphasin Thaweesak, and Lianzhou Wang. "Noble-metal-free MoS2/Ta3N5 heterostructure photocatalyst for hydrogen generation." Progress in Natural Science: Materials International 28, no. 2 (2018): 189-193.

358.   Jones, Daniel R., Michael EA Warwick, James D. McGettrick, and Charles W. Dunnill. "Composition analysis of Ta3N5/W18O49 nanocomposite through XPS." Surface Science Spectra 25, no. 2 (2018).

359.   Jiang, Yinhua, Peipei Liu, YeCheng Chen, Zhengzhong Zhou, Haijian Yang, Yuanzhi Hong, Fan Li, Liang Ni, Yongsheng Yan, and Duncan H. Gregory. "Construction of stable Ta3N5/g-C3N4 metal/non-metal nitride hybrids with enhanced visible-light photocatalysis." Applied Surface Science 391 (2017): 392-403.

360.   Cui, Junyan, Yu Qi, Beibei Dong, Linchao Mu, Qian Ding, Gang Liu, Mingjun Jia, Fuxiang Zhang, and Can Li. "One-pot synthesis of BaMg1/3Ta2/3O3-xNy/Ta3N5 heterostructures as H2-evolving photocatalysts for construction of

visible-light-driven Z-scheme overall water splitting." Applied Catalysis B: Environmental 241 (2019): 1-7.

361.   Zhang, Guping, Hao Wu, Dongyun Chen, Najun Li, Qingfeng Xu, Hua Li, Jinghui He, and Jianmei Lu. "A mini-review on ZnIn2S4-Based photocatalysts for energy and environmental application." Green Energy & Environment 7, no. 2 (2022): 176-204.

362.   Jo, Wan-Kuen, and Thillai Sivakumar Natarajan. "Fabrication and efficient visible light photocatalytic properties of novel zinc indium sulfide (ZnIn2S4)–graphitic carbon nitride (g-C3N4)/bismuth vanadate (BiVO4) nanorod-based ternary nanocomposites with enhanced charge separation via Z-scheme transfer." Journal of colloid and interface science 482 (2016): 58-72.

363.   Xiao, Yan, Wenli Zhang, Qingzeng Xing, Xintao Feng, Yinhua Jiang, Yuhang Gao, Haiqing Xu, Jianming Zhang, Liang Ni, and Zhanchao Liu. "Eco-friendly synthesis of core/shell ZnIn2S4/Ta3N5 heterojunction for strengthened dual-functional photocatalytic performance." International Journal of Hydrogen Energy 45, no. 55 (2020): 30341-30356.

364.   Jia, Xiaowei, Wenjing Chen, Yunfeng Li, Xuanbo Zhou, Xiaodan Yu, and Yan Xing. "Enhanced photoexcited carrier separation in Ta3N5/SrTaO2N (1D/0D) heterojunctions for highly efficient visible light-driven hydrogen evolution." Applied Surface Science 514 (2020): 145915.

365.   Hojamberdiev, Mirabbos, Ronald Vargas, Fuxiang Zhang, Katsuya Teshima, and Martin Lerch. "Perovskite BaTaO2N: From Materials Synthesis to Heterogeneous Solar Water Splitting." Advanced Science (2023): 2305179.

366.   Zhao, Tao, Zilin Ye, Mingjun Zeng, Wenbo Li, Wei Luo, Qi Xiao, and Jingsan Xu. "Molten Salt Synthesis of Mg-Doped Ta3N5 Nanoparticles with

Optimized Surface Properties for Enhanced Photocatalytic Hydrogen Evolution." Energy & Fuels (2023).

367.   Zhan, Xiaoqiang, Deliu Ou, Yapeng Zheng, Bing Li, Leyao Xu, Hongli Yang, Wenxiang Yang, Haitao Zhang, Huilin Hou, and Weiyou Yang. "Boosted photocatalytic hydrogen production over two-dimensional/two-dimensional Ta3N5/ReS2 van der Waals heterojunctions." Journal of Colloid and Interface Science 629 (2023): 455-466.

368.   Peng, ZhiYuan, Yinhua Jiang, Yan Xiao, Haiqing Xu, Wenli Zhang, and Liang Ni. "CdIn2S4 surface-decorated Ta3N5 core-shell heterostructure for improved spatial charge transfer: In-situ growth, synergistic effect and efficient dual-functional photocatalytic performance." Applied Surface Science 487 (2019): 1084-1095.

369.   Xiao, Jiadong, Junie Jhon M. Vequizo, Takashi Hisatomi, Jabor Rabeah, Mamiko Nakabayashi, Zheng Wang, Qi Xiao et al. "Simultaneously Tuning the Defects and Surface Properties of Ta3N5 Nanoparticles by Mg–Zr Codoping for Significantly Accelerated Photocatalytic H2 Evolution." Journal of the American Chemical Society 143, no. 27 (2021): 10059-10064.

370.   Hsu, Wan-Pyng, Mrinalini Mishra, Wei-Szu Liu, Chung-Yi Su, and Tsong-Pyng Perng. "Fabrication of direct Z-scheme Ta3N5-WO2.72 film heterojunction photocatalyst for enhanced hydrogen evolution." Applied Catalysis B: Environmental 201 (2017): 511-517.

371.   Zhan, Xiaoqiang, Huilin Hou, Deliu Ou, Haitao Zhang, Bing Li, Lan Jiang, Fengmei Gao, Leyao Xu, and Weiyou Yang. "Heterojunction engineering between 2D MoSe2 nanosheets and 1D Ta3N5 nanofibers for boosted photocatalytic hydrogen production." Materials Today Energy 34 (2023): 101311.

372. Jiang, Hongquan, Xuesong Li, Shuying Zang, and Wenli Zhang. "Mixed cobalt-nitrides CoxN and Ta2N bifunction-modified Ta3N5 nanosheets for enhanced photocatalytic water-splitting into hydrogen." Journal of Alloys and Compounds 854 (2021): 155328.

373. Zeng, Weixuan, Sheng Cao, Lulu Qiao, Anquan Zhu, Pengfei Tan, Yongjin Ma, Yuan Bian, Rui Dong, Ziyu Wang, and Jun Pan. "One-pot nitridation route synthesis of SrTaO2N/Ta3N5 type II heterostructure with enhanced visible-light photocatalytic activity." Journal of colloid and interface science 554 (2019): 74-79.

374. Yang, Qing, Yunfeng Li, Zhiling Xia, Wei Chang, and Yan Xing. "Preparation of two-dimensional mesoporous Ta3N5 by utilizing a biological template for enhanced photocatalytic hydrogen production." Ceramics International 48, no. 15 (2022): 22338-22345.

375. Zhan, Xiaoqiang, Haitao Zhang, Huilin Hou, Fengmei Gao, Lin Wang, Deliu Ou, Bing Li, Leyao Xu, and Weiyou Yang. "Rationally designed Ta3N5/ZnO Core-shell nanofibers for significantly boosts photocatalytic hydrogen production." Applied Surface Science 611 (2023): 155788.

376. Dao, Van-Duong, Nguyen Thi Phuong Le Chi, Doan Van Thuan, Thanh-Dong Pham, Dinh-Trinh Tran, Minh Phuong Nguyen, Phuong Thao et al. "Superior stability and photocatalytic activity of Ta3N5 sensitized/protected by conducting polymers for water splitting." Journal of Alloys and Compounds 775 (2019): 942-949.

377. Truc, Nguyen Thi Thanh, Dinh Trinh Tran, Nguyen Thi Hanh, and Thanh-Dong Pham. "Novel visible light-driven Nb-doped Ta3N5 sensitized/protected by PPy for efficient overall water splitting." International Journal of Hydrogen Energy 43, no. 33 (2018): 15898-15906.

378. Niu, Bo, and Zhenming Xu. "A stable Ta3N5@ PANI core-shell photocatalyst: shell thickness effect, high-efficient photocatalytic performance and enhanced mechanism." Journal of Catalysis 371 (2019): 175-184.

379. Putri, Lutfi K., Boon-Junn Ng, Wee-Jun Ong, Hing Wah Lee, Wei Sea Chang, and Siang-Piao Chai. "Heteroatom nitrogen-and boron-doping as a facile strategy to improve photocatalytic activity of standalone reduced graphene oxide in hydrogen evolution." ACS applied materials & interfaces 9, no. 5 (2017): 4558-4569.

380. Tanc, Yi-haO CheWa, and SianG-piaO Chai. "Functionalization of Chemically Derived Graphene for Solar Energy Conversion." Chemically Derived Graphene: Functionalization, Properties and Applications 46 (2018): 102.

381. Latorre-Sánchez, Marcos, Ana Primo, and Hermenegildo García. "P-doped graphene obtained by pyrolysis of modified alginate as a photocatalyst for hydrogen generation from water–methanol mixtures." Angewandte Chemie International Edition 52, no. 45 (2013): 11813-11816.

382. Liu, Sen, Honglei Zhu, Wenqing Yao, Kai Chen, and Daimei Chen. "One step synthesis of P-doped g-C_3N_4 with the enhanced visible light photocatalytic activity." Applied Surface Science 430 (2018): 309-315.

383. Madhusudan, Puttaswamy, S. Wageh, Ahmed A. Al-Ghamdi, Jun Zhang, Bei Cheng, and Yan Yu. "Graphene-$Zn_{0.5}Cd_{0.5}S$ nanocomposite with enhanced visible-light photocatalytic CO_2 reduction activity." Applied Surface Science 506 (2020): 144683.

384. Uğuz, Özlem, and Atıf Koca. "Hybrid photoelectrochemical–photocatalytic hydrogen evolution reaction with reduced graphene oxide–binary metal chalcogenide composites." International Journal of Energy Research 45, no. 13 (2021): 19303-19315.

385. ÖZKAYA, ALİ RIZA. "Metal chalcogenide based photocatalysts decorated with heteroatom doped reduced graphene oxide for photocatalytic and photoelectrochemical hydrogen production." (2019).

386. Park, Sunghak, Woo Je Chang, Chan Woo Lee, Sangbaek Park, Hyo-Yong Ahn, and Ki Tae Nam. "Photocatalytic hydrogen generation from hydriodic acid using methylammonium lead iodide in dynamic equilibrium with aqueous solution." Nature Energy 2, no. 1 (2016): 1-8.

387. Xu, Yang-Fan, Mu-Zi Yang, Bai-Xue Chen, Xu-Dong Wang, Hong-Yan Chen, Dai-Bin Kuang, and Cheng-Yong Su. "A CsPbBr3 perovskite quantum dot/graphene oxide composite for photocatalytic CO2 reduction." Journal of the American Chemical Society 139, no. 16 (2017): 5660-5663.

388. Wang, Guoqing, Fengjun Zhang, Yingrui Wang, and Jie Ma. "Research Progress on Photocatalytic Reduction of CO2 Based on CsPbBr3 Perovskite Materials." ChemNanoMat 8, no. 8 (2022): e202200230.

389. Chen, Zhoujie, Yangguang Hu, Jin Wang, Qing Shen, Yaohong Zhang, Chao Ding, Yu Bai, Guocan Jiang, Zhengquan Li, and Nikolai Gaponik. "Boosting photocatalytic CO2 reduction on CsPbBr3 perovskite nanocrystals by immobilizing metal complexes." Chemistry of Materials 32, no. 4 (2020): 1517-1525.

390. Xiao, Ya, and Tongming Su. "Application of MXene-Based Photocatalyst for Photocatalytic CO2 Reduction." In MXene-Based Photocatalysts, pp. 135-165. CRC Press, 2022.

391. Huang, Wenxuan, Qiliang Zhu, Yihua Zhu, Cheng Chen, and Jianhua Shen. "Tailoring perovskite quantum dots heterojunction nanocomposite toward photocatalytic reduction of CO2." Materials Today Energy (2023): 101458.

392.   Chen, Yu-Hung, Kai-An Tsai, Tzu-Wei Liu, Yao-Jen Chang, Yu-Chen Wei, Meng-Wei Zheng, Shou-Heng Liu et al. "Charge Carrier Dynamics of CsPbBr3/g-C3N4 Nanoheterostructures in Visible-Light-Driven CO2-to-CO Conversion." The Journal of Physical Chemistry Letters 14, no. 1 (2022): 122-131.

393.   Wan, Shipeng, Man Ou, Qin Zhong, and Xinming Wang. "Perovskite-type CsPbBr3 quantum dots/UiO-66(NH2) nanojunction as efficient visible-light-driven photocatalyst for CO2 reduction." Chemical Engineering Journal 358 (2019): 1287-1295.

394.   Ding, Lan, Fenghua Bai, Burenbayaer Borjigin, Yuning Li, Huiqin Li, and Xiaojing Wang. "Embedding $Cs_2AgBiBr_6$ QDs into Ce-UiO-66-H to in situ construct a novel bifunctional material for capturing and photocatalytic reduction of CO_2." Chemical Engineering Journal 446 (2022): 137102.

395.   Sun, Zhimin, Wei Fang, Lei Zhao, Hui Chen, Xuan He, Weixin Li, Pan Tian, and Zhaohui Huang. "g-C_3N_4 foam/Cu_2O QDs with excellent CO_2 adsorption and synergistic catalytic effect for photocatalytic CO_2 reduction." Environment international 130 (2019): 104898.

396.   Li, Huiling, Yonggen Lei, Ying Huang, Yueping Fang, Yuehua Xu, Li Zhu, and Xin Li. "Photocatalytic reduction of carbon dioxide to methanol by Cu_2O/SiC nanocrystallite under visible light irradiation." Journal of Natural Gas Chemistry 20, no. 2 (2011): 145-150.

397.   Olowoyo, Joshua O., Manoj Kumar, Tapan Dash, Sandeep Saran, Sahil Bhandari, and Umesh Kumar. "Self-organized copper impregnation and doping in TiO_2 with enhanced photocatalytic conversion of H_2O and CO_2 to fuel." international journal of hydrogen energy 43, no. 42 (2018): 19468-19480.

398.   Ali, Khozema Ahmed, Ahmad Zuhairi Abdullah, and Abdul Rahman Mohamed. "Visible light responsive TiO_2 nanoparticles modified using Ce and La for photocatalytic reduction of CO_2: effect of Ce dopant content." Applied Catalysis A: General 537 (2017): 111-120.

399.   Huang, Chun-ying, Rui-tang Guo, Wei-guo Pan, Jun-ying Tang, Wei-guo Zhou, Hao Qin, Xing-yu Liu, and Peng-yao Jia. "Eu-doped TiO2 nanoparticles with enhanced activity for CO2 phpotcatalytic reduction." Journal of CO2 Utilization 26 (2018): 487-495.

400.   Xiong, Zhuo, Ze Lei, Siming Ma, Xiaoxiang Chen, Bengen Gong, Yongchun Zhao, Junying Zhang, Chuguang Zheng, and Jeffrey CS Wu. "Photocatalytic CO_2 reduction over V and W codoped TiO_2 catalyst in an internal-illuminated honeycomb photoreactor under simulated sunlight irradiation." Applied Catalysis B: Environmental 219 (2017): 412-424.

401.   Alli, Yakubu Adekunle, Peter Olusakin Oladoye, Abdulmujeeb T. Onawole, Hazleen Anuar, Sheriff Adewuyi, Olutobi Daniel Ogunbiyi, and Karine Philippot. "Photocatalysts for CO2 reduction and computational insights." Fuel 344 (2023): 128101.

402.   Tsounis, Constantine, Ryo Kuriki, Kengo Shibata, Junie Jhon M. Vequizo, Daling Lu, Akira Yamakata, Osamu Ishitani, Rose Amal, and Kazuhiko Maeda. "Copolymerization approach to improving Ru (II)-complex/C3N4 hybrid photocatalysts for visible-light CO2 reduction." ACS Sustainable Chemistry & Engineering 6, no. 11 (2018): 15333-15340.

403.   Yamanaka, Ken-ichi, Shunsuke Sato, Masayo Iwaki, Tsutomu Kajino, and Takeshi Morikawa. "Photoinduced electron transfer from nitrogen-doped tantalum

oxide to adsorbed ruthenium complex." The Journal of Physical Chemistry C 115, no. 37 (2011): 18348-18353.

404.   Huang, Peipei, Sebastian A. Pantovich, Norbert O. Okolie, N. Aaron Deskins, and Gonghu Li. "Hybrid Carbon Dioxide Reduction Photocatalysts Consisting of Macrocyclic Cobalt (III) Complexes Deposited on Semiconductor Surfaces." ChemPhotoChem 4, no. 6 (2020): 420-426.

405.   Roy, Souvik, and Erwin Reisner. "Visible-light-driven CO_2 reduction by mesoporous carbon nitride modified with polymeric cobalt phthalocyanine." Angewandte Chemie International Edition 58, no. 35 (2019): 12180-12184.

406.   Woo, Sung-Jun, Sunghan Choi, So-Yoen Kim, Pil Soo Kim, Ju Hyoung Jo, Chul Hoon Kim, Ho-Jin Son, Chyongjin Pac, and Sang Ook Kang. "Highly selective and durable photochemical CO_2 reduction by molecular Mn (I) catalyst fixed on a particular dye-sensitized TiO_2 platform." ACS Catalysis 9, no. 3 (2019): 2580-2593.

407.   Xiong, Zhuo, Ze Lei, Siming Ma, Xiaoxiang Chen, Bengen Gong, Yongchun Zhao, Junying Zhang, Chuguang Zheng, and Jeffrey CS Wu. "Photocatalytic CO2 reduction over V and W codoped TiO2 catalyst in an internal-illuminated honeycomb photoreactor under simulated sunlight irradiation." Applied Catalysis B: Environmental 219 (2017): 412-424.

408.   Wang, Congjun, Robert L. Thompson, Paul Ohodnicki, John Baltrus, and Christopher Matranga. "Size-dependent photocatalytic reduction of CO 2 with PbS quantum dot sensitized TiO2 heterostructured photocatalysts." Journal of Materials Chemistry 21, no. 35 (2011): 13452-13457.

409.   Wang, Qinglong, Leiming Tao, Xingxing Jiang, Mingkui Wang, and Yan Shen. "Graphene oxide wrapped CH3NH3PbBr3 perovskite quantum dots hybrid for

photoelectrochemical CO2 reduction in organic solvents." Applied Surface Science 465 (2019): 607-613.

410.   Shu, Mengyang, Zhijie Zhang, Zhongliang Dong, and Jiayue Xu. "CsPbBr3 perovskite quantum dots anchored on multiwalled carbon nanotube for efficient CO2 photoreduction." Carbon 182 (2021): 454-462.

411.   Basri, Siti Hajar. "Fabrication and Characterization of Zinc Oxide Thin Films for Optoelectronic Applications." PhD diss., University of Malaya (Malaysia), 2017.

412.   Sharma, Anuradha, Ahmad Hosseini-Bandegharaei, Naveen Kumar, Suresh Kumar, and Kavitha Kumari. "Insight into ZnO/carbon hybrid materials for photocatalytic reduction of CO2: An in-depth review." Journal of CO2 Utilization 65 (2022): 102205.

413.   Liu, Lijun. "Controllable ZnO nanorod arrays@ carbon fibers composites: towards advanced CO_2 photocatalytic reduction catalysts." Ceramics International 42, no. 10 (2016): 12516-12520.

414.   Uchida, Hiroyuki, Shigeyoshi Itoh, and Hiroshi Yoneyama. "Photocatalytic decomposition of propyzamide using TiO_2 supported on activated carbon." Chemistry Letters 22, no. 12 (1993): 1995-1998.

415.   Pan, Jiaqi, Yingzhuo Sheng, Jingxiang Zhang, Jumeng Wei, Peng Huang, Xin Zhang, and Boxue Feng. "Preparation of carbon quantum dots/TiO 2 nanotubes composites and their visible light catalytic applications." Journal of Materials Chemistry A 2, no. 42 (2014): 18082-18086.

416.   Zhang, Qian, Cheng-Fang Lin, You Hai Jing, and Chang-Tang Chang. "Photocatalytic reduction of carbon dioxide to methanol and formic acid by graphene-TiO_2." Journal of the Air & Waste Management Association 64, no. 5 (2014): 578-585.

417.   Dehkordi, Ali Banitalebi, Abolfazl Ziarati, Jahan B. Ghasemi, and Alireza Badiei. "Preparation of hierarchical g-C3N4@TiO2 hollow spheres for enhanced visible-light induced catalytic CO2 reduction." Solar Energy 205 (2020): 465-473.

418.   Wang, Huiqin, Hongda Li, Zhuowen Chen, Jinze Li, Xin Li, Pengwei Huo, and Qian Wang. "TiO2 modified g-C3N4 with enhanced photocatalytic CO2 reduction performance." Solid State Sciences 100 (2020): 106099.

419.   El-Hossary, F. M., A. Ghitas, A. M. Abd El-Rahman, A. A. Ebnalwaled, M. Abdelhamid Shahat, and M. H. Fawey. "Effect of UV-activated TiO2 nanoparticles on the properties and performance of Pani-TiO2 nanocomposite films for solar cell applications." In IOP Conference Series: Materials Science and Engineering, vol. 956, no. 1, p. 012015. IOP Publishing, 2020.

420.   Liang, Mengfang, Timur Borjigin, Yuhao Zhang, Beihong Liu, Hui Liu, and Hong Guo. "Controlled assemble of hollow heterostructured g-C3N4@CeO2 with rich oxygen vacancies for enhanced photocatalytic CO2 reduction." Applied Catalysis B: Environmental 243 (2019): 566-575.

421.   Wang, Shaomang, Yuan Guan, Lei Lu, Zhan Shi, Shicheng Yan, and Zhigang Zou. "Effective separation and transfer of carriers into the redox sites on Ta3N5/Bi photocatalyst for promoting conversion of CO2 into CH4." Applied Catalysis B: Environmental 224 (2018): 10-16.

422.   Nguyen, Thi Dieu Cam, Thi Phuong Le Chi Nguyen, Hung Thanh Tung Mai, Van-Duong Dao, and Minh Phuong Nguyen. "Novel photocatalytic conversion of CO_2 by vanadium-doped tantalum nitride for valuable solar fuel production." Journal of catalysis 352 (2017): 67-74.

423.   Feng, Shouhua, and Ruren Xu. "New materials in hydrothermal synthesis." Accounts of chemical research 34, no. 3 (2001): 239-247.

424.   Somiya, Shigeyuki, ed. "Hydrothermal reactions for materials science and engineering: an overview of research in Japan." (2012).

425.   Lai, Jianping, Wenxin Niu, Rafael Luque, and Guobao Xu. "Solvothermal synthesis of metal nanocrystals and their applications." Nano Today 10, no. 2 (2015): 240-267.

426.   Louis, Catherine. "Deposition-precipitation synthesis of supported metal catalysts." Catalyst Preparation (2016): 333-354.

427.   Borgwardt, R. H. "Calcination kinetics and surface area of dispersed limestone particles." AIChE Journal 31, no. 1 (1985): 103-111.

428.   Nordin, Nurfatirah, Zainab Hamzah, Othman Hashim, Farizul Hafiz Kasim, and Rozaini Abdullah. "Effect of temperature in calcination process of seashells." Malaysian Journal of Analytical Sciences 19, no. 1 (2015): 65-70.

429.   Grzybowski, Bartosz A., Adam Winkleman, Jason A. Wiles, Yisroel Brumer, and George M. Whitesides. "Electrostatic self-assembly of macroscopic crystals using contact electrification." Nature materials 2, no. 4 (2003): 241-245.

430.   Galwey, Andrew Knox, and Michael E. Brown. Thermal decomposition of ionic solids: chemical properties and reactivities of ionic crystalline phases. Elsevier, 1999.

431.   Shen, Yafei. "Carbothermal synthesis of metal-functionalized nanostructures for energy and environmental applications." Journal of Materials Chemistry A 3, no. 25 (2015): 13114-13188.

432.   Mann, Stephen, Sandra L. Burkett, Sean A. Davis, Christabel E. Fowler, Neil H. Mendelson, Stephen D. Sims, Dominic Walsh, and Nicola T. Whilton. "Sol-gel synthesis of organized matter." Chemistry of materials 9, no. 11 (1997): 2300-2310.

433.   Therese, G. Helen Annal, and P. Vishnu Kamath. "Electrochemical synthesis of metal oxides and hydroxides." Chemistry of materials 12, no. 5 (2000): 1195-1204.

434.   Tsuzuki, Takuya. "Mechanochemical synthesis of metal oxide nanoparticles." Communications Chemistry 4, no. 1 (2021): 143.

435.   Hong, Zonghan, Davin Tan, Rohit Abraham John, Yong Kang Eugene Tay, Yan King Terence Ho, Xin Zhao, Tze Chien Sum, Nripan Mathews, Felipe García, and Han Sen Soo. "Completely solvent-free protocols to access phase-pure, metastable metal halide perovskites and functional photodetectors from the precursor salts." Iscience 16 (2019): 312-325.

436.   Kumar, Santosh, Miriam Regue, Mark A. Isaacs, Emma Freeman, and Salvador Eslava. "All-inorganic CsPbBr3 nanocrystals: gram-scale mechanochemical synthesis and selective photocatalytic CO2 reduction to methane." ACS Applied Energy Materials 3, no. 5 (2020): 4509-4522.

437.   Yang, Wenlong, Sarish Rehman, Xin Chu, Yanglong Hou, and Song Gao. "Transition metal (Fe, Co and Ni) carbide and nitride nanomaterials: structure, chemical synthesis and applications." ChemNanoMat 1, no. 6 (2015): 376-398.

438.   Lie, S. T., S. P. Chiew, and S. Sun. "Experimental investigation of T-tubular joint subjected to complex loading conditions." In Second International Conference on Experimental Mechanics, vol. 4317, pp. 351-356. SPIE, 2001.

439.   Mathur, S., P. Singh, and B. M. Moudgil. "Advances in selective flocculation technology for solid-solid separations." International Journal of Mineral Processing 58, no. 1-4 (2000): 201-222.

440.   Zhao, Huaizhou, Ming Lei, Xiaolong Chen, and Weihua Tang. "Facile route to metal nitrides through melamine and metal oxides." Journal of Materials Chemistry 16, no. 45 (2006): 4407-4412.

441.   Guillon, Olivier, Jesus Gonzalez-Julian, Benjamin Dargatz, Tobias Kessel, Gabi Schierning, Jan Räthel, and Mathias Herrmann. "Field-assisted sintering technology/spark plasma sintering: mechanisms, materials, and technology developments." Advanced Engineering Materials 16, no. 7 (2014): 830-849.

442.   Copeland, Llewellyn Everard, and Robert H. Bragg. "Quantitative X-ray diffraction analysis." Analytical Chemistry 30, no. 2 (1958): 196-201.

443.   Pope, Christopher G. "X-ray diffraction and the Bragg equation." Journal of chemical education 74, no. 1 (1997): 129.

444.   Kuptsov, A. H., and German Nikolaevich Zhizhin. Handbook of Fourier transform Raman and infrared spectra of polymers. Elsevier, 1998.

445.   Spence, John CH, and W. Hawkes Peter, eds. Springer handbook of microscopy. Springer, 2019.

446.   Kumar, Challa SSR, ed. UV-VIS and photoluminescence spectroscopy for nanomaterials characterization. Berlin: Springer, 2013.

447.   Crosby, Glenn A., and James N. Demas. "Measurement of photoluminescence quantum yields. Review." The Journal of Physical Chemistry 75, no. 8 (1971): 991-1024.

448.   Srinivasan, Ramanathan, and Fathima Fasmin. An Introduction to Electrochemical Impedance Spectroscopy. CRC Press, 2021.

449.   Sing, Kenneth. "The use of nitrogen adsorption for the characterisation of porous materials." Colloids and Surfaces A: Physicochemical and Engineering Aspects 187 (2001): 3-9.

450.   Vossoughi, Shapour, Gordon W. Bartlett, and G. Paul Willhite. "Development of a kinetic model for in-situ combustion and prediction of the process variables using

TGA/DSC techniques." In SPE Annual Technical Conference and Exhibition?, pp. SPE-11073. SPE, 1982.

451.   Su, Dang Sheng, Bingsen Zhang, and Robert Schlögl. "Electron Microscopy of Solid Catalyst Transforming from a Challenge to a Toolbox." Chemical reviews 115, no. 8 (2015): 2818-2882.

452.   Taylor, Temis G., and Joseph A. Tainter. "The nexus of population, energy, innovation, and complexity." American Journal of Economics and Sociology 75, no. 4 (2016): 1005-1043.

453.   Bard, Allen J. "Photoelectrochemistry." Science 207, no. 4427 (1980): 139-144.

454.   Gielen, Dolf, Ricardo Gorini, Nicholas Wagner, Rodrigo Leme, Laura Gutierrez, Gayathri Prakash, Elisa Asmelash et al. "Global energy transformation: a roadmap to 2050." (2019).

455.   Kabir, Ehsanul, Pawan Kumar, Sandeep Kumar, Adedeji A. Adelodun, and Ki-Hyun Kim. "Solar energy: Potential and future prospects." Renewable and Sustainable Energy Reviews 82 (2018): 894-900.

456.   Wells, Stephen A., Asel Sartbaeva, Vladimir L. Kuznetsov, and Peter P. Edwards. "Hydrogen economy." (2011).

457.   Fujishima, Akira, and Kenichi Honda. "Electrochemical photolysis of water at a semiconductor electrode." nature 238, no. 5358 (1972): 37-38.

458.   Qi, Jing, Wei Zhang, and Rui Cao. "Solar-to-hydrogen energy conversion based on water splitting." Advanced Energy Materials 8, no. 5 (2018): 1701620.

459.   Ganguly, Aparna, Oruganti Anjaneyulu, Kasinath Ojha, and Ashok K. Ganguli. "Oxide-based nanostructures for photocatalytic and electrocatalytic applications." CrystEngComm 17, no. 47 (2015): 8978-9001.

460. Gujral, Harpreet Singh, Gurwinder Singh, Arun V. Baskar, Xinwei Guan, Xun Geng, Abhay V. Kotkondawar, Sadhana Rayalu, Prashant Kumar, Ajay Karakoti, and Ajayan Vinu. "Metal nitride-based nanostructures for electrochemical and photocatalytic hydrogen production." Science and Technology of Advanced Materials 23, no. 1 (2022): 76-119.

461. Li, Zihao, Ling Wang, Yu Li, Yiyu Feng, and Wei Feng. "Carbon-based functional nanomaterials: Preparation, properties and applications." Composites Science and Technology 179 (2019): 10-40.

462. Reddy, N. Ramesh, U. Bhargav, M. Mamatha Kumari, K. K. Cheralathan, and M. Sakar. "Review on the interface engineering in the carbonaceous titania for the improved photocatalytic hydrogen production." International Journal of Hydrogen Energy 45, no. 13 (2020): 7584-7615.

463. Kang, Yuyang, Yongqiang Yang, Li-Chang Yin, Xiangdong Kang, Gang Liu, and Hui-Ming Cheng. "An amorphous carbon nitride photocatalyst with greatly extended visible-light-responsive range for photocatalytic hydrogen generation." Advanced materials 27, no. 31 (2015): 4572-4577.

464. Silva, Claudia G., Maria J. Sampaio, Rita RN Marques, Liliana A. Ferreira, Pedro B. Tavares, Adrian MT Silva, and Joaquim L. Faria. "Photocatalytic production of hydrogen from methanol and saccharides using carbon nanotube-TiO2 catalysts." Applied Catalysis B: Environmental 178 (2015): 82-90.

465. Yu, Zhengmin, Jianling Meng, Yang Li, and Yongdan Li. "Efficient photocatalytic hydrogen production from water over a CuO and carbon fiber comodified TiO2 nanocomposite photocatalyst." International journal of hydrogen energy 38, no. 36 (2013): 16649-16655.

466.   Li, Rengui, and Can Li. "Photocatalytic water splitting on semiconductor-based photocatalysts." In Advances in catalysis, vol. 60, pp. 1-57. Academic Press, 2017.

467.   Bellani, Sebastiano, Maria Rosa Antognazza, and Francesco Bonaccorso. "Carbon-Based Photocathode Materials for Solar Hydrogen Production." Advanced Materials 31, no. 9 (2019): 1801446.

468.   Choudhary, Ram Bilash, Sarfaraz Ansari, and Mandira Majumder. "Recent advances on redox active composites of metal-organic framework and conducting polymers as pseudocapacitor electrode material." Renewable and Sustainable Energy Reviews 145 (2021): 110854.

469.   Wang, Huanhuan, Jianyi Lin, and Ze Xiang Shen. "Polyaniline (PANi) based electrode materials for energy storage and conversion." Journal of science: Advanced materials and devices 1, no. 3 (2016): 225-255.

470.   Zhang, Peng, Jijie Zhang, and Jinlong Gong. "Tantalum-based semiconductors for solar water splitting." Chemical Society Reviews 43, no. 13 (2014): 4395-4422.

471.   Liu, Guiji, Sheng Ye, Pengli Yan, Fengqiang Xiong, Ping Fu, Zhiliang Wang, Zheng Chen, Jingying Shi, and Can Li. "Enabling an integrated tantalum nitride photoanode to approach the theoretical photocurrent limit for solar water splitting." Energy & Environmental Science 9, no. 4 (2016): 1327-1334.

472.   Ge, Jianlong, Yifan Zhang, and Soo-Jin Park. "Recent advances in carbonaceous photocatalysts with enhanced photocatalytic performances: a mini review." Materials 12, no. 12 (2019): 1916.

473.   Zhong, Miao, Takashi Hisatomi, Yutaka Sasaki, Sayaka Suzuki, Katsuya Teshima, Mamiko Nakabayashi, Naoya Shibata et al. "Highly active GaN-stabilized

Ta_3N_5 thin-film photoanode for solar water oxidation." Angewandte Chemie 129, no. 17 (2017): 4817-4821.

474.   Hou, Jungang, Yunzhen Wu, Shuyan Cao, Fei Liang, Zheshuai Lin, Zhanming Gao, and Licheng Sun. "In Situ Phase-Induced Spatial Charge Separation in Core–Shell Oxynitride Nanocube Heterojunctions Realizing Robust Solar Water Splitting." Advanced Energy Materials 7, no. 17 (2017): 1700171.

475.   Munusamy, S., K. Sivaranjan, P. Sabhapathy, V. Narayanan, Faruq Mohammad, and Suresh Sagadevan. "Enhanced electrochemical and photocatalytic activity of g-C_3N_4-PANI-PPy nanohybrids." Synthetic Metals 272 (2021): 116669.

476.   Chatterjee, Shreyam, Rama K. Layek, and Arun K. Nandi. "Changing the morphology of polyaniline from a nanotube to a flat rectangular nanopipe by polymerizing in the presence of amino-functionalized reduced graphene oxide and its resulting increase in photocurrent." Carbon 52 (2013): 509-519.

477.   Zhang, Qinghong, and Lian Gao. "Ta3N5 nanoparticles with enhanced photocatalytic efficiency under visible light irradiation." Langmuir 20, no. 22 (2004): 9821-9827.

478.   Wang, Chao, Li Wang, Jun Jin, Jing Liu, Yu Li, Min Wu, Lihua Chen, Binjie Wang, Xiaoyu Yang, and Bao-Lian Su. "Probing effective photocorrosion inhibition and highly improved photocatalytic hydrogen production on monodisperse PANI@ CdS core-shell nanospheres." Applied Catalysis B: Environmental 188 (2016): 351-359.

479.   Hou, Jungang, Zheng Wang, Chao Yang, Huijie Cheng, Shuqiang Jiao, and Hongmin Zhu. "Cobalt-bilayer catalyst decorated Ta3N5 nanorod arrays as integrated electrodes for photoelectrochemical water oxidation." Energy & Environmental Science 6, no. 11 (2013): 3322-3330.

480.   Zhang, Hao, Ruilong Zong, Jincai Zhao, and Yongfa Zhu. "Dramatic visible photocatalytic degradation performances due to synergetic effect of TiO2 with PANI." Environmental science & technology 42, no. 10 (2008): 3803-3807.

481.   Liu, Li, Lan Ding, Yongguang Liu, Weijia An, Shuanglong Lin, Yinghua Liang, and Wenquan Cui. "A stable Ag3PO4@ PANI core@ shell hybrid: enrichment photocatalytic degradation with π-π conjugation." Applied Catalysis B: Environmental 201 (2017): 92-104.

482.   Wang, Chao, Li Wang, Jun Jin, Jing Liu, Yu Li, Min Wu, Lihua Chen, Binjie Wang, Xiaoyu Yang, and Bao-Lian Su. "Probing effective photocorrosion inhibition and highly improved photocatalytic hydrogen production on monodisperse PANI@ CdS core-shell nanospheres." Applied Catalysis B: Environmental 188 (2016): 351-359.

483.   Nurlaela, Ela, Moussab Harb, Silvano Del Gobbo, Manish Vashishta, and Kazuhiro Takanabe. "Combined experimental and theoretical assessments of the lattice dynamics and optoelectronics of TaON and Ta3N5." Journal of Solid State Chemistry 229 (2015): 219-227.

484.   Liqiang, Jing, Qu Yichun, Wang Baiqi, Li Shudan, Jiang Baojiang, Yang Libin, Fu Wei, Fu Honggang, and Sun Jiazhong. "Review of photoluminescence performance of nano-sized semiconductor materials and its relationships with photocatalytic activity." Solar Energy Materials and Solar Cells 90, no. 12 (2006): 1773-1787.

485.   Zhang, Qinghong, and Lian Gao. "Ta3N5 nanoparticles with enhanced photocatalytic efficiency under visible light irradiation." Langmuir 20, no. 22 (2004): 9821-9827.

486.   Khan, Sherdil, Sérgio Ribeiro Teixeira, and Marcos Jose Leite Santos. "Controlled thermal nitridation resulting in improved structural and photoelectrochemical properties from Ta3N5 nanotubular photoanodes." RSC advances 5, no. 125 (2015): 103284-103291.

487.   Pihosh, Yuriy, Vikas Nandal, Ryota Shoji, Raman Bekarevich, Tomohiro Higashi, Valeria Nicolosi, Hiroyuki Matsuzaki, Kazuhiko Seki, and Kazunari Domen. "Nanostructured Tantalum Nitride for Enhanced Solar Water Splitting." ACS Energy Letters 8, no. 5 (2023): 2106-2112.

488.   Zheng, Yaru, Jie Dong, Cunping Huang, Ligang Xia, Qiang Wu, Qunjie Xu, and Weifeng Yao. "Co-doped Mo-Mo$_2$C cocatalyst for enhanced g-C$_3$N$_4$ photocatalytic H$_2$ evolution." Applied Catalysis B: Environmental 260 (2020): 118220.

489.   Yang, Chao, Sushu Zhang, Yi Huang, Kangle Lv, Shun Fang, Xiaofeng Wu, Qin Li, and Jiajie Fan. "Sharply increasing the visible photoreactivity of g-C$_3$N$_4$ by breaking the intralayered hydrogen bonds." Applied Surface Science 505 (2020): 144654.

490.   Paulraj, P., Ahmad Umar, K. Rajendran, A. Manikandan, R. Kumar, E. Manikandan, K. Pandian et al. "Solid-state synthesis of Ag-doped PANI nanocomposites for their end-use as an electrochemical sensor for hydrogen peroxide and dopamine." Electrochimica Acta 363 (2020): 137158.

491.   Dao, Van-Duong, Nguyen Thi Phuong Le Chi, Doan Van Thuan, Thanh-Dong Pham, Dinh-Trinh Tran, Minh Phuong Nguyen, Phuong Thao et al. "Superior stability and photocatalytic activity of Ta3N5 sensitized/protected by conducting polymers for water splitting." Journal of Alloys and Compounds 775 (2019): 942-949.

492. Chae, Sang Youn, and Eun Duck Park. "Enhanced photoelectrochemical stability of Ta3N5 in the acidic electrolyte conditions." Applied Surface Science 583 (2022): 152566.

493. Munusamy, S., K. Sivaranjan, P. Sabhapathy, P. S. Ramesh, V. Narayanan, Faruq Mohammad, and Suresh Sagadevan. "Electrochemical and photocatalytic studies of Ta3N5-TaON-PEDOT-PANI nanohybrids." Chemical Physics Letters 780 (2021): 138947.

494. Yu, Zong Bao, Ying Peng Xie, Gang Liu, Gao Qing Max Lu, Xiu Liang Ma, and Hui-Ming Cheng. "Self-assembled CdS/Au/ZnO heterostructure induced by surface polar charges for efficient photocatalytic hydrogen evolution." Journal of Materials Chemistry A 1, no. 8 (2013): 2773-2776.

495. Hu, Yidong, Gang Chen, Chunmei Li, Yansong Zhou, Jingxue Sun, Sue Hao, and Zhonghui Han. "Fabrication of {010} facet dominant BiTaO 4 single-crystal nanoplates for efficient photocatalytic performance." Journal of Materials Chemistry A 4, no. 14 (2016): 5274-5281.

496. Jiang, Hongquan, Xuesong Li, Shuying Zang, and Wenli Zhang. "Mixed cobalt-nitrides CoxN and Ta2N bifunction-modified Ta3N5 nanosheets for enhanced photocatalytic water-splitting into hydrogen." Journal of Alloys and Compounds 854 (2021): 155328.

497. Omer, Abdeen Mustafa. "Demand for energy efficient, eco-friendly environment, applications and sustainable development." Energy 5000 (2013): 10000.

498. Moustakas, K., M. Loizidou, M. Rehan, and A. S. Nizami. "A review of recent developments in renewable and sustainable energy systems: Key challenges and future perspective." Renewable and Sustainable Energy Reviews 119 (2020): 109418.

499. Xu, Jiuping, Qiulin Li, Heping Xie, Ting Ni, and Chi Ouyang. "Tech-integrated paradigm based approaches towards carbon-free hydrogen production." Renewable and Sustainable Energy Reviews 82 (2018): 4279-4295.

500. Shen, Shaohua, Jinwen Shi, Penghui Guo, and Liejin Guo. "Visible-light-driven photocatalytic water splitting on nanostructured semiconducting materials." International Journal of Nanotechnology 8, no. 6-7 (2011): 523-591.

501. Wang, Zheng, Yasunobu Inoue, Takashi Hisatomi, Ryo Ishikawa, Qian Wang, Tsuyoshi Takata, Shanshan Chen, Naoya Shibata, Yuichi Ikuhara, and Kazunari Domen. "Overall water splitting by Ta_3N_5 nanorod single crystals grown on the edges of $KTaO_3$ particles." Nature Catalysis 1, no. 10 (2018): 756-763.

502. Nurlaela, Ela, Samy Ould-Chikh, Moussab Harb, Silvano Del Gobbo, Mimoun Aouine, Eric Puzenat, Philippe Sautet, Kazunari Domen, Jean-Marie Basset, and Kazuhiro Takanabe. "Critical role of the semiconductor–electrolyte Interface in photocatalytic performance for water-splitting reactions using Ta3N5 particles." Chemistry of Materials 26, no. 16 (2014): 4812-4825.

503. Zhou, Chenguang, Junkang Zhou, Lei Lu, Jiajia Wang, Zhan Shi, Bing Wang, Lang Pei, Shicheng Yan, Yu Zhentao, and Zhigang Zou. "Surface electric field driven directional charge separation on Ta3N5 cuboids enhancing photocatalytic solar energy conversion." Applied Catalysis B: Environmental 237 (2018): 742-752.752

504. Fu, Cen-Feng, Xiaojun Wu, and Jinlong Yang. "Material design for photocatalytic water splitting from a theoretical perspective." Advanced Materials 30, no. 48 (2018): 1802106.

505. Wei, Xiaoqian, Xinghou He, Pian Wu, Fangjie Gong, Danqi Wang, Shanlin Wang, Siyu Lu et al. "Recent advances in the design of semiconductor hollow

microspheres for enhanced photocatalytic water splitting." International Journal of Hydrogen Energy 46, no. 55 (2021): 27974-27996.

506.   Wang, Tong, and Tao Xu. "Effects of vanadium doping on microstructures and optical properties of TiO2." Ceramics International 43, no. 1 (2017): 1558-1564.

507.   Chang, Sue-min, and Wei-szu Liu. "Surface doping is more beneficial than bulk doping to the photocatalytic activity of vanadium-doped TiO2." Applied Catalysis B: Environmental 101, no. 3-4 (2011): 333-342.

508.   Liu, Hongyan, and Lian Gao. "(Sulfur, Nitrogen)-Codoped Rutile-Titanium Dioxide as a Visible-Light-Activated Photocatalyst." Journal of the American Ceramic Society 87, no. 8 (2004): 1582-1584.

509.   Umebayashi, T., T. Yamaki, S. Yamamoto, A. Miyashita, S. Tanaka, T. Sumita, and K. Asai. "Sulfur-doping of rutile-titanium dioxide by ion implantation: photocurrent spectroscopy and first-principles band calculation studies." Journal of Applied Physics 93, no. 9 (2003): 5156-5160.

510.   Namsheer, K., and Chandra Sekhar Rout. "Conducting polymers: A comprehensive review on recent advances in synthesis, properties and applications." RSC advances 11, no. 10 (2021): 5659-5697.

511.   Sarkar, Sudipta, Eric Guibal, Françoise Quignard, and A. K. SenGupta. "Polymer-supported metals and metal oxide nanoparticles: synthesis, characterization, and applications." Journal of Nanoparticle Research 14 (2012): 1-24.

512.   Vijayakanth, Thangavel, David J. Liptrot, Ehud Gazit, Ramamoorthy Boomishankar, and Chris R. Bowen. "Recent advances in organic and organic–inorganic hybrid materials for piezoelectric mechanical energy harvesting." Advanced Functional Materials 32, no. 17 (2022): 2109492.

513.   Kumar, Ravindra, Satyendra Singh, and B. C. Yadav. "Conducting polymers: synthesis, properties and applications." International Advanced Research Journal in Science, Engineering and Technology 2, no. 11 (2015): 110-124.

514.   Riaz, Ufana, S. M. Ashraf, and Jyoti Kashyap. "Enhancement of photocatalytic properties of transitional metal oxides using conducting polymers: A mini review." Materials Research Bulletin 71 (2015): 75-90.

515.   Lu, Xiaofeng, Wanjin Zhang, Ce Wang, Ten-Chin Wen, and Yen Wei. "One-dimensional conducting polymer nanocomposites: Synthesis, properties and applications." Progress in Polymer Science 36, no. 5 (2011): 671-712.

516.   Le Chi, Nguyen Thi Phuong, Nguyen Thi Dieu Cam, Doan Van Thuan, Thanh Tam Truong, Nguyen Thi Thanh Truc, Cao Van Hoang, Tran Thi Thu Phuong et al. "Synthesis of vanadium doped tantalum oxy-nitride for photocatalytic reduction of carbon dioxide under visible light." Applied Surface Science 467 (2019): 1249-1255.

517.   Higgins, Drew, Md Ariful Hoque, Min Ho Seo, Rongyue Wang, Fathy Hassan, Ja-Yeon Choi, Mark Pritzker, Aiping Yu, Jiujun Zhang, and Zhongwei Chen. "Development and simulation of sulfur-doped graphene supported platinum with exemplary stability and activity towards oxygen reduction." Advanced Functional Materials 24, no. 27 (2014): 4325-4336.

518.   Singla, Shelly, Pooja Singh, Soumen Basu, and Pooja Devi. "BiVO4/MoSe2 Photocatalyst for the photocatalytic Abatement of tetracycline and photoelectrocatalytic water splitting." Materials Chemistry and Physics 295 (2023): 127111.

519.   Nasir, Muhammad, Zhenhao Xi, Mingyang Xing, Jinlong Zhang, Feng Chen, Baozhu Tian, and Segomotso Bagwasi. "Study of synergistic effect of Ce-and S-

codoping on the enhancement of visible-light photocatalytic activity of TiO_2." The Journal of Physical Chemistry C 117, no. 18 (2013): 9520-9528.

520.   Dong, Beibei, Junyan Cui, Yuying Gao, Yu Qi, Fuxiang Zhang, and Can Li. "Heterostructure of 1D Ta_3N_5 nanorod/$BaTaO_2N$ nanoparticle fabricated by a one-step ammonia thermal route for remarkably promoted solar hydrogen production." Advanced Materials 31, no. 15 (2019): 1808185.

521.   Gomez, Humberto, Manoj K. Ram, Farah Alvi, Elias Stefanakos, and Ashok Kumar. "Novel synthesis, characterization, and corrosion inhibition properties of nanodiamond− polyaniline films." The Journal of Physical Chemistry C 114, no. 44 (2010): 18797-18804.

522.   Hadjiivanov, Konstantin. "Use of overtones and combination modes for the identification of surface NO x anionic species by IR spectroscopy." Catalysis letters 68 (2000): 157-161.

523.   Nekrasov, A. A., O. D. Iakobson, O. L. Gribkova, and S. I. Pozin. "Raman spectroelectrochemical monitoring of conducting polymer electrosynthesis on reflective metallic electrode: Effects due to double excitation of the electrode/film/solution interfaces." Journal of Electroanalytical Chemistry 873 (2020): 114415.

524.   De Matas, M., H. G. M. Edwards, E. E. Lawson, L. Shields, and P. York. "FT-Raman spectroscopic investigation of a pseudopolymorphic transition in caffeine hydrate." Journal of molecular structure 440, no. 1-3 (1998): 97-104.

525.   Ou, Duan Li, and Angela B. Seddon. "Near-and mid-infrared spectroscopy of sol–gel derived ormosils: vinyl and phenyl silicates." Journal of non-crystalline solids 210, no. 2-3 (1997): 187-203.

526.   Asemani, Morteza, and Ahmad Reza Rabbani. "Detailed FTIR spectroscopy characterization of crude oil extracted asphaltenes: Curve resolve of overlapping bands." Journal of Petroleum Science and Engineering 185 (2020): 106618.

527.   Bonelli, Barbara, Barbara Onida, Bice Fubini, C. Otero Arean, and Edoardo Garrone. "Vibrational and thermodynamic study of the adsorption of carbon dioxide on the zeolite Na− ZSM-5." Langmuir 16, no. 11 (2000): 4976-4983.

528.   Lahmer, M. A. "Effect of (S, V) codoping on the electronic, optical and photocatalytic properties of β-TaON: A DFT+ U study." Computational Condensed Matter 32 (2022): 00706.

529.   Peng, ZhiYuan, Yinhua Jiang, Yan Xiao, Haiqing Xu, Wenli Zhang, and Liang Ni. "$CdIn_2S_4$ surface-decorated Ta_3N_5 core-shell heterostructure for improved spatial charge transfer: In-situ growth, synergistic effect and efficient dual-functional photocatalytic performance." Applied Surface Science 487 (2019): 1084-1095.

530.   Fan, Gongduan, Xia Li, Xiaolei Chen, Yifan You, Wenxin Dai, Fangshu Qu, Dingsheng Tang, and Zhongsen Yan. "Z-scheme Ag_3PO_4@ polyaniline core-shell nanocomposite with high visible light photocatalytic performance for Microcystis aeruginosa inactivation." Chemical Engineering Journal 427 (2022): 132005.

531.   Narkeviciute, Ieva, and Thomas F. Jaramillo. "Effects of Ta3N5 Morphology and Composition on the Performance of Si-Ta3N5 Photoanodes." Solar RRL 1, no. 11 (2017): 1700121.

532.   Wang, Xin, Siqing Ma, Boyan Liu, Songcan Wang, and Wei Huang. "Imperfect makes perfect: defect engineering of photoelectrodes towards efficient photoelectrochemical water splitting." Chemical Communications (2023).

533.   Dao, Van-Duong, Nguyen Thi Phuong Le Chi, Doan Van Thuan, Thanh-Dong Pham, Dinh-Trinh Tran, Minh Phuong Nguyen, Phuong Thao et al. "Superior stability

and photocatalytic activity of Ta3N5 sensitized/protected by conducting polymers for water splitting." Journal of Alloys and Compounds 775 (2019): 942-949.

534.   Nagar, Aashna, and Soumen Basu. "Fabrication of 3D porous peony flower-like β-Bi_2O_3/BiOCl heterostructure for synergistically boosting the visible-light-driven degradation of organic pollutants." Environmental Technology & Innovation 24 (2021): 101956.

535.   Zhan, Xiaoqiang, Deliu Ou, Yapeng Zheng, Bing Li, Leyao Xu, Hongli Yang, Wenxiang Yang, Haitao Zhang, Huilin Hou, and Weiyou Yang. "Boosted photocatalytic hydrogen production over two-dimensional/two-dimensional Ta_3N_5/ReS_2 van der Waals heterojunctions." Journal of Colloid and Interface Science 629 (2023): 455-466.

536.   Fu, Hai-hai, Long Chen, Haojie Gao, Xiaokun Yu, Juan Hou, Gang Wang, Feng Yu et al. "Walnut shell-derived hierarchical porous carbon with high performances for electrocatalytic hydrogen evolution and symmetry supercapacitors." International journal of hydrogen energy 45, no. 1 (2020): 443-451.

537.   Chae, Sang Youn, and Eun Duck Park. "Enhanced photoelectrochemical stability of Ta3N5 in the acidic electrolyte conditions." Applied Surface Science 583 (2022): 152566.

538.   Cravanzola, Sara, Federico Cesano, Fulvio Gaziano, and Domenica Scarano. "Sulfur-doped TiO2: Structure and surface properties." Catalysts 7, no. 7 (2017): 214.

539.   Zhou, Wenfang, Qingju Liu, Zhongqi Zhu, and Ji Zhang. "Preparation and properties of vanadium-doped TiO2 photocatalysts." Journal of Physics D: Applied Physics 43, no. 3 (2010): 035301.

540.   Zhang, Jun, Tao Li, Jili Zheng, YanQiu Xiao, Xiaotian Li, Jun Song, Chuanxiao Cheng, Wei Yang, and Gang Chen. "Hole transport layer in photoelectrochemical water splitting." Solar RRL.

541.   Zeng, Weixuan, Sheng Cao, Lulu Qiao, Anquan Zhu, Pengfei Tan, Yongjin Ma, Yuan Bian, Rui Dong, Ziyu Wang, and Jun Pan. "One-pot nitridation route synthesis of SrTaO2N/Ta3N5 type II heterostructure with enhanced visible-light photocatalytic activity." Journal of colloid and interface science 554 (2019): 74-79.

542.   Zhu, Qian, Yan Wang, Fu Chen, Xiaohong Yang, Hui Ou, Shixian Xiong, and Haitao Fu. "Enhanced photocatalytic H2 production performance of Au@Cu2O-Ta3N5 discrete ternary core-shell spheres." Applied Surface Science (2023): 157682.

543.   Niu, Bo, and Zhenming Xu. "A stable Ta3N5@PANI core-shell photocatalyst: shell thickness effect, high-efficient photocatalytic performance and enhanced mechanism." Journal of Catalysis 371 (2019): 175-184.

544.   Tahir, Muhammad, and NorAishah Saidina Amin. "Performance analysis of nanostructured NiO–In2O3/TiO2 catalyst for CO2 photoreduction with H2 in a monolith photoreactor." Chemical Engineering Journal 285 (2016): 635-649.

545.   Gao, Tian, YiLi Zhang, YaQin Qiu, Zhuo Xiong, JianPing Yang, YongChun Zhao, and JunYing Zhang. "Mercury removal performance over a Ce-doped VW/TiO2 catalyst in an internally illuminated honeycomb photoreactor." Science China Technological Sciences 64, no. 11 (2021): 2441-2452.

546.   Qazi, Umair Yaqub. "Future of hydrogen as an alternative fuel for next-generation industrial applications; challenges and expected opportunities." Energies 15, no. 13 (2022): 4741.

547. Wang, Zheng, Can Li, and Kazunari Domen. "Recent developments in heterogeneous photocatalysts for solar-driven overall water splitting." Chemical Society Reviews 48, no. 7 (2019): 2109-2125.

548. Moniz, Savio JA. "Recent Developments in Heterostructure-Based Catalysts for Water Splitting." Visible Light-Active Photocatalysis: Nanostructured Catalyst Design, Mechanisms, and Applications (2018): 191-226.

549. Higashi, Tomohiro, Hiroshi Nishiyama, Vikas Nandal, Yuriy Pihosh, Yudai Kawase, Ryota Shoji, Mamiko Nakabayashi et al. "Design of semitransparent tantalum nitride photoanode for efficient and durable solar water splitting." Energy & Environmental Science 15, no. 11 (2022): 4761-4775.

550. Eichhorn, Johanna, Simon P. Lechner, Chang-Ming Jiang, Giulia Folchi Heunecke, Frans Munnik, and Ian D. Sharp. "Indirect bandgap, optoelectronic properties, and photoelectrochemical characteristics of high-purity Ta3N5 photoelectrodes." Journal of Materials Chemistry A 9, no. 36 (2021): 20653-20663.

551. Kannichankandy, Drishya, Pratik M. Pataniya, Chetan K. Zankat, Mohit Tannarana, Vivek M. Pathak, Gunvant K. Solanki, and Kireet D. Patel. "Paper based organic–inorganic hybrid photodetector for visible light detection." Applied Surface Science 524 (2020): 146589.

552. Chang, Jui-Che, Jens Birch, Gueorgui Kostov Gueorguiev, Babak Bakhit, Grzegorz Greczynski, Fredrik Eriksson, Per Sandström, Lars Hultman, and Ching-Lien Hsiao. "Domain epitaxial growth of Ta3N5 film on c-plane sapphire substrate." Surface and Coatings Technology 443 (2022): 128581.

553. Fu, Jie, Zeyu Fan, Mamiko Nakabayashi, Huanxin Ju, Nadiia Pastukhova, Yequan Xiao, Chao Feng, Naoya Shibata, Kazunari Domen, and Yanbo Li. "Interface

engineering of Ta3N5 thin film photoanode for highly efficient photoelectrochemical water splitting." Nature communications 13, no. 1 (2022): 729.

554.   Tang, Weiqiang, Rongjie Yang, Tao Zeng, Jianmin Li, Jinghui Hu, Xuyuan Zhou, Enzhou Jiang, and Yuxuan Zhang. "Positive effects of organic fluoride on reduction of slag accumulation in static testing of solid rocket motors of different diameters." Acta Astronautica 194 (2022): 277-285.

555.   Chen, Shanshan, Yu Qi, Qian Ding, Zheng Li, Junyan Cui, Fuxiang Zhang, and Can Li. "Magnesia interface nanolayer modification of Pt/Ta3N5 for promoted photocatalytic hydrogen production under visible light irradiation." Journal of Catalysis 339 (2016): 77-83.

556.   Yang, Qing, Yunfeng Li, Zhiling Xia, Wei Chang, and Yan Xing. "Preparation of two-dimensional mesoporous Ta3N5 by utilizing a biological template for enhanced photocatalytic hydrogen production." Ceramics International 48, no. 15 (2022): 22338-22345.

557.   Truc, Nguyen Thi Thanh, Dinh Trinh Tran, Nguyen Thi Hanh, and Thanh-Dong Pham. "Novel visible light-driven Nb-doped Ta3N5 sensitized/protected by PPy for efficient overall water splitting." International Journal of Hydrogen Energy 43, no. 33 (2018): 15898-15906.

➢ **Achievments**
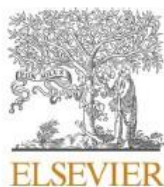
Office of the Principal Scientific Adviser to the Government of India

WASTE TO WEALTH

INVEST INDIA
NATIONAL INVESTMENT PROMOTION & FACILITATION AGENCY

This is to certify

Monika Sindhu

has been awarded the

Swachhta Saarthi Fellowship
2021-22

Thank you for your contribution
to waste management. every step matters!

Dr. (Mrs.) Parvinder Maini
Scientific Secretary
Office of the Principal Scientific Adviser
to the Government of India

Fabrication and characterization of novel V, S co-doped Ta_3N_5 protected with PANI composite materials for hydrogen generation from light-driven water splitting

Monika Sindhu [a], Ajit Sharma [a,*,b], Karan Singh Maan [a], Vijaykumar Patel [a],
Prabal Pratap Singh [c], Van-Huy Nguyen [d,*]

[a] Department of Chemistry, School of Chemical Engineering and Physical Sciences, Lovely Professional University, Jalandhar, 144411, India
[b] Institute of Advanced Materials, IAAM, Gammalkilsvägen 18, Ulrika, 590 53, Sweden
[c] Department of Chemistry, GLA University, Mathura (UP), India, 281406
[d] Centre for Herbal Pharmacology and Environmental Sustainability, Chettinad Hospital and Research Institute, Chettinad Academy of Research and Education, Kelambakkam, 603103, Tamil Nadu, India

ARTICLE INFO

ABSTRACT

Background: The rising global demand for energy and the associated environmental problems calls for the rapid development of renewable and eco-friendly energy systems. Due to advantages like low cost, and high catalytic efficiency, V, S co-doped Ta_3N_5 protected with polyaniline (PANI) photocatalyst as a photocatalyst has attracted more and more attention.

Methods: Herein, co-doped $V@S-Ta_3N_5$/PANI composite materials were synthesized by two different approaches. Fourier transform infrared spectra (FTIR), X-ray diffraction (XRD), and field emission scanning electron microscopy (FE-SEM) were used to analyze the structural and morphological properties of the synthesized composites. In contrast, the optical properties were analyzed with the help of UV–Vis diffuse reflectance spectroscopy (DRS) techniques. Electrical impedance spectroscopy (EIS) and photoluminescence (PL) tests were used to investigate charge separation efficiency and the degree of recombination.

Significant findings: As a dopant, V and S were incorporated into the lattice of Ta_3N_5, where their presence as an intermediate between the valance and conduction band of Ta_3Na_5 narrowed down its band gap. These intermediate bands of the metal (V) and non-metal (S) dopant also exhibit superior efficiency in electron-hole pair separation and prevent their recombination, extending the period of the electron-hole pairs. As a sensitizer/

Characteristic studies of Ta₃N₅/BSC@PANI nanocomposites for hydrogen production via water-splitting under visible light irradiation

Monika Sindhu[a], Ajit Sharma[a,b,*], Vijaykumar Patel[a], Amika Gahlawat[a], Prabal Pratap Singh[c], Karan Singh Maan[a], Deepak Kumar[a], Van-Huy Nguyen[d,**]

[a] Department of Chemistry, School of Chemical Engineering and Physical Sciences, Lovely Professional University, Jalandhar 144411, India
[b] Institute of Advanced Materials, IAAM, Gammalkilsvägen 18, Ulrika 590 53, Sweden
[c] Department of Chemistry, GLA University, Mathura 281406, Uttar Pradesh, India
[d] Centre for Herbal Pharmacology and Environmental Sustainability, Chettinad Hospital and Research Institute, Chettinad, Academy of Research and Education, Kelambakkam 603103, Tamil Nadu, India

ABSTRACT

Hydrogen (H₂) production in water-splitting could be significantly increased by designing cost-effective photocatalysts with remarkable performance. The main objective of this study is to recognize the behavior of soot carbon-based metal nitrides nanocomposites on its photocatalytic activity when exposed to solar lights. This study synthesized a p-n heterojunction Ta₃N₅/PANI composite photocatalyst modified by eco-friendly and low-cost biomass soot carbon (BSC) using hydrothermal and chemisorption methods. BSC materials are photoactive when exposed to UV light because of their band gap ($E_g < 4$ eV), indicating they behave as semiconductors. Compared to pure Ta₃N₅, the hydrogen production rate of a photocatalyst containing polyaniline (PANI) can reach up to 76.9 µmol g^{-1} h^{-1}, equivalent to 3.42 times superior to pristine Ta₃N₅. The formation of a p-n heterojunction at the interface of PANI and Ta₃N₅ was primarily responsible for improving the H₂ evolution activity. This successfully prevents the self-photocorrosion of Ta₃N₅ by providing a rapid route for the migration and separation of photogenerated charges. It also confirms the long-term stability of the materials by repeating the experiments up to 6 cycles with more than 95 %.

Synthesis and characterization of Bismuth titanate perovskite materials for hydrogen production

Amika Gahlawat [a], Monika Sindhu [a], Ajit Sharma [a,d,*], Karan Singh Maan [a], Prabal Pratap Singh [b], Radhamanohar Aepuru [c], Deepak Kumar [a,*]

[a] Deptartment of Chemistry, School of Chemical Engineering and Physical Sciences, Lovely Professional University Phagwara, Punjab 144411. India
[b] Department of Chemistry, GLA University, Mathura, Uttar Pradesh 281406, India
[c] Departamento de Ingeniería Mecánica, Facultad de Ingeniería, Universidad Tecnológica Metropolitana, Santiago, Chile
[d] Institute of Advanced Materials, IAAM, Gammalkilsvägen 18, Ulrika, 590 53, Sweden

ARTICLE INFO

ABSTRACT

In this work, a simple, low-cost, precursor free and a single step synthetic technique has been used for synthesis of Bismuth titanate (BT) perovskite nanomaterials, under surfactant free conditions. The powdered X-ray diffraction method has been employed for confirmation of crystal structure and surface morphology of synthe-sized nanoparticles were confirmed by FESEM analysis. The nanoparticles showed the band gap of 3.25 eV, calculated with the help of Tauc plot by diffused reflectance spectroscopy (DRS-UV). The efficiency of nano-particles to act as photocatalyst was assessed by hydrogen evolution reaction carried out by water splitting, utilizing a photochemical cell reactor having xenon lamp. The reaction was carried out in the presence of triethanolamine (TEOA) and methanol acting as scavengers. It was reported that maximum hydrogen yield 39.24 μmol/g was obtained with methanol.

1. Introduction

because of absorption of light in visible region [7–10].The valence band of bismuth doped semiconducting material is composed of hybrid or

Nb-Ta$_3$N$_5$ protected with PANI nanocomposite for enhanced photocatalytic water-splitting towards hydrogen production under visible light irradiation

Monika Sindhu[1], Ajit Sharma[1]*, Karan Singh Maan[1], Vijaykumar Patel[1], Prabal Pratap Singh[2], Ba-Son Nguyen[3], Van-Huy Nguyen[4]*, Dai-Viet N. Vo[5]

[1]Department of Chemistry, School of Chemical Engineering and Physical Sciences, Lovely Professional University, Jalandhar, 144411, India

[2]Department of Chemistry, GLA University, Mathura (UP), India-281406

[3]Institute of Intelligent and Interactive Technologies, College of Technology and Design, University of Economics Ho Chi Minh city (UEH)

[4]Faculty of Allied Health Sciences, Chettinad Hospital and Research Institute, Chettinad Academy of Research and Education, Kelambakkam-603103, Tamil Nadu, India

[5]Institute of Applied Technology and Sustainable Development, Nguyen Tat Thanh University, Ho Chi Minh City, 755414, Viet Nam

* Corresponding authors: Ajit Sharma (ajitsharma2003@gmail.com); Van-Huy Nguyen (vhnguyen.ChE@gmail.com)

Nutshell-derived efficient carbon nanomaterials as a potential smart electrode material for electrocatalytic hydrogen production

Monika Sindhu[1], Ajit Sharma[1*, 2, 3], Dai-Viet N. Vo[4]

[1]School of Chemical Engineering and Physical Science, Lovely Professional University, Phagwara, Punjab, India
[2]KTH Engineering Sciences in Chemistry, Biotechnology and Health, Stockholm, Sweden
[3]Institute of Advanced Materials, IAAM, Sweden
[4]Institute of Applied Technology and Sustainable Development, Nguyen Tat Thanh University, Ho Chi Minh City, 755414, Viet Nam

Corresponding author: ajitsharma2003@gmail.com

Abstract

As part of on-going exertions by researchers to develop sustainable solutions to curtail the problem of continuous emissions of greenhouse gases produced by the use of fossil fuels, attention has been directed toward biomass (organic matter that can be converted into useful energy). Green nanotechnology is advancing to address society's global sustainability disquiets by recycling a variety of industrial and bio-wastes to generate functional carbonaceous nanomaterials that include biochar, activated carbon. Biomass can serve as the

ORIGINAL ARTICLE

Facile Synthesis of CdS Doped Bismuth Titanate Perovskites: A Cocatalyst-Free Promising Photocatalyst for Hydrogen Generation

Amika[1] · Monika Sindhu[1] · Ajit Sharma[1,2] · Karan Singh Maan[1] · Prabal Pratap Singh[3] · Shubham Ladiya[1] · Deepak Kumar[1] · Rajesh Sharma[4] · Pardeep Dahiya[5]

Abstract

A low temperature hydrothermal method has been adapted for synthesis of Bismuth titanate based perovskite nanomaterials taking Bismuth nitrate pentahydrate ($Bi(NO_3)_2 \cdot 5H_2O$) and titanium isopropoxide as precursors. Different concentrations (0.1%, 0.3% and 0.6% w/w) of Cadmium sulfide nanoparticles were introduced into the lattice site of Bismuth titanate by means of mechanical method for a cocatalyst free hydrogen generation by photocatalytic splitting of water. The powdered X-ray diffraction method was employed for determination of crystallite size (30.20 nm) and spherical morphology of as-synthesized nanoparticles has been deduced from FESEM. The photochemical reactor having Xenon lamp was used to check the photocatalytic performance of the nanoparticles for hydrogen generation in presence of different scavengers. It was observed that out of various scavengers, 0.6% CdS doped BT shows maximum hydrogen yield of 171 µmol/g with methanol and for hydrogen generation the order of scavengers is Methanol > EDTA > TEOA for 0.6% CdS doped Bismuth titanates.

Graphical abstract
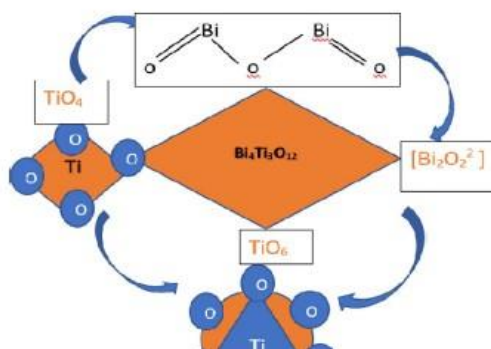
Review

The progress and roadmap of metal–organic frameworks for high-performance supercapacitors

P.E. Lokhande [a], Sahana Kulkarni [b], Sandip Chakrabarti [b,*], H.M. Pathan [c], Monika Sindhu [d], Deepak Kumar [d,*], Jashanpreet Singh [d], Anupam Kumar [e], Yogendra Kumar Mishra [f], Dana-Cristina Toncu [g,h], Mikael Syväjärvi [h], Ajit Sharma [d,h,*], Ashutosh Tiwari [h,*]

[a] Department of Mechanical, Manufacturing and Biomedical Engineering, Trinity College Dublin, Ireland
[b] Amity Institute of Nanotechnology, Amity University, Noida, UP 201303, India
[c] Advanced Physics Laboratory, Department of Physics, Savitribai Phule Pune University, Pune 411007, India
[d] Department of Chemistry, School of Chemical Engineering and Physical Sciences, Lovely Professional University, Phagwara 144411, India
[e] Department of Biotechnology, School of Bioengineering and Biosciences, Lovely Professional University, Phagwara 144411, India
[f] Mads Clausen Institute, NanoSYD, University of Southern Denmark, Alsion 2, 6400 Sønderborg, Denmark
[g] School of Chemistry, University College Dublin, Belfield, Dublin 4, Ireland
[h] Institute of Advanced Materials, IAAM, Gammalkilsvägen 18, Ulrika 590 53, Sweden

ARTICLE INFO

ABSTRACT

The ever-increasing energy demand has led to the need of new smart materials to overcome the present crises in energy generation and storage. Amongst various cross-functional platforms, metal–organic framework (MOF) has turned up as an efficient class of porous organic–inorganic ordered structure due to their flexibility, tunable structures, and composition, which allow them to play an important role in building blocks for synthesizing highly efficient energy materials for advanced applications. Recent progress in metal–organic framework based derived materials have revealed impressive efficiency in energy conversion and storage by overcoming many of the challenges which are generally faced by the individual materials and/or compounds utilized in fabrication of supercapacitor electrodes. In this review, we discuss the performances of different types of nano/micro hybrid structures derived from the metal–organic framework as electrode materials for supercapacitor applications. For the detailed understanding, a special section is devoted to MOF precursors-based electrodes as advanced energy materials. In each section, the emerging feasibility of large-scale production, challenges and future perspectives is system-atically discussed. Further open strategies for the MOF-based supercapacitors that could accomplish high

Green Carbon Dots: Advanced Material For Renewable Energy Sources

Monika Sindhar, Pinku Nath, Ajit Kumar Sharma*

Department of Chemical Engineering and Physical Sciences, Lovely Professional University, Jalandhar, Punjab, India

(*Corresponding author: Dr Ajit K Sharma; ajitsharmaiit@gmail.com)

Abstract: Fluorescent carbon dots (CDs) are an emerging category of nanomaterials in the carbon family. There are different inexpensive and renewable resources that can be used to synthesize green CDs, which include received immense consideration from researchers because of their improved aqueous solubility, high biocompatibility, and eco-friendly nature compared with chemically derived CDs. Additional surface passivation is not necessary as heteroatoms be present on the surface of green CDs in the form of amine, hydroxyl, carboxyl, or thiol functional groups, which be able to improve their physicochemical properties, quantum yield, and the probability of visible light absorption. Green CDs boast potential applications in the fields of bioimaging, drug/gene delivery systems, catalysis, and sensing. While their discovery, there have been several review articles that describe the synthesis of green CDs and some of their applications. Nevertheless, there are no review articles describing the synthesis and complete applications of green CDs. Here, we provide detailed information concerning their synthesis and applications based on the available literature. In addition, we discuss a number of the less explored applications of green CDs and the challenges that continue to be overcome.

Keywords: carbon dots; nanomaterials; green; energy; renewable sources

Carbon Based Nanocomposites For Environmental Applications: Current Progress, Challenges, And Future Possibilities

Monika, PinkuNath, Ajit Kumar Sharma*

Department of Chemistry, School of Chemical Engineering and Physical Sciences,
Lovely Professional University, Jalandhar, Punjab, India

Abstract

Carbon is normally produced by incomplete combustion or pyrolysis as an unwanted substance. Flammable powder consists primarily of carbon sphere aggregates. The domestic fireplace chimneys soot contains few aggregates but can produce large amounts of coke or char. Soot from diesel engines is mainly composed of aggregates with tars and resins. carbon-based nanocomposites are carbon nanomaterials that are formed from green sources. The term green refers to materials that are natural or harvest of natural renewable sources. Green sources grant outstanding properties, such as low cost, high yield, high availability, high biocompatibility, and high renewability. In this review, we discuss different applications of green carbon-based nanocomposites, such as H_2 production, water splitting, hydrogen storage, and utilization. Among these applications, renewable energy production is the mainly studied application of carbon-based nanocomposites. Carbon-based nanocomposites are fascinating because of their unique properties, such as wavelength-pitched color production, low toxicity, high water solubility, and high biocompatibility. In addition, the optical, physical, and chemical properties of carbon-based nanocomposites can be improved by surface doping. carbon-based nanocomposites are too considered an active photocatalyst because they can act as an electron acceptor and a donor leading doping among several heteroatoms, metal ions, and assorted functional groups

RESEARCH ARTICLE | SEPTEMBER 08 2023

Synthesis of highly efficient novel electrocatalyst for hydrogen production via microbial process ⊘

Monika Sindhu ✉; Karan Singh Maan; Sahima Tabasum; Vijay Patel; Pratima Gajbhiye; Anupam Kumar; Jashanpreet Singh; Ajit Kumar Sharma ✉

Check for updates

CrossMark

View Online

Export Citation

Articles You May Be Interested In

A functional integral formalism for quantum spin systems

J. Math. Phys. (July 2008)

Preparation of vanadium oxide from various route of synthesis process for energy storage application ⊘

Neetu Vishwakarma ✉; Monika Sindhu; Karan Singh Maan; Sahima Tabasum; Suman Rani; Vijay Patel; Jashanpreet Singh; Amar Srivastava; Ajit Kumar Sharma

Check for updates

CrossMark

View Online

Export Citation

Articles You May Be Interested In

A functional integral formalism for quantum spin systems

J. Math. Phys. (July 2008)

Synthesis and characteristic study of La/ZnO nanocomposites via hydrothermal route for pesticide degradation from agriculture aquatic waste ⊘

Suman Rani ✉; Sahima Tabasum; Ashima Thakur; Rohit Patra; Monika Sindhu; Karan Singh Maan; Upasana; Pratima Gajbhiye; Deepak Kumar; Ajit Kumar Sharma

Check for updates

CrossMark

View Online

Export Citation

Articles You May Be Interested In

A functional integral formalism for quantum spin systems

J. Math. Phys. (July 2008)

Photo-catalytic detoxification of chlorpyrifos pesticide from the aquatic environment using g-C$_3$N$_4$ doped with GO nano-composite ⊘

Sahima Tabasum ✉; Suman Rani; Ashima Thakur; Monika Sindhu; Karan Singh Maan; Upasana; Vijay Patel; Sarika; Azad Qayoom Malik; Pratima Gajbhiye; Deepak Kumar; Ajit Kumar Sharma

Check for updates

View Online   Export Citation   CrossMark

13 September 2023 05:13:53

Structural and morphological properties of bismuth oxide nanostructured materials ⊘

Amika; Deepak Kumar ✉; Rajesh Sharma; Monika Sindhu

Check for updates

View Online   Export Citation   CrossMark

Articles You May Be Interested In

The effect of reaction temperature on the particle size of bismuth oxide nanoparticles synthesized via hydrothermal method

AIP Conference Proceedings (May 2018)

Methodology for the recording and analysis of heart rate and oxygen saturation in adolescents, when they are playing video games

AIP Conference Proceedings (April 2023)

Facile synthesis of ZnS and Ni doped ZnS quantum dots and enhanced photocatalytic property of Ni doped ZnS nanoparticle

AIP Conf. Proc. (September 2023)

Conferences	Topic	Organized by	Date
International Conclave	International Conclave on Materials, Energy and Climate	Organized by IAAM Sweden	12-14 December 2022 (Oral Presentation)
International Conference	International Conference on Emerging Materials for Sustainable Development	Organized by CSIR-CISO Chandigarh	9-11 October 2022 (Poster Presentation)
International Conference	International Conference on Materials for Emerging Technologies	Department of Research Impact and Outcome (DRD) Lovely Professional University	18-19 Feb 2022 (Oral Paper Presentation)
International Conference	Recent Advances in Fundamentals and Applied Sciences	Department of Chemical Engineering and Physical Sciences, Lovely Professional University	25-26 June 2021 (Oral Presentation)
International Conference	Recent Advances in Chemical Sciences	Department of Chemistry, J.C. Bose University of Science and Technology, YMCA, Faridabad	14-16 July 2021 (Poster Presentation)

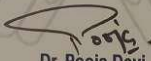| International Conference	Multinational Advanced Materials	Department of Chemistry, JVM Degree College	9-10 August 2021 (Oral Presentation)
International Conference	Recent Advances in Basic and Applied Sciences	Faculty of Sciences BMU Rohtak	27-28 August 2021 (Oral Presentation)

➢ **Certificates**

CERTIFICATE

This is to certify that

Ms.Monika Sindhu

Lovely Professional University, India

Delivered **Oral**

On

"Development of a highly efficient Co-doped Ta3N5 solar catalyst immobilized with BSC/PANI for H2 production"

In the

International Conclave on Materials, Energy & Climate,

12 December to 14 December 2022

ONSITE - ONLINE LIVE ▶

Onsite Venue

Indira Gandhi Delhi Technical University for Women, Delhi, India

Organized by

IAAM® International Association of Advanced Materials — IGDTUW — Shoolini University

Date
12 to 14 December 2022

Place and Country
New Delhi, India

Secretary General

International Association of
Advanced Materials
Org. 802503-6784

Gammalkilsvägen 18
Ulrika 590 53, Sweden

Web : www.iaamonline.org
Tel. : (+46) 1313-2424
E-mail : contact@iaamonline.org

Certification of Oral / Poster Presentation

This is to certify that Dr./Mr./Ms. ----Monika Sindhu---------------- from--Lovely Professional University----------------------- presented an oral / poster titled "Development of a highly efficient Nb-doped Ta₂N₅ solar catalyst immobalized with biomass soot carbon protected by PANI for H₂ production via water electrolysis "under the theme --Materials for clean Energy----in the "International Conference On Emerging Materials For Sustainable Development (EMSD-2022)" Jointly organized by CSIR-CSIO, Chandigarh and IEEE AcSIR-CSIO student chapter during October 9th -11th, 2022 held at CSIR-CSIO, Chandigarh.

Dr. Vinod Karar
Chief Scientist, CSIR-CSIO ,
Branch Counsellor,
IEEE AcSIR-CSIO SB, Chandigarh

Dr. Pooja Devi
Principal Scientist, CSIR-CSIO ,
Faculty Advisor, IEEE NTC, AcSIR-CSIO
Convenor, EMSD-2022

Ms. Aditi Chopra
Chair
IEEE AcSIR-CSIO SB, Chandigarh
Student Convenor, EMSD-2022

DIVISION OF RESEARCH AND DEVELOPMENT

[Under the Aegis of Lovely Professional University, Jalandhar-Delhi G.T. Road, Phagwara (Punjab)]

Certificate of Participation
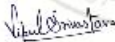
This is to certify that **Ms. Monika Sindhu** of **Lovely Professional University, Phagwara, Punjab, India** has presented paper on **Synthesis of Highly Efficient Novel Electrocatalyst for Hydrogen Production** in the **International Conference on Materials for Emerging Technologies (ICMET-21)** held on February 18-19, 2022, organized by Department of Research Impact and Outcome, Division of Research and Development, Lovely Professional University, Punjab.

Date of Issue: 16-03-2022
Place: Phagwara (Punjab), India
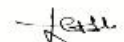
Prepared by
(Administrative Officer-Records)

Dr. Vipul Srivastava
Convener
(ICMET-21)

Dr. Manish Vyas
Organizing Secretary
(ICMET-21)

Dr. Chander Prakash
Co-Chairperson
(ICMET-21)

International Conference (Virtual) on Recent Advancements in Chemical Sciences - 2021 [ICRACS-2021]

July 14-16, 2021

Organized by

DEPARTMENT OF CHEMISTRY

CERTIFICATE

E-Certificate No.:
CHEM/2021-22/ICRACS/243

This is certified that Prof/Dr/Mr/Ms/Mrs **MONIKA**

of **LOVELY PROFESSIONAL UNIVERSITY JALANDHAR, PUNJAB** has presented a poster and title is

Highly Efficient V-doped Ta3N5 Photocatalyst for H2 Production via Water Splitting Process Under Solar

Irradiation

in "International Conference (Virtual) on Recent Advancements in Chemical Sciences - 2021 [ICRACS-2021]"

conducted by J. C. Bose University of Science and Technology, YMCA from July 14 to July 16, 2021.

Dr. Ravi Kumar	Dr. Sunil Kumar	Dr. Amit Rajput
Convener	**Organizing Secretary**	**Organizing Secretary**
Chairman, Chemistry	Assistant Professor, Chemistry	Assistant Professor, Chemistry

Certificate of Participation

This is to certify that   **Ms. Monika Sindhu**

of   **Lovely Professional University**

has given oral presentation on   **Development of a highly efficient Nb-doped Ta3N5 solar catalyst immobilized with**

biomass soot carbon for H2 production via water

in the International Conference on "Recent Advances in Fundamental and Applied Sciences" (RAFAS 2021) held on June 25-26, 2021, organized by School of Chemical Engineering and Physical Sciences, Lovely Faculty of Technology and Sciences, Lovely Professional University, Punjab.

Date of issue : 15-07-2021
Place of issue: Phagwara (India)

Prepared by
(Administrative Officer-Records)

Organizing Secretary
(RAFAS 2021)

Convener
(RAFAS 2021

283

284

INTERNATIONAL CONFERENCE

ON

"RECENT ADVANCES IN BASIC AND APPLIED SCIENCES"

(ICRABAS-2021)

Celebrating
Azadi Ka
Amrit Mahotsav

Organized by

FACULTY OF SCIENCES, BABA MASTNATH UNIVERSITY, ROHTAK
In Association with Internal Quality Assurance Cell (IQAC)

On

27th-28th August, 2021

CERTIFICATE

Unique ID_ICR- 4692

This is to certify that Mr./Ms./Dr./Prof. **Monika, Department of Chemistry, Lovely Professional University, Punjab, India** has presented **Oral** entitled **"Development of a highly efficient V-doped Ta3N5 photocatalyst immobilized with biomaas soot carbon for H2 production via water splitting process under solar irradiation"** at the International Conference on "Recent Advances in Basic and Applied Sciences" held at Faculty of Sciences, Baba Mastnath University, Asthal Bohar (Rohtak), on 27th-28th August, 2021.

Dr. Manoj Antil
Convener
ICRABAS-2021

Dr. Praveen Bhatt
Organizing Secretary
ICRABAS-2021

Dr. Manoj Kumar
Dean
FACULTY OF SCIENCES